Exploiting New GNSS Signals to Monitor, Model and Mitigate the Ionospheric Effects in GNSS

Zeynep Günsu Elmas, MSc

Thesis submitted to the University of Nottingham for the degree of Doctor of Philosophy

APRIL 2013

PREFACE

This thesis is submitted in fulfilment of the requirements for a degree of Doctor of Philosophy at Nottingham Geospatial Institute (NGI), University of Nottingham, UK, April, 2013. The research was conducted in the Innovative Navigation using new GNSS Signals with Hybridised Technologies, *iNsight*, project funded by the Engineering and Physical Sciences Research Council (EPSRC), UK, and it was supervised by Dr. Marcio Aquino (main supervisor), Prof. Terry Moore and Dr. Chris Hill at NGI.

This thesis should be cited as:

Elmas, Z.G. (2013) *Exploiting New GNSS Signals to Monitor, Model and Mitigate the Ionospheric Effects in GNSS.* Ph.D. dissertation, Nottingham Geospatial Institute, The University of Nottingham, Nottingham, UK.

ABSTRACT

Signals broadcast by the Global Navigation Satellite Systems (GNSS) enable global, autonomous, geo-spatial positioning exploited in the areas such as geodesy, surveying, transportation and agriculture. The propagation of these signals is affected as they propagate through the Earth's upper atmosphere, the *ionosphere*, due to the ionic and electronic structure of the ionosphere. The ionosphere, a highly dynamic and spatially and temporally variable medium, can be the largest error source in Global Navigation Satellite System (Klobuchar 1991) in the absence of the Selective Availability.

Propagation effects due to the ionosphere lead to errors in the range measurements, impact on receiver signal tracking performance and influence the GNSS positioning solution. The range error can vary from 1 to 100m depending on time of day, season, receiver location, conditions of the earth's magnetic field and solar activity (Hofmann-Wellenhof et al. 2001).

This thesis focuses on modelling, monitoring and mitigating the ionospheric effects in GNSS within the scope of GNSS modernization, which introduces new signals, satellites and constellations. The ionosphere and its effects on GNSS signals, impact of the ionospheric effects at the receiver end, predicted error bounds of these effects under different solar, geomagnetic and ionospheric conditions, how these effects can be modelled and monitored with current and new (possible with GNSS modernization) correction approaches, degradation in the GNSS positioning solution and mitigation techniques to counter such degradation are investigated in this thesis.

Field recorded and simulated data are considered for studying the refractive and diffractive effects of the ionosphere on GNSS signals, signal tracking performance and position solution. Data from mid-to-high latitudes is investigated for the refractive effects, which are due to dispersive nature of the ionosphere. With the use of multi-frequency, multi-constellation receivers, modelling of the refractive effects is discussed through elimination and estimation of these effects on the basis of dual and triple frequency approaches, concentrating on the benefit of

the new GNSS signals. Data from the low latitudes is considered for studying the diffractive effects of the ionosphere, scintillation in particular, in GNSS positioning, and possible mitigation techniques to counter them. Scintillation can have a considerable impact on the performance of GNSS positioning by, for instance, increasing the probability of losing phase lock with a signal and reducing the accuracy of pseudoranges and phase measurements. In this sense, the impact of scintillation on signal tracking performance and position solution is discussed, where a novel approach is proposed for assessing the variance of the signal tracking error during scintillation. The proposed approach also contributes to the work related with scintillation mitigation, as discussed in this thesis.

The timeliness of this PhD due to the recent and increasingly active period of the next Solar Cycle (predicted to reach a peak around 2013) and to the ongoing GNSS modernization give this research an opportunity to enhance the ionospheric knowledge, expertise and data archive at NGI, which is rewarding not only for this PhD but also for future research in this area.

TABLE OF CONTENTS

LIST OF TABLES

LIST OF FIGURES

LIST OF ACRONYMS

.csv	Extension for a comma separated values file
.ucd	Extension for a user commands file
3D	Three dimensions (horizontal and vertical components)
AGC	Automatic Gain Control
AltBOC	Alternative Binary Offset Code
BOC	Binary Offset Code
BPSK	Bi-Phase Shift Key
BSW	Bernese GPS Software
C/N_0	Normalized signal to noise ratio (given in dB-Hz)
c/n_0	Fractional form of C/N_0 ($c/n_0 = 10^{0.1\ C/N0}$);
L1 C/A	Coarse-Acquisition Code on L1 carrier
CDMA	Code Division Multiple Access
CGM	Corrected Geomagnetic Model
CODE	Center for Orbit Determination in Europe
CP	Carrier Phase
CSM	Cornell Scintillation Model
dB	Decibels
DCB	Differential Code Bias
DLL	Delay Locked Loop
DOP	Dilution of Precision
DOY	Day of year
E1	Galileo E1 signal at 1575.42 MHz
E5a	Galileo E5 signal at 1176.45 MHz
E5b	Galileo E5 signal at 1207.14 MHz
EGNOS	European Geostationary Navigation Overlay Service
ESA	European Space Agency
FDMA	Frequency Division Multiple Access
FEC	Forward Error Correction
FFT	Fast Fourier Transformation
FOC	Full Operational Capability
GAGAN	GPS and GEO Augmented Navigation
GEO	Geostationary Earth orbit
GIM	Global Ionospheric Map
GISM	Global Ionospheric Scintillation Model
GLONASS	Global Navigation Satellite System (Russia)
GNSS	Global Navigation Satellite System
GPS	Global Positioning System (USA)
HO	Higher Order
I,Q or I/Q	In-phase, Quadra-phase
IF	Ionosohere-free
IGRF	International Geomagnetic Reference Field

IGS	International GPS Service
IGSO	Inclined geosynchronous orbit (IGSO)
IOC	Initial Operational Capability
ION	Institute of Navigation
IONEX	Ionosphere Map Exchange
Iono1	First order ionospheric effect
Iono2	Second order ionospheric effect
Iono3	Third order ionospheric effect
IOV	In-orbit validation
IPP	Ionospheric Pierce Point
IRNSS	Indian Regional Navigational Satellite System
ISRO	Indian Space Research Organization
JPL	Jet Propulsion Laboratory
Kp	Planetary K index
L1	GPS L1 signal at 1575.42 MHz
L2	GPS L2 signal at 1227.6 MHz
L2C	L2 signal with C code in GPS
L2P(Y)	P(Y) code on L2 signal in GPS
L5	GPS L5 signal 1176.45 MHz
LC	Linear Combination
LoL	Loss of Lock
LoS	Lone of Sight
LSQ	Least Squares
MEO	Medium Earth Orbit
NGI	Nottingham Geospatial Institute
N_{max}	Maximum electron density
NRCan	Natural Resources Canada
OS	Open Service
P1	Precision code on L1 carrier
P2	Precision code on L2 carrier
PANDA	*P*ositioning *A*nd *N*avigation *D*ata *A*nalyst
PLL	Phase Locked Loop
PPP	Precise Point Positioning
PR	Pseudorange
PRN	Pseudorandom noise
PRS	Public Regulated Service
PRU1, PRU2	Two stations in Brazil at about 300m distance
QZSS	The Quasi-Zenith Satellite System
RAIM	Receiver Autonomous Integrity Monitoring
RHCP/LHCP	Right/Left Hand Circularly Polarized
RHS	Right hand side
RINEX	Receiver Independent Exchange Format
RMS	Root Mean Square
RRE	Residual Range Error

RTK	Real Time Kinematic
S4	Amplitude scintillation index
SBAS	Satellite Based Augmentation System
SNR	Signal to noise ratio (in dB units)
SoL	Safety of Life
STD	Standard Deviation
STEC	Slant Total Electron Content
SV	Satellite Vehicle
TEC	Total Electron Content
TEC	Total Electron Content
TECU	Total Electron Content Units (10^{16} electrons per m^2)
UTC	Universal Time Coordinated
VTEC	Vertical Total Electron Content
WAAS	Wide Area Augmentation System
WBMOD	Wide-Band Model, WBMOD, for ionospheric scintillation

ACKNOWLEDGEMENTS

This work was partially funded by an EPSRC studentship award and by a Research Studentship from the School of Civil Engineering at the University of Nottingham, UK.

First and foremost I would like to thank my main supervisor Dr. Marcio Aquino for his guidance, support and motivation, making my research years at NGI unquestionably rewarding and memorable. I would also like to thank Prof. Terry Moore and Dr. Chris Hill for their inspiring feedback and encouraging supervision.

Heartfelt thanks to Sreeja Veettil for her friendship and support, Alan Dodson for his encouragement and stimulating questions and Biagio Forte for his contribution to our discussions during the CIGALA project. My thanks extend to Dr. Hal Strangeways at the University of Leeds for his elaborate lectures and Jean Marie Sleewagen at Septentrio Satellite Navigation for his patience with my inquisition about GNSS receiver details.

I am indebted to my colleagues Haroldo Marques and Heloisa da Silva, supervised by J.F. Galera Monico at UNESP, for their courtesy and support while making available useful GNSS software deployed in this thesis.

This thesis would not be possible without the unconditional support of my beloved family.

CHAPTER 1

1. INTRODUCTION

Signals broadcast by the Global Navigation Satellite Systems (GNSS) enable global, autonomous, geo-spatial positioning exploited in the areas such as geodesy, surveying, construction, offshore operations, mining, aviation and agriculture. These signals (electromagnetic waves) travel through the Earth's upper atmosphere, the *ionosphere*, which affects the propagation of these radio signals due to its ionic and electronic structure; these propagation effects lead to errors in range measurements, impact on receiver signal tracking performance and affect the GNSS positioning solution.

This thesis concentrates on an investigation of the ionospheric effects in GNSS within the scope of GNSS modernization: what the ionosphere is and how it affects the GNSS signals, observed impact at the receiver end, predicted error bounds of these effects under different background (solar, geomagnetic, ionospheric) conditions, how these ionospheric effects can be modelled and monitored, correction approaches, possible degradation in the GNSS positioning solution and mitigation techniques to counter such degradation.

This PhD research has been conducted as part of the project Innovative Navigation using new GNSS SIGnals with Hybridized Technologies, *iNsight*, funded by the EPSRC and carried out by the four leading UK universities – Imperial College, University of Nottingham (UoN), University College London, University of Westminster (UoW), in collaboration with nine commercial companies and government agencies: Air Semiconductors, Civil Aviation Authority, EADS Astrium, Leica Geosystems, Nottingham Scientific Limited, Ordnance Survey, QinetiQ, ST Microsystems, and Thales Research and Technology. The University of Nottingham leads two work packages (WP) in this project: one related with the effects of the atmosphere in GNSS (WP5) and the other (WP6) with GNSS positioning, both of which aim to exploit the new GNSS signals. This PhD research is conducted within WP5 and has focused on the ionospheric effects and new GNSS signals for modelling, monitoring and mitigation purposes.

Research in the iNsight project is conducted aiming for an input-output based interface between WPs. In this sense, WP5 of UoN can inform the WP7 of UoW (University of Westminster) that focuses on the software GNSS receiver. It should be mentioned that during this PhD work, the software GNSS receiver developed by UoW had just started tracking live signals thus data made available from it could not be included into this thesis; however, design requirements from WP5 for a (software) GNSS receiver that can be used as a reliable equipment for future studies about ionospheric effects in GNSS were discussed with the team members of UoW. Further details on the iNsight project can be found at http://www.insight-gnss.org/.

Within the time frame of this PhD, participation in the other GNSS related projects participated by NGI such as the Concept for Ionospheric Scintillation Mitigation for Professional GNSS in Latin America, *CIGALA*, and Predicting Observing Locating And Redressing Ionospheric Scintillation, *POLARIS*, have helped to conduct the research during this PhD by observing the effects on the new signals such as GPS L2C, L5 and Galileo E1, to correlate the ionospheric effects to range measurements and positioning solutions and to provide a technical opportunity to learn GNSS receiver architecture and station deployment at a necessary level.

- The CIGALA project aims to implement a novel scintillation and tracking model into an advanced multi-frequency GNSS receiver that is capable of countering the ionospheric scintillation effects in Latin America. Experience obtained through the CIGALA project has contributed to this PhD from the aspects of understanding the causes of scintillation and state of the art models for signal tracking and focusing on an improved receiver signal tracking error model sensitive to the scintillation effects on the GNSS signals especially at the low latitudes. Through analysis of data logged by the scintillation specific receiver *PolaRxS* (manufactured by Septentrio N.V. Belgium), it was possible to model, implement and test receiver robustness against scintillation and scintillation mitigation techniques. Significant contribution to the CIGALA project facilitated the investigation of the ionospheric scintillation effects on the GNSS signals as well as acquiring experimental knowledge about receiver architecture.

■ Through the POLARIS project funded by EPSRC, it was possible to access data from receivers in a widely spaced network at the equatorial, mid and high latitudes as well as the arctic region. Particular interest was given to the receivers capable of tracking the new Galileo signals E1 and E5a/b signals, however, only the data made available until the end of the research period of this PhD could be considered in this thesis.

1.1. MOTIVATION AND PURPOSE OF THE RESEARCH

GNSS supports a wide range of applications from construction, surveying, aviation, precision-agriculture to earth sciences and space weather research (Gleason & Egziabher 2009). Ionospheric effects are the largest and most variable error sources in GNSS (Doherty et al. 2000; Langley 2000; Dubey et al. 2006). As GNSS based applications are more widespread than before, there is more emphasis and need to understand how the ionosphere affects the GNSS.

After removal of the Selective Availability[a] in 2000, the ionosphere became the dominant error source in the GNSS error budget (El-Rabbany 2002). The ionosphere is a medium of free electrons and ions and as such (the all-time background ionosphere) perturbs the transionospheric (through the ionosphere) signal propagation by introducing errors in the range measurements computed by a GNSS receiver (Leick 1995; Beach 1998; Knight et al. 1999; Langley 2000; Humphreys et al. 2005). Furthermore, at certain times and geographical locations ionospheric conditions may get adverse, which can make this medium less predictable (the disturbed ionosphere). While the undisturbed background ionosphere causes errors that are rather deterministic i.e. the magnitude of the error in the range measurement can be estimated and/or corrected, effects of the disturbed ionosphere can be random. It is generally known *when* (for instance, during the local post-sunset to local midnight hours) and *where* (for instance, the low latitude regions) they are "more likely to happen", and their impact on the signals and receiver performance.

[a] *Selective Availability (SA) was an intentionally introduced error source to the public GPS navigation signals by the US Department of Defence. It was turned off in May 2000 by the U.S. Department of Defence.*

With modernization in GNSS, which involves new signals and satellites as in GPS and GLONASS, and new GNSS systems such as Galileo and BeiDou, it is possible to expand the research about monitoring, modelling and mitigating the ionospheric effects in GNSS to a level that can provide higher accuracy, less computational burden and faster positioning solutions, to name a few of the possible advantages. Details and advantages of GNSS modernization within the scope of the ionospheric effects are discussed in Chapter 2.

Modelling and correcting the ionospheric effects has become more crucial given the greater user demand (such as higher accuracy) and the greater worldwide dependence on GNSS applications (for instance, by the agriculture, oil and gas industries, transportation, navigation etc). This requires the ionospheric effects to be better understood, and modelling and correction approaches revisited and improved. With this *motivation*, this research *aims* to understand the ionospheric effects and focus on the modelling and correction approaches which can benefit from GNSS modernization, as well as to advance the mitigation technique suggested by Aquino et al. (2009) against the ionospheric effects in GNSS positioning.

In the work by Aquino et al. (2009), a mitigation technique is proposed that improves the stochastic model that is related with the statistical quality, *precision*, of the measurements. Such statistical quality is determined in terms of the tracking error (jitter) variance and the measurements are assigned weights that are inversely proportional to the estimated jitter variances. The authors demonstrate that instead of considering each observable with a constant precision (i.e. an "equal weights" approach), regarding the measurements with individual weights makes the stochastic model more realistic in terms of the impact of scintillation and this improves the estimated position solution. The same authors make use of the model of Conker et al. (2003) (referred to as the "Conker model") to estimate the variances in order to modify the stochastic model and test and validate their technique of mitigation against scintillation. However, the Conker model, as investigated in the respective section of this thesis, may not be valid for use at times of strong scintillation. With this limitation of the Conker model it is not possible to estimate the jitter variance for strong scintillation conditions; and with such non-availability of the jitter variance it is also not possible to apply

the mitigation technique of Aquino et al. (2009) when it can be especially advantageous – during strong scintillation.

A novel approach is suggested in this PhD in order to estimate the jitter variance continuously and during any level of scintillation. Such estimation is achieved by exploring the data from the signal tracking loops of a receiver - more specifically, from the output of the correlators, referred to as the "post-correlator" data[b]. The suggested approach enables estimation of the jitter variance during strong scintillation levels which may not be possible when the Conker model is applied; and it helps to carry forward the scintillation mitigation work of Aquino et al. (2009) in terms of investigating, testing and validating their mitigation technique making use of a larger data set from stations at the equatorial latitudes where strong scintillation effects are a well-observed threat to GNSS.

The timeliness of this PhD is remarkable given that the period 2009-2012 coincides well with the ongoing GNSS modernization as well as the recent and increasingly active period of the *Solar Cycle 24*[c] (Bureau of Meteorology 2009). Opportunity to enhance the ionospheric knowledge, expertise and data archive at NGI in the next solar maximum is rewarding not only for this PhD but also the future research.

It is anticipated that the analysis methods about receiver signal tracking performance and scintillation mitigation in positioning set out during this PhD and the collected data may contribute positively to the field of research about the ionospheric effects in GNSS for current and future

[b] *It can serve as a raw source of data helpful to infer scintillation effects on the signals that can affect the performance of the tracking loops.*

[c] *The sun exhibits a reliable periodic cycle of activity, going from a low activity phase at a solar minimum to a high at a solar maximum (Banks 1976). The periodicity of this activity is characterized by the number of dark areas, spots, which are relatively cooler areas observed on the solar surface. Monthly averages for these "sunspots" give the Sunspot Cycle, which reflects the observed maxima and minima in the solar activity that repeat every 11 years (Fig. 1.1.). As of 2008 the Solar Cycle 24 is in progress, expected to peak around 2013 (Bureau of Meteorology 2009).*

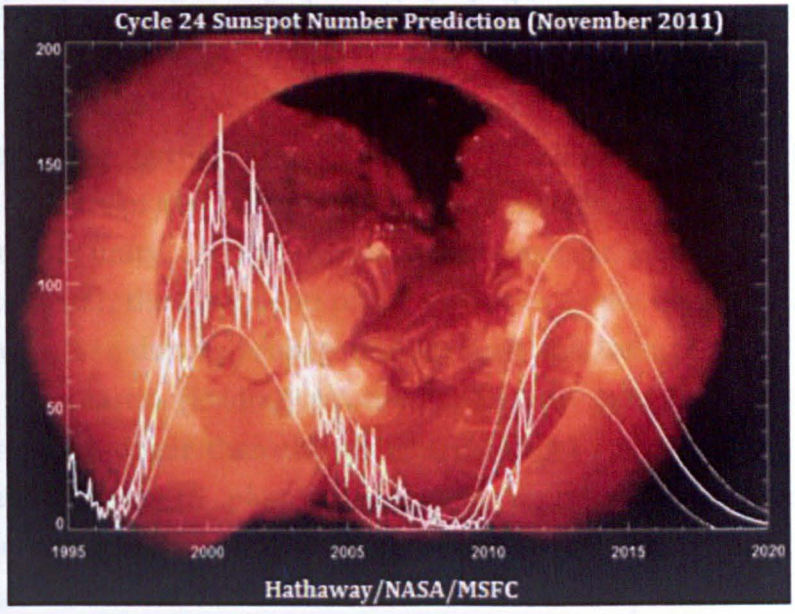

Figure 1.1. Variation in solar activity in terms of the monthly average sunspot number since 1995 (NASA 2012).

researchers. Use of the Spirent GNSS signal simulator at NGI for studying the scintillation effects making use of both open sky and model output data as a source of scintillation effects has proved to be helpful for simulation-based research. An alternative method proposed in this research for estimating the increase in thermal noise due to scintillation, which helps to assess code tracking loop jitter variance during (especially strong) amplitude scintillation, may also be helpful for real-time, continuous assessment of receiver signal tracking performance. Furthermore, during the period of this PhD research, GNSS modernization has been in progress but not yet complete; therefore, open sky data for the new signals recorded during and beyond the period of this research is deemed to contribute to the scintillation data archive of NGI for research purposes.

1.2. LITERATURE OVERVIEW

The ionosphere which is not a vacuum but a dispersive medium with ionic and electronic structure affects the speed and direction of the GNSS signals during propagation. Signals are refracted and diffracted by the ionosphere; the former gives rise to range errors in the pseudoranges and carrier phase measurements whereas the latter is related with rapid fluctuations

in the signal intensity and phase that challenge tracking of the signal within the receiver.

The all-time background ionosphere can be taken as to constitute the predictable part of the ionosphere. As the ionospheric refractive index is different from unity, i.e. radio waves do not travel at the speed of light but slower or faster, the group and phase velocities of the GNSS signals differ from each other during propagation through the ionosphere: the group velocity decreases (leading to the so-known *group delay* i.e. code measurements longer than the geometric range) and the phase velocity increases (leading to *phase advance* in carrier phase). Background ionosphere can be considered as an all-time error source for the GNSS range measurements; this is discussed in detail in Chapter 3.

Due to the dispersive nature of the ionosphere, the ionospheric effects can be accounted for by making use of the measurements on distinct signal frequencies (Hofmann-Wellenhof et al. 2001). Common practice of eliminating the refractive (delay) effects caused by the ionosphere by linearly combining the observables (pseudoranges or carrier phases) on different frequencies gives the so-called *ionosphere free* (IF) observable. This can be achieved using the observables on L1 and L2 frequencies (or also L1 and L5 with the modernized GPS) and can account for about 99% of the total ionospheric error; this is known as the first order approximation. The remaining 1% residual range error (RRE) in the IF observable is due to the higher (second and third) order ionospheric effects. Higher order terms are related with the electron content along the signal path; moreover, the second order term is associated with the influence of the geomagnetic field on the ionospheric refractive index along the signal path and the third order term with the ray bending effect of the ionosphere which can cause significant deviation in the ray trajectory from the line of sight (due to strong electron density gradients in the ionosphere) (Kim & Tinin 2007) especially at low elevation angles (Strangeways & Ioannides 2002). When the phase and group velocities are affected, the ray trajectory is also likely to be affected *unless* the wave is travelling perpendicular to the gradients in the ionosphere (Cairo & Cerisier 1976). This effect, also known as the ray bending effect, is inversely proportional to the signal frequency and highly dependent on the satellite elevation angle. The error due to the ray bending effect is

orders of magnitude smaller than the first order ionospheric error – it is indeed comparable in magnitude to that of the higher order error terms (Petrie et al. 2010). A single frequency receiver would need to estimate the error due to the ionosphere using an ionosphere correction model as provided in the GPS broadcast message, which can remove about 50-60% of the delay (Klobuchar 1996), or by receiving corrections and/or measurements by a reference station. In this thesis, focus is on how a receiver can benefit from the new GNSS signals to better account for the ionospheric error in stand-alone mode by making use of the currently available and new signals to correct the frequency dependent effect of the ionosphere, to monitor or estimate the electronic content of the ionosphere more precisely.

Since the higher order error terms do not cancel out in the first order approximation (as discussed in Section 3.1.2.), they can degrade the accuracy of GNSS positioning, depending on the level of the solar activity and the geomagnetic and ionospheric conditions (Hoque & Jakowski 2007). Simulation results from early 1990s show that these error terms can contribute to the ionospheric error budget by up to about 1% of the first order error term at GPS frequencies (Datta-Barua et al. 2008) leading to cm-mm level range errors, subject to the background ionospheric conditions. Although the IF observable may provide sufficient accuracy for most GNSS applications, the higher order error terms need to be considered for high accuracy demanding applications especially at times of elevated solar activity. In this respect, GNSS modernization brings some new strategies to account for the range errors due to the ionosphere such as: (i) with the new civil code on GPS L2 signal, L2C, can obviate the need for codeless or semi-codeless tracking of L2 signal making a civil dual frequency tracking possible; (ii) with the availability of three signal frequencies (L1, L2, L5), it is possible to use three frequencies to construct the IF observable instead of the dual-frequency approach; this enables a second order approximation to correct for both the first and second order ionospheric error terms. (iii) more accurate modelling of the total electron content (TEC) which is an important parameter estimated by GNSS data regarding the ionospheric conditions.

With a wide range of applications, varying from vertical land motion estimates for calibration of tide gauges and comparison with glacial

isostatic adjustment (Bouin & Wöppelmann 2010) to tectonic strain (Calais et al. 2005) comes a requirement for precision which has brought into attention the higher order ionospheric effects in the past few years (Petrie et al. 2011). An increasing emphasis on correcting the higher order error terms, focusing on the second order term, can be noticed in Hernandez-Pajares et al. (2008), Elsobeiey & El-Rabbany (2009), and Elsobeiey & El-Rabbany (2012). While the need for a review of the higher order ionospheric effects in GNSS is more obvious, it is also more feasible / possible to study these effects with modernized GNSS that offers more signals and satellites (Petrie et al. 2011). Improvement in precision has been possible not only due to advances in receiver technology, but also to an improved understanding of systematic errors, such as the ionospheric effects, affecting GPS signals and modelling of these errors.

Recent work by some authors highlights the importance of the new signals in modelling the ionospheric effects in GNSS: Lightsey & Humphreys (2011) emphasize the importance of the new GPS L2C signal for L1, L2 linear combination over the next decade for eliminating the ionospheric error (to the first order), EU METSAT (2008) draws attention to a triple frequency approach for the IF observable LC using wide lane and extra wide lane signals[d] and also mention the larger amount of residual error in IF when constructed from L1 and L5 instead of the L1 and L2 signals (due to the lower frequency of the L5 signal which is more affected by the ionosphere than L2), Richert & El-Sheimy (2007) emphasize the choice of coefficients for linearly combining the triple frequency observations which can yield significantly different accuracies for reducing the contribution of the error sources to the resultant observable.

Regarding the ionosphere that is more random in nature. The effects of a disturbed ionosphere are related with electron density *irregularities* (small scale fluctuations in the refractive index of the ionosphere (Stevanovic 2012)) along the signal propagation path that diffract the GNSS signals (Wernik et al. 1990; Kintner et al. 2001). Such diffractive

[d] *Wide lane combination is used to create signals with wide wavelengths, where the longer wavelength can help in cycle-slip detection and ambiguity resolution.*

effects of the ionosphere are observed as rapid (less than 15s variations, (Langley 2000)) fluctuations in the intensity and phase of the received signal. Such effects are different than the background ionosphere which is refractive in nature for the GNSS signals. Electron density gradients along the signal propagation path can cause difficulty in the receiver's ability to track especially the phase of the incoming signal. Diffractive effects of the ionosphere, known as scintillation, can challenge the code and carrier tracking loops of a GNSS receiver such that phase tracking can be degraded leading to cycle slips (jumps of the carrier phase by an integer number of cycles causing the phase ambiguity to change while leaving the fractional part of the phase observable unchanged (Seeber 1993)), or even complete loss of signal lock under extreme conditions and navigation data bit errors (Leick 1995; Beach 1998; Knight et al. 1999; Humphreys et al. 2005).

On a global scale, scintillation activity is observed more often at the equatorial latitudes extending to about 20^0 on both sides of the geomagnetic equator and at the auroral latitudes from about 65^0 to 75^0 north and south latitudes (Pi et al. 2002). In addition to its latitudinal variation, scintillation occurrence has temporal, seasonal, solar and geomagnetic activity dependence (Aarons 1982; Groves et al. 1997; Beniguel et al. 2004). Scintillation shows strong diurnal dependence such that it is mostly strongest around local sunset and gets milder towards midnight and almost disappears during day time. It is characterized by the 11-year Sunspot Cycle - approximately every 11 years a solar maximum happens which is associated with elevated ionospheric activity. Around the solar maximum, increase in the high-energy electromagnetic radiation and particles from the Sun enhance the content and variability of electrons in the ionosphere (Langley 2000; Kintner et al. 2007). Influence of the geomagnetic effects, such as disturbances in the Earth's geomagnetic field influencing the ionization levels of the ionosphere, can extend towards the mid-latitudes causing the scintillation events be observable at these extended latitudes (Doherty et al. 2000; WAAS 2010); as such is also more likely to happen around the years of solar maximum.

Scintillation affects the GNSS receivers at signal tracking loop level leading to difficulty in signal acquisition and tracking, as well as causing degradation in accuracy and availability of measurements. For this reason

it is not possible, or at least it is not a general practical solution, to correct for the error due to scintillation by making use of measurements on multiple frequencies. Moreover, impact of scintillation on different receivers will be different depending on the hardware and software specifications, for instance, tracking loop bandwidth (important for the thermal noise and robustness of receiver to signal dynamics), oscillator quality (important for precise carrier phase tracking) as well as carrier phase based versus code-only receivers (Langley 2000). It has been understood in this PhD research that scintillation may disrupt signal tracking causing the number of visible satellites to abruptly decrease, introduce errors to range measurements and eventually degrade the positioning solution (Coco et al. 1999). Scintillation is not likely to affect all line-of-sight (LoS) signal paths at the same time – however, complete outages causing insufficient number of trackable satellites for a positioning solution may occur under extreme conditions as was observed in Cerruti et al. (2008). By degrading the relative geometry with the available constellation (as well as increasing the noise during signal tracking) scintillation can affect the precision with which a positioning solution can be achieved. Investigations are carried out in this work analyzing open sky data with moderate-to-strong levels of scintillation when typical GNSS receivers start losing lock. This helps to conclude that the spatial distribution of scintillation causing irregularities, coverage of the satellites and the level of scintillation are important factors for the impact of scintillation in GNSS positioning. A recent strong scintillation event in 26 March 2011 is investigated by the authors Sreeja et al. (2011a) who draw attention to the impact of equatorial scintillation on the tracking of signal phase. The authors show that recovering the phase lock after a loss under strong scintillation can be very difficult and the variance of the phase jitter increases with the intensity of scintillation. Positioning solutions may be impaired due to a loss of lock (LoL) on one or more satellites (in a limited sky-view tracking condition, this can make a positioning solution not available), general increase in the noise level of the received signal while keeping lock with all satellites or a combination of the two cases. This, indeed, is important for the mitigation strategies against the effects of scintillation developed in this PhD: Mitigating the scintillation effects at positioning level relies on all line-of-sight (LoS) signals that are not lost but perturbed by scintillation. If a satellite is lost,

then mitigation, as described in this thesis, cannot reconstruct the impaired relative satellite-receiver geometry.

Another impact of scintillation is that it may increase the susceptibility of a GNSS receiver to jamming (Volpe 2001). Scintillation can already degrade the power of the received signal due to signal fading. For instance, scintillation can cause fading so severe that the power level of the received signal can fall below the threshold for the receiver to keep lock or challenge reacquisition after a LoL. Under such conditions, jamming the already weakened tracking channels to make them lose lock can become easier during scintillation (NovAtel 2012). This issue of receiver susceptibility to jamming during scintillation, however, is not investigated within this thesis.

Robust signal tracking during scintillation can be achieved by receiver hardware as well: for instance, scintillation related parameters (statistical measures using signal intensity and phase fluctuations) can be monitored (in real time by the receiver itself) or estimated (by a scintillation model[e] which may need geographical, geomagnetic and time data as input) such that increasing severity triggers, for example, a change in the bandwidth of the carrier tracking loop to decrease the possibility of a loss of lock (Hegarty et al. 2001; Humphreys et al. 2009a).

Scintillation effects can be avoided by simply by turning off the receiver at certain times (such as when a threshold for scintillation detection is exceeded) in certain geographical regions that are known to be more prone to scintillation effects; or by tracking the satellites that remain visible but achieving a position solution using the erroneous measurements. The latter has been considered in this thesis while applying the mitigation strategy in GNSS positioning as shown earlier by Aquino et al. (2009) that makes use of all range measurements (some impaired due to scintillation) for obtaining a position solution. Contribution of this PhD to mitigating the scintillation effects is discussed in detail in Chapter 6.

[e] *Appendix A provides details about models that can be exploited regarding ionospheric scintillation*

1.3. THESIS OUTLINE

This thesis is composed of nine chapters as shown in Figure 1.2.

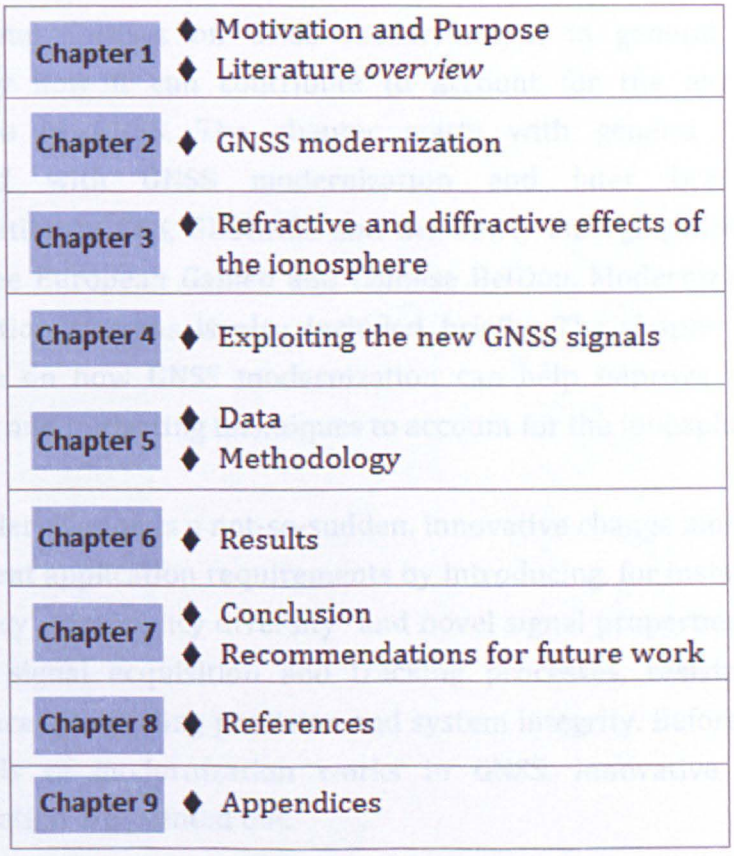

Figure 1.2. Schematic for the thesis outline.

Chapter 1 is the introduction chapter for this thesis including the motivation and purpose of the research as well as an *overview* of the literature about the ionospheric effects in GNSS (Literature *review* about the subjects discussed in Chapters 2, 3 and 4 is reserved to relevant sections of these chapters). Chapter 2 gives an up-to-date status of GNSS modernization. Chapter 3 concentrates on the diffractive and refractive effects of the ionosphere in GNSS. Chapter 4 focus on how the new GNSS signals can be exploited to monitor, model and mitigate the ionospheric effects - in a theoretical approach. Chapter 5 presents the data and methodology considered in the investigations of this thesis. Chapter 6 contains the results and discussion for the refractive and diffractive effects of the ionosphere in two respective sections. Chapter 7 includes the conclusion for the thesis and puts forward recommendations for the future work. Chapter 8 contains a list of the references and Chapter 9 provides the appendices.

CHAPTER 2

2. GNSS MODERNIZATION

This chapter focuses on GNSS modernization in general and more specifically how it can contribute to account for the effects of the ionosphere in GNSS. The chapter starts with general innovations introduced with GNSS modernization and later branches into modernization in GPS, GLONASS and the newly emerging GNSS systems such as the European Galileo and Chinese BeiDou. Modernization in the augmentation systems is also included briefly. The chapter ends with discussion on how GNSS modernization can help improve monitoring, modelling and mitigating techniques to account for the ionospheric effects.

GNSS modernization is a not-so-sudden, innovative change aiming to meet the different application requirements by introducing, for instance, "signal redundancy", "frequency diversity" and novel signal properties which can improve: signal acquisition and tracking processes, resistance to RF interference, positioning precision and system integrity. Before going into the details of modernization works in GNSS, innovative aspects of modernization are pointed out.

It should be noted that during this PhD, GNSS modernization was not yet complete thus the Spirent GNSS signal simulator has been advantageous to track the new signals like GPS L2C and L5 at a constellation level and investigate tracking performance especially during different scintillation scenarios. While the open sky data was limited in terms of the modernized signals as well as scintillation events, the Spirent simulator provided the capability to consider weak (S4<0.4) to strong (S4>0.6) ionospheric conditions to investigate the signal tracking robustness while at the same time enabling application and improvement of the knowledge on implementing scintillation effects on the generated signals.

- More signal frequencies:

Figure 2.1. shows the L band (L1, L2 and L5 (referred to as L3 in GLONASS)) signals for GPS, GLONASS and Galileo with respective modulation of the signals.

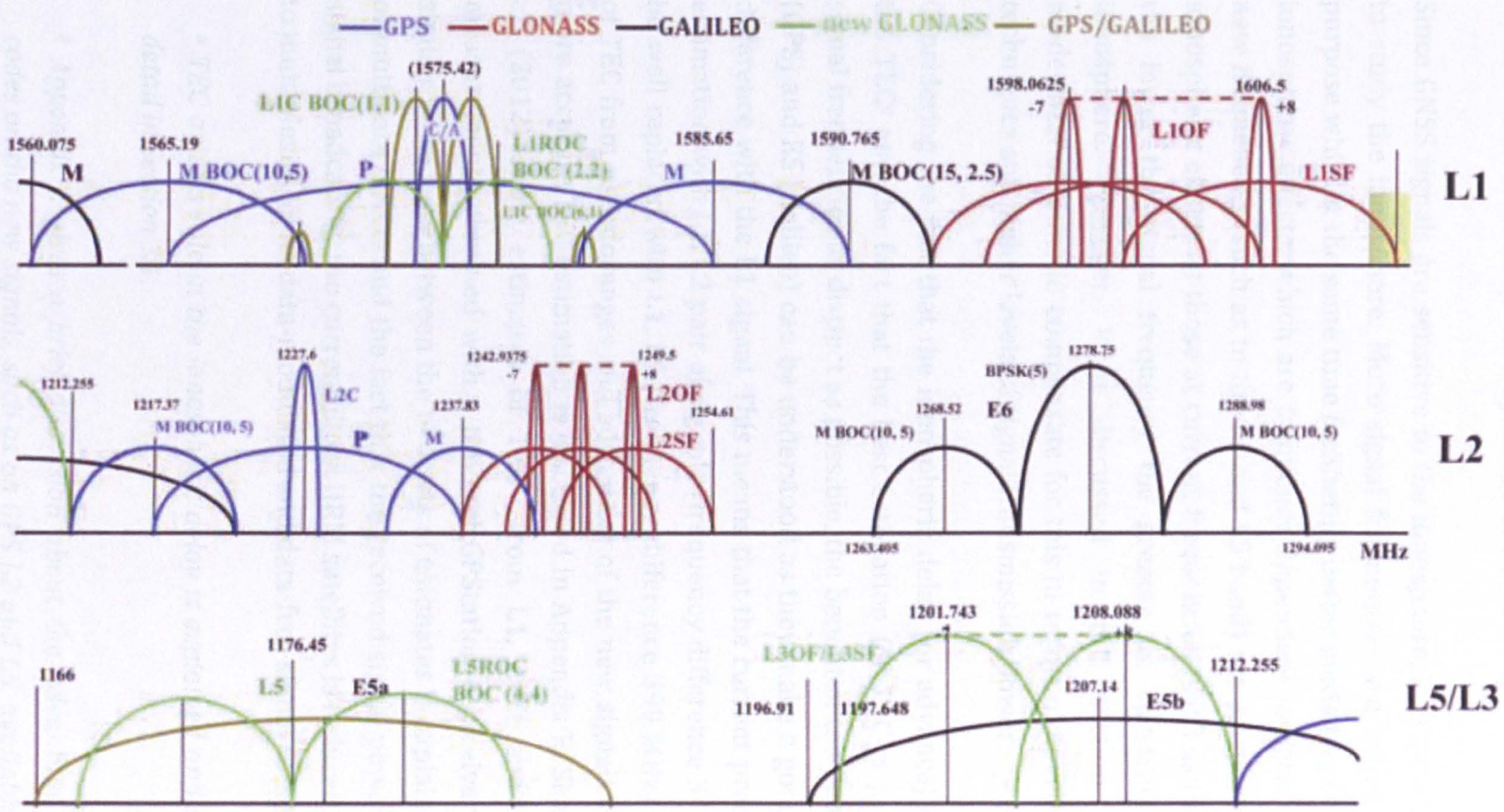

Figure 2.1. Evolution of the GPS signals from the Block I through the Block III satellites. The normalized power spectral densities are shown in decibels (Gibbons 2008).

The spectrum for the Chinese Beidou, which plans to broadcast three signals at the frequencies 1575.42MHz, 1191.795 MHz and 1268.52MHz, can be found at a recent work by Inside GNSS (2009a).

Since GNSS signals are sensitive to the ionosphere, they provide a means to study the ionosphere. More signal frequencies are beneficial for this purpose while at the same time facilitating better modelling efforts for the ionospheric effects, which are frequency dependent in nature. Signals at new frequencies (such as in the L2 and L5 band) are as vulnerable to the ionospheric effects as those at current frequencies (such as the L1 band); the lower the signal frequency the greater its vulnerability to the ionosphere. However, it is discussed in this section that GNSS modernization aims to compensate for this in terms of novel modulation techniques and higher levels of signal transmission power.

Considering the fact that the ionospheric delay (or advance) depends on the TEC[a] and the fact that the best estimation for TEC is possible with signal frequencies as distinct as possible, the benefit of the new signals L5 (GPS) and E5 (Galileo) can be understood as they make a good frequency difference with the L1 signal. This means that the current practice of TEC estimation with L1, L2 pair of signals (frequency difference 348 MHz) can be well replaced with L1, L5 (frequency difference 399 MHz). Estimation of TEC from pseudoranges and advantage of the new signals related with more accurate TEC estimation is discussed in Appendix B. Shanmugam et al. (2012) show estimates of TEC from L1, L2C[b] and L1, L2P(Y) measurements obtained with a NovAtel GPStation-6 receiver where the similar noise level between the two sets of estimates is explained in terms of multipath effects and the fact that the received signal power of the L2C signal broadcast by the current Block IIRM satellites is reduced by 3dB due to multiplexing of its data-modulated and data-free signal components.

[a] *TEC and its role in the ionospheric delay is explained and discussed in detail in Section 3.1.*

[b] *Appendix C gives a brief discussion about the advantage of the civil codes on the new signals, such as on GPS L2 and L5, available with GNSS modernization.*

The new L2C signal, introduced in 2005, aims to improve the accuracy, tracking and redundancy of the GPS system for civilian users who can derive dual-frequency observables based on code-tracking instead of the current practice of semi-codeless tracking which suffers from a squaring loss that depends on the SNR of the L2 signal. Furthermore, in order to account for this squaring loss, semi-codeless techniques depend strongly on L1 C/A tracking to minimize the squaring loss by achieving narrow bandwidth code and carrier tracking loops. Such narrow bandwidth tracking conditions may not be favourable for calculation of the scintillation indices (Shanmugam et al. 2012). The new L2C signal, therefore, can overcome the squaring loss related problem of semi-codeless tracking in the dual-frequency approach. Leandro et al. (2001) point out that L2C can be tracked at a higher SNR compared to L2P(Y) and allow for better tracking at lower satellite elevation angles. The same authors also show in their results that the number of L2 observations increases when the observables for L2C are recorded, and the number of cycle slips detected above 10^0 elevation angle decreases when the L2C signal is tracked. Further to their results, enabling the L2C tracking does not affect the behaviour of the L2P(Y) phase observations or the calculated position solution for a given receiver.

Within the ionospheric context, dual frequency operation can improve SBAS capability in terms of robustness against ionospheric gradients and reliability especially for the equatorial areas where the current single-frequency, two dimensional grid can be a poor fit to the actual temporal and spatial conditions of the ionosphere in these regions. Dual frequency operation can also benefit scintillation monitoring in these regions as these regions may not be accurately modelled within the thin shell model approach of the grid providing corrections in SBAS (Shanmugam et al. 2012).

Another impact of more signal frequencies is related with the linear combination (LC) of observations to eliminate or reduce the total ionospheric error. The current dual-frequency practice of linear combination, making use of code and phase observables on L1, L2 signals, can be advanced to triple-frequency L1, L2, L5. While the former provides a first order correction to the total ionospheric error leaving behind residual errors due to Iono2 and Iono3, the latter can help eliminate

further Iono2 in a second order approximation. Although a noise increase in such triple-frequency linear combination is expected (Urquhart 2009), the benefit of more signal frequencies remains evident.

The frequency bands of the different GNSS constellations may overlap or be adjacent to each other. This can favour the combined use of several constellations to increase performance, robustness and integrity of the GNSS services offered to the user communities (Hegarty & Chatre 2008).

- Higher chipping rate (in spreading codes):

Higher chipping rate ("faster" codes) can be associated with a narrower/ sharper peak in the autocorrelation functions (which are related with comparing the local and received spreading code in time-shifted versions) so that the received signal can be distinguished easily from other satellite signals or those arriving through different paths. For instance, the new GPS L5 signal has ten times a greater chipping rate than that of L1C/A signal (i.e. 1 code chip of L5 is $1/10^{th}$ that of L1C/A); the result of this is a correlation peak of L5 ten times narrower/ sharper than that of L1C/A, which makes the correlation peak more "distinguishable". This can be advantageous for tracking during ionospheric scintillation when the signal power can be degraded. Higher chipping rate allows better ranging accuracy as it has a direct influence on the accuracy with which the position can be determined: whereas a rate of 1.023MHz corresponds to about 300m, a chipping rate ten times greater (10.23MHz) corresponds to about 30m.

Possible drawbacks for higher chipping rates can be the need for wider front end bandwidth in a receiver and for greater power consumption to track the *faster* code. Thermal noise within the receiver is also expected to be greater in the case of higher chipping rates (Humphreys et al. 2008a) which can additionally stress the loops if effects like scintillation already enhance thermal noise in the loops. In the case of the new GPS L2C signal, which has a chipping rate same as the L1C/A signal, robustness against ionospheric perturbations are expected to be similar to that of L1C/A.

- Longer codes:

Choice of pseudorandom noise (PRN) codes is crucial for the system performance of GNSS. Code length is important for auto- and cross-

correlation and the cold start signal acquisition time (Hein et al. 2002) both of which can be especially important for tracking through ionospheric effects on signal propagation. There is a trade off between how long the PRN code can/should be and the system performance: it should be long enough to provide protection against interference and at the same time short enough to provide quick (re)acquisition of the signal. For instance, a loss of lock during scintillation would degrade the navigation solution if the lock is not re-acquired shortly after.

Longer PRN codes make the sidelobes (secondary peaks around the main lobe of the signal shown in Fig. 2.2.) in the autocorrelation and cross correlation functions have lower peaks. This means that when the signal is faint, tracking can still happen since the sidelobes will be relatively much smaller than the main peak of the correlation function. Greater capability to track even weaker signals makes it possible to have a lower threshold for data demodulation: it becomes feasible to demodulate the navigation message while barely tracking the signal which can occur due to scintillation - in other words, longer codes *can* enhance tracking robustness during scintillation.

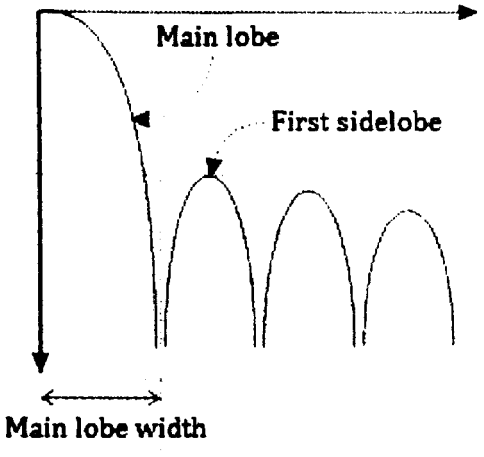

Figure 2.2. Three sidelobes (the first one marked) shown next to the main lobe (MikroElektronica 1998).

GPS L1C/A signal has not-so-good *cross correlation* properties, i.e. distinguishing a GPS L1C/A signal tracked with one satellite from another satellite can be difficult. The new signals, such as GPS L2C and L5, have longer codes that can help overcome this difficulty by improving the 21dB cross correlation performance of GPS L1C/A to 45dB – in the case of the

L2C signal (Parkins 2009). The L2C signal already has less received power (2.3dB) and its frequency causes about 65% more refraction in the ionosphere; therefore, use of a longer code instead of the C/A code seems a reasonable choice.

Another advantage of long codes is that they can decrease the possibility of a false lock through providing lower peaks in sidelobes (Fig. 2.3.). Shape of the correlation curve is important for the signal tracking performance: whereas the main lobe's peak is the correct point for acquisition of the signal, side lobes (especially when not significantly distinguished from the peak of the main lobe) can cause false lock during signal acquisition.

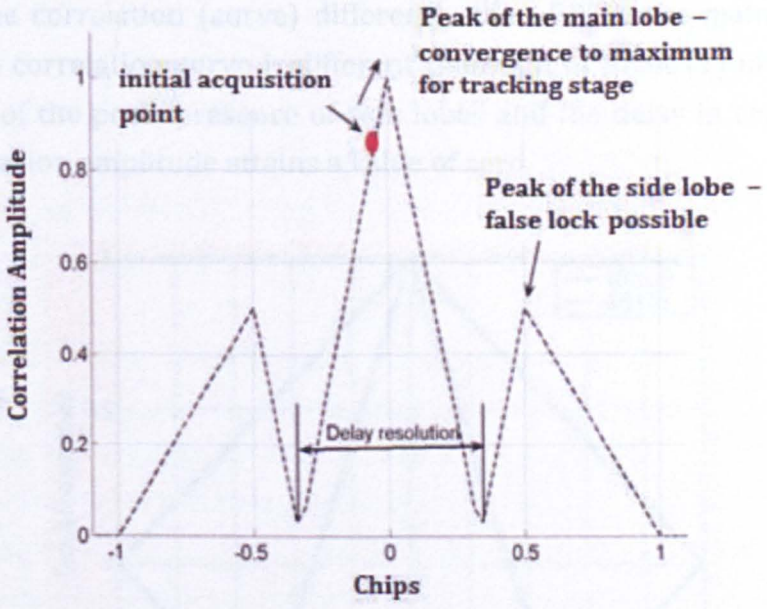

Figure 2.3. Shape of the correlation curve, which depends on the modulation technique as well as the PRN code length (Lohan 2011).

Although longer codes can bring better correlation properties, a disadvantage can be related with longer signal acquisition time. For practical purposes acquisition of long codes may require prior knowledge of time to enhance the signal acquisition time. Another drawback of longer codes is greater computational burden on receiver processing.

- <u>New modulation techniques:</u>

The need for new modulation techniques can be associated with the populated spectrum on the L band (Fig. 2.1.), which raises concern on issues such as interference. Modulation techniques are important for acquisition and tracking capabilities of a GNSS receiver.

One new modulation technique in GNSS modernization is the Binary Offset Carrier, BOC, which can provide efficient spectral sharing of the L band spectrum by multiple civilian and military users (Burian et al. 2007). Spectral efficiency between BOC and shift-keying modulation (bi-phase shift key, BPSK) is achieved by locating the signal energy away from the centre of the band. BOC can minimize interference with BPSK signals and provide better code tracking as well as resistance to multipath and narrowband interference (Burian et al. 2007). In this sense, comparison of the Galileo OS signal, which has BOC modulation and a longer PRN code, with GPS L1 signal, which has BPSK modulation, can help to note the advantage of BOC modulation. As can be seen in Fig. 2.4, BOC modulation shapes the correlation (curve) differently than BPSK: the main peak of BOC (1,1) correlation curve is different than that of BPSK (1) in terms of its width of the peak, presence of side lobes and the delay in chips when the correlation amplitude attains a value of zero.

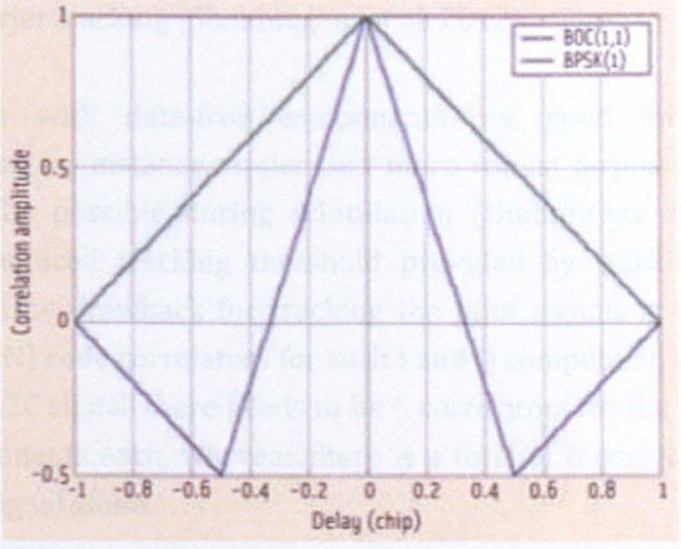

Figure 2.4. Correlation curves compared for BOC (1,1) and BPSK (1) signals – the former is deployed in Galileo OS signals and the latter in GPS L1C/A (Borio & Lo Presti 2007).

A smaller step (mostly in decimal chips) for shifting the code in the acquisition process is required for the BOC modulation in order to achieve such a narrower main lobe peak; this increases the computational burden in signal acquisition. However, it can be noted in Fig. 2.4. that it is easier to distinguish the correlation peak of the BOC modulation than that of BPSK.

- Data-free signal components (*pilot* signal):

Data-free signal components indicate when the PRN code is not modulated with the navigation data; they are also referred to as the "pilot" signal.

Most of the modernized signals, such as GPS L5, L1C and Galileo signals, are broadcast as In-phase (I) and Quadra-phase (Q) signal components. The two parts can have the same (as in GPS L5 where the I and Q components each have half of the total signal transmission power) or a different (as in GPS L1C) share of the total transmission power. Moreover, they can have the same (GPS L1C) or different length PRN codes modulating them.

The new GPS L2C signal is expected to have greater performance by having no navigation data modulated on its CL code (one of its PRN codes): this enables "full-wavelength" carrier phase measurements, which can help to resolve the carrier phase ambiguity more easily. For instance, while tracking the GPS L2C signal, its pilot component can be used for coherent carrier tracking (Shanmugam et al. 2012).

New signals with data-free components are good for low C/N_0 environments, for instance, easier and more robust acquisition of weak signals can be possible during scintillation (Humphreys et al. 2008a) through a reduced tracking threshold provided by tracking the pilot component. One drawback for tracking the pilot signals is the need for separate (PRN) code correlators for each I and Q component. For instance, for the GPS L2C signal, there needs to be 6 correlators for the I component and Q components each, whereas there is a total of 6 correlators for the GPS L1C/A signal alone.

- Higher signal power:

More signal power can improve every aspect of GNSS; it can improve operation under foliage and interference (Gruber 2012) and it can make the signal less vulnerable to ionospheric diffractive effects where received signal power may suffer fades. GPS L5 signal has the highest transmission power among the modernized signals: its received power is at least 3.7 dB higher than that of L1 C/A, and is 5.1 dB higher in received power than the L2C signal (Lohan 2011). Moreover, L5 signal transmission power is planned to be higher by another 0.9 dB on future Block III GPS satellites –

the L2C signal power will also be 1.5 dB stronger on those satellites (IS-GPS-705A 2010; IS-GPS-200F 2011; Shanmugam et al. 2012). Stronger signals are expected to contribute to the acquisition and tracking performance of GNSS receivers, which can be important when the signals are subject to degradations due to the ionosphere.

N.B. GPS L2C signal has 2.3dB less power than GPS L1C/A - however its modulation attempts to compensate for this deficit.

- Forward Error Correction (FEC):

FEC introduces "redundancy" into the navigation data to enable correction of possible decoding errors (such as bit decision error) that may occur during demodulation of the navigation message. FEC is expected to improve acquisition and tracking capabilities (Tran & Hegarty 2004); especially in challenged environments such as indoor mobile positioning. The benefit of FEC to counter the ionospheric effects can occur when navigation data demodulation is likely to be affected, such as during deep signal fading.

- Number of visible satellites:

An increased number of satellites gives the advantage of measuring/monitoring the ionospheric effects through more pierce points in the ionosphere – for the purpose of modelling the ionosphere, more sample points can provide better statistics. Moreover, they can also contribute to monitoring of the ionospheric conditions which can provide more accurate corrections made available to users, for instance, in Real-Time Kinematic (RTK) positioning. More satellites *can* provide better relative receiver-satellite geometry[c] and contribute to the *"time to first fix"*, which is the time required by a GNSS receiver from signal acquisition to a position solution.

[c] *The effect of geometry between the receiver and satellites on the position error is known as "dilution of precision". Larger the volume of the tetrahedron formed between the receiver and four satellites, better the relative geometry; and the size of the tetrahedron body remains maximal if one satellite is in zenith and all others are evenly distributed in azimuth (Dawoud 2010). When the satellites are near to each other in orbits, the geometry is relatively "weak" and the associated DOP value (ratio of the*

positioning accuracy to the measurement accuracy), which is not an actual prediction of the measurement error, is high. A relatively "strong" geometry, on the other hand, i.e. well distributed satellites in elevation and azimuth, means a good angular separation and gives a low DOP value.

With more number of satellites, it is possible for a receiver to maintain good receiver-satellite geometry for a longer period of time while the satellites move across the sky. Selection of satellites to achieve an acceptably low DOP can be practically more possible with more number of satellites in view.

When a certain region of the ionosphere challenges a signal through inhomogeneities or electron density gradients, a satellite at a different azimuth and elevation in the sky can compensate a possible LoL and help keep the number of satellites optimum for a positioning solution meeting the accuracy/precision of interest. If neglecting the measurements with certain signals is foreseen then as redundancy is important to perform a positioning solution, the number of visible satellites can be crucial to maintain redundancy.

As for modelling the ionospheric effects, an increase in the number of satellites can help to eliminate the low elevation satellites while estimating TEC, which can contribute to the accuracy of TEC estimation without sacrificing redundancy.

- <u>More GNSS constellations:</u>

Whereas the total number of satellites a GPS-only receiver tracks can change around an average of 9 over a day, this number can shift to an average of 18 in a GPS and GLONASS capable receiver (Shanmugam et al. 2012). A receiver with enough channels to track more satellites can have a greater number of visible satellites. Assuming the possibility of cross-combination of measurements between different constellations, there is an obvious advantage to redundancy in the number of visible satellites which can benefit convergence time[d] for a position solution, or provide

[d] *The quality of a positioning solution is optimal when the carrier phase ambiguities converge/are resolved (Elsobeiey & El-Rabbany 2011).*

better sampling of the ionosphere through more signals. There may, however, be differences in the quality of the measurements between different constellations which can influence the accuracy of the position solution; however, this may still be better than a lack of redundancy or non-availability of a position solution.

2.1. MODERNIZATION IN GPS

The Global Positioning System, GPS, is a space-based global navigation satellite system development started by the U.S. Air Force in 1978 and became fully operational in 1995 (El-Rabbany 2002), and is owned by the U.S. government which has the policy to meet growing demands by improving the performance of GPS services, and to remain competitive with international satellite navigation systems (GPS Governance 2012a).

Modernization in GPS is a long-term, multibillion-dollar commitment to upgrade the GPS space and control segments with new features including new civilian and military signals to improve GPS performance (GPS Governance 2012b). It can be said that modernization in GPS started in May 2000 with the disabling of the SA feature. Overnight this led to an improvement in accuracy from a hundred meters down to ten meters for civil users (GPS Governance 2012b). New signals introduced by GPS Modernization for civilian use – although of limited use until broadcast at constellation level, are L2C, L5, and L1C. With the legacy civil signal L1 C/A a total of four civil GPS signals will be available for the future GPS users (GPS Governance 2013a).

- L2C (1227.6 MHz): The most important benefit of the L2C signal (available since 2005 with the launch of the first IIR-M satellite (Gruber 2012) is that the IF observable can be constructed in dual-frequency civil GPS receivers. Compared with current technique based on L2P(Y) signal, L2C can provide faster signal acquisition, enhanced reliability, and greater operating range. It broadcasts at a higher effective power than the legacy L1 C/A signal which makes L2C easier to be received under trees and even indoors. It is expected that L2C will be broadcast at full constellation by 2016.

- L5 (1176.45 MHz): L5 signal, available since 2010 with the launch of Block IIF satellites, is broadcast in a radio band reserved for aviation safety services. Future aircrafts will use L5 in combination with L1 C/A to improve accuracy against ionospheric errors and robustness through signal redundancy. L5 is transmitted at a higher power than current civil GPS signals, and has a wider bandwidth.

- L1C (1575.42 MHz): This signal (not investigated in this thesis) is designed for interoperability with Galileo, and other systems also adopt L1C as a future standard for international operability. Broadcast at a higher level, L1C will be backward compatible with the current L1 C/A signal. Its design aims to improve mobile signal reception in challenging environments. This signal is planned for launch in 2014 with Block IIIA satellites.

N.B. Modernization in the GPS civil signals is focused on here, there is also plan for an M code on L1 and L2 frequencies (Fontana et al. 2001).

When fully operational, the L2C and L5 signals of GPS modernization will obviate the need for codeless or semi-codeless techniques which are deployed today using L1C/A and L2P(Y) signals for achieving high accuracy through dual frequency capability.

N.B. As of April 2013, 10 GPS SVs broadcast at L2C and 3 GPS SVs at L5.

GPS modernization includes not only new signals but also new satellites and an improved Ground Segment where the new Operational Control Segment (OCX) is planned to replace the current GPS Operational Control System placed at Schriever Air Force Base (GPS Governance 2012a). The new generation of satellites, referred to as blocks, are (GPS Governance 2013b):

- Satellites in GPS Block IIR(M) are *m*odernized versions of IIR series satellites developed by Lockheed Martin and launched between 2005 and 2009. Important features of this block are L2C and two new military signals.
- Block IIF series satellites are a *f*ollow-on for IIR(M) block developed by Boeing and started to be launched in 2010. With inclusion of a third

civil signal L5 in IIF, higher accuracy, signal strength and quality is expected.

- Block III is the future block of GPS satellites under development by Lockheed Martin with a first launch expected in 2014. They are planned to provide more powerful signals, one of which is the new civil signal L1C for international interoperability.

2.2. MODERNIZATION IN GLONASS

The Government of the Russian Federation acknowledged GLONASS as a top priority in 2001 aiming to improve both the space and ground-based segments. In 2010, GLONASS reached full coverage in Russian territory and in 2011 full operational capability with the full orbital constellation of 24 satellites was restored in GLONASS (Davydov & Revnivykh 2012).

N.B. GLONASS may be perceived to perform worse than GPS due to factors such as the performances of the on-board atomic clocks, the number of satellites in the constellation and the ground segment monitoring and control being confined largely to the Russian territory.

Traditionally, GLONASS satellites transmit navigational radio signals on two frequency sub-bands (L1 ~ 1602 MHz and L2 ~ 1246 MHz), relying on the Frequency Division Multiple Access (FDMA) technique. However, aiming to provide better accuracy, multipath resistance and especially, greater interoperability with GPS and future GNSS Systems, new GLONASS-K satellites will transmit CDMA signals in addition to FDMA.

With launch of the first GLONASS-K satellite (Inside GNSS 2011), a new L3 CDMA signal (centred at 1207.14 MHz, in the region allocated to the Aeronautical Radio 1 Navigation Service (ARNS)) is already being transmitted and tracked by several receiver companies. By 2020 GLONASS is scheduled to have all satellites transmitting both the new CDMA and legacy FDMA signals (Inside GNSS 2011).

Satellite modernization of GLONASS started with the second generation of satellites, GLONASS-M and further flight tests for GLONASS-K satellites, which will transmit both legacy FDMA and CDMA signals (Oleynik &

Revnivykh 2011), are already undertaken in 2012 (Davydov & Revnivykh 2012).

Regarding the new signals in GLONASS, a *m*odernized block of GLONASS-KM that is for launch after 2015 (Langley 2010) may also transmit on the L5 frequency.

2.3. EMERGING GNSS SYSTEMS

2.3.1. GALILEO

Galileo is the first global satellite positioning, navigation and timing system which is designed and operated under civil control (Celestino 2012). It is financed and co-funded by the European Union (EU) and European Space Agency (ESA); and managed by the European Commission (EC) where ESA acts as design and procurement agent on behalf of the EC (Anon. 2012). Planned to consist of 30 satellites, Galileo will provide a highly accurate, guaranteed global positioning service under civilian control (European Commission 2013) that is interoperable with other GNSS at four levels of service (compared with two in GPS, civil and military): the open Service (OS), the Safety-of-Life (SoL) service, the Commercial Service (CS) and the Public Regulated Service (PRS) – (GNSS Solutions, 2006). The Galileo program has been structured (Fig. 2.5.) according to three main phases (European Commission 2012; European Commission 2011c):

1. In-Orbit Validation (IOV) phase which consists of qualifying the system through tests and the operation of two experimental satellites (launched in 2005 and 2008 with a purpose to characterize the Medium-Earth Orbit (MEO) environment (radiations, magnetic field etc) and to test in such environment the performance of critical payload technology (atomic clocks and radiation hardened digital technology)) and a reduced constellation of four operational satellites and their related ground infrastructure.

   The first 2 Galileo operational satellites were launched by ESA in October 2011 and are both operational since 2012 (European Commission 2011b). The next two Galileo satellites, completing the

IOV quartet, were launched in October 2012 and as of December 2012 were not yet operational (Anon. 2012).

2. Initial Operational Capability (IOC) phase which is planned to be the partial commissioning of the ground and space infrastructure from 2014-2015 and the provision of the Open Service, the Search And Rescue service and the Public Regulated Service.

   IOC phase includes the first batch of satellites (14 additional satellites, planned to be launched by the end of 2015, to the 4 satellites in IOV), the launch services, the needed mission and control ground infrastructure, the system support services and the corresponding operations (Europa Press Releases 2010).

3. Full Operational Capability (FOC) phase, planned to be achieved on 2019-2020, consists of the deployment of the full system of 30 satellites, control centres located in Europe and a network of sensor stations and uplink stations installed around the globe.

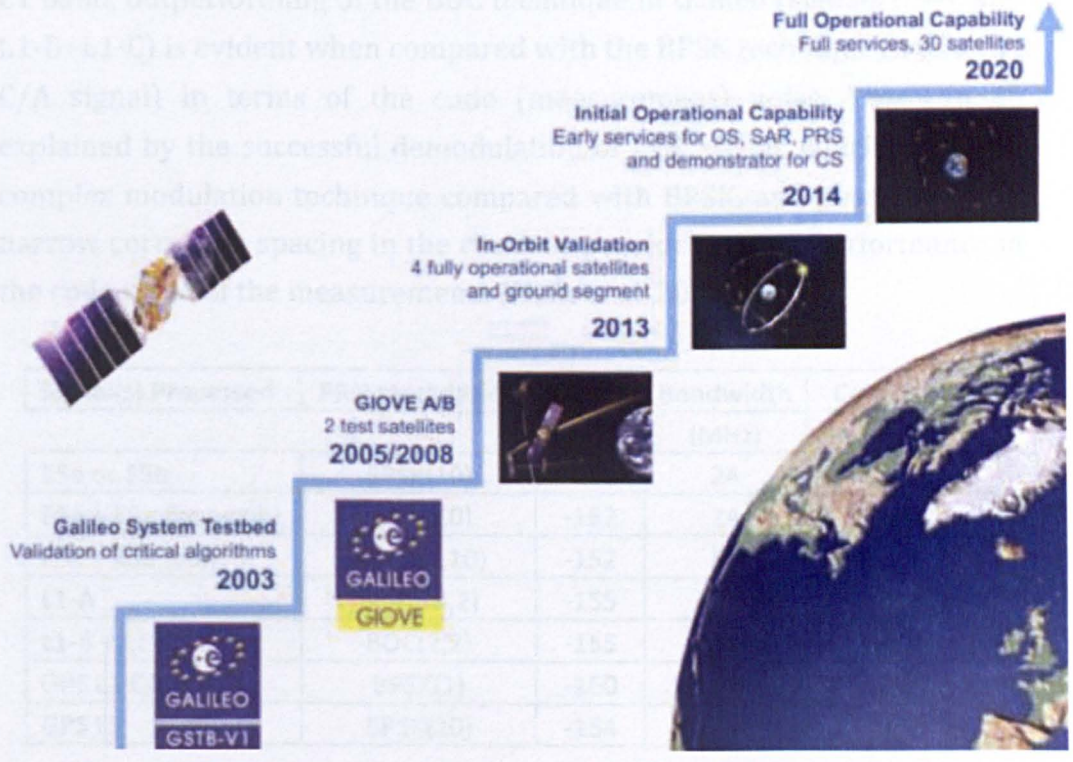

Figure 2.5. Timeline for the phases of Galileo (Celestino 2012).

Performance of the first 4 operational satellites has been good so far. The two Galileo In-Orbit Validation Element, GIOVE, -A and –B missions have ended and early services from Galileo (Open Service, Search and Rescue, Public Regulated Services) are planned in 2014. Full constellation is expected by 2020.

Galileo is to transmit in three frequency bands such that E5 signal gives users a choice of 3 signals (E5a/E5b/E5AltBOC) and open services will be through L1 (E1) and E5 because E6 will have encryption for authorized users. A detailed schematic of the signals transmission frequencies, modulation techniques and spectrum details regarding signals of other constellations can be found at Hein et al. (2002).

Galileo provides 10 navigation signals on four frequency bands, E5a/b, E6 and E1 (Hein et al. 2002). Compared with GPS signals, one important difference of Galileo signals is the BOC modulation technique (Betz 1999; Pany et al. 2002; Ries et al. 2002) as well as a large bandwidth need for most of its signals. One immediate consequence is the code measurement error due to *thermal noise.* Table 2.1. compares the code accuracy due to thermal noise for Galileo and GPS signals with different modulation techniques on different GPS and Galileo signals (Hein et al. 2002). For the L1 band, outperforming of the BOC technique in Galileo (signals L1-A, and L1-B+L1-C) is evident when compared with the BPSK technique in GPS (L1 C/A signal) in terms of the code (measurement) noise. This can be explained by the successful demodulation of BOC signal, which is a more complex modulation technique compared with BPSK, and possible use of narrow correlator spacing in the receiver provides a good performance in the code noise of the measurements (Hein et al. 2002).

Signal(s) Processed	PRN modulation	Power	Bandwidth	Code Noise
		(dBW)	(MHz)	(cm)
E5a or E5b	BPSK(10)	-155	24	4.6
E5a + E5b (non-coh)	BPSK(10)	-152	24	3.2
E5a + E5b (coh [e])	BOC(15,10)	-152	51	0.8
L1-A	BOC(14,2)	-155	32	1.2
L1-B + L1-C	BOC(2,2)	-155	24	5.5
GPS L1 C/A	BPSK(1)	-160	24	23.9
GPS L5	BPSK(10)	-154	24	4.1

Table 2.1. Comparison of the code accuracy due to thermal noise for Galileo (E5a, E5b, L1-A, L1-B, L1-C) and GPS (L1 C/A, L5) signals for different modulation techniques on different signals (Hein et al. 2002).

[e] *Coherent tracking of E5a and E5b provides high code tracking accuracy; however, this requires the need of a wide front-end filter, such as 51Hz.*

Whereas the tracking of GPS L5 signal can provide less code noise than tracking of either of E5a or E5b for the same receiver front-end bandwidth (former 4.1 cm, latter 4.6 cm in Table 2.1.), combined tracking of E5a and E5b can bring significant advantage (0.8 cm compared with the other values in Table 2.1.) to the coded tracking if a large bandwidth can be allocated to the reception of this signal.

Another comparison is shown in Table 2.2. in terms of the noise STD of code and phase measurement noise for GPS L1 C/A and Galileo E5a/b signals (Simsky & Sleewagen 2005; Simsky et al. 2008).

	Noise STD	
Signal	**Code**	**Phase**
	(m)	(m)
GPS L1 C/A	0.18	0.0019
Gal E5a	0.11	0.0025
Gal E5b	0.11	0.0024

Table 2.2. Noise STD of code and phase measurements for GPS L1C/A and Galileo E5a/b signals.

2.3.2. BEIDOU

The Compass Navigation Satellite System (CNSS), also named BeiDou-2 after the regional BeiDou system which is being expanded into a global system, is China's second-generation satellite navigation system that will be capable of providing positioning, navigation, and timing services to users on a continuous worldwide basis and it is expected to reach the FOC by 2020 when it would provide global navigation services, similar to the GPS, GLONASS or Galileo systems.

Beidou is planned to be developed and deployed in three phases (Shen 2009):

Phase 1 (2003 onwards) consists of the regional navigation system, BeiDou-1, providing active navigation service.

Phase 2 (2012 onwards) aims to deploy a system with passive positioning and timing capability over a regional area.

Phase 3 (2020 onwards) refers to the planned FOC with a constellation of 27 medium Earth orbit (MEO) satellites, 5 geostationary

Earth orbit (GEO) satellites and 5 inclined geosynchronous orbit (IGSO) satellites (Shen 2009; Anon. 2012).

By December 2011, the BeiDou system went into operation on a trial basis providing initial passive positioning navigation and timing services for the whole Asia-Pacific region with a constellation of 10 satellites (5 GEO satellites and 5 IGSO satellites) (Dingding 2011) and the Initial Operational Service was declared officially available. During 2012, more launches placed in orbit two additional GEO and four MEO satellites to expand the service area to Asian-Pacific users and improve positioning accuracy to better than 10m (EU METSAT 2008; China Satellite Navigation Office 2011).

2.3.3. QZSS

The Quasi-Zenith Satellite System (QZSS) authorized by the Japanese government in 2002 is a proposed three-satellite regional time transfer system and enhancement for the GPS that would be receivable within Japan. QZSS is not intended to provide standalone positioning capability but rather improve the performance of GPS in Japan (Hegarty & Chatre 2008). The QZSS service area covers East Asia and Oceania region and its platform is multi-constellation GNSS. It is not required to work in a stand-alone mode, but together with data from other GNSS satellites (IS-QZSS 2011).

QZSS space segment consists of three satellites in elliptical orbits at geosynchronous altitude in three orbital planes with the same ground track (IS-QZSS 2011). The first satellite was launched in 2010 and full operational status is expected by 2013. The ground track forms a figure-eight pattern (Fig. 2.6.) with the northern portion of the ground track covering a much smaller geographical area than the southern portion due to the eccentricity of the orbit. The design aims that at least one satellite out of three exists near zenith over Japan and given its orbit, each satellite appears almost overhead most of the time therefore the term "quasi-zenith".

The QZSS satellites will broadcast six CDMA navigation signals on four carrier frequencies: 1575.42 MHz (common with GPS L1 and Galileo E1),

1278.75 MHz (common with Galileo E6), 1227.6 MHz (common with GPS L2), and 1176.45 MHz (common with GPS L5) (Hegarty & Chatre 2008).

The ground segment is composed of a master control station responsible for navigation message generation, tracking control stations, laser ranging stations and monitoring stations. The network of monitoring stations covers East Asia and Oceania region, with stations in Japan and abroad (IS-QZSS 2011).

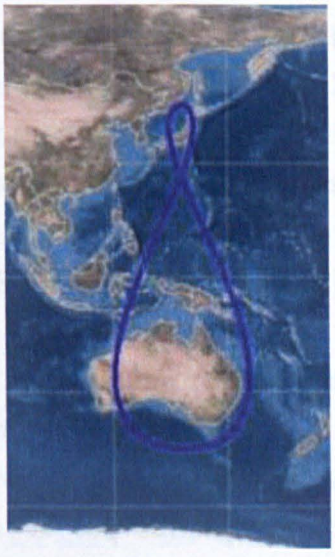

Figure 2.6. Ground track for QZSS' highly elliptical orbit (IS-QZSS 2011).

There are 6 signals planned for the QZSS system (IS-QZSS 2011). Among these L1 C/A, L1C, L2C and L5 interoperable signals are used by combining with GNSS. There is an L1 band sub-meter class augmentation signal that is interoperable with GPS-SBAS and another experimental signal on the L2 band that provides high precision (3 cm level) service compatible with Galileo E6 signal.

2.3.4. IRNSS

The Indian Regional Navigational Satellite System (IRNSS) is a *regional* satellite navigation system owned by the Indian government and developed by Indian Space Research Organization (ISRO). IRNSS is aimed as an independent and autonomous regional navigation system consisting of seven satellites covering India. Plan for the first launch in 2012-2013 and the rest with six months periodic launches means that the IRNSS

system should be functional by 2015 (Anandan 2010). Space segment aims to minimize maximum DOP with minimum number of satellites.

As all GNSS systems, IRNSS consists of ground, user and space segments aiming at three kinds of services: Standard Positioning Service with signals at 1191.795 MHz and 2491.005 MHz, Precise Positioning Service at the same frequencies with a higher (10 times as greater) chipping rate, and Restricted Services.

Ionospheric studies including scintillation in the L band are planned to be carried out as part of the initial phase of the GAGAN system (Coordinates 2011).The ionospheric corrections are planned for a grid of 80 points to assist single frequency users in India (Coordinates 2008).

2.4. AUGMENTATION SYSTEMS AND MODERNIZATION

Augmentation in GNSS aims to improve the accuracy, reliability and availability of the system through integration of external information (such as differential corrections, integrity parameters, information about the error sources such as the satellite orbits, clock drifts and the ionospheric delay) into the calculation processes (Hegarty & Chatre 2008). Augmentation systems can be satellite-based, ground-based or aircraft-based (Hegarty & Chatre 2008); in this section the satellite based augmentation systems (SBAS) are focused on within the scope of ionospheric effects and GNSS modernization. The Wide-Area Augmentation System (WAAS) in the United States, the European Geostationary Navigation Overlay Service (EGNOS) in Europe, the GPS and GEO Augmented Navigation (GAGAN) system in India and the Multifunctional Transport Satellite Based Augmentation System (MSAS) in Japan are examples to current SBAS (Hegarty & Chatre 2008).

SBAS might be in particular useful and necessary for helping users to correct the ionosphere induced error in GNSS especially in certain global regions. SBAS service in the low and high latitudes can be especially important given the variability of the ionosphere in these regions. For instance, ionospheric conditions of the equatorial latitudes produce large spatial gradients and temporal gradients in the ionospheric delay. The equatorial anomaly effects (near-midnight TEC enhancements, TEC

depletions and scintillation observed in the region about 20^0 to the north and south of the magnetic equator (ICTP 2013)) may not be well represented by the 5^0x5^0 grid thin shell model of the current SBAS standards. Similarly, plasma bubbles associated well with the ionospheric conditions of the equatorial region can cause large gradients over short periods of time. Another important threat to GNSS is ionospheric scintillation which may cause tracking and noise problems that may challenge user equipments.

It is important to note that all these error sources can equally affect the SBAS links (between the ground segment and the SBAS satellites as well as between the user segment and the SBAS satellites). Therefore two points emerge regarding the relation between the SBAS and the ionosphere:

(i) Augmentation can be crucial for users at regions largely affected by the ionosphere – this emphasizes the need for continuous and reliable SBAS service;

(ii) The augmentation system itself should be robust to maintain its service despite the degrading effects of the ionosphere.

Not taking into account the physical conditions of the ionosphere or not alerting users about them can make it difficult for users to achieve the expected performance levels with SBAS. With the above raised points, this section continues with the details of and the modernization works in WAAS, EGNOS and GAGAN.

2.4.1. WAAS

The Satellite Based Augmentation System of US government is the Wide Area Augmentation System (WAAS) started in 1992 and declared operational in 2003 (GPSLAB 2004) and run by Federal Aviation Agency (FAA) (FAA 2009) especially for the civil aviation community (FAA 2010b). WAAS is a system in continuous development planning to improve its capabilities in parallel with the evolution of the SBAS standards towards a dual-frequency augmentation service (FAA 2008). Its service area includes Continental US, Alaska, Canada and Mexico (FAA 2010a) and supports thousands of aircraft instrument approaches at airports in USA and Canada (FAA 2013).

Recent development in WAAS services include two second-generation GEOs broadcasting at the GPS L1 and L5 carrier frequencies (although presently the L5 signal is only for use by the WAAS ground network) (Hegarty & Chatre 2008). The dual frequency (L1, L5) operational capability in WAAS, expected during 2014-2028 (Clore 2011), can be interesting regarding the ionospheric effects: the L5 signal is affected by the ionosphere (i.e. refracted and diffracted) more than the L1 signal due to its lower signal frequency; however the L5 signal's greater transmission power and modulation technique can compensate for this. It is also possible that tracking of the data-free signal component of L5 signal can maintain lock on the carrier phase.

2.4.2. EGNOS

EGNOS is an open service operational since October 2009 and with its own data access service declared in July 2012. It Safety-of-Life service is operational since March 2011 and within Europe about a hundred approach procedures that rely on EGNOS for aircraft landing have been approved (Celestino 2012). The EC intends to ensure the future of EGNOS services for GPS L1 legacy users until at least 2030 (European Commission 2011a).

Major EGNOS system evolutions towards a multi frequency and multi constellation configuration are currently being assessed with the objective of having them operational by 2020 (European Commission 2011a). A technical assessment of the potential EGNOS evolution, EGNOS V3, is currently (2013) being undertaken by the ESA within the European GNSS Evolution Programme. The EC defines the evolution of the EGNOS mission in steps (current EGNOS with annual updates, EGNOS-V2 envisaged in 2006 and EGNOS-V3 with an implementation phase beyond 2013 (Rodriguez et al. 2009):

(i) En-route service based on augmentation of GPS L1 with Safety-of-Life service being offered by EGNOS from early 2011 onwards on a regional basis until 2030,

(ii) EGNOS-V3, planned to include the fulfilment of SBAS L1/L5, aiming to expand the augmentation service to dual frequency and improve towards a multi-constellation concept.

The EC and ESA actively take role in different international co-operations for SBAS standardisation and interoperability ensuring co-ordination of the EGNOS evolution with the other SBAS. Concerning the provision of additional services such as maritime, high precision, land-users, objective is to ensure that EGNOS has sufficient built-in expandability and upgrade the capability to allow the provision of new products (European Commission 2011a).

2.4.3. GAGAN

The GPS Aided Geo Augmented Navigation, GAGAN, is the SBAS implementation by the Indian government for which the Airports Authority of India and ISRO have an agreement for establishment (Bhaskaranarayana 2008). In 2009, Raytheon was awarded the contract to build the complete GAGAN system (Inside GNSS 2009b).

Like other systems, GAGAN also has phases for development and deployment: Technology Demonstration System (completed in 2007), Initial Experimental Phase (completed in 2007) and the Final Operational Phase. As of 2012, two satellites with GAGAN SBAS payload were in orbit (Inside GNSS 2012) broadcasting SBAS navigation data using L1 and L5 signals, with GPS type modulation (ISRO 2012).

In principle, implementation of an SBAS in India is anticipated to be motivated by the highly variable ionosphere in this region. India's location in the low latitudes brings in concerns related with the equatorial anomaly associated with strong enhancements in TEC during post-sunset to midnight hours, depletions in TEC leading to what is known as "plasma bubbles" and scintillation events. The highly variable ionosphere in these low latitudes makes GAGAN service not a trivial one (Doherty et al. 2001; Wu et al. 2001; Lejeune et al. 2002)

Table 2.3. (up-to-date as of December 2012) gives information about each SBAS with the PRN numbers of their satellites, complementary to the Sections 2.4.1-2.4.3.

SBAS	Signals	PRN #	
WAAS	L1/L5	133, 135, 138	Enroute precision and non-precision approach
EGNOS	L1, L1/L5	120, 124, 126, 136	SoL service available
GAGAN	L1/L5	127, 128	Signals in test mode
QZSS	L1	183	Signal in test mode

Table 2.3. The number of satellites for each SBAS with their designated PRN numbers (IGS 2013).

2.5. BENEFITS OF GNSS MODERNIZATION FOR THE IONOSPHERIC EFFECTS

The new GNSS signals can contribute to the correction techniques for the ionospheric effects, through elimination and estimation.

- In terms of eliminating the ionospheric effects, within the dual frequency approach it is possible to make use of the new civil signals such as GPS L2C and L5 to linearly combine with the L1C/A signal so that the disadvantageous (due to dependence of L2P(Y) on acquisition of L1C/A signal) semicodeless tracking of L2P(Y) can be avoided. For the same elimination purpose, a triple frequency approach can enable a second order approximation to the total ionospheric error (as opposed to the first order approximation) and eliminate the Iono2 error term (along with the Iono1 term which is the only term eliminated in the first order approximation) by linearly combining the observations on three signal frequencies (instead of on two signal frequencies in the first order approximation).

- In terms of estimating the ionospheric effects, new GNSS signals can improve the accuracy of estimating TEC based on a dual-frequency approach, such as through higher accuracy range measurements. This can be achieved through, for instance, using GPS L5 or L2C signals instead of L2P(Y) with GPS L1C/A signal (explained in Appendix B). In addition to

this, it is also possible to reconstruct TEC in a triple frequency approach, as shown by Spits & Warnant (2011), who claim to improve the accuracy of TEC values using undifferenced code and phase measurements on L1, L2 and L5 signals, first by performing the ambiguity resolution and then by estimating the TEC based on only the phase measurements.

Higher chipping rates, greater signal transmission power and novel modulation techniques applied in GNSS can improve signal tracking, and this can be advantageous during adverse ionospheric conditions that can impair the received signal power and cause rapid fluctuations in the signal phase. Improved tracking robustness can provide quick reacquisition of a signal after a LoL. Faster signal acquisition, as possible with a reduced acquisition threshold (i.e. signal can be acquired even at a lower signal-to-noise ratio), can be crucial for meeting the required levels of system performance during ionospheric scintillation. This can provide less "time to first fix" even in the absence of a priori receiver state or almanac information.

It can be understood that a significant part of the research and development in SBAS focus on defining and mitigating ionospheric challenges. SBAS system development in the low latitude regions, such as South America and India, will have to contend with much more extreme ionospheric conditions, which include strong spatial and temporal gradients, plasma depletions and scintillation. Such conditions can limit SBAS performance in these regions. As SBAS is planning to switch to a dual-frequency operation, the physics of low latitude ionosphere need to be addressed and understood, for instance, the level of impact the ionospheric disturbances induce on the system during severe solar and/or geomagnetic activity and prediction methods for the spatial and temporal variability of the ionosphere at these latitudes.

It was also brought into attention that GNSS modernization includes new signals at the L2 and L5 bands at lower frequencies than the L1 band, which are expected to be more influenced by the ionospheric diffraction (scintillation in particular) and refraction (delay/advance effect). For instance the new GPS L5 signal at 1176.45MHz is more likely to be affected in intensity and phase due to scintillation compared with GPS L1C/A; however, GPS L5's design parameters (such as transmission power and

chipping rate) aim for better performance than L1C/A. Refractive effects like ranging errors are greater at lower signal frequencies. For instance, regarding the ray bending error, high signal frequency can prevent significant bending of the wave. Ray bending error for the dual frequency L1, L2 IF observable may exceed 3mm at the equatorial latitudes (Petrie et al. 2010). With the new lower frequency signals introduced in GNSS modernization, an elevation cutoff angle (about 7^0-10^0) can help to eliminate the error due to signal bending.

It can be briefly remarked that:

- A useful common feature of GNSS modernization for the ionospheric effects is the availability of at least two frequencies for the civil users, which can help correct for the frequency dependent ionospheric error in measurements. Availability of three signal frequencies is aimed at in most constellations which can help to correct the ionospheric error even further, for instance, allowing to take into account the second order ionospheric error term. Three distinct frequencies also provide redundancy in a dual-frequency approach to the ionospheric error.
- Whereas an increase in the number of satellites can contribute to a better sampling of the ionosphere, it can also provide a good relative geometry between the receiver and satellites. Cross-combination of (observations with) satellites between different constellations can also contribute to redundancy, which may be affected during adverse ionospheric conditions, such as scintillation.
- The new modulation techniques, such as BOC, are important to enhance tracking performance in poor conditions induced by the ionosphere, such as during scintillation, which can challenge the acquisition and tracking of a signal through rapid fluctuations in the signal intensity and phase. In this sense, the modulation technique can help the reacquisition of a lost signal lock during scintillation, or provide more robust tracking even when the signal power is affected by fading. Similarly, higher chipping rates can also benefit signal tracking during adverse ionospheric conditions by allowing robustness against perturbations along signal propagation.

CHAPTER 3

3. IONOSPHERE AND IONOSPHERIC EFFECTS IN GNSS

High energy radiation (mostly in the form of UV and X-ray) and emissions from the surface of the Sun influence Earth's upper atmosphere causing heating in the region. The atmospheric layer of altitude between about 100-1000km is known as the *ionosphere*, where solar radiation strips off electrons from atoms leading to an ionized gaseous medium, known as *plasma*. In addition to electrons being stripped off, a *recombination* process (by which a free electron is captured by a positive ion) also takes place. Low "atomic" density due to low gravitational force at these aforementioned altitudes leads to a low rate of recombination *letting free ions and electrons dominate the ionosphere* (Ratcliffe 1956). The balance between ionization and recombination determines the level of ionization present at any time at a particular altitude in the ionosphere. The ionic structure makes the ionosphere a conductive medium which can support electric currents and magnetic field (Davies 1966).

Depending on how *deep* the solar radiation penetrates through the ionosphere, *layers* form with *different balances* of ionization. Moreover, ionization depends on the solar zenith angle and radiation intensity. Different balance levels at different altitudes give a *layered* structure (spherically stratified) to the ionosphere. There are three layers associated with the ionosphere: *D layer* extends up to about 90km; it is mostly due to photoionization under X-rays (mostly disappears at night) and has no measureable effect on GPS frequencies. E layer is at about 90-150km; it is a conductive layer with a high collisional frequency (its conductivity is known to reduce day-time scintillation) and has minimal effect in normal conditions. The most variable and irregular F layer causes most of the problems for radiowave propagation at GNSS frequencies. It has two sub-layers, F1, approximately between 150-210km, and F2, approximately between 210-600km. The F1 layer has a highly predictable density from known solar emissions and together with the E region can account for up to 10% of the ionospheric time delay in GNSS signals. The F2 layer has the highest variability and density causing most of the potential effects in GNSS. It contains a region of maximum electron density between about 250-400km. The altitude of the maximum electron density

can change under the influence of geomagnetic storms[a] and it may increase during evening hours (and decrease at dawn) such that at low geomagnetic latitudes it may reach about 450km altitude at local post-sunset hours (Doherty et al. 2001; Petrie et al. 2011; ICTP 2013). Figure 3.1. illustrates the layered structure of the ionosphere.

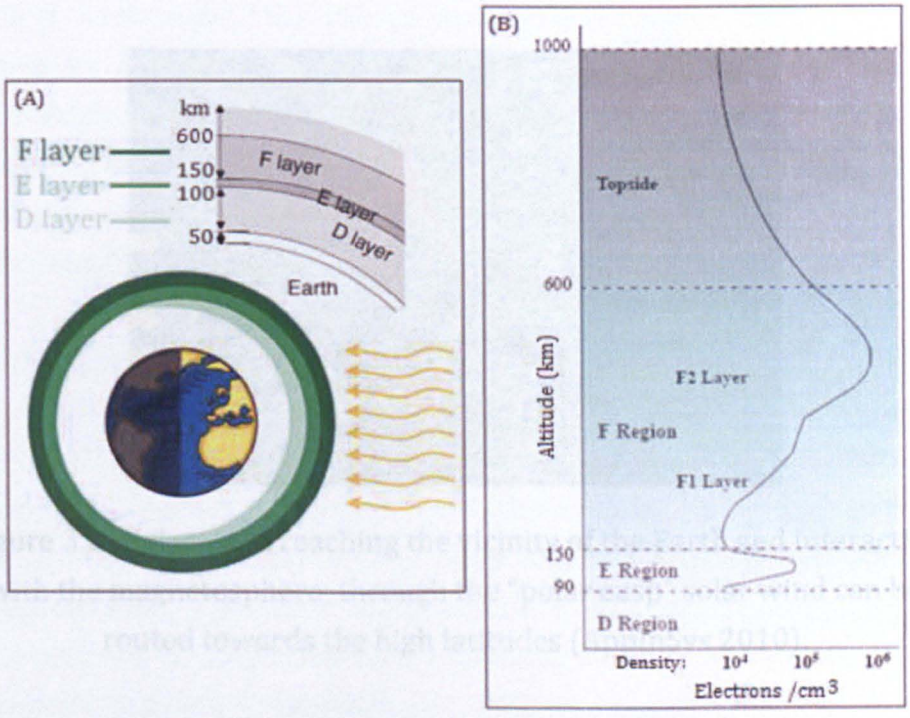

Figure 3.1. *(A)* Layered structure of the ionosphere (altitudes within the ionosphere) under the influence of solar radiation. *(B)* Changes in the electron density at different layers of the ionosphere with altitude in the ionosphere.

Along with radiation, there is also emission of matter from the sun, known as the "solar wind", in which solar particles convey a magnetic field that makes up the "interplanetary magnetic field" (IMF) (Davies 1990; AppInSys 2010). Solar wind is deflected by the geomagnetic field (Fig. 3.2.) thus it cannot penetrate into the atmosphere *in the first place,* however it can influence the geomagnetic field. For instance, bursts of energy at the surface of the Sun cause plasma and radiation emission that can influence the geomagnetic field. The interaction between solar activity, geomagnetic

[a] *Geomagnetic storms occur due to charged particles from solar flares (caused by solar activity) arriving to the vicinity of the earth and affecting the earth's magnetic (geomagnetic) field.*

field and ionospheric conditions can be easily understood when considering the orientation of the geomagnetic field lines at the high latitudes: particles arriving at the vicinity of the Earth can be routed towards lower altitudes of the ionosphere through the "polar cusp" at the high latitudes, where the geomagnetic field lines are almost vertical towards the Earth (AppInSys 2010).

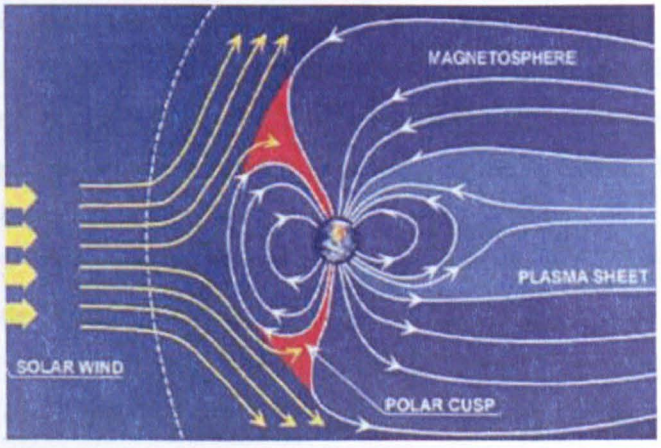

Figure 3.2. Solar wind reaching the vicinity of the Earth and interacting with the magnetosphere; through the "polar cusp" solar wind can be routed towards the high latitudes (AppInSys 2010).

GNSS signals penetrating the ionosphere (Fig. 3.2.) are modified due to (i) the ionospheric electron content, (ii) variations in the electron density and (iii) small scale electron density irregularities (Hunsucker 1991). A list of the ionospheric effects on GNSS signals can be summarized as:

- Delay/advance in signal propagation time caused by ionospheric refractivity,
- Dispersion which makes the ionospheric delay/advance depend on the signal frequency (Fig. 3.3.),
- Ray bending, which is a change in the apparent direction of arrival of the signal,
- Scintillation due to small scale electron density irregularities,
- Doppler shift[b],
- Change in the angle of arrival,
- Polarisation rotation.

[b] *Liu et al. (2004) show theoretically that the time rate of change in TEC is well correlated with Doppler shift in signals.*

TEC is a parameter related with the ionization in the ionosphere such that its value increases as the number of the sunspots increases and on a daily average the value of TEC varies mainly with the solar radiation i.e. it increases after sunrise, makes a peak around midday and decreases at sunset (Leick 1995). In addition to this diurnal variation, there is also a seasonal dependence in TEC such that during the equinoxes (spring and autumn) maximum TEC values in the ionosphere can be noticed throughout a year (Ratcliffe 1956). TEC and variations in TEC are important factors for the above listed effects. The last three of these effects are not focused on in this thesis, but the others, refractive and diffractive effects, are concentrated on in this research, as discussed in further detail in the remainder of this chapter.

The ionosphere can be characterized as:

a) Inhomogeneous due to spatial and temporal variability of ionospheric electron density. Electron density gradients within the ionosphere cause the ionospheric refractive index to vary along the signal propagation path. Considering the types of errors in GNSS – random (i.e. not predictable), systematic (i.e. predictable thus can be corrected) and gross (outliers or blunders such as human error), the inhomogeneous ionosphere can lead to deterministic (such as propagation delay affecting the range measurements which is a systematic error) and random errors (such as signal fluctuations leading to scintillation). The deterministic part of the inhomogeneous ionosphere (referred to as background ionosphere) can be characterised by TEC along the signal path giving rise to advance/delay on the range measurements. The random part of the ionosphere associated with electron density irregularities[c] and variations in TEC causes phase fluctuations on the penetrating signal and the received signal is observed to have rapid variations in phase and intensity, known as scintillation.

b) Anisotropic, i.e. ionospheric refractivity that depends on the propagation direction of the GNSS signals. An anisotropic medium contains right and left hand transverse modes of propagation where each has a distinct group and phase velocity such that these two modes

[c] *Appendix D provides further details about the electron density irregularities responsible for the scintillation effects on GNSS signals.*

propagate along different ray trajectories. Anisotropic effects at GNSS signal frequencies can be represented in terms of the refractive index "η" as a series in inverse powers of frequency (Eq. 1):

$$n_{\pm,p}^2 = 1 - \frac{2X(1-X)}{2(1-X)-Y_\perp^2 \pm \sqrt{Y_\perp^4+4(1-X)^2Y_{||}^2}} \qquad \text{(Eq. 1)}$$

In Eq. 1, "±" denotes two different modes rising from the double refraction of GNSS signals in the ionosphere ("+" for left-hand polarized signals, and "-" for right-hand polarized signals such as GNSS, thus adapted hereafter). Terms X, $Y_\perp$ and $Y_{||}$ as well as the derivation of Eq. 1 are explained in Appendix E.

An ionospheric refractive index different from unity makes different frequencies travel at different speeds (Davies 1966, 1990; Hunsucker 1991). Thus the propagation velocity of GNSS signals change, which causes delay in code measurements and advance in phase measurements (where the pair deviate from each other giving what is known as "code-carrier divergence"). Phase refractive index is less than unity (making the phase velocity *greater* than the speed of light); this causes phase advance and makes the carrier phase based range measurements less than the geometric (true) range. Group refractive index, on the other hand, is greater than unity (making the group velocity *less* than the speed of light); this causes the group delay which makes the pseudoranges longer than the true range. Such propagation delay can amount from 1 to 100m at GPS L1 frequency.

c) Layered structure, due to photochemical processes where solar energy gets absorbed by particles in the atmosphere (*photodissociation*: molecules separating into atoms, *photoionization*: an electron coming off from a molecule/atom under solar radiation), and plasma transportation (such as motion of charged particles in the ionosphere, plasma diffusion, electromagnetic drift) (Fig. 3.1.). In the absence of sunlight, photoionization does not take place thus D and F1 layers almost disappear at night while E and F2 remain due to recombination and transportation processes.

Ionospheric electron content is the main reason why the ionosphere affects GNSS signals; the other reason is the presence of the geomagnetic field that also interacts with the ionosphere. It can be said that the ionosphere is under the influence of *solar* and *geomagnetic activities* such that it can be enhanced by solar activity and influenced by changes/disturbances in the geomagnetic field (such as geomagnetic storms). How the ionosphere is exposed to the Sun affects the TEC. For instance, diurnal and seasonal variations in TEC are due to such exposure. Solar activity, which can be associated with the Sunspot Cycle[d], can cause large gradients in TEC (with or without causing disturbances in the geomagnetic field). Geomagnetic activity[e] also influences TEC; for instance, geomagnetic storms and storm induced conditions can enhance and cause variations in TEC.

In terms of a geographic distribution of the ionospheric effects on GNSS, three global regions can be considered based on the ionospheric electron content and its interaction with the geomagnetic field: equatorial region, mid-latitudes and high latitudes (including the auroral region and polar cap[f]). Figure 3.3 illustrates these three regions according to the Wide-Band Model, WBMOD, predictions of the S4 index (90^{th} percentile) considering DOY 91 (corresponding to an equinox month) for GPS L1 signal with high solar activity (Sunspot number 150) and low geomagnetic disturbances (K_p=0) for 23:00 local time at all longitudes. The two global regions where scintillation occurs predominantly can be seen in Fig. 3.4.: high latitudes between 60^0 to 90^0 N and S geographic latitudes, and the equatorial belt extending between 30^0 N and S geographic latitudes.

[d] *A solar minimum occurs when sunspot numbers are lowest, and a solar maximum when numerous sunspots are observed on average in a month; the latter can increase the intensity/occurrence rate of geomagnetic storms and radiation showers in the atmosphere, affecting the ionization levels of the ionosphere.*

[e] *Appendix F provides a brief description of the commonly used indices related with monitoring of the geomagnetic activity.*

[f] *Polar cap is considered as the region with geomagnetic latitude >75^0 (Pi et al. 2002).*

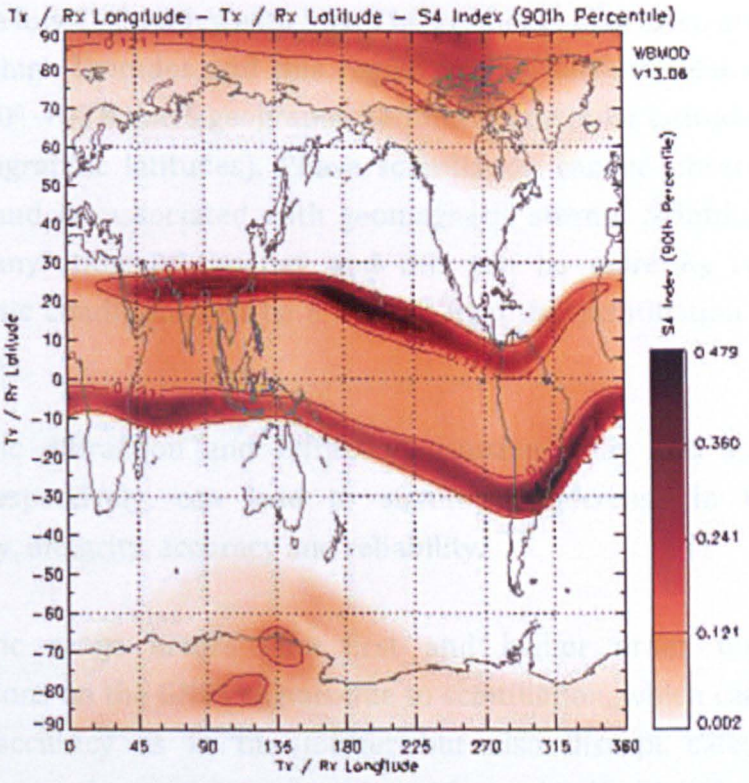

Figure 3.3. Three main global regions of distinguished ionospheric conditions (Bureau of Meteorology 2010).

1. The low latitude region between about ±20^0 N and S geomagnetic latitudes can be referred to as the *equatorial belt/region* where the ionospheric conditions are known to have high spatial and temporal variability. High TEC values as well as high TEC gradients can be observed in general in this region. Scintillation in both amplitude and phase is more likely to occur during the active phase of the Solar Cycle and more predictable to happen during certain hours of the day, for instance, during post-sunset into mid-night hours (Basu 1981; Aarons 1985).

2. The region with negligible S4 values observed in Fig. 3.3. refers to the mid-latitudes (30^0-60^0 N and S geographic latitude) where rather moderate TEC values may be observed and practically no severe scintillation events are expected – however, these conditions may change subject to the background solar and geomagnetic conditions. For instance, depending on the strength of geomagnetic disturbances, it is possible that the enhanced high latitude ionospheric conditions affect the mid-latitudes, which can happen especially around the peak periods of the Solar Cycle.

3. The region with the geographic latitude greater than 60^0 N and S in Fig. 3.3., where low TEC values with high TEC gradients may exist, are referred to as the high latitudes and this region can be further subdivided into auroral (60^0-70^0 N and S geographic latitudes) and polar latitudes (>70^0 N and S geographic latitudes). Phase scintillation can be observed more common and be associated with geomagnetic storms. Scintillation may happen "any" time of the day and this can be more K_p related i.e. geomagnetic conditions can be a driving force for scintillation events at this region.

Ionospheric diffraction and refraction, causing delay and scintillation effects, respectively, can lead to significant decrease in the GNSS availability, integrity, accuracy and reliability.

Ionospheric range errors (the first and higher order terms) and perturbations on the GNSS signals due to scintillation, which can not only degrade accuracy as in the former but also disrupt safety critical applications such as aviation, constitute the major limiting factor in the high precision demanding GNSS applications that (are relied on more heavily in the modern society), such as Precise Point Positioning and network RTK positioning.

3.1. REFRACTIVE EFFECTS OF THE IONOSPHERE

Range measurement between a receiver and satellite can be based on the code and carrier phase of the incoming signal, as represented by Eq. 2 and Eq. 3, respectively.

$$PR_{fi} = \rho + c(dt_r - dt^s) + I_{fi} + T + M_{PR,fi} + \varepsilon_{PR,fi} \quad \text{(Eq. 2)}$$

PR_{fi} is the pseudorange for the GPS signal frequency f_i where i=1,2,5 for L1, L2 and L5, respectively. In Eq. 2, ρ is the geometric (true) distance between the receiver and satellite at the times of reception and transmission, dt_r is the receiver clock offset, dt^s is the satellite clock offset, I_{fi} is the ionospheric error for f_i frequency, T is the tropospheric delay, $M_{PR,fi}$ is the multipath effect and $\varepsilon_{PR,fi}$ is the noise in the PR measurement for f_i frequency.

$$L_{fi} = \rho + c(dt_r - dt^s) - I_{fi} + T + M_{L,fi} + \varepsilon_{L,fi} + \lambda_{fi} \cdot N_\lambda \quad \text{(Eq. 3)}$$

L_{fi} is the carrier phase range measurement for GPS signal frequency f_i. In Eq. 3, ρ, dt_r, dt^s, I_{fi} and T are same as explained above for Eq.2. Moreover, $M_{L,fi}$ is the multipath effect, $\varepsilon_{L,fi}$ is the noise on the carrier phase range measurement for f_i frequency, $\lambda_{f1} \cdot N_\lambda$ is the ambiguity term where λ_{fi} is the wavelength of the signal at f_i frequency and N_λ is the ambiguity in the carrier phase measurement.

The refractive effect of the ionosphere giving rise to the total ranging error is derived and shown for code and phase measurements further below (f is taken for a generic frequency) (Bassiri & Hajj 1993):

$$\delta\rho_g = \frac{\kappa}{f^2}\int N ds + \frac{\kappa e \int N B_0 \cos\theta \, ds}{\pi m f^3} + \frac{3\kappa^2}{2f^4}\int N^2 ds \qquad \text{(Eq. 4)}$$

$\delta\rho_g$ is the *total* delay due to the ionosphere on the code (group) observation (in other words $+I_{fi}$ term in Eq.2). κ is a constant (40.3, no units). N is the electron density distribution along the signal path and the integral $\int N ds$ is taken along this path in increments of ds. e is the electron charge, m is the electron mass and B_0 is the magnitude of the geomagnetic field at the ionospheric pierce point (IPP) where the signal from the satellite pierces through the ionosphere (about 3.12 $*10^{-5}$ Tesla at the equator). θ is the angle between the signal wave vector and the geomagnetic field vector at the IPP.

Equation 5 follows from Eq. 4 by replacing the integral $\int N ds$ in the first and second terms on the right hand side (RHS) of Eq. 4 with *slant* TEC, *STEC*; by taking the $B_0 \cos\theta$ term out of the integral (assuming that this product is LoS independent) in the second term on the RHS and by approximating the integral $\int N^2 ds$ in the third term on the RHS based on the shape parameter η (Hartmann & Leitinger 1984).

$$\delta\rho_g = \frac{\kappa}{f^2} STEC + \frac{\kappa e B_0 \cos\theta}{\pi m f^3} STEC + \frac{3\kappa^2}{2f^4} \eta N_{max} STEC \qquad \text{(Eq. 5)}$$

The first, second and third terms on the RHS of Eq. 5 are the first (Iono1), second (Iono2) and third (Iono3) order ionospheric error terms, respectively. The shape parameter η in the Iono3 term is independent of satellite elevation and the maximum electron density

in the vertical electron density profile (N_{max}), where all integrals are assumed along LoS between the receiver ("rec") and satellite ("sat") (Hartmann & Leitinger 1984):

$$\eta = \frac{\int_{rec}^{sat} N^2 ds}{N_{max} \int_{rec}^{sat} N ds} \quad \text{(Eq. 6)}$$

Equation 5 can be written more compactly as:

$$\delta\rho_g = Ion1 + Ion2 + Ion3 \quad \text{(Eq. 7)}$$

Equation 8 represents the advance on the carrier phase range measurement due to the ionospheric effect ($-I_{fi}$ term in Eq. 3) (Bassiri & Hajj 1993).

$$\delta\rho_P = -\frac{\kappa}{f^2} STEC - \frac{\kappa e B_0 cos\theta}{2\pi m f^3} STEC - \frac{\kappa^2}{2f^4} \eta N_{max} STEC \quad \text{(Eq. 8)}$$

Common parameters of Eq. 5 and Eq. 8 are as defined for Eq. 5. Similar to Eq. 7, Eq. 8 can be written as:

$$\delta\rho_P = -Ion1 - \frac{Ion2}{2} - \frac{Ion3}{3} \quad \text{(Eq. 9)}$$

The total ionospheric error due to refraction depends on the background solar, ionospheric and magnetic conditions. At times of high background solar activity, such as during the peaks of the Solar Cycle or days of an ionospheric storm, increase in solar radiation leads to enhanced TEC. This can cause the slant ionospheric delay on GPS L1 to be as large as 100m in the uncorrected observable - in general, contribution of the first order error term is about 10 to 100 meters (Klobuchar & Kunches 2003). For high accuracy demanding GNSS applications like PPP and RTK, especially during the peaks of the Solar Cycle and during geomagnetic storms, the higher order error terms need to be considered as they can cause range errors of a few to tens of centimetres (Wang et al. 2005).

In general, most of the ionospheric range error can be eliminated depending on the type of positioning technique deployed and the number of signal frequencies in the observations:

(i) In stand-alone mode, users with dual frequency receivers can benefit from the dispersive nature of ionospheric errors and account for

the first order ionospheric effect (in real-time) by the IF observable[g] correcting about 99% of the total ionospheric error. This would yield an accuracy sufficient for most GNSS applications. The higher order ionospheric errors, however, remain in this ionospherically corrected observable. If multi-frequency receivers are available, then it is also *possible* to correct for the second order error term with an IF observable which shall leave less residual error in the IF observable.

Users with single frequency GNSS receivers can (a) resort to the ionospheric correction data that is broadcast in the GNSS navigation message, or (b) benefit from the Satellite Based Augmentation Systems (SBAS) as another source of corrections. The correction data broadcast in the navigation message are based on ionospheric models[h] like the Klobuchar and NeQuick – the former gives the vertical TEC for a receiver location in time for GPS single frequency users, and the latter describes spatial and temporal variation of the electron density for a receiver location in time for Galileo single frequency users – although it can also be used (at least in post-processing) by GPS and GLONASS users (Leick 1995; Klobuchar 1996; Memarzadeh 2009; Jakowski et al. 2011). An ionospheric model like the Klobuchar model can correct about 50-60% of the total ionospheric effect and its performance for users outside the mid-latitudes can be limited (Orus et al. 2002). The broadcast ionospheric corrections can be fairly effective during periods of low to moderate ionospheric activity; however, they may fail to represent the actual physical conditions of the ionosphere correctly at times of enhanced ionospheric activity as during geomagnetically influenced ionospheric conditions (NovAtel 2012). Regarding SBAS like the Wide Area Augmentation System (WAAS),

[g] *While this can account for the ionospheric error, non-integer nature of ambiguities as well as increase in noise of the new observable can be non-favourable to some users.*

[h] *Models can be empirical (i.e. based on ionospheric measurements), GNSS data driven (global or regional maps in a grid form providing the values of an ionospheric parameter such as TEC in a TEC map), analytical (which can be computationally exhaustive) or physical models (based on theory of ionospheric formation).*

European Geostationary Navigation Overlay Service (EGNOS), Indian GPS-Aided GEO-Augmented Navigation (GAGAN) and Japan's MTSAT Space-based Augmentation System (MSAS) as a source of ionospheric corrections, (WAAS 1999; NovAtel 2012) these augmentation systems provide vertical ionospheric grid delay and grid ionospheric vertical error (GIVE) considering a 5^0-5^0 grid at an altitude of 350km (REF) to users as part of WAAS message (Wanner 2002). User interpolates this information to correct range measurements along each signal path. Such correction can improve the navigation solution of single frequency users; however during severe conditions they may represent the actual ionosphere not so accurately. It should be noted that such SBAS are also vulnerable to ionospheric effects which may impair system performance during enhanced solar, geomagnetic and ionospheric activities.

(ii) In differential mode, for users on a baseline or in a network (as in RTK) ionospheric error can be eliminated by observations and/or corrections obtained from a reference station assuming a spatially and temporally correlated ionosphere between the user and reference; thus it can be expected that shorter baselines can be more successful at eliminating the ionospheric error that is more likely to be common to both the reference and rover. However, during adverse ionospheric conditions spatial and temporal correlation of the ionospheric errors can decrease between the rover and reference.

3.1.1. FIRST ORDER IONOSPHERIC EFFECT

As can be seen in Eq. 5 and Eq. 8, the first order error term *Iono1* depends on the inverse frequency squared and is proportional to the integral of the electron density along LoS (Hofmann-Wellenhof et al. 2001). Neglecting the ionospheric ray bending effect which would give STEC differently on propagation paths for different signal frequencies since bending is frequency dependent (this is indeed discussed later in Section 3.1.2.3.), a linear combination of measurements on two frequencies can account for the first order error term eliminating about 99% of the total ionospheric delay/advance error; this is known as the first order approximation (Hofmann-Wellenhof et al. 2001) providing sub-meter accuracy in stand-alone positioning which can be sufficient for many GNSS applications.

$$Iono1_{g,i} = \frac{40.3}{f_i^2} STEC \qquad \text{(Eq. 10)}$$

Figure 3.4 shows for different GNSS signal frequencies the theoretical estimation of the first order error term under different ionospheric conditions considered in terms of the slant TEC values.

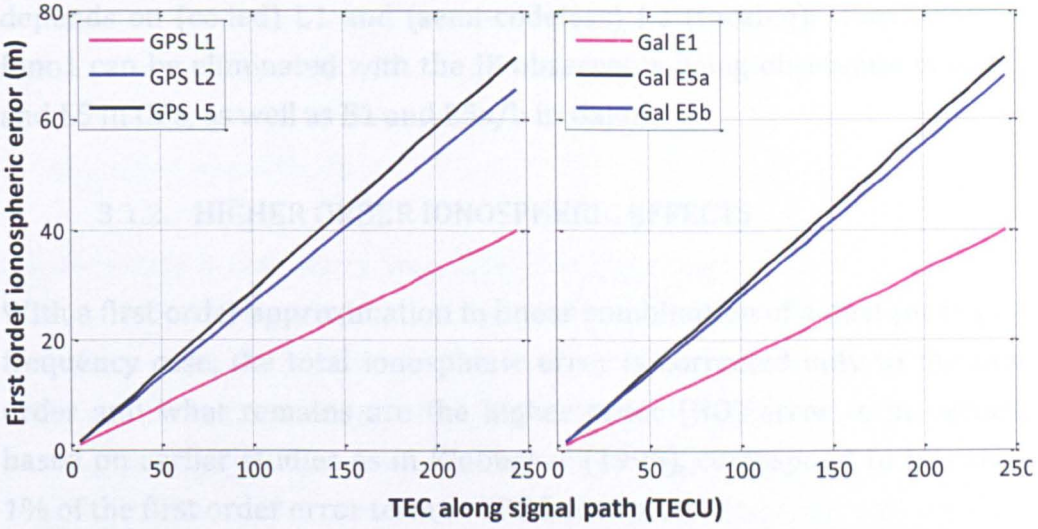

Figure 3.4. The first order ionospheric error ("Iono1") on GPS (*left*) and Galileo (Gal) (*right*) signals for different TEC along the signal path.

Lower elevation satellites pierce through a thicker slab of the ionosphere thus the TEC along the signal path is larger. High values of TEC in Fig. 3.4 can be due to low elevation or adverse ionosphere in real conditions; in either case Iono1 is influenced. As expected, lower frequencies are influenced more by Iono1 as can be seen especially for the GPS L5 and Galileo E5a signals. For TEC values of about 40-50 TECU along LoS that can represent "normal conditions", about 8 to 15m of range error can occur along the L1 (or E1) to L5 (or E5) frequency range. Under enhanced electron densities of, for instance, 180 TECU, this can increase to about 30 to 55m error for the same signal frequency range.

Depending on the receiver type (single or dual frequency) in stand-alone mode, the error due to Iono1 can be corrected by a single frequency receiver using an ionosphere model (Appendix G) or a TEC map (such as the Global Ionospheric Maps made available by CODE to obtain TEC along LoS) whereas dual frequency receiver code and carrier measurements can be used to either calculate TEC or as an IF linear combination to eliminate $Iono1^i$.

It is discussed in Section 4 and shown from open sky data in Section 6 how GNSS modernization can benefit accounting for the Iono1 term. With modernization of GNSS, it can be preferred to use, for instance, GPS L2C signal instead of L2P(Y) to construct the IF observable as *coded* tracking of L2C is expected to be more robust[j] than the semi-codeless or codeless tracking of L2P (The current practice of removing ionospheric error depends on (coded) L1 and (semi-codeless) L2 tracking). Furthermore, Iono1 can be eliminated with the IF observable using observations on L1 and L5 in GPS, as well as E1 and E5a/b in Galileo.

3.1.2. HIGHER ORDER IONOSPHERIC EFFECTS

With a first order approximation in linear combination of a dual (or triple) frequency case, the total ionospheric error is corrected only to the first order and what remains are the higher order (HO) error terms which, based on earlier studies as in Klobuchar (1996), correspond to less than 1% of the first order error term at GPS frequencies.

During periods of high solar/ionospheric/storm activity, total delay on ranges can be as large as a 100m with HO terms reaching tens of centimeters (Datta-Barua et al. 2008). Unlike the Iono1 term, HO terms are not equal in magnitude and opposite in sign for code and carrier observations. This can lead to accumulation of error in carrier smoothing of the first order IF code observable as shown by Datta-Barua et al. (2008)

[i] *Residual range error (RRE) in the first order approximation of dual frequency IF observable can reach tens of centimetres: the Iono2 term contributes about several centimetres of range error as shown by Bassiri & Hajj (1993), Kedar et al. (2003), Fritsche et al. (2005), Morton et al. (2009) and Iono3 term about 1 cm or less, such as during disturbed ionospheric background conditions with geomagnetic storms as discussed by Brunner & Gu (1991), Bassiri & Hajj (1993) and Kedar et al. (2003).*

[j] *Semi-codeless techniques to track L2 P(Y) signal suffer from SNR loss that can range between 15-35dB with dependence on the quality of L1 tracking (Woo 1999). With the new L2C civil signal, semi-codeless tracking can be avoided.*

who state that errors in the carrier smoothed code measurements are due to HO error terms.

HO terms can be neglected in a wide range of applications; however, these errors can degrade accuracy of geodetic applications and augmentation systems (Datta-Barua et al. 2008). HO ionospheric effects get more attention with the growing accuracy needs of GNSS applications. For instance, ambiguity resolution in RTK positioning can benefit from higher order corrections for ionospheric effects even in short baselines (Shanmugam et al. 2012).

Earlier works in literature investigate the higher order ionospheric effects considering i) the series expansion of ionospheric refractive index and Chapman theory for the layered structure of the ionosphere; ii) the influence of the geomagnetic field on the refractive index, which leads to a second order approximation of the total ionospheric error and iii) the bending effect of the ionosphere on the GNSS signals (frequency and satellite elevation angle dependent), which in general is neglected due to its small contribution to the ionospheric error budget. Authors of earlier works approach these concepts differently to estimate the contribution of the second and third order ionospheric effects to the GNSS error budget.

Brunner & Gu (1991) observed that the RREs due to Iono2 and Iono3 in the dual frequency solution (i.e. using the IF observable) can reach several centimetres at low satellite elevations when the ionospheric electron density is as high as during the active period of the Solar Cycle. Their proposed model (using two separate Chapman functions to represent the top and bottom sides of the ionospheric electron density profiles) can eliminate the RREs to better than 1mm by considering a series expansion of the ionospheric refractive index, an accurate ionosphere model (that provides the electron density as a function of height in the ionosphere), the International Geomagnetic Reference Field (IGRF) and also by accounting for the differential bending effect (important especially at low elevation angles) of the GPS signals (along with the tropospheric effect on the curvature of the GPS signals).

Bassiri & Hajj (1993) proposed an approach which can reduce the RREs to the millimetre level by considering a series expansion of the ionospheric

refractive index, a thin shell model for the ionosphere (as a sum of E, F1 and F2 Chapman layers), a tilted dipole model for the geomagnetic field and by neglecting the bending effect on the GPS signals (since they assume that the bending effect is insignificant for satellite elevation angles greater than 30^0).

Strangeways & Ioannides (2002) showed an analytical perturbation technique to determine the Iono2 and Iono3 terms whereby they account for the ray bending effect, and the authors compare these results with those obtained from precise ray-tracing calculations for the GPS frequencies. They conclude that the refracted geometrical path increases compared with the LoS and there is a corresponding increase in the TEC with an associated phase advance. If the influence of the magnetic field for the L band signals is neglected then the total curvature error is of comparable magnitude with the increase in the geometrical path length related with the longer curved path but of opposite sign; this represents the phase advance. The authors thereafter suggest that both terms do not need to be determined since the total curvature error is of the same magnitude but opposite sign of the increase in the geometrical path.

Kedar et al. (2003) focused on the impact of Iono2 on PPP by considering a co-centric tilted magnetic dipole and the GIM software (Global Ionospheric Mapping software from the Jet Propulsion Laboratory, JPL) which provides two-dimensional electron density maps for the ionosphere taken as a thin layer at 400km altitude. They use the satellite clock and orbit products that are not corrected for Iono2. In their comparison of the coordinate time series corrected for Iono2 with the original uncorrected coordinates, they find sub-centimeter level error contribution by the Iono2 term to the GNSS positioning error.

Fritsche et al. (2005) investigated the impact of correcting the satellite orbits and Earth rotation parameters in estimating the station coordinates in a PPP approach using the Bernese GPS Software (BSW) Version 5.0 (V5.0) (Beutler et al. 2007; Dach et al. 2007). Following the mathematical model of Bassiri & Hajj (1993) for Iono2 and Iono3 and using a thin shell model for the ionosphere, they apply GIMs for TEC data and a co-centric tilted magnetic dipole for the geomagnetic field. They show that both the station coordinates and the satellite orbits can change at the centimeter

level when the corrections for Iono2 and Iono3 are applied. Contrary to Kedar et al (2003), they emphasize that a consistent correction method for RREs should use the corrected GPS observations and products rather than the corrected observations without taking into account the RREs for the products.

In Wang et al. (2005) a multi-GNSS approach was taken to estimate the higher order error terms; and the authors focus on the techniques of eliminating/estimating the ionospheric errors through new linear combinations possible with the new signal frequencies of the modernized GNSS. They present a triple-frequency method for correcting Iono2 and propose an ionosphere-free linear combination method based on three frequencies, claiming that their triple-frequency method can correct the effects to the millimetre level. Moreover, they derive a formula for Iono3 for which they apply the semi-empirical ionospheric model developed by Anderson et al. (1987) who define TEC as a linear function of the maximum electron density (N_{max}) in the ionosphere which gives N_{max} as 4.405×10^{-6} TEC - this agrees well with the linear interpolation applied by Fritsche et al. (2005). After obtaining TEC from pseudorange (PR) measurements with L1 and L2, Wang et al. (2005) can estimate Iono3 with an accuracy of about 1mm.

Hernandez-Pajares et al. (2007) consider the impact of Iono2 on the satellites clocks and show that the estimates of the RREs on the receiver coordinates, satellite positions and clocks are correlated. Regarding the receiver positions, they infer that Iono2 has a sub-daily impact of less than 1mm during March in 2001 – a year during the previous peak of the Solar Cycle. As for the satellite positions, they show that Iono2 causes a daily mean global southward displacement of several millimetres, depending on the ionization level in the ionosphere. Regarding the satellite clocks, which are most affected by the higher order ionospheric effects according to their results, RREs can cause deviations even larger than 30 picoseconds (corresponding to about 1cm) depending on latitude and local time of the receiver position.

Hoque & Jakowski (2007) quantified the residual "phase" error due to Iono2 and neglect that due to Iono3 (differential bending of the GNSS signals also neglected) claiming that on a disturbed day (about 100 TECU)

the RRE due to Iono3 is at the sub-millimetre level. Their model, which can provide better than 2mm accuracy for GNSS users in Germany, does not require knowledge of the instantaneous geomagnetic field since they take the geomagnetic field component for a reference user position in central Germany. Knowledge about the electron distribution along the propagation path is also not required. These assumptions make the model suitable for real time GNSS applications but only in central Germany.

Kim & Tinin (2007) used perturbation theory to study the residual error in the dual frequency ionosphere free observable; they investigate in particular the Iono3 term associated with the ray bending effect on the GNSS signals penetrating through an inhomogeneous ionosphere. Taking into account that Iono3 term includes not only the quadratic correction due to the refractive index but also the correction for the ray bending effect, they show that the ray bending effect may dominate the Iono2 error contribution. They consider both the regular large scale and random small scale irregularities in the ionosphere such that the latter can, at times, cause residual error comparable to or greater than that of the Iono2 term, dominating the contribution to the residual error in the IF observable.

Datta-Brua et al. (2008) showed that, unlike the Iono1 term which has the same magnitude but opposite signs for the group and carrier phase measurements, the Iono2 and Iono3 have different magnitudes and signs for these two types of measurements. For this reason, the authors claim that the higher order errors accumulate in the carrier smoothing of the IF (to the first order) code observable; the authors show that the errors in the carrier-smoothed code measurements are mostly due to Iono2 and Iono3. In other words the unaccounted higher order group errors contribute to the error in the carrier smoothing. Although they can be neglected in many applications, these residual errors can be crucial in high precision applications.

Hernandez-Pajares et al. (2008) focus on Iono2 and different methods to obtain slant TEC (STEC) and the geomagnetic field component projected onto the receiver-satellite path. Considering the error due to Iono2 on positioning, they emphasize that correction for Iono2 must be applied to all fiducial stations during product generation - application only to the unknown station (user) can lead to errors in the estimated coordinates

that can be worse than applying no correction at all at the any receiver involved.

In a more recent study, Kim & Tinin (2011) explored the possible ways of eliminating the higher order ionospheric error terms considering a multi-frequency GNSS approach and show how the GNSS accuracy can be improved considering the propagation of the signals through an inhomogeneous and random structure of the ionosphere. Through numerical simulation they show that the systematic, residual ionospheric errors can be significantly reduced (under certain ionospheric conditions) through triple frequency modelling.

Moore & Morton (2011) focused on the Iono2 term introduced by the interaction between the GNSS signal and the magnetic field of the Earth. The anisotropy of the ionosphere causes the right hand circularly polarized (RHCP) GPS signals to propagate in two (ordinary and extraordinary) modes, as a linear combination of them, depending on the angle between the GPS signal wave normal and the Earth's magnetic field. These two modes correspond to two different magneto-ionic polarizations each with a particular refractive index that needs to be considered in the Iono2 term. The authors show that near the geomagnetic equator signals arriving from the north propagate with the ordinary polarization (associated with left hand circularly polarized wave) yielding a "positive" Iono2 term for the carrier phase; and those arriving from the south propagate in the extraordinary mode polarization (associated with right-hand circularly polarized wave) making the Iono2 term "negative" for the carrier phase. A "positive" Iono2 term corresponds to the presence of error that needs to be accounted for in the (first order) ionospherically corrected measurements. The authors also point out a *misconception* in the work of Bassiri & Hajj (1993) who assume that the left hand circularly polarized (LHCP) component of GPS signals propagates in the ordinary mode and do not realize the fact that the RHCP signal component may indeed travel in either of the propagation modes. Moore & Morton (2011) show that the magneto-ionic polarization of the predominantly RHCP GPS signal depends on the direction of the GPS signal wave vector with respect to the magnetic field line. Considering three different geographic locations to show the influence of this fact on the Iono2 term, the same authors infer that Iono2 is asymmetric with respect to the geomagnetic equator such

that a RHCP wave has different propagation modes depending on the magnitude of the angle between the wave vector and the magnetic field line. Therefore, the authors suggest that considering only one propagation mode can lead to mismodelling of inaccuracies while estimating the error due to the Iono2 term.

From the above literature review, therefore, it is understood that the higher order ionospheric error terms may contribute up to cm level range errors subject to background ionospheric conditions. Greater accuracy can be achieved while estimating the magnitudes of the higher order error terms by 1) using a more precise geomagnetic field model like the IGRM instead of the dipole model, 2) obtaining accurate estimates for the electron content along the signal path (slant TEC, STEC) which can be either retrieved from Global Ionospheric Maps (GIMs)[k], estimated from PR measurements[l] or by using the geometry-free observable[m], and 3) using

[k] *GIMs produced daily at an update rate of 5-15 minutes in IONEX format by CODE using data from about 150 global, continuously operating, dual frequency sites of IGS and other institutions provide instantaneous, accurate TEC distributions from spatial and temporal interpolations of 6-8 simultaneous TEC measurements from each receiver (JPL 2012). Estimating P1-P2 DCBs for all GPS satellites and receivers for each day, and using P1-C1 DCBs, CODE determines STEC and converts it into VTEC using a modified single layer model mapping function, which changes vertical ionospheric delay at IPP into slant delay (Beutler et al. 2007).*

[l] *STEC can be obtained from PRs (non-ambiguous) on L1 and L2 – or on L1 and L5 in future practice. Details about calculating STEC in this method are given in Appendix B.*

[m] *This method offers an easy computation of STEC as it depends on code and phase observations on dual frequency (phase observations used due to their higher accuracy), CP ambiguity in the case of the phase observations, and satellite and receiver DCBs which are almost constant in time (even if they vary, this contributes to RRE due to Iono2 at sub-millimeter level (Beutler et al. 2007; Hernandez-Pajares et al. 2008).*

the satellite orbit and clock products estimated by applying corrections for the higher order ionospheric error terms - this is particularly important for a systematic and accurate analysis of the impact of the higher order terms in the GNSS positioning.

3.1.2.1. SECOND ORDER IONOSPHERIC EFFECT

The second order ionospheric error term, Iono2, is due to the interaction between the geomagnetic field and ionospheric refractivity. It is inversely proportional to the third power of frequency and depends on TEC along the signal path. Due to its geomagnetic field dependence (evident in the $B_0 cos\theta$ term, Eq. 11), the magnitude of the Iono2 term can depend on the receiver latitude and conditions of the geomagnetic field at the IPP.

$$Iono2_{g,i} = \frac{\kappa e B_0 cos\theta}{\pi m f_i^3} STEC \qquad \text{(Eq. 11)}$$

Geomagnetic field properties can be obtained using, for instance, the International Geomagnetic Reference Field, IGRF-11 (11^{th} generation for IGRF), which is a more sophisticated model than the dipole approach in which the geomagnetic field is approximated in terms of a bar magnet tilted 11^0 from the spin axis of the Earth (Macmillan 2005; Georgia State University 2008). Earth's main field and its annual rate of change is mathematically represented in IGRF through a multipole expansion with updated estimates for coefficients that are involved in the definition of the scalar magnetic field potential (Walt 1994). The IGRF model was made publicly available in Fortran code by Tsyganenko (2005). An approximation for Iono2 can be based on taking an average value for "B" and value of $cos\theta$ at IPP of 350km altitude. This helps avoid integration in the mathematical model that facilitates calculations.

In the case of Iono2, IGRF-11 outputs for 350km ionospheric shell height can be considered.

The $B_0 cos\theta$ term attains different values depending on the receiver location, which relates with relative satellite geometry, and altitude in the ionosphere, which relates with the geomagnetic field (as the B vector varies from location to location in the ionospheric altitudes). For instance,

if the signal is propagating perpendicular to the geomagnetic field in which case the angle θ is close to 90^0, Iono2 range error approaches zero due to the *cosine* function. Furthermore, depending on the angle θ and the *cosine* function, the Iono2 term can be positive or negative.

For a receiver in the southern hemisphere,

- Signal arriving at a small elevation angle from the south gives *positive* $B_0 cos\theta$ values (delay on the pseudorange measurement),
- Signal arriving at a small elevation angle from the north gives *negative* $B_0 cos\theta$ values (advance on pseudorange measurement).

This means that the signal arriving from the south with respect to the receiver contains delay due to the Iono2 term, whereas that arriving from the north has advance due to Iono2.

In addition to the sign of the Iono2 term, the magnitude of the error depends on the TEC along the propagation path (which can be affected by patchy electron density irregularities affecting the propagation) and the angle θ such that smaller the angle θ, larger the magnitude of the error due to Iono2.

Regarding the influence of the geomagnetic field in the Iono2 error term, knowledge about the Kp or Dst parameters (Appendix F) which can tell about disturbances in the geomagnetic field for the high and low latitude regions, respectively, can also be important to consider (Morton 2008).

Figures 3.5. and 3.6. show, respectively, theoretical magnitudes of Iono2 on pseudoranges for GPS L1, L2 and L5 signals, considering a receiver at the mid and equatorial latitudes (for relevant values of B) as functions of TEC along the signal path and angle θ between the signal path and geomagnetic field at IPP. Choice of latitudes is for assigning meaningful values to B for magnitude analysis of Iono2 under possible values of TEC and the angle between the signal path and geomagnetic field line at IPP. Theoretical magnitudes of Iono2 for Galileo E1-E5a-E5b signals for a receiver at mid- and equatorial latitudes are shown in Fig. 3.7. and Fig. 3.8.

N.B. In Fig 3.5. - 3.8. the magnitude of Iono2 in absolute terms is considered such that its sign needs to be determined according to relative geometry between receiver and satellite.

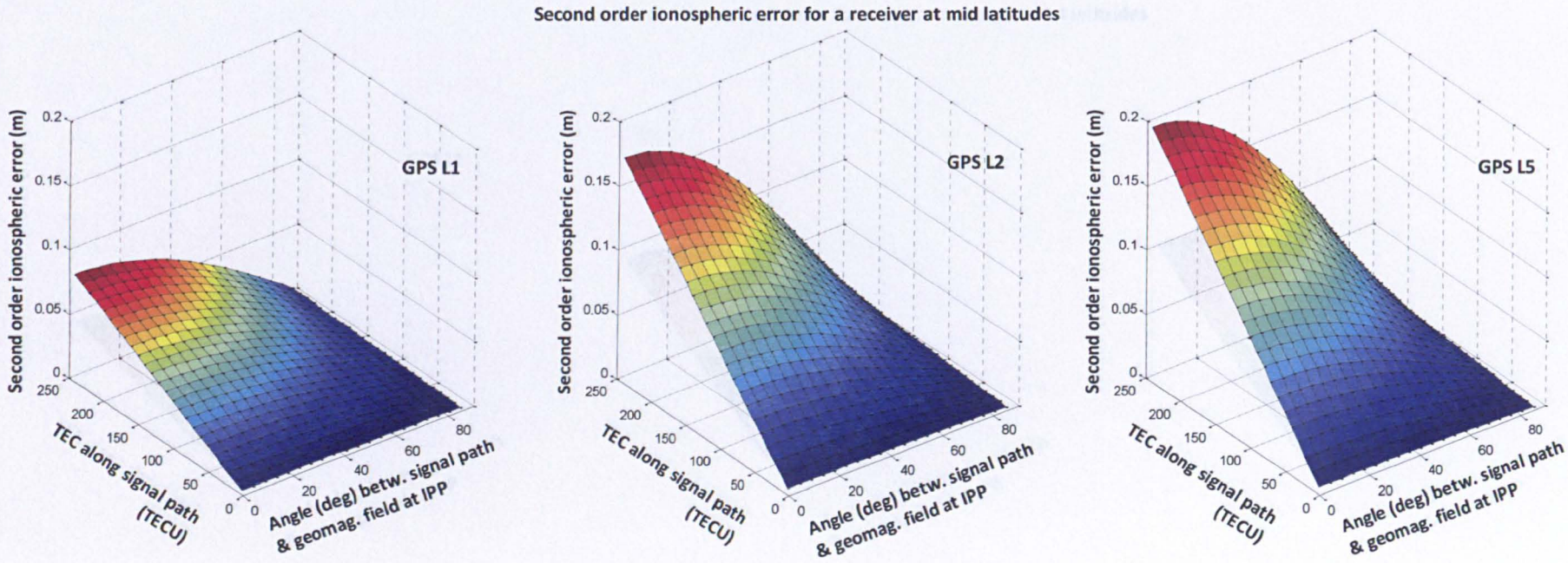

Figure 3.5. The magnitude of Iono2 for GPS L1, L2 and L5 signal frequencies for a receiver at mid latitudes.

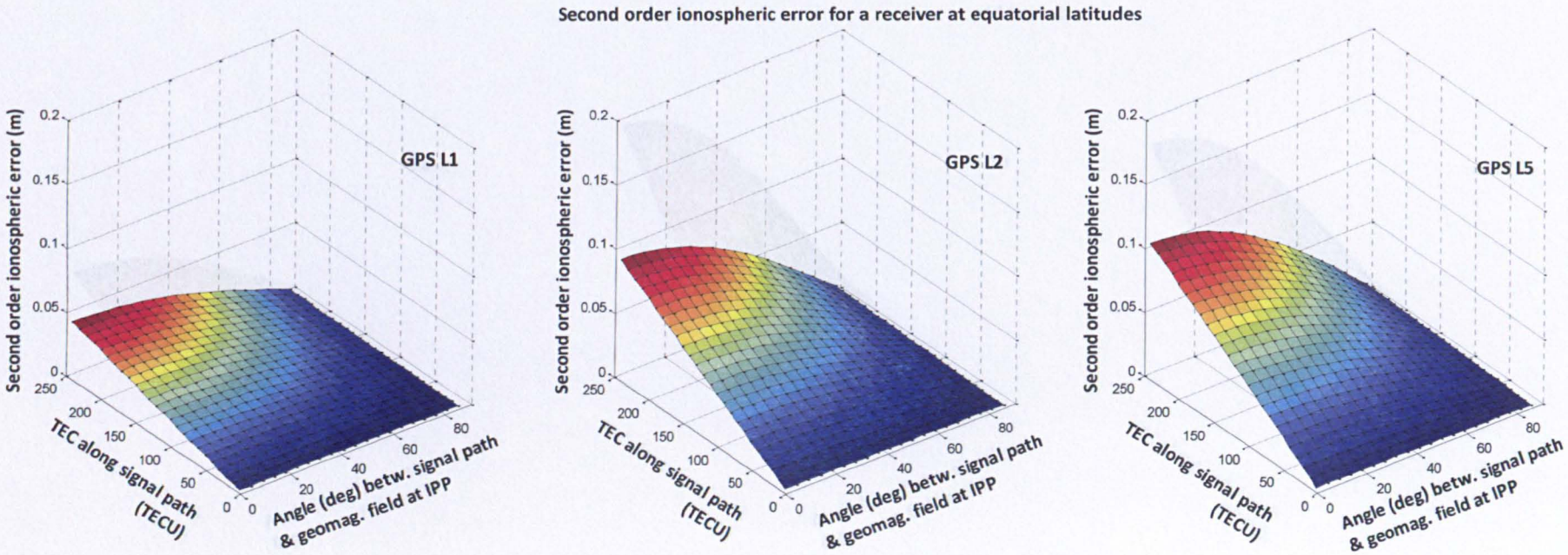

Figure 3.6. The magnitude of Iono2 for GPS L1, L2 and L5 signal frequencies for a receiver at equatorial latitudes.

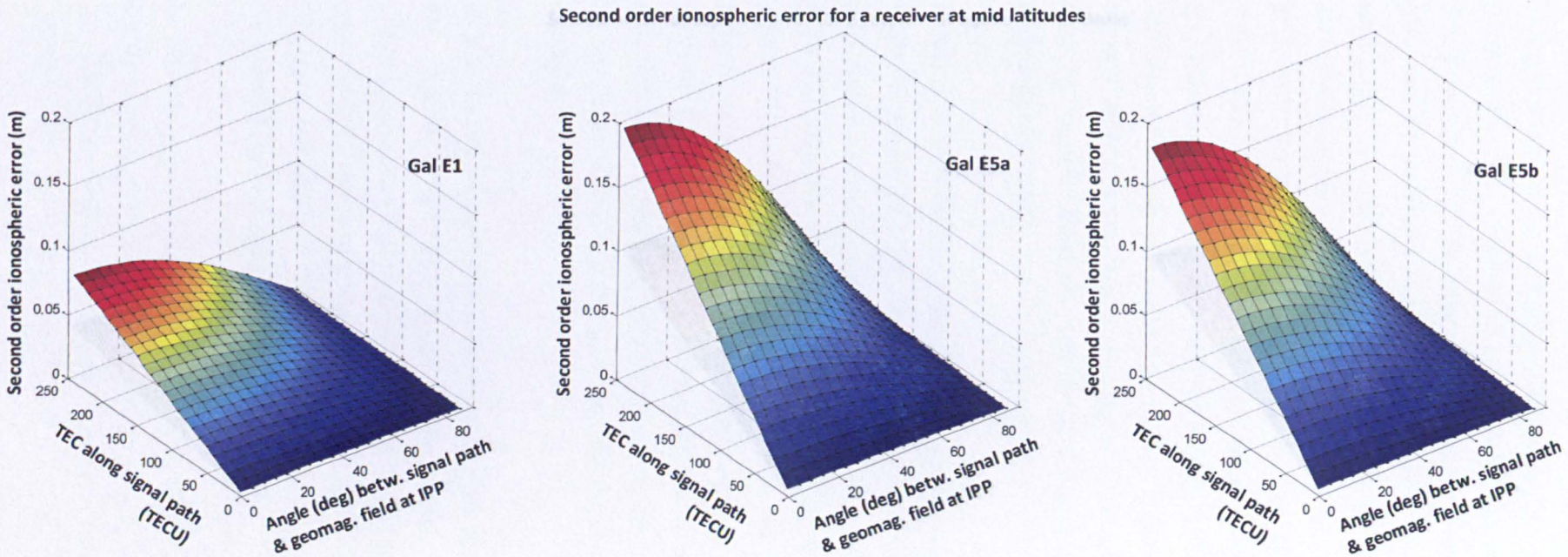

Figure 3.7. The magnitude of Iono2 for Galileo E1, E5a and E5b signal frequencies for a receiver at mid latitudes.

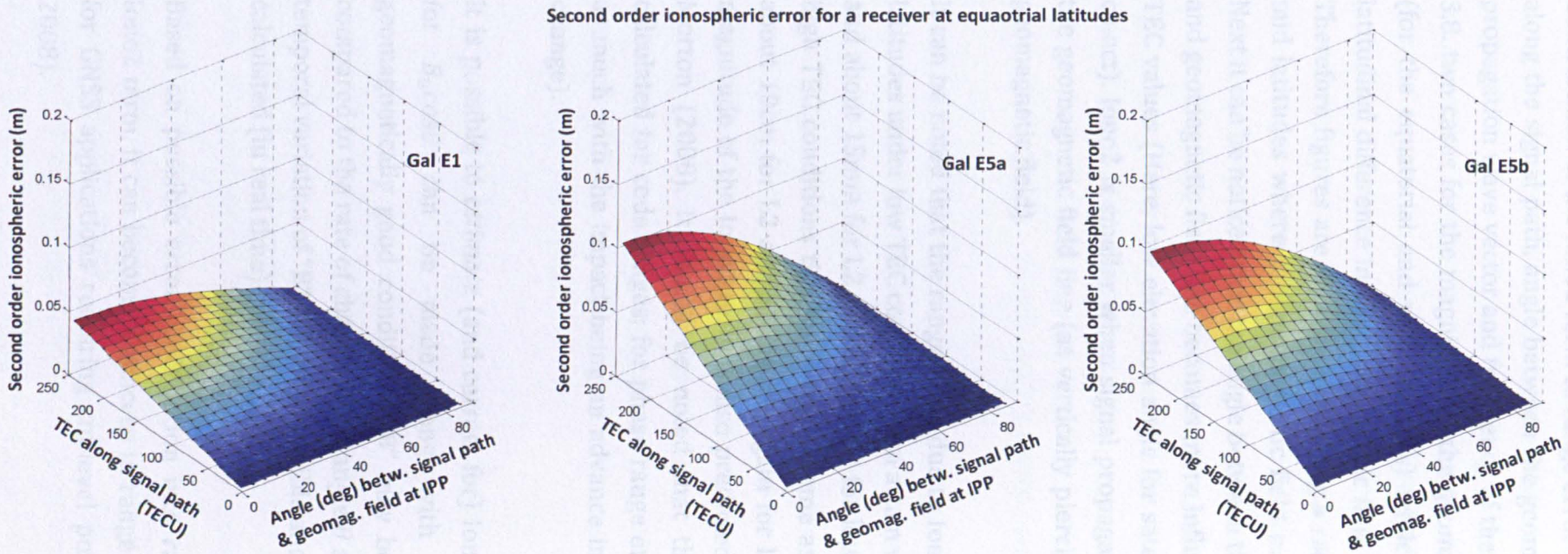

Figure 3.8. The magnitude of Iono2 for Galileo E1, E5a and E5b signal frequencies for a receiver at equatorial latitudes.

Contribution of the Iono2 term to range error in principle depends on TEC along the signal path, angle between the geomagnetic field line and signal propagation wave vector and frequency of the signal (Eq. 11). In Fig. 3.5. - 3.8. two cases for the magnitude of the geomagnetic field are considered (for the equatorial and mid latitudes) while estimating Iono2 as such, latitudinal difference in the geomagnetic field is expected at IPP altitudes. Therefore figures are shown considering a receiver at the equatorial and mid latitudes where the geomagnetic field may be different in strength. Next it can be noticed that the angle between the propagating signal vector and geomagnetic field line becomes more influential especially for greater TEC values (Here, low elevation angle for satellite and angle θ at IPP can co-act). Iono2 is smaller when signal propagates almost perpendicular to the geomagnetic field line (as vertically piercing through the plane of the geomagnetic field).

It can be noted that the range error due to Iono2 for a receiver at the mid latitudes under low TEC conditions can attain values of about 10mm for L1 and about 15mm for L2 and L5 signals for low elevation satellites; during high TEC conditions this error can become as large as 45mm for L1 and about 10cm for L2 and L5 signals again for low elevation satellites. The magnitude of the Iono2 term is also predicted to vary between 1-4cm by Morton (2008). It should be noted that these error magnitudes are calculated for code ranges; for phase range errors Iono2 contributes half as much with the impact being an advance instead of a delay (i.e. a sign change).

It is possible to *estimate* (and correct for) Iono2 if a good approximation for $B_0 cos\theta$ can be made along with TEC information. Under geomagnetically good conditions, "B" may be considered as a constant compared to the rate of change in the angle θ and TEC; in other words, the temporal variation of "B" may be negligible and the angle θ and TEC can be calculated (in real time).

Based on possible error contribution into range measurements by the Iono2 term, it can become a concern in range measurement error budget for GNSS applications requiring cm-level positioning accuracy (Morton 2008).

As discussed in Section 4, GNSS modernization makes it possible to do a second order approximation to *eliminate* the Iono2 term giving a further reduced IF observable by linearly combining observations on three frequencies. However, the commonly acknowledged disadvantage of this approach is the increased noise level of the achieved observable.

Correcting the Iono2 term in the observations can influence GNSS positioning results where sub-mm level shift in receiver position towards south at the low latitudes and north at the high latitudes can be observed (Hernandez-Pajares et al. 2007). In Section 6, Iono2 is estimated using open sky data with the software tool *Rinex_HO* (described in Section 5.2.1.) that considers the IGRF estimates for the geomagnetic field.

3.1.2.2. THIRD ORDER IONOSPHERIC EFFECT

The third order error term, Iono3, is due to d*eviations of the ray trajectory from a straight line* (i.e. ray bending effect due to refraction leading to non-LoS propagation) and depends on the maximum electron density along the signal path. Iono3 involves the square of the electron density (third term at the RHS of Eq. 4) which makes the mathematical approach rather difficult for evaluating this term analytically. In order to facilitate this, an approximation suggested by Hartmann & Leitinger (1984) is applied that redefines the squared electron density in terms of a maximum electron density and shape parameter whose value can be taken as constant under different link geometries.

$$Iono3_{g,i} = \frac{3\kappa^2}{2f_i^4}\eta N_{max} STEC \qquad \text{(Eq. 12)}$$

N.B. Bending effect is discussed separately in Section 3.1.2.3.

With this approximation it can be seen that Iono3 depends on N_{max}, the peak electron density value, which characterizes electron density in an ionospheric sub-layer (Pireaux et al. 2010). A linear interpolation (considering ionization levels at different altitudes in the ionosphere) can be used to approximate N_{max} in terms of TEC based on a relation between normal/typical and solar maximum ionospheric conditions (Fritsche et al. 2005). Anderson et al. (1987) also suggest a relation defining TEC in terms

of N_{max}. A further modified version of this linear interpolation is suggested by Pireaux et al. (2010):

$$N_{max} = \frac{(20-6)\times10^{12}}{(4.55-1.38)\times10^{18}}\{VTEC - 4.55 \times 10^{18}\} + 20 \times 10^{12} \quad \text{(Eq. 13)}$$

$$N_{max} = \frac{(20-6)\times10^{12}}{(4.55-1.38)\times10^{18}}\{STEC \times [1 - (\frac{R_E}{R_E+H})^2 \cos^2(\alpha \times z)]^{1/2} - 4.55 \times 10^{18}\} + 20 \times 10^{12} \quad \text{(Eq. 14)}$$

In Eq. 13 and Eq. 14, H is the altitude of the ionospheric single layer; R_E is radius of the Earth; α is a correction factor (depending on zenith angle and H) and z is the zenith angle for the signal path piercing the ionospheric single layer with respect to the local vertical. For a zenith angle of 80^0 and H=506.7km, α has a value of 0.9782 (Pireaux et al. (2010)).

N.B. Equation 14 contains a modified single layer model mapping function to express VTEC in Eq. 13 in terms of STEC.

For quantifying Iono3, the relation suggested by Fritsche et al. (2005) is considered for practical implementation into the Iono3 equation, i.e. N_{max} = 4.415*10^{-6} TEC. Thereafter, it is possible to obtain realistic error bounds for Iono3 for different TEC values along the signal path for different signal frequencies as shown in Fig. 3.9.

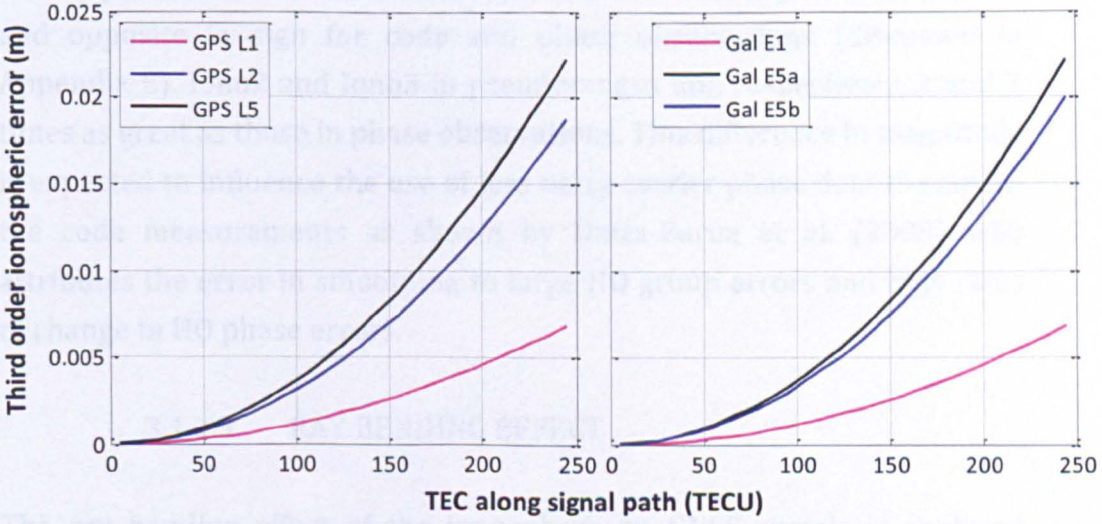

Figure 3.9. The magnitude of Iono3 error term estimated for GPS (*left*) and Galileo (Gal) (*right*) signal frequencies, based on the linear relation between N_{max} and TEC, suggested by Fritsche et al. (2005).

Different from the Iono1 term, a quadratic dependence on TEC can be seen for Iono3 which is due to expressing N_{max} in terms of TEC as an approximation. For low levels of TEC of about 40-50 TECU, as during low TEC conditions, the error contribution of Iono3 to pseudoranges is about a few mm. For higher values of TEC, this can reach cm level, which is comparable to the error contributed by Iono2. Kim & Tinin (2007) remark that the Iono3 term in RRE may exceed the Iono2 term, depending on ionospheric conditions. It is important to note that for phase measurements, Iono3 contributes one third of the contribution for code measurements.

Before continuing with the ray bending error term in the next section, it should be stated that RRE due to Iono2 and Iono3 in the IF observable contributes less than 1% of the Iono1 term at GPS frequencies corresponding to about mm/cm level errors at geodetic precision. RRE can be neglected during quiet ionospheric (low ionization levels in the ionosphere evident in low TEC values) and solar background conditions (during a solar minimum); however, several tens of centimetres of range error can occur during high solar activity and especially at low elevation angles. Fristche et al. (2005) show that cm-level changes in the estimated station coordinates can occur when HO error terms are considered in GNSS positioning (Fritsche et al. 2005).

It is important to note that Iono2 and Iono3 are not equal in magnitude and opposite in sign for code and phase observations (discussed in Appendix E). Iono2 and Iono3 in pseudoranges are, respectively, 2 and 3 times as great as those in phase observations. This difference in magnitude is expected to influence the use of less noisy carrier phase data to smooth the code measurements as shown by Datta-Barua et al. (2008) who attributes the error in smoothing to large HO group errors and high rates of change in HO phase errors.

3.1.2.3. RAY BENDING EFFECT

The ray bending effect of the ionosphere on GNSS signals is analyzed separately from the Iono3 term, although they both have inverse frequency dependence to the fourth power – this is a reason why the ray bending error can be in general grouped with the Iono3 term. Ray bending

is a consequence of the ionospheric refraction. The signal propagation path becomes no longer a straight LoS but a curved path which bears the excess path length. One consequence of the bending effect is that it causes TEC to be estimated differently along the two (curved and LoS) paths leading to a TEC difference between the curved and LoS paths. In order to avoid error contribution from the ray bending while estimating the TEC, it can be preferred to exclude the low elevation observations which may be more affected by the ray bending.

The magnitude of the bending depends on the signal frequency and satellite elevation, for instance, lower frequency signals are bent more than higher frequency ones (Fig. 3.10.), and greater bending occurs at lower elevation. Neglecting the ray bending effect means to assume that the delay effects occur along LoS signal propagation. However, it should be noted that the fact that the bending effect is different on different frequency signals, the paths taken by these signals is slightly different from each other therefore the 'ionosphere-free' linear combination may no longer completely cancel the first error term in the first order approximation (Petrie et al. 2011).

In this thesis, the ionospheric ray bending effect is discussed in a theoretical approach rather than on the basis of data analysis. It should be remarked that the bending error may, under adverse conditions, exceed or be comparable in magnitude to the second order error term (Hoque & Jakowski 2008). Neglecting the bending effect means to assume that GNSS signals travel along straight LoS paths (Hoque & Jakowski 2007) instead of two slightly different (bent and LoS) paths.

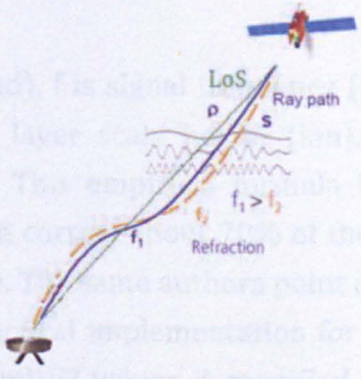

Figure 3.10. Difference between the line-of-sight (LoS), "ρ", and actual ray path, "s", due to ionospheric refractivity. The individual ray paths for two signals at frequencies f_1 and f_2, where $f_1 \neq f_2$.

This assumption of neglecting a bent path implies that TEC and geomagnetic field effect are the same for different signal frequencies. Ray bending effect on GNSS signals becomes significant especially at low satellite elevation angles, such as below 10^0 (Hoque & Jakowski 2007). More detailed analyses about the impact of ray bending on GNSS signal propagation and observations have been shown, among other researchers, by Hoque & Jakowski (2008) who provide an empirical formula for the geometric bending of the GPS signals; Hartmann & Leitinger (1984) who consider the geometric bending of GNSS signals in their analysis of RREs due to the atmosphere; and Petrie et al. (2010) who use the International Reference Ionosphere (IRI) 2007 model (Bilitza & Reinish 2008) to estimate the potential size of the ray bending effect on the estimated GPS parameters and positioning.

It can be mentioned at this point that a greater number of satellite paths through the ionosphere can help neglect some paths near the horizon for more accurate TEC estimation. To the first order, estimated TEC is a sum of TEC along LoS path and that due to the bent path (the latter being negligible for high elevation satellites). Under favourable geometry conditions, contribution to TEC from the bent paths can be neglected or avoided if redundancy can be achieved with a greater number of visible satellites.

Ray bending causes excess path length to occur due to geometric bending which can be modelled as (Jakowski et al. 2008):

$$d_g = \frac{7.5*10^{-5}*STEC^2*e^{-2.13*\beta}}{f^4*HF_2*(h_mF_2)^{1/8}} \qquad \text{(Eq. 15)}$$

where β is elevation (rad), f is signal frequency (GHz), HF_2 (described in Appendix H) is the F_2 layer scale height (km), and h_mF_2 is the peak ionisation height (km). This empirical formula is derived by Hoque & Jakowski (2008) and can correct about 70% of the error remaining in the first order IF observable. The same authors point out that this formulation falls rather far from practical implementation for real time purposes due to the need for H and hmHF2 values. A modified version is suggested for "excess path" i.e. range error due to bending (Hoque & Jakowski 2012) as:

$$d_{ben} = \frac{2.9344*10^7}{f^4}\left(\frac{1}{\sqrt{1-0.8260*\cos^2\beta}} - 1\right) TEC^2 \qquad \text{(Eq. 16)}$$

where d_{ben} is the ray bending error in cm, f is frequency of GNSS signal in MHz, TEC is in TECU and β is elevation angle in radians (Hoque & Jakowski 2012). Figure 3.11. and Fig. 3.12. show range error due to ionospheric ray bending for GPS and Galileo signals, respectively.

It can be seen in Fig. 3.11. and Fig. 3.12. that LoS assumption of GNSS signal propagation needs correction especially for low elevation angles and during enhanced TEC conditions. Comparing the impact on different signal frequencies, it can be seen that for 8^0 elevation angle (considered since ray bending is more important at low elevation angles) and 155 TECU, ray bending causes a non-LoS range error of about 0.15 cm on GPS L1, 0.40 cm on GPS L2 and 0.48 cm on GPS L5. Accounting for ray bending error can be necessary in particular for dual or triple frequency linear combinations of observations.

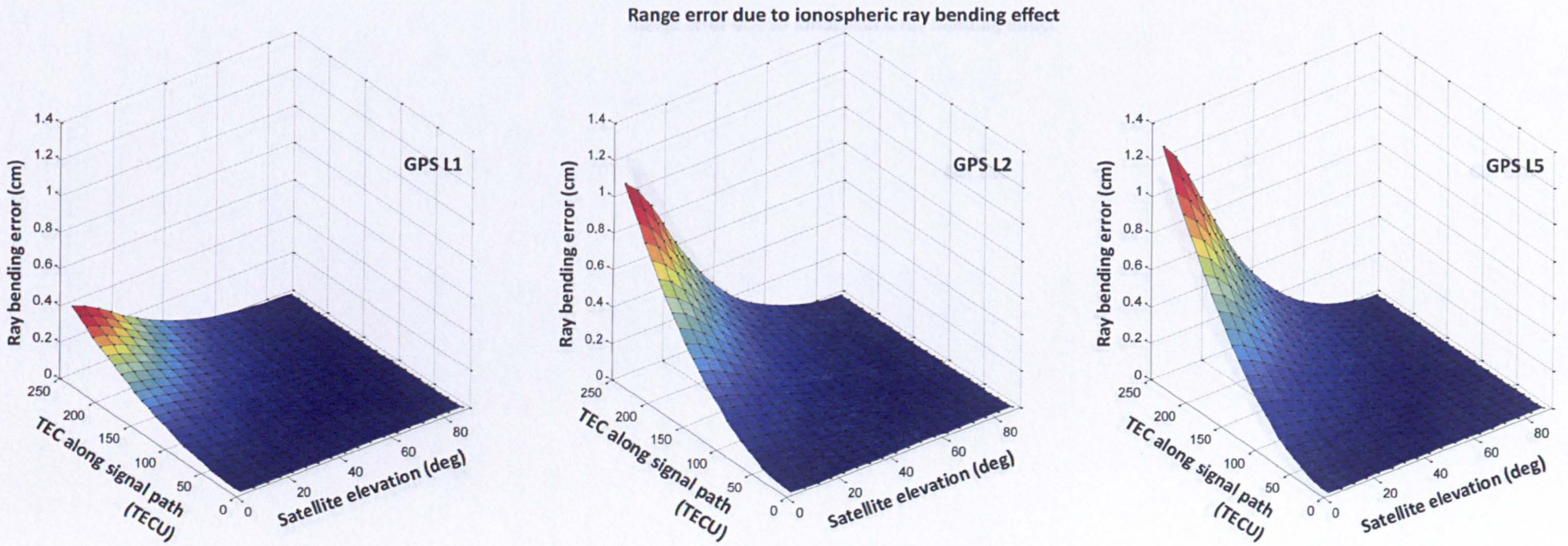

Figure 3.11. Range error due to the ray bending effect for GPS signals.

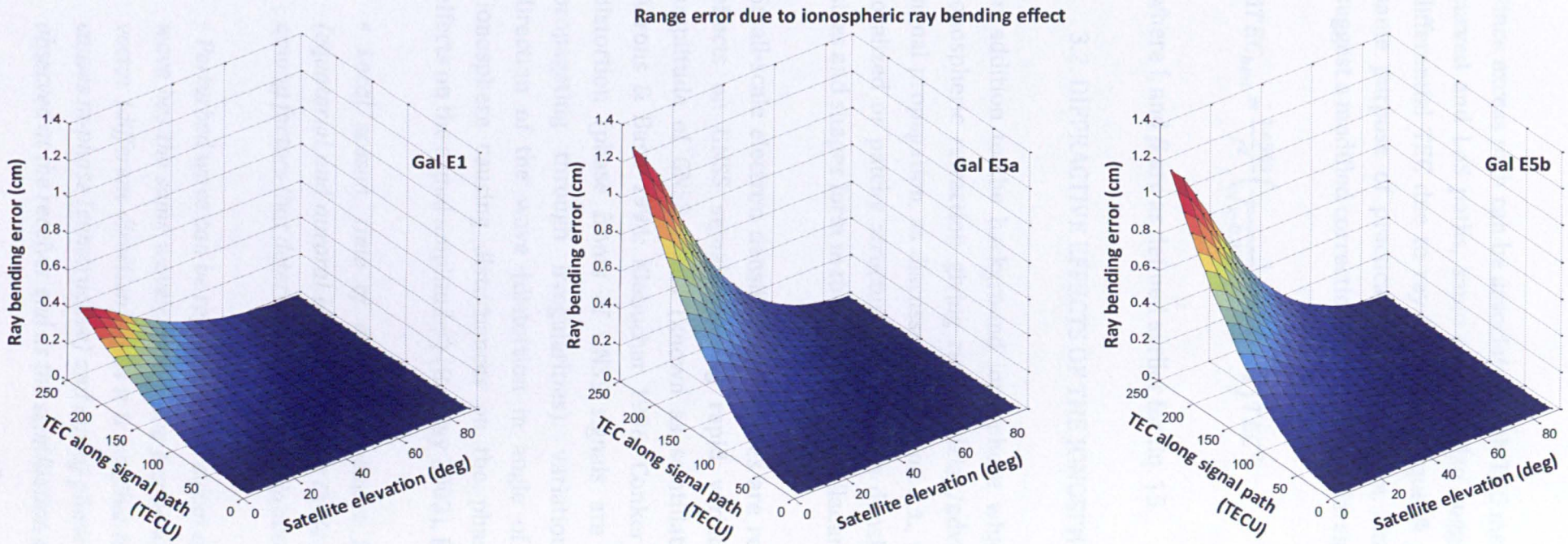

Figure 3.12. Range error due to the ray bending effect for Galileo signals.

Since excess path can be associated with TEC measured differently on the curved and LoS paths, same authors also suggest a correction for this differential TEC due to ray bending (Hoque & Jakowski 2008). For the same purpose of practical implementation, Hoque & Jakowski (2012) suggest a modified correction formula for differential TEC:

$$\Delta TEC_{ben} = \frac{1.4563}{f^2}\left(\frac{1}{\sqrt{1-0.8260*\cos^2\beta}} - 1\right) TEC^2 \qquad \text{(Eq. 17)}$$

where f, and β are as defined earlier for Eq. 15.

3.2. DIFFRACTIVE EFFECTS OF THE IONOSPHERE

In addition to the background ionosphere which is the main cause of ionospheric refraction giving rise to delay/advance/bending effects on signal propagation, as discussed in Section 3.1., there can be times when localized or patchy structures of electron density gradients of different sizes and shapes form in the ionosphere (Valladares et al. 1999).

Small-scale electron density irregularities are responsible for diffraction effects on GNSS signals causing rapid variations in the phase and amplitude of GNSS signal (known as scintillation[n]) (Wanninger 1993; Aarons & Basu 1994; Klobuchar 1996; Conker et al. 2003), wavefront distortion (phase fronts of GNSS signals are no longer planar after propagating through irregularities), variations in the propagation direction of the wave (distortion in angle of arrival) and scattering (ionosphere causing disturbances on the phase front with negligible effects on the signal amplitude[o]) (Barclay 2003). Fluctuations in amplitude

[n] *Local season, time of day (post sunset hours), receiver location (equatorial and auroral latitudes), Solar Cycle (11-year Solar Cycle) are among factors that determine when scintillation is more likely to happen.*

[o] *Perturbed wave can be represented as a sum of plane waves where each wave has the same wavelength (same frequency) but with its own wave vector (different direction); thus it is possible to expect interference that causes in-phase (constructive) and out-of-phase (destructive) waves to be observed at the receiver end as the scintillation effects.*

and phase of the received signal are known as *amplitude* and *phase scintillation.*

(i) Amplitude scintillation is observed as fluctuations and fading on the amplitude (intensity) of the received signal, which primarily affects the signal-to-noise ratio causing what is observed as fading in the signal. Amplitude scintillation may be monitored in terms of the S4 index which is the normalized STD (over 60s) of detrended[p] high frequency (50Hz) signal intensity (Van Dierendonck 1999). The S4 index is observed to agree (during this research) with the Nakagami-m statistics which can be applied to high rate signal intensity data (described in detail in Section 4.2.) to estimate S4, as shown for GPS L1 in Fig. 3.13. Such a statistical relation between Nakagami statistics and fading in the signal amplitude (related to S4) is also suggested by the authors Nakagami (1960) and Humphreys et al. (2008b, 2009a-b).

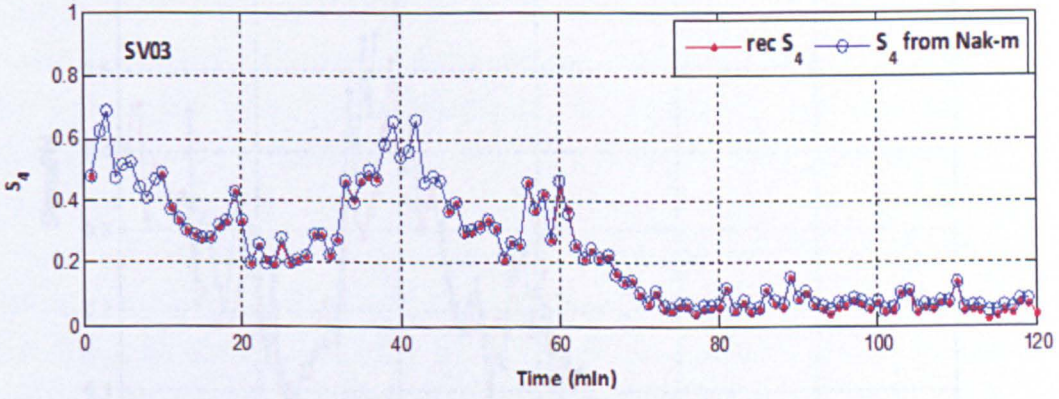

Figure 3.13. The S4 index for SV03 (for GPS L1) obtained from the receiver, "*rec S_4*", and calculated using high rate signal intensity data applying Nakagami-m statistics, "*S_4 from Nak-m*".

(ii) Phase scintillation which causes rapid changes in the phase (frequency) of the received signal may cause the Doppler shift on the received signal to exceed the bandwidth of the phase tracking loop (phase locked loop, PLL). Such stress on the tracking loop of a GNSS receiver can challenge an accurate phase estimate of the received signal. Large, rapid and random phase fluctuations can degrade the carrier tracking

[p] *Detrending is performed to extract the high frequency fluctuations in signal intensity and phase that are induced by scintillation*

performance which can introduce cycle slips causing several measurement epochs to be missed and requiring the carrier phase ambiguity search to be reset - a time consuming task. Acquisition of the incoming or lost signal can be impeded, lock on an incorrect phase can occur or the carrier lock can be lost completely (Mao et al. 2004; Pullen et al. 1998). Phase scintillation is quantified in terms of the SigmaPhi index which is STD (over 60s) of the detrended high frequency signal phase (Van Dierendonck 1999). SigmaPhi obeys Gaussian distribution with zero mean. It is possible to approximate SigmaPhi index making use of the high rate signal intensity data similar to the case with S4 – however, here instead of applying a statistical approach, an approximation is performed with high rate signal intensity and phase data. Figure 3.14. shows the estimated SigmaPhi (for GPS L1) index compared with that output by the receiver.

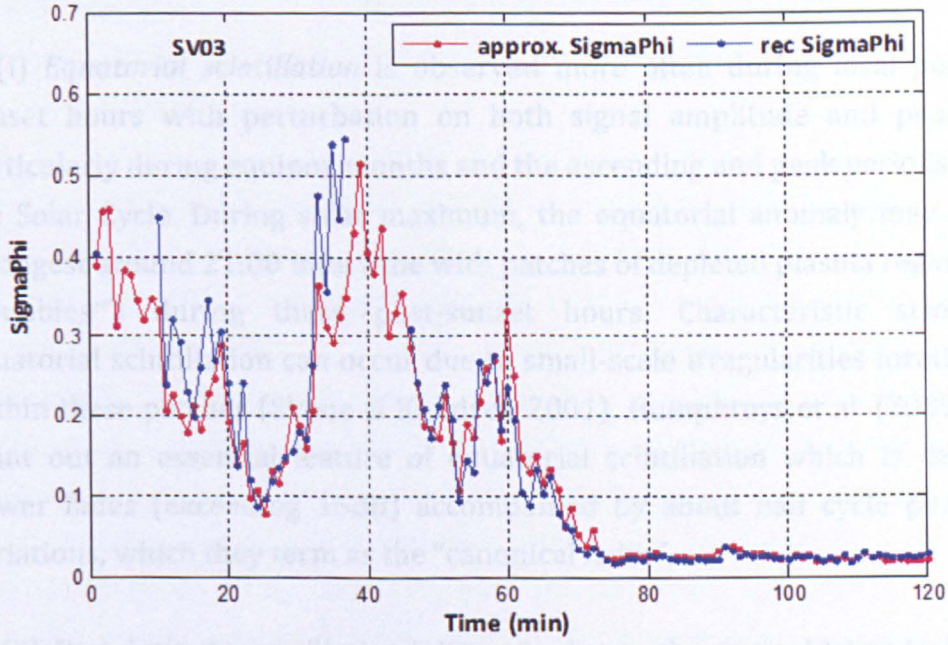

Figure 3.14. The SigmaPhi index for SV03 (for GPS L1) obtained from the receiver, "*rec SigmaPhi*", and approximated with high rate signal intensity data "*approx. SigmaPhi*".

N.B. Both amplitude and phase scintillations can cause cycle slips which are caused more often by phase scintillation (Humphreys et al. 2009a).

N.B. Kim & Tinin (2011) suggest that phase scintillation effects appear as a third order ionospheric error term which may indicate an inverse frequency dependence to the third power for scintillation. The same

authors also highlight that this error induced by phase scintillation can sometimes exceed the second order ionospheric range error term.

Both S4 and SigmaPhi are statistically meaningful estimates over 0.1-1 range.

On a global scale[q], scintillation activity is observed more often at the equatorial region, extending to 10-20^0 geomagnetic latitudes on both sides of the geomagnetic equator; and at the auroral latitudes beyond about 75^0 N-S geomagnetic latitude (Skone & Knudsen 2001). In addition to this latitudinal variation, occurrence of scintillation has temporal (post-sunset hours at the equatorial latitudes), seasonal, solar (most frequent occurrence during peak of Solar Cycle) and geomagnetic activity dependence (Hegarty et al. 2001; Beniguel et al. 2004).

(i) *Equatorial scintillation* is observed more often during local post-sunset hours with perturbation on both signal amplitude and phase, particularly during equinox months and the ascending and peak periods of the Solar Cycle. During solar maximum, the equatorial anomaly may be strongest around 21:00 local time with patches of depleted plasma regions ("bubbles[r]") during these post-sunset hours. Characteristic strong equatorial scintillation can occur due to small-scale irregularities forming within these patches (Skone & Knudsen 2001). Humphreys et al. (2009a) point out an essential feature of equatorial scintillation which is deep power fades (exceeding 15dB) accompanied by about half cycle phase variations, which they term as the "canonical fades".

(ii) *High latitude scintillation* (also referring to the auroral latitudes) is associated with geomagnetic storms, rather than presenting a daily pattern.

[q] *Appendix I contains details about the globally observed regions for scintillation.*

[r] *Equatorial Plasma Bubbles are structures of depleted TEC which form at the edges of equatorial anomalies; they are often accompanied by increased scintillation activity*

Occurrence and severity of scintillation is greater during a solar maximum (Doherty et al. 2000); however strong scintillation can be observed even during solar minimum (Seo et al. 2007).

3.2.1. SCINTILLATION EFFECTS

Scintillation affects the propagation of GNSS signals in the ionosphere when they pierce through localized "patchy" electron density structures, challenges the signal tracking loops of a GNSS receiver, can have an impact on the accuracy of the range measurements, and consequently influence the GNSS positioning solution. Strong scintillation may cause the dual-frequency signal tracking to drop to single frequency in which case the dual frequency first order ionospheric correction may not be possible (Hegarty et al. 2001). This can pose a problem not only to multi-frequency receiver users but also in, for instance, the networks of receivers providing ionospheric grid models for the single frequency users of SBAS such as EGNOS and WAAS.

Due to rapid fluctuations in the received signal phase, signal lock can be challenged (causing cycle slips or even complete loss of lock) in the tracking loop even if the signal-to-noise ratio does not drop drastically (Hegarty et al. 2001). It is also possible that during rapid phase fluctuations the signal lock can be maintained however be challenged if the received signal power level drops below a critical value ("signal-to-noise ratio threshold") due to amplitude fluctuations. This can explain the difficulty imposed by the equatorial scintillation in particular on the receiver tracking loops given that both the amplitude and phase of the received signal can be largely affected by scintillation at these low latitudes.

The level of scintillation can be classified in general as *weak*, *moderate* and *strong* in terms of the scintillation indices, S4 and SigmaPhi, despite the difficulty of drawing a line between the levels. Hegarty et al. (2001) suggest the values given in Table 3.1. for levels of equatorial scintillation in reference to the Wide-Band Model for ionospheric scintillation (Secan 1996) such that the values of S4 up to 0.4 can be regarded as weak, between 0.4 and 0.6 as moderate and between 0.6 and 0.9 as strong scintillation (and saturated for S4~1). Other classifications are also

possible, for instance, in Bureau of Meteorology (2013), weak scintillation is defined as S4<0.3, moderate when 0.3<S4<0.6 and strong when S4>0.6.

Scintillation level	S_4 on L1 (no unit)	σ_Φ on L1 (rad)
Strong	0.9	0.6
Moderate	0.6	0.3
Weak	0.4	0.2

Table 3.1. Possible definition of scintillation levels based on the scintillation indices, S4 and SigmaPhi, for the L1 signal.

The impact of the ionospheric scintillation on GNSS receivers can be in the form of cycle slips, or even complete loss of phase lock during severe scintillation, fading in signal power, navigation data bit errors (Loh et al. 1995; Knight et al. 1999), degraded range measurements and positioning solution (NovAtel 2012). Research conducted at NGI in the area of ionospheric scintillation has brought into attention the impact observed at the receiver tracking and positioning levels during moderate to strong levels of scintillation: Sreeja et al. (2011a) analyse equatorial scintillation events observed that challenge receiver signal tracking loops where the observed impact is greater with increasing scintillation level[s]; Aquino et al. (2009) focus on scintillation at the high latitudes claiming that the scintillation indices alone may not be adequate to assess the actual tracking errors due to scintillation and the authors apply suitable receiver tracking models (in this case the Conker model) to compute the jitter variance, which expresses the quality of the range measurements; in another work, involving the NGI, Strangeways et al. (2011) focus on high latitude scintillation where significant difference is noted in the scintillation level on the paths from different satellites received simultaneously and the results are shown for improvement of accuracy in relative positioning, which is achieved by applying the mitigation technique introduced by Aquino et al. (2009). Associated with the

[s] *As shown in the results of this thesis (Section 6.2.2.), the jitter variance at the output of the code and carrier tracking loops increases with the level of scintillation, making this statistical component a good metric to assess the impact of scintillation on the signal tracking performance.*

challenge in the phase tracking loops, it is possible to have missing carrier phase range measurements in the observations due to scintillation – this has been observed in the field collected data at low latitudes stations deployed in the CIGALA project.

It can be observed in open sky data that different satellite-receiver paths are affected by scintillation at different levels at a given time. Considering the receivers on a baseline or in a network, it is expected that the influence of scintillation on a receiver's signal will be different than the influence on another receiver's signal with the same satellites. Correlation of the observed effects between different signals ("link correlation") will depend on the relative signal path/baseline geometry and the ionospheric conditions. For instance, error due to the scintillation on the signal paths of two "nearby" receivers with the same satellite can be decorrelated in space and time. This decorrelation of the ionospheric errors under scintillation can be important for the differential GNSS techniques. For instance, scintillation may cause the ionospheric corrections computed by the reference station to be less accurate/applicable for the rover due to "spatial and temporal decorrelation of the errors" over (even) short distances or time intervals, respectively. In this case (assuming scintillation impact on range measurements), for instance, a user who could during non-scintillation times benefit from the corrections provided by a reference station at a certain distance from the reference station may fail to achieve similar positioning accuracy with the corrections at times of scintillation. This can be associated with two reasons:

1) Corrections may not correspond well to the user's location (assuming that the signal paths at the reference station and those of the rover pierce through considerably different parts of the ionosphere during a scintillation event to the same satellites),

2) Corrections may not be relevant to the rover by the time they are provided.

These two points related with link correlation during scintillation are not investigated in this thesis.

Significant loss of redundancy in the number of tracked satellites can occur during a scintillation event. For instance, a solar radio burst can leave receivers unable to achieve a positioning solution due to tracking fewer than 4 satellites, as observed on 6 December 2006 by Cerruti et al.

(2008) (Fig. 3.15.), when peak positioning errors in the horizontal and vertical directions of about 20 and 60 m, respectively, were observed. Degradation in SNR exceeding 25 dB were also observed by the authors during this solar burst, which was strong enough to substantially degrade GPS tracking and positioning accuracy. Simultaneous loss of lock to a significant number of satellites can the cause discontinuity in GNSS service (Cerruti et al. 2008).

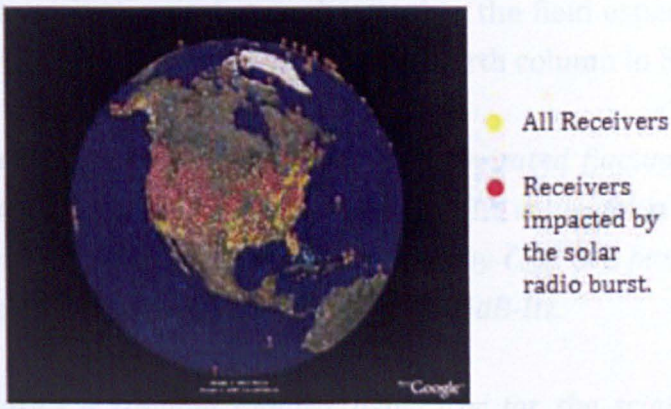

Figure 3.15. Impact of the solar radio burst on 6 December 2006: yellow markers indicate GPS receivers and red markers show the receivers tracking less than 4 satellites during the peak of the burst.

A point of interest is the level of impact a certain level of scintillation can have on the range measurements. The Cornell Scintillation Model (CSM)[t] can help to explain this point. CSM maps the scintillation induced variations in signal phase onto variations in the carrier phase ranges, and those in signal amplitude onto variations in the received signal intensity. Variations in the carrier phase ranges can help to explain the above raised point; and to illustrate this the CSM is run with different input values (to indicate a different level of scintillation) and its outputs of time series for the carrier phase ranges and signal intensity are plotted in Fig. 3.16. The levels of scintillation is determined by two input parameters, S4 and Tau0 (τ_0) – former is the amplitude scintillation index and latter is a time parameter which is related with the rapidity of phase fluctuations (smaller Tau0 corresponds to a more rapidly changing phase, vice versa). Each column of plots in Fig. 3.16. refer to a set of S4 and Tau0 that is used to run the CSM; as such there are four runs where S4=0.3 and Tau0=1.9s refers to weak scintillation and S4=0.9 and Tau0=0.1s to strong scintillation (representing a very strong case owing to the very small value given to

Tau0). Two types of time histories are obtained from the CSM: variations in the carrier phase range (m) and in signal intensity (dB-Hz) as shown in the first and second row in Fig. 3.16., respectively.

It can be seen in Fig. 3.16. for the CSM outputs for different scintillation levels that the scintillation induced fluctuations in carrier phase can lead to (most reasonably) cm level variations in the phase measurements and deep fades in the signal level as much as -30dB-Hz. The model outputs may not be as realistic as what is observed in the field especially for the cases of saturating level of scintillation (the fourth column in Fig. 3.16.).

N.B.: Elevation angle dependence for the generated fluctuations can be modelled in terms of the expected nominal C/N_0 value; for a set of S4 and Tau0 parameters the time series generated by CSM are more degrading for an expected nominal CN0 of 35 than for 45dB-Hz.

N.B.: CSM uses a random number generator for the scintillation time series. Every time CSM is run for a pair of S4 and Tau0, the "seed" for this random number generator is different, therefore even for the same pair of S4 and Tau0, each run of CSM returns different scintillation time series. In other words, the fades and carrier phase variations are different in each run (for the same pair of S4 and Tau0); indeed significant differences can be observed as in the power fades. If the particular code "scintModel04.m" in CSM MatLAB package is edited to start with "st=randn('state')" command line and the instances of "randn" function in the same code are edited to precede with the command line "randn('state', st)", then different runs of CSM for the same pair of S4 and Tau0 return the same time series.. This suggestion aims to provide repeatability of scintillation time series for the same pair of S4 and Tau0 and comparability of the time series for different pairs of S4 and Tau0 in every run of CSM.

[t] *CSM is described in greater detail in Section 5.1.2. to which the reader is recommended to refer to for a better understanding of this model.*

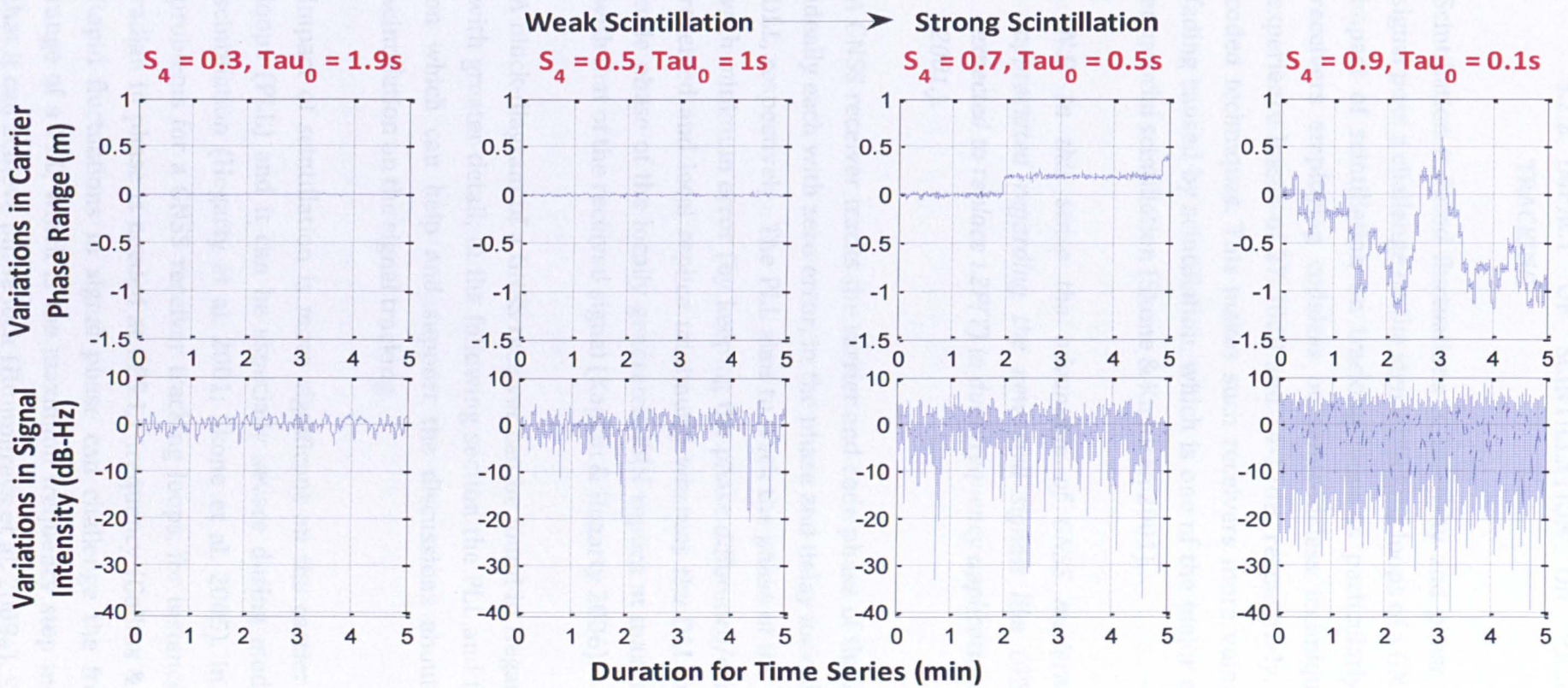

Figure 3.16. Generated time series in carrier phase (*top row*) and in signal intensity (*bottom row*) obtained from CSM are shown for weak (*leftmost column*) to strong (*rightmost column*) scintillation levels which are determined by the pair of S_4 and Tau_0 parameters. While a small S_4 coupled with a large Tau_0 gives weak scintillation level, a large S_4 with a small Tau_0 corresponds to strong scintillation effects.

.

3.2.2. IMPACT OF SCINTILLATION ON RECEIVER SIGNAL TRACKING

Scintillation induced fluctuations in intensity and phase of the received signal pose a challenge on the signal tracking loops of a GNSS receiver. The impact of scintillation on tracking loops is particularly important for receivers employing codeless or semicodeless techniques, which may experience losses of 27-30dB and 14-17dB, respectively, compared with coded techniques. This makes such receivers more vulnerable to signal fading caused by scintillation, which is one of the major consequences of equatorial scintillation (Skone & Knudsen 2001).

N.B. In this sense the advantage of GNSS modernization can be appreciated regarding the new civil signals like GPS L2C which is expected to replace L2P(Y) in dual frequency applications (Leandro et al. 2001.).

A GNSS receiver tracks the carrier and code phase of the incoming signal, ideally each with zero error, in the phase and delay locked loops, PLL and DLL, respectively. The PLL aims to track the phase of the incoming signal with minimum error (by keeping the phase difference/error between the received and local replica minimum) whereas the DLL tries to keep the code phase of the locally generated PRN replica at maximum correlation with that of the received signal (Kaplan & Hegarty 2006).

A block-diagram of a GNSS receiver can be found in Hegarty et al. (2001) with greater detail; in the following section the PLL and DLL are focused on which can help and support the discussions about the impact of scintillation on the signal tracking.

Impact of scintillation is more significant on the carrier phase tracking loops (PLL) and it can be especially severe during moderate to strong scintillation (Hegarty et al. 2001; Skone et al. 2005). In order to cause problems for a GNSS receiver tracking loops, for instance, a change of 1 radian in phase is needed at GPS L1 frequency (Collins & Langley 1996). Rapid fluctuations in signal phase can challenge the frequency pull-in range of a PLL, which is the maximum frequency step input to a PLL so that it can achieve phase lock (Humphreys et al. 2009a). Scintillation may

increase the phase tracking loop error variance, cause loss of lock on carrier phase and possibly cycle slips (Gupta 1975; Ascheid & Meyr 1982; Conker et al. 2003; Gardner 2005; Humphreys et al. 2009a). Scintillation can cause L1 and L2 carrier phases to lose coherence which would invalidate the assumption of similar dynamics on L1 and L2 that enables use of very narrow loop bandwidths for semi-codeless L2 carrier tracking. Hegarty et al. (2001) show that the DLL is in general more robust to both amplitude and phase scintillation than PLL.

Previous works show that at the low latitudes amplitude scintillation and long-term signal fades challenge the signal tracking (El-Arini et al. 2003; Ganguly et al. 2003; Morrissey et al. 2004); and at the high latitudes large phase variations cause problem at the receiver end (Pi et al. 2002; Skone et al. 2005).

3.2.2.1. INSIDE OF A GNSS RECEIVER

A basic introduction to the details of a generic GNSS receiver can assist the understanding of how scintillation affects the signal tracking loops (Fig. 3.17.). A GNSS signal arriving at the antenna goes through an RF front-end processing which includes (details not shown in Fig. 3.17.) preamplification of the received signal rejecting noise and out-of-band interference. After preamplification, the frequency of the RF signal is brought *down* to a convenient intermediate frequency. The resultant frequency signal goes through into the tracking loops of the receiver (number of the loops given by the number of channels in a receiver). More details about the tracking loops are provided next; outputs from the tracking loops "Pseudoranges, pseudorange-rates" are shown in Fig. 3.17. as input to the navigation processor which yields the position, velocity and time (PVT) information from the receiver.

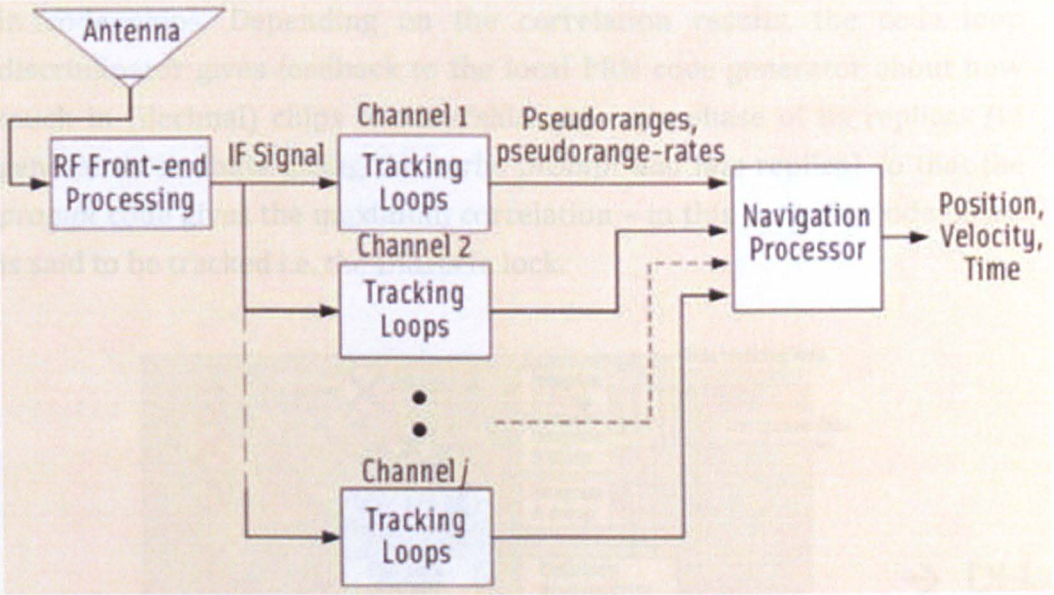

Figure 3.17. Receiver architecture for a generic GNSS receiver (Lashley & Bevly 2009).

The DLL and PLL are the tracking loops for the signal code and carrier phase, respectively. Figure 3.18. illustrates the two loops generically (different receivers can have specific designs of the loops in terms of the feedback between the PLL and DLL) which are explained next.

The PLL aims to keep the carrier phase difference between the incoming and the local replica signals (i.e. the phase error) minimum, ideally zero. Any misalignment of the prompt I,Q components from the correlators are detected by the carrier loop discriminator (Mao et al. 2008). The phase error indicates to the PLL loop filter how much the carrier phase adjustment is necessary so that the phase error can be minimized. The loop filter's output is input to the oscillator (mostly numerically controlled) which adjusts the frequency of its oscillation (Abramovitch 2002). A small phase error is assumed in a PLL so that a linearization of the phase error can be possible, i.e. it can be analyzed in the linear regime. However, scintillation can cause large phase errors which can bring the PLL out of the linear regime. This renders the models that are based on the PLL linearity invalid, which is also the case of the Conker model which assumes weak scintillation i.e. small carrier phase changes (Knight 2000).

The DLL aims to keep the prompt code phase of the local PRN code replica at the maximum correlation with the code phase of the incoming signal. This is achieved with the correlators which *compare* the two PRNs shifted

in code chips. Depending on the correlation results, the code loop discriminator gives feedback to the local PRN code generator about how much in (decimal) chips to vary/shift the code phase of its replicas (in general three shifts giving the early, prompt and late replica) so that the *prompt* code gives the maximum correlation – in this case, the code phase is said to be tracked i.e. the DLL is in lock.

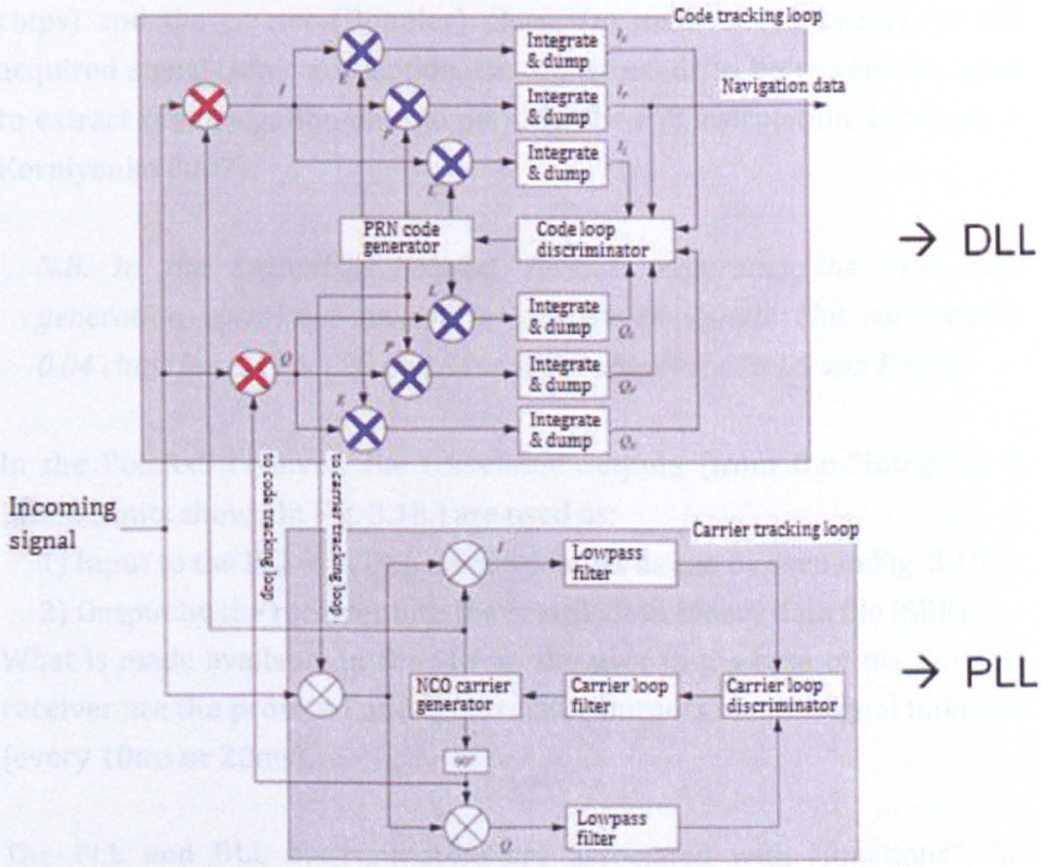

Figure 3.18. Generic block diagrams for the DLL and PLL (Andreotti 2011).

The intermediate frequency signal arriving at the tracking loops is first multiplied (indicated with red crosses in the DLL part of Fig. 3.18.) with the cosine and sine carrier wave replicas to wipe-off the carrier in the signal. Ideally, the replica carrier wave is a *good* match to the carrier of the incoming signal so that this wipe off is successful. This multiplication in the two arms sets up the In-phase (I) and Quadra-phase (Q) arms which are termed so due to the 90^0 shift between them. The signal in I and Q arms is next stripped off the PRN code that is achieved through multiplication with the locally generated PRN code (indicated with blue crosses in the DLL part of Fig. 3.18.) – there are in general 3 replicas for each arm: early, prompt and late codes that are stepped in decimal chips.

The resulting 6 signal components[u] (3 for each of I and Q) go into the *correlators* named as "Integrate[v] & Dump" units in the DLL (Fig. 3.18.).

When the time (PRN code shift) alignment of the incoming PRN code and local replica is achieved, (and the Doppler frequency is retrieved), the signal is said to be "acquired" - the receiver knows which satellite is visible (for a particular channel, Fig. 3.17.), the code phase (in units of chips) and the carrier (Doppler) phase (in units of frequency) for the acquired signal. After acquisition, the signal needs to be tracked in order to extract the navigation data to perform the PVT calculation. (Sharawi & Korniyenko 2007).

N.B. In the Septentrio PolaRxS receiver regarding the PRN code generation, correlator spacing is 40ns for all signals. This corresponds 0.04 chips for L1C/A, L2C and E1; and 0.4 chips for GPS L5 and E5a/b.

In the PolaRxS receiver, the correlator outputs (from the "Integrate & Dump" units shown in Fig. 3.18.) are used as:

1) Input to the PLL and DLL discriminators as can be seen in Fig. 3.18.
2) Output by the receiver into the scintillation binary data file (SBF).

What is made available in the SBF to the user in the case of the PolaRxS receiver are the prompt I and Q correlator outputs for the signal intensity (every 10ms or 20ms).

The PLL and DLL discriminators are associated with "functions"; for instance, in the case of the PolaRxS receiver the PLL discriminator performs the mathematical *atan* (arctangent) function for the GPS L1C/A signal and *atan2*[w] (*extended arctangent* function, which enables a wider

[u] *Depending on the code shift (i.e. the code delay) that is applied by the PRN code generator, each I and Q arm has that many subcomponents.*

[v] *"Summation in discrete units" is more suitable for a digital signal.*

[w] *By this arrangement, the lock range of L2C, L5 PLL becomes twice as large as that of L1C/A and this in turn provides lower probability of cycle slips for L2C, L5 compared to L1C/A.*

linear tracking range) for the L2C, L5 signals (Septentrio private communication). From the noise aspect of the PLL discriminator, there is no significant difference between these two types of functions associated with the PLL discriminator. This hints that the calculations involving the *atan* function can be applied for the *atan2* function as well.

The discriminator output is the difference between what is measured and received; this difference is also referred to as the error. From the PLL discriminator, output is an estimate of the phase error for the received and local replica signal; and from the DLL discriminator it is the error in the code phase measured for the received and local replica. The discriminator should be ideally zero. In the case of the PLL, a *small* phase error is assumed so that it can be analyzed in the *linear* regime. However, linearity of the error at the PLL output may not hold during strong scintillation; large phase errors can bring the PLL out of the linear regime and during rapid large phase changes - characteristic of canonical fading (Humphreys et al. 2009a), the PLL behaviour may no longer be in the linear regime and the loop signal-to-noise ratio may no longer be constant but vary due to amplitude scintillation (Forte 2011). This renders the models that are based on PLL linearity invalid, as in the case of the Conker model which assumes small carrier phase changes during scintillation (Kaplan & Hegarty 2006).

In a generic GNSS receiver, what follows the discriminators are the loop filters (although not shown in Fig. 3.18. for the DLL, a filter can be assumed after the code loop discriminator just as that which takes input from the carrier loop discriminator in the PLL). Function of the filters in the DLL and PLL is to remove the noise from the estimated code and carrier phase errors, respectively. The phase error at the discriminator output informs the PLL loop filter how much to adjust the carrier phase and with this the loop filter updates the oscillator to adjust the frequency of its oscillation (Abramovitch 2002).

Receiver simulations performed by Hegarty et al. (2001) show that the "non-coherent" DLL (where the DLL is able to track the PRN code with the navigation data bits present and the PLL not necessarily being in lock) is in general very robust to amplitude and phase scintillation effects; whereas the PLL is more susceptible to the scintillation effects.

The correlators, code loop discriminator and code loop filter determine two important performance characteristics for the DLL: the DLL thermal noise error and the maximum LoS dynamic stress (such as scintillation) threshold. Although the PLL can be considered as the weak link regarding the dynamic stress, the DLL (the more robust to this stress) aiding the PLL would be unfavourable because the thermal noise figure of DLL is orders of magnitude greater than that of the PLL (Kaplan & Hegarty 2006).

Optimum PLL design aims to reduce the effect of dynamics in the presence of additive white noise. When the STD of phase jitter (while tracking GPS L1 C/A) is greater than about 15^0, the phase discriminator output can no longer be considered in the linear regime. In this case, the PLL is more likely to lose lock on the tracked signal (Kaplan & Hegarty 2006).

Improved tracking loop models can minimize phase errors and loss of lock during scintillation (Skone et al. 2005); loss of lock can be a problem in particular for narrow bandwidth tracking loops. Robustness against high levels of scintillation can be handled in the receiver design; for instance, a "scintillation-intelligent" receiver can update its tracking loop bandwidth i.e. can automatically adjust the tracking loop bandwidth to account for fast signal dynamics due to strong scintillation (Fu et al. 1999; Morrissey et al. 2004). Such adjustment can be based on its estimates of scintillation indices or the jitter variance at DLL and PLL outputs, or positioning error during scintillation.

3.2.2.2. RECEIVER SIGNAL TRACKING PERFORMANCE DURING SCINTILLATION

Signal tracking performance of a GNSS receiver can provide useful information in terms of accuracy and reliability of the range measurements. As described in Section 3.2.2.1, code and carrier phase tracking loops can have difficulty in maintaining lock on the code and carrier phases, respectively, during scintillation. This difficulty can lead to an increase in the variance of the tracking error (jitter) at the output of the loops (Hegarty et al. 2001; Conker et al. 2003). This variance is a good measure of the scintillation effect on the tracking loops (Conker et al. 2003). Scintillation makes estimation of this variance not a trivial task.

Based on the earlier work by Knight & Finn (1998) and Hegarty et al. (1999), Conker et al. (2003) propose a model that is sensitive to the scintillation effects on the signal tracking performance. For modelling the impact of scintillation, Conker et al. (2003) focus on the code and carrier phase tracking loops (DLL and PLL, respectively) which enable GNSS receivers to handle weak-to-moderate levels of scintillation. In their approach, the impact of scintillation is modelled in terms of DLL and PLL jitter variances (as an increase due to scintillation): In the case of the DLL jitter variance, the authors consider the thermal noise and in the case of the PLL jitter variance, the model focuses on contribution from three error sources: thermal noise, phase variations and oscillator noise (Conker et al. 2003).

The scintillation sensitive model suggested by Conker et al. (2003) to calculate the jitter variance for a 3rd order PLL and a 1st order DLL can be considered as state-of-the-art (Eq. 18 - Eq. 23). The authors considered some assumptions while devising their scintillation sensitive tracking model:

(i) no correlation is considered between amplitude and phase scintillation while modelling the jitter variance at the PLL output,

(ii) phase scintillation is assumed to have little effect on the DLL jitter therefore the DLL jitter variance is modelled in terms of thermal noise, amplitude scintillation and interference - independent of phase scintillation,

(iii) the tracking loop signal-to-noise ratio is taken to remain constant (although in actual physical conditions this may vary due to amplitude scintillation).

This model represents statistically the influence of scintillation in the error variances at the output of the code and carrier phase tracking loops. In this sense, the impact of stronger scintillation manifests itself as greater variance on the tracking loops performance. Greater variance can be associated with a less healthy tracking that can in turn cause less accurate and reliable measurements especially under strong levels of scintillation. While less accuracy may mean more erroneous range measurements that would affect the positioning solution, less reliability means decreased ability to detect outliers in the observations that can also affect the positioning solution.

The jitter variance for a 3rd order PLL for GPS L1 is given according to the Conker model as:

$$\sigma^2_{\phi_\varepsilon} = \sigma^2_{\phi_S} + \sigma^2_{\phi_T} + \sigma^2_{\phi_{OSC}} \qquad \text{(Eq. 18)}$$

where the first term on the RHS of Eq. 18 is associated with scintillation induced phase variations:

$$\sigma^2_{\phi_S} = \frac{\pi T}{k f_n^{p-1} \sin\frac{[2k+1-p]\pi}{2k}} \qquad \text{(Eq. 19)}$$

and the second term on the RHS of Eq. 18 is related with modelling the impact of amplitude fading in terms of (an increase in) the thermal noise (Conker et al. 2003):

$$\sigma^2_{\phi_T} = \frac{B_n}{(c/n_0)_{L1C/A}(1-S4^2_{L1})}\cdot\left(1+\frac{1}{2\eta(c/n_0)_{L1C/A}(1-2S4^2_{L1})}\right) \qquad \text{(Eq. 20)}$$

The third term on the RHS of Eq. 18, $\sigma^2_{\phi_{OSC}}$, is the effect of the oscillator noise which is suggested as about $(0.1^{rad})^2$ (Conker et al. 2003).

In the term $\sigma^2_{\phi_S}$, p (inverse power law of phase power spectral density, PSD, no units) and T (spectral power of phase PSD at 1Hz, in units of rad^2/Hz) are the previously mentioned scintillation spectral parameters[x]; k is the loop order (3 in this case for PLL); f_n is the natural frequency of the loop (1.91Hz for a 3rd order PLL); B_n is the one-sided loop bandwidth (10-15Hz); c/n_0 is the fractional form of C/N_0 ($c/n_0 = 10^{0.1\ C/N0}$); η is the predetection integration time (20ms for L1 C/A code); $S4_{L1}$ is the S4 measured on the L1 carrier.

[x] *The spectral parameters, p and T, can be estimated from the phase spectrum, where p is the negative of the slope of the line fit on the phase PSD and T is the value of the PSD at 1Hz. Another technique for estimating p and T makes use of the scintillation indices (Strangeways 2009). Whereas the former technique requires FFT on the high rate carrier phase data, the latter has less computational burden as it avoids*

FFT. Effect of the (lower and higher) cutoff frequencies while estimating p in the former technique is discussed in Strangeways et al. (2011). Work related with estimation of p and T from the scintillation indices was presented by Elmas et al. (2010a) and Elmas & Aquino (2010b).

In the case of a 2nd order semi-codeless phase tracking loop for GPS L1-aided L2 carrier, the RHS components of Eq. 18 are valid except that the thermal noise term now depends also on S4 on the GPS carrier L2, $S4_{L2}$:

$$\sigma_{\phi_T}^2 = \frac{B_n}{(c/n_0)_{L2P}(1-S4_{L2}^2)}\left(1+\frac{1}{2\eta_Y(c/n_0)_{L1P}(1-2S4_{L1}^2)}\right) \qquad \text{(Eq. 21)}$$

with $B_n \sim 0.25$Hz and $\eta_Y = 1.91\mu$s for the P(Y) code (Conker et al. 2003).

The jitter variance of a 1st order DLL for GPS L1 accounting for the impact of scintillation is modelled in terms of an increase in the thermal noise:

$$\sigma_\tau^2 = \frac{B_n d\left[1+\frac{1}{\eta(c/n_0)_{L1C/A}(1-2S4_{L1}^2)}\right]}{2(c/n_0)_{L1C/A}(1-S4_{L1}^2)} \qquad \text{(Eq. 22)}$$

where d is the correlator spacing in C/A chips (such as 0.1 chips) and B_n is the DLL bandwidth in Hz (0.25Hz in PolaRxS receiver).

In the case of a 1st order DLL for GPS L1-aided L2 carrier, Eq. 22 is modified to depend also on $S4_{L2}$:

$$\sigma_\tau^2 = \frac{B_n\left[1+\frac{1}{2\eta_Y(c/n_0)_{L1P}(1-2S4_{L1}^2)}\right]}{2(c/n_0)_{L2P}(1-S4_{L2}^2)} \qquad \text{(Eq. 23)}$$

Similar modelling is also suggested by Kim et al. (2001) for the tracking error variance of GPS L5 signal during scintillation. For a receiver tracking the phase of the GPS L5 carrier (i.e. a PLL is considered) which has the I, Q components, the variance at the PLL output is:

$$\sigma_{\phi_\varepsilon}^2 = \frac{\pi T}{k f_n^{p-1} \sin\frac{[2k+1-p]\pi}{2k}} + \sigma_{\phi_T}^2 + \sigma_{\phi_{osc}}^2 \qquad \text{(Eq. 24)}$$

where the oscillator noise term is about $(0.122^{rad})^2$. The thermal noise term has two cases depending on which signal component of L5 is tracked; these are shown in Eq. 25, where the formulation for the data-free (i.e. no navigation data) component (represented by "*Q*") and data component (represented by "*I*") are provided.

$$\sigma_{\phi_T}^2 = \begin{cases} \dfrac{B_n}{a_1 (c/n_0)_{L5}(1-S4_{L5}^2)}\left(1+\dfrac{1}{2a_1\eta_1(c/n_0)_{L5}(1-2S4_{L5}^2)}\right), I \\ \dfrac{B_n}{a_2 (c/n_0)_{L5}(1-S4_{L5}^2)}, Q \end{cases} \qquad \text{(Eq. 25)}$$

where a_1 and a_2 refer to the ratio of the total signal power allocated to each signal component ($a_1+a_2=1$) and for the GPS L5, $a_1=a_2=1/2$ (Kim et al. 2001).

N.B. The I and Q signal components in Eq. 25 are different from what is referred to as I/Q post-correlator data described in Section 4.2. In Eq. 25, they refer to the broadcast signal components with (I) and without (Q) the navigation data.

As seen in Eq. 25, $S4_{L5}<0.707$ if the *I* component is tracked, whereas $S4_{L5}<1$ for the *Q* (data free) component. This is an immediate benefit of the data-free signal component to signal tracking performance.

For a receiver tracking the code on GPS L5 (i.e. a DLL is considered), the effect of scintillation is represented as an increase in the thermal noise. Similar to Eq. 22, the jitter variance for DLL due to scintillation is given (in units of L5 data code chips squared) as (Kim et al. 2001):

$$\sigma_\tau^2 = \begin{cases} \dfrac{B_n d\left[1+\dfrac{1}{a_1\eta_1(c/n_0)_{L5,I}(1-2S4_{L5}^2)}\right]}{2a_1(c/n_0)_{L5,I}(1-S4_{L5}^2)}, I \\ \dfrac{B_n d}{2a_2(c/n_0)_{L5}(1-S4_{L5}^2)}, Q \end{cases} \quad \text{(Eq. 26)}$$

N.B. Eq. 25 and Eq. 26 are applicable in the case of the new GNSS signals which have I and Q signal components. It can be further noticed that these equations are applicable for S4<0.707 and S4<1 in the case of the I and Q components, respectively.

Although the Conker model is easy to implement, there are two immediate concerns with its use:

(i) Its limited applicability to weak-to-moderate scintillation levels can be seen in the thermal noise and DLL terms. Eq. 20 and Eq. 22 are only valid for $S4_{L1} < 0.707$, whereas Eq. 21 and Eq. 23 for $S4_{L1} < 0.687$. Regarding this limitation, the authors of the model claim that such instances of $S4_{L1} > 0.707$ indeed do not pose a problem since, according to their model, LoL occurs when $S4_{L1} > 0.707$ thus error in the ranges or the DLL jitter variance becomes irrelevant. However, in the open sky data analyzed during this PhD it has been observed in the scintillation data collected in the field that there are instances of $S4_{L1} > 0.707$ while the lock on the carrier is still maintained (It is anticipated that the carrier tracking is challenged yet the lock is kept). Therefore, this limitation in the Conker model cannot be neglected.

(ii) Scintillation spectral parameters *p* and *T* are needed in the first RHS component of Eq. 18. Retrieving accurate p and T values can be crucial, in particular for real-time use of the model: high rate (50Hz) signal phase and intensity data from scintillation specific receivers like the NovAtel *GSV4004B* or Septentrio *PolaRxS* need to be manipulated in the frequency domain to obtain p and T (Aquino et al. 2007) which is computationally intensive and availability of such data remains as an extra issue.

Such an approach is valid for up to moderate levels of scintillation; in severe cases the assumption of PLL linearity breaks down and the mathematical models behind this approach are no longer applicable as

shown below. In this thesis, one of the tasks has been to address the limitation of these mathematical models because assessment of signal tracking performance should be possible even during strong scintillation conditions – as long as signal is tracked.

One reason why the jitter variance is a subject of interest is its use for mitigation of scintillation induced errors in GNSS positioning as shown in earlier works by Aquino et al. (2009). Estimates for the loop variances can be used to assign weights on the GNSS observations to account for scintillation induced errors in positioning (Aquino et al. 2009). However, the above raised issue about limitation in the use of the Conker model to moderate to strong levels of amplitude scintillation prevents an "all time, any scintillation level" application of the model. For moderate-to-strong levels of amplitude scintillation can occur in the local post-sunset hours at the low latitudes especially around the peak of the Solar Cycle (Doherty et al. 2001; Petrie et al. 2011; ICTP 2013). From the mitigation work point of view, as focused on in this thesis, an alternative approach has been introduced (Section 4.2.) to overcome this limitation in estimating the DLL jitter variance for continuous evaluation considering any GNSS signal and ideally during any level of scintillation as long as the signal is tracked.

In this chapter, the diffractive and refractive effects of the ionosphere are discussed giving the mathematical background for the effects and within the scope of the new signals. Nature of the ionosphere (inhomogeneous, anisotropic and layered structure) is described to facilitate the understanding of how the ionosphere interferes with the propagation of GNSS signals.

- In a mathematical approach, the total error due to ionospheric refractivity is provided introducing the first and HO error terms for pseudorange and carrier phase measurements. The recent work in literature was reviewed for the formulation of the second and third order error terms.
- Based on this mathematical approach, the error bounds are estimated for the error terms considering reasonable approximations for the parameters involved with these terms, such as the geomagnetic field magnitude for Iono2, and maximum electron density for Iono3.

- Although mostly neglected as an error source to ranging, the ray bending error is also described - its negligible error contribution can help to understand why this error term is not considered in general.
- The diffractive effects of the ionosphere, scintillation in particular, are discussed from the aspects of background solar/magnetic conditions, global regions where the scintillation effects are more significantly observed, impact on GNSS signals and possible degradation in receiver signal tracking performance. It is attempted to suggest a qualitative relation between the level of scintillation and the magnitude of perturbations in signal intensity and carrier phase fluctuations, making use of the CSM.
- With a brief introduction to the architecture of a typical GNSS receiver's tracking loops, impact of scintillation on receiver signal tracking performance is also discussed. Within this scope, the scintillation sensitive model of Conker et al. (2003) is described for evaluating the tracking error variance of the code and carrier phase tracking loops, drawing attention to the disadvantage of the model in terms of its limited applicability for strong level of amplitude scintillation.

CHAPTER 4

4. EXPLOITING NEW GNSS SIGNALS TO MONITOR, MODEL AND MITIGATE THE IONOSPHERIC EFFECTS

This section takes the ionospheric effects introduced in Section 2 to a level of investigation putting emphasis on the *contribution* of new GNSS signals. A theoretical approach is taken while discussing how GNSS modernization can benefit the tasks of monitoring, modelling and mitigating the ionospheric effects.

This chapter starts with a focus on the refractive ionospheric effects where the first order approximation is discussed from a new signals point of view. Then, the second order approximation is considered which takes the common practice of dual frequency ionosphere-free linear combination to a triple frequency level. Investigation of the refractive effects finally considers the bending effect in a theoretical approach with consideration of the new GNSS signals. The chapter then addresses the diffractive effects where focus is placed on a proposed alternative technique for assessing signal tracking performance during scintillation, in particular when the model of Conker is not applicable. The foundation of this technique is explained here, reserving the results based on open sky data to Chapter 6. This chapter closes with consideration of the new satellites from an ionospheric effects perspective.

4.1. NEW SIGNALS AND THE IONOSHERIC REFRACTIVE EFFECTS

As the ionospheric effect on GNSS signals is frequency dependent, availability of new GNSS signals within the GNSS modernization offers further advantages for correcting the ionospheric errors: Wang et al. (2005) consider a "triple frequency" approach and suggest that both estimation and elimination of the higher order ionospheric error terms can benefit from the third signal L5 (or E5 as referred to in Galileo); Richert & El-Sheimy (2007) show that elimination of the first order ionospheric effect using the dual frequency IF observable can be modified to include the new L5 signal code and phase observables and also draw attention to the choice of coefficients while linearly combining observations on three distinct frequencies that can yield significantly

different accuracies in the resultant ionosphere-free observable and Lightsey & Humphreys (2011) emphasize the importance of the new GPS L2C signal for the L1, L2 linear combination to eliminate the first order ionospheric error. In this section, a similar investigation is pursued in order to put forward how the new GNSS signals can benefit the methods that account for the refractive and diffractive ionospheric effects.

4.1.1. FIRST ORDER APPROXIMATION

In a first order approximation, observations on two signal frequencies considering only the first order ionospheric error term are linearly combined in order to eliminate the ionospheric error to the first order, in this case. Since only the Iono1 term is taken into account in the initial observations, there remains a residual ionospheric range error in the IF observable. In the current practice, such dual frequency approach is based on the L1 and L2P(Y) code and phase observations where a semi-codeless (or codeless) tracking approach can be applied since the civil users cannot decrypt the L2P(Y) signal. As mentioned in Appendix C semi-codeless tracking is not advantageous due to a greater level of noise and dependence of acquisition of L2 P(Y) on the L1 signal (Hegarty et al. 2001). With the advent of the new signals like GPS L2C and L5, full coded tracking is possible which can eliminate disadvantages associated with L2P(Y).

Separating only the (frequency dependent) ionospheric error term and including all other (frequency-independent) error terms with the geometric range "ρ", the pseudorange observation equation for a signal frequency "i" can be written as:

$$PR_i = \rho + Iono_i \qquad \text{(Eq. 27)}$$

The ionospheric error "$Iono_i$" includes indeed all three orders of error terms (Iono1, Iono2, Iono3) as well as the ray bending effect which can be neglected for convenience here. The first order approximation considers only the Iono1 term for each observation (i.e. $Iono_i$ taken as Iono1 only), and in this case the linear combination based on the L1 and L2 observables leads to the IF observable "$PR_{IF\ 1,2}$" as:

$$PR_{IF\,1,2} = \frac{f_1^2}{f_1^2-f_2^2} \cdot (\rho + Iono1_1) - \frac{f_2^2}{f_1^2-f_2^2} \cdot (\rho + Iono1_2) = \rho \qquad \text{(Eq. 28)}$$

N.B. There is no difference in this notation when L2 tracking is for the P(Y) code or the new C code on L2.

However, in practice $Iono_i$ has a contribution from the HO terms as well, and the more complete result for the above linear combination becomes:

$$PR_{IF\,1,2} = \frac{f_1^2}{f_1^2-f_2^2} \cdot (\rho + Iono1_1 + Iono2_1 + Iono3_1) - \frac{f_2^2}{f_1^2-f_2^2} \cdot (\rho + Iono1_2 + Iono2_2 + Iono3_2)$$

$$= \rho + \frac{eB_0 cos\theta}{\pi m} \cdot \frac{K \cdot STEC}{f_1^2-f_2^2} \cdot \left(\frac{1}{f_1} - \frac{1}{f_2}\right) + \frac{3\eta N_{max}}{2} \cdot \frac{K^2 STEC}{f_1^2-f_2^2} \cdot \left(\frac{1}{f_1^2} - \frac{1}{f_2^2}\right) \qquad \text{(Eq. 29)}$$

As can be seen in the RHS Eq. 29, there is contribution from Iono2 and Iono3 error terms, referred to as RRE, which is neglected in the first order approximation. Figure 4.1. shows *residual error due to Iono2* in the L1, L2 IF observable: maximum error shown is about 0.06m which is about 72% of the maximum error for Iono2 on GPS L1 for a receiver at the mid-latitudes – as indicated by Morton (2008).

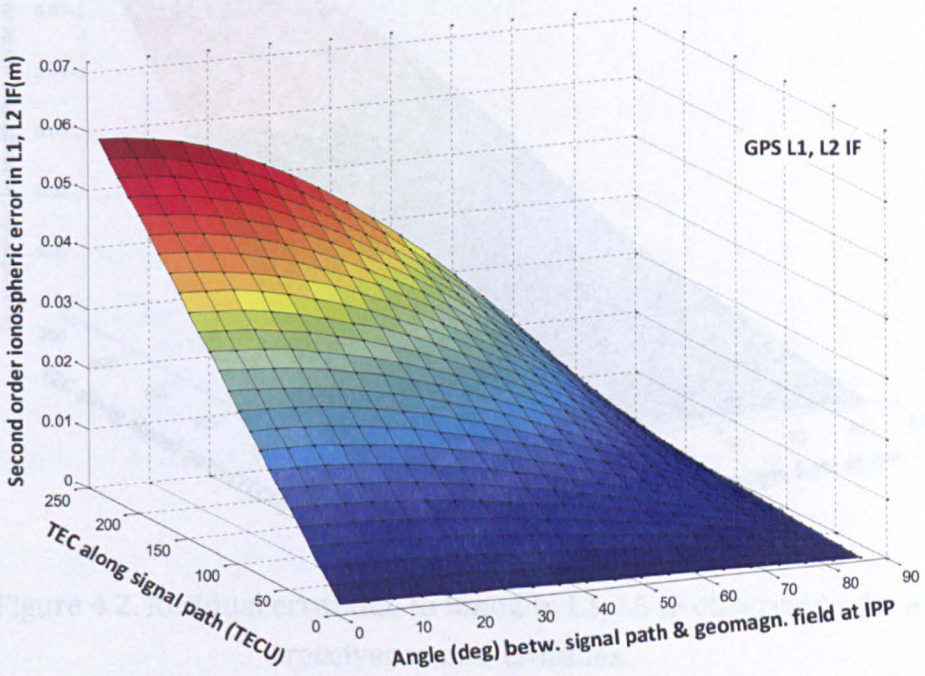

Figure 4.1. Residual error due to Iono2 in L1, L2 IF observable, for a receiver at mid-latitudes.

It is possible to create the IF observable from observations on L1 and L5 signals. In this case, the residual range error (due to Iono2 and Iono3) that is neglected in the first order approximation is given by the second and third terms in the RHS of the equation for $PR_{IF\ 1,5}$:

$$PR_{IF\ 1,5} = \frac{f_1^2}{f_1^2-f_5^2} \cdot PR_1 - \frac{f_5^2}{f_1^2-f_5^2} \cdot PR_5$$

$$= \rho + \frac{eB_0 cos\theta}{\pi m} \cdot \frac{K \cdot STEC}{f_1^2-f_5^2} \cdot \left(\frac{1}{f_1} - \frac{1}{f_5}\right) + \frac{3\eta N_{max}}{2} \cdot \frac{K^2 STEC}{f_1^2-f_5^2} \cdot \left(\frac{1}{f_1^2} - \frac{1}{f_5^2}\right) \qquad \text{(Eq. 30)}$$

As before, the first order approximation would neglect the inverse frequency dependent terms in the RHS of the Eq. 30, however this residual error can be significant subject to ionization levels. Figure 4.2. shows the *residual error due to Iono2* in the L1, L5 IF observable: the maximum error shown is about 0.062m which is about 77% of the maximum error for Iono2 on GPS L1 for a receiver at the mid-latitudes (Fig. 3.6. in Section 3).

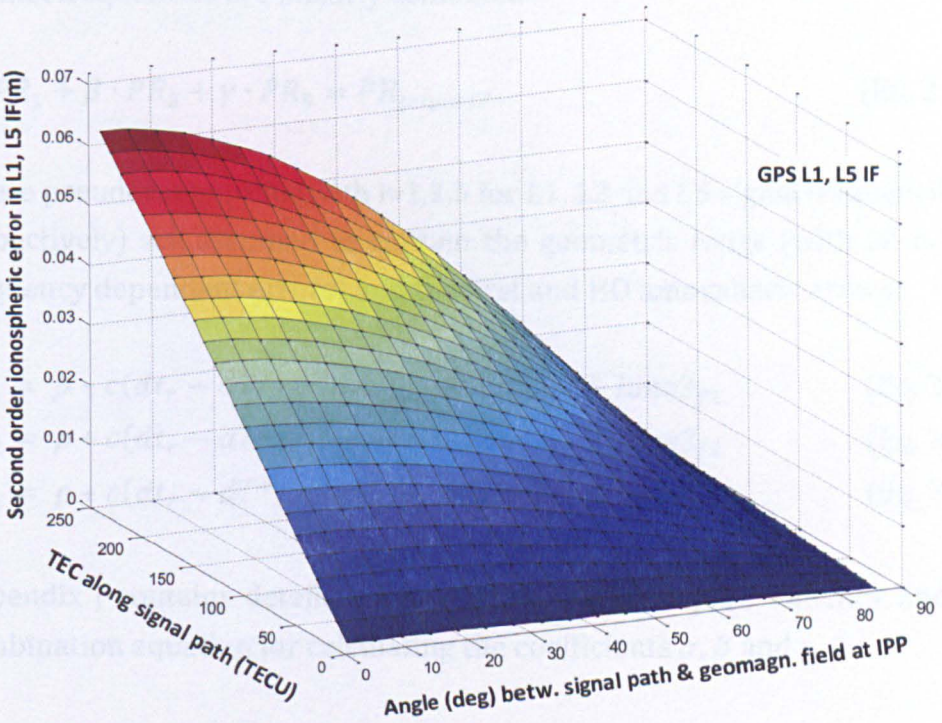

Figure 4.2. Residual error due to Iono2 in L1, L5 IF observable, for a receiver at mid-latitudes.

Higher order error terms are kept deliberately in Eq. 29 and Eq. 30 to show that the first order approximation has residual range error due to Iono2 and Iono3 which together may cause cm level range error (Petrie et

al. 2011) if enhanced ionization levels affect the signal paths. In practice it can be challenging to split the residual range error to its contributing parts for Iono2 and Iono3.

Furthermore, the same linear combination approach applies for phase observations as well, taking into account an ambiguity term for each carrier phase observation.

4.1.2. SECOND ORDER APPROXIMATION

In a second order approximation, observations are considered to include the first *and second* order ionospheric error terms such that linearly combining these observations leads to an IF observable independent of any ionospheric error term that is inverse frequency dependent to the second or third power. Such ionospheric correction eliminating both the first and second order error terms is possible if observations on three distinct frequencies are linearly combined:

$$\alpha \cdot PR_1 + \beta \cdot PR_2 + \gamma \cdot PR_5 = PR_{triple\ IF} \qquad \text{(Eq. 31)}$$

where pseudoranges PR_i (with i=1,2,5 for L1, L2 and L5 signal frequencies, respectively) are assumed to contain the geometric range (with all non-frequency dependent errors) and the first and HO ionospheric errors:

$$PR_1 = \rho + c(dt_r - dT^S) + Iono1_{f1} + Iono2_{f1} + Iono3_{f1} \qquad \text{(Eq. 32)}$$
$$PR_2 = \rho + c(dt_r - dT^S) + Iono1_{f2} + Iono2_{f2} + Iono3_{f2} \qquad \text{(Eq. 33)}$$
$$PR_5 = \rho + c(dt_r - dT^S) + Iono1_{f5} + Iono2_{f5} + Iono3_{f5} \qquad \text{(Eq. 34)}$$

Appendix J contains details for solving the above triple frequency linear combination equation for calculating the coefficients α, β and γ.

Based on the above formulation, the triple-frequency IF observable $PR_{triple\ IF}$ becomes independent of ionospheric errors that are inverse frequency dependent to the second and third powers. This can be noted on the RHS of $PR_{triple\ IF}$ where the first and second order ionospheric error terms are eliminated. Furthermore, it is evident that such second order

approximation cannot exclude the total ionospheric error while a residual error associated with Iono3 term remains in $PR_{triple\ IF}$.

$$PR_{triple\ IF} = \rho + \frac{3\,K^2\,\eta\,N_{max}\,STEC}{2} \cdot \frac{1}{f_1{}^2(f_2-f_5)(f_1+f_2+f_5)} \cdot \left(\frac{f_2+f_1}{f_2} - \frac{f_5+f_1}{f_5}\right) \quad \text{(Eq. 35)}$$

The main disadvantage of a second order approximation that eliminates both the Iono1 and Iono2 terms in the IF observable is the increased noise level of the resultant observable (Urquhart 2009). When the error propagation law is applied (see Appendix J) to figure out how much "more noisy" the IF observable gets, it can be seen that the noise disadvantage of such triple frequency combination may outweigh its advantage of correcting the ionospheric error further; as it is about 60 times as noisy an observable.

4.2. NEW SIGNALS AND THE IONOSPHERIC DIFFRACTIVE EFFECTS - PROPOSED TECHNIQUE TO ASSESS SIGNAL TRACKING PERFORMANCE DURING SCINTILLATION

In the mitigation technique proposed by Aquino et al. (2009), the stochastic model, which is related with the statistical quality of the measurements, in the Least Squares positioning solution is modified. In this modification, the measurements are assigned "weights" which are inversely proportional to the jitter variance at the DLL and PLL outputs. In this sense, the "best estimates" of the jitter variances are used to improve the stochastic model.

The estimation of the variances in the work of Aquino et al. (2009) is accomplished using the Conker model (model details can be found in Section 3.2.2.2.) in order to test and validate the proposed mitigation technique.

When attempting to apply the mitigation technique of Aquino et al. (2009) considering data collected at the low latitudes with strong amplitude scintillation, it was observed during this research that the use of the Conker model remains limited in the case of strong amplitude scintillation (i.e. when S4>0.707) due to a singularity inherent in the mathematical formulation of the model for the thermal noise (Eq. 20 and Eq. 21) and the

DLL jitter variance (Eq. 22 and Eq. 23). In order to proceed with this mitigation technique, the need for an alternative approach emerged during this PhD in order to estimate the tracking error variances since the Conker model may not be applicable for the instances when $S4_{L1}$ is greater than 0.707.

This need for an alternative approach to assess the jitter variance was the motivation for exploring the receiver logged post-correlation in-phase "I" and quadra-phase "Q" (I/Q) data which are output at a high rate (such as 50Hz) by the receiver for the signal intensity (at non-relevant units) that is given as $\sqrt{I^2 + Q^2}$.

As described in the following bullet points in this section, I/Q data is intended to be used since the influence of scintillation can be observed in this data which is considered statistically to estimate the jitter variance for DLL and PLL outputs. Where a comparison can be made (as shown in this section later), the results obtained with the I/Q data, for instance, for DLL jitter variance agree well with those obtained from the Conker model for the tracking of GPS L1 signal – in addition, the I/Q data can provide more continuous estimation of the jitter variance which may not be possible when using the Conker model for the same estimation purpose. The proposed estimation approach using the I/Q data can help to assess the signal tracking performance at "any" scintillation level *as long as* the signal is tracked (i.e. lock is maintained), and such assessment can be particularly important in a real time application with significant scintillation.

A patent has been filed (by the Nottingham Geospatial Institute, file number JL59468P.GBA) where the proposed jitter variance estimation approach utilizing the post-correlator I/Q data assists the mitigation technique of Aquino et al. (2009). The author of this PhD thesis is a co-author in this patent which claims to improve the accuracy of GNSS coordinate estimation during ionospheric scintillation.

Background information about I/Q data, justification for the use of and details about the formulation based on I/Q data to assess signal tracking performance are provided in this section. Advantages and disadvantages of the technique are also discussed in this section.

■ **I/Q Post-Correlator Outputs:** Prompt correlator outputs of I/Q data that is recorded in the SBF file by a Septentrio PolaRxS receiver can be represented approximately as (Kaplan & Hegarty 2006):

$$I_P = \sqrt{\frac{P}{2}} \cdot d(t - \tau(t)) \cdot R(\varepsilon_T) \cdot \frac{\sin(\pi \cdot \Delta f \cdot T_I)}{\pi \cdot \Delta f \cdot T_I} \cdot \cos(\varepsilon_\phi) + \text{Noise}_I \quad \text{(Eq.36)}$$

$$Q_P = \sqrt{\frac{P}{2}} \cdot d(t - \tau(t)) \cdot R(\varepsilon_T) \cdot \frac{\sin(\pi \cdot \Delta f \cdot T_I)}{\pi \cdot \Delta f \cdot T_I} \cdot \sin(\varepsilon_\phi) + \text{Noise}_Q \quad \text{(Eq. 37)}$$

where P is the total inter-frequency signal power, $d(t - \tau(t))$ is related with the navigation message where $\tau(t)$ is the code delay at time t, $R(\varepsilon_T)$ is the PRN auto-correlation function based on the error in code delay estimation denoted with ε_T, T_I is integration period of the correlator, Δf is carrier frequency estimation error, ε_ϕ is the carrier phase estimation error and the additive term in both I_P and Q_P is for noise, which can be taken as zero mean, Gaussian (Kaplan & Hegarty 2006). This noise is expected to be the same for either arm and be zero mean Gaussian statistics (Kaplan & Hegarty 2006).

What is of interest is the term involving the phase error ε_ϕ therefore the preceding terms can be shown by {...} for a more compact representation of I/Q as a ratio:

$$\frac{Q_P}{I_P} = \frac{\{...\} \cdot \sin(\varepsilon_\phi) + \text{Noise}_Q}{\{...\} \cdot \cos(\varepsilon_\phi) + \text{Noise}_I} \quad \text{(Eq. 38)}$$

Considering a vector representation of the baseband signal on the xy-plane such that +x axis represents the (amplitude of) I correlator output and y axis that of Q output, under *quiescent* conditions this vector traces across the +x axis with a small angular deviation from the +x axis such that there is greater projection onto the +x axis (greater magnitude in the I arm) and less onto the y axis (ideally very small magnitude in the Q arm).

Figure 4.3. illustrates the correlation products where I and Q samples are mapped with a vector which extends from the origin to the point on the xy-plane indicated by the values of I (x value) and Q (y value). The angle forming between the two is also shown in this "vector" representation.

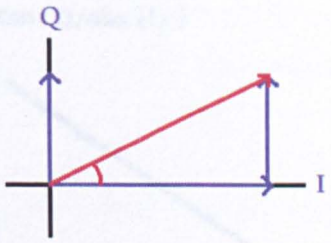

Figure 4.3. I and Q correlation outputs (not drawn to scale) represented in a vector form.

During good tracking conditions, the I correlator output is expected to have the maximum magnitude and the Q minimum; any divergence from such allocation of power can be due to perturbations on the incoming signal – this can be caused by scintillation induced signal fading or rapid variations in signal phase. For ionospheric effects from signal propagation point of view, it is expected that the magnitude and orientation of this (symbolic) vector should be affected.

The amplitude of such a vector will depend on the constructive or destructive interference (such as due to scintillation) which may increase or decrease the signal amplitude. There can also be amplitude/power amplifications applied by the receiver that may influence the magnitudes of the correlator outputs; however during this research the Automatic Gain Control (AGC) in the receiver was turned off[a] while collecting data. This means that I/Q samples are not (expected to be) enhanced by any receiver amplification.

Incorporating I/Q into this research is possible through considering the magnitude of this vector (shown in x-axis in Fig. 4.4.) as well as the angle formed between I and Q in the vector representation (shown in y-axis in Fig. 4.4.). The solid line in Fig. 4.4. is based on the assumption that while the magnitude of the representative vector shown in Fig. 4.3. is large, the corresponding angle also illustrated in Fig. 4.3. should be small – this is well expected during healthy tracking conditions. Yet for small values of magnitude of this vector, the corresponding angle shall be large.

[a] *This aims to avoid influence of the AGC on the observed impact of the amplitude and phase scintillation on the received signal.*

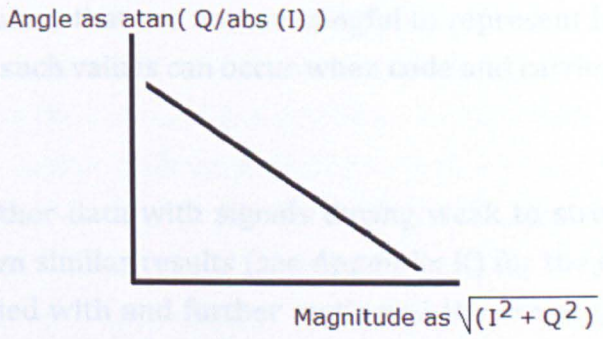

Figure 4.4. Relation between the angle and magnitude calculated from I/Q.

Considering open sky data (for PRU2 station in Brazil on 26 September 2011 at 00:00-03:00 GPS Time) with scintillation effects on the GPS L1 signal from SV02, the real case corresponding to Fig. 4.4. is given in Fig. 4.5.

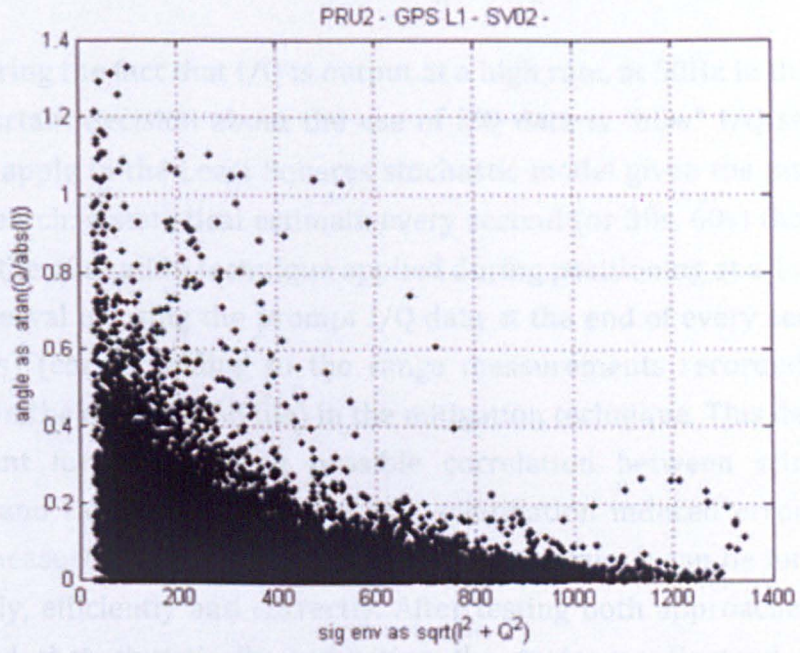

Figure 4.5. Signal envelope ("sig env", constructed from I/Q as sqrt(I^2+Q^2) versus angle (magnitude calculated from *atan*(Q/abs(I)) where abs is for absolute value) shown from open sky data collected at PRU2 station on 26 September 2011 at 00:00-03:00 GPS Time.

Figure 4.5. shows the scattering of angle and envelope components using data with strong scintillation on a GPS L1 signal. When the signal envelope/ magnitude is small the angular information is large, and vice versa. It can be noted that there are instances when scattering lies outside the majority of the data points. Such deviations in scattering can be due to

I/Q attaining values that are not meaningful to represent healthy tracking conditions and such values can occur when code and carrier tracking loops are challenged.

Analysis of further data with signals during weak to strong scintillation levels has shown similar results (see Appendix K) for the use of I/Q. Such findings complied with and further motivated the use of I/Q for research involving scintillation effects in signal propagation.

N.B. Figure 4.5. refers to post-correlator level, therefore it can be said that outliers in this plot may pose difficulty for filters in DLL and PLL.

N.B. "Amplitude/Magnitude" and "Phase" are not used to denote the received signal's amplitude and phase, respectively.

Considering the fact that I/Q is output at a high rate, at 50Hz in this thesis, an important decision about the use of I/Q data is "how" I/Q should be used to apply in the Least Squares stochastic model given the purpose of this research: a statistical estimate every second (or 30s, 60s) that can be used in the mitigation technique applied during positioning at a 1s (or 30s, 60s) interval or using the prompt I/Q data at the end of every second (or 30s, 60s) (corresponding to the range measurements recorded at that instant in the observation file) in the mitigation technique. This decision is important for investigating possible correlation between scintillation impact and range measurements (i.e. scintillation induced errors in the range measurements) so that the mitigation technique can be formulated optimally, efficiently and correctly. After testing both approaches, it was observed that statistically estimating the variances (instead of using prompt I/Q samples as mentioned above) using the I/Q data in order to apply the inverse of the variances as weights in the stochastic model in the mitigation technique gives improvement in the positioning solution.

- **Use of I/Q in Assessing Signal Tracking Performance:**

Based on the assumption that a decrease in the magnitude of the I component (or equally increase in that of Q) can occur when tracking is "less" healthy, for instance, due to signal propagation related perturbations, a negative correlation between the amplitude of the I

component and the code tracking error variance was assumed initially. In this sense, increase in the DLL jitter variance corresponds to a decrease in the magnitude of the I component. As shown in Fig. 4.6, negative values of the I correlator output (unit neglected) seems to be correlated (in profile) with the estimated (using the Conker model) DLL jitter variance for GPS L1C/A.

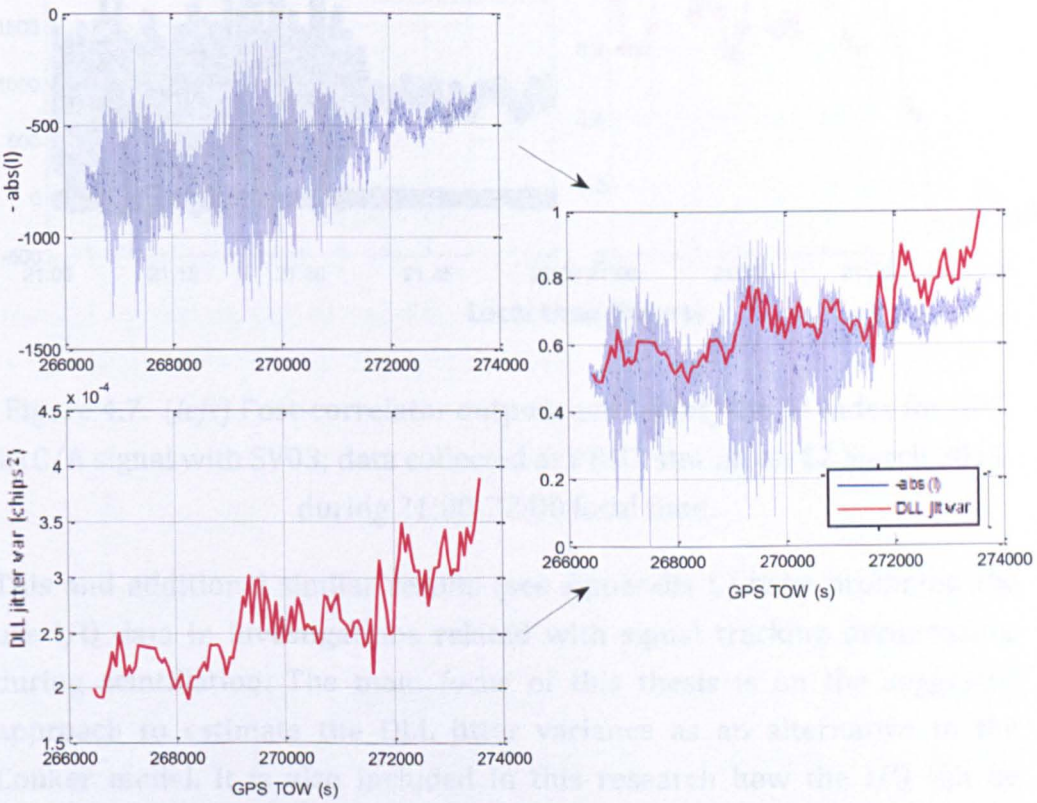

Figure 4.6. Negative of the absolute value of I correlator output (*top left*) and the DLL jitter variance in chips squared calculated with Conker model (*bottom left*). The two time series *normalized* (by dividing each series with its maximum) to superimpose both results within the same range (0-1, no units) (*far right*).

It is anticipated that the two series in the superimposed plot in Fig. 4.6. depart from each other (at the beginning and end) due to the changing elevation angle which can be associated with the signal-to-noise ratio whose effects would be different to observe in the I component and the calculated DLL jitter variance. The decreasing elevation angle (with correspondingly smaller C/N_0) in the last quarter of the series in this case may increase the DLL jitter variance while leading to a less noisy time series of the I component. This correlation led to further analysis of the I as well as the Q component about how they can be explored in the subject

of ionospheric scintillation and its impact on the signal and signal tracking. Indeed, the use of both correlator samples seems reasonable when one considers in Fig. 4.7. how the I and Q components change when the S4 index indicates strong amplitude scintillation.

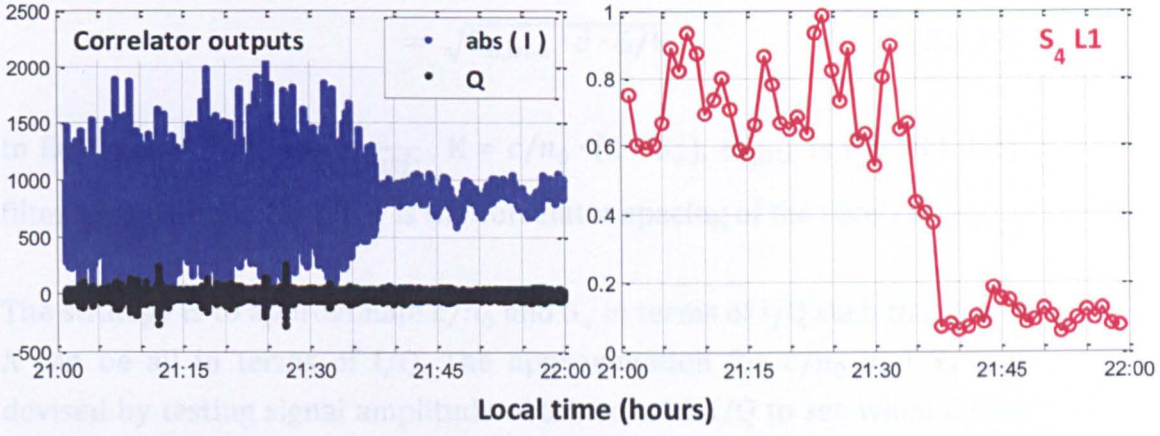

Figure 4.7. (*left*) Post-correlator outputs and (*right*) the S4 index for GPS L1C/A signal with SV03; data collected at PRU2 station on 12 March 2011, during 21:00-22:00 local time.

This and additional similar results (see Appendix L) have prompted the use I/Q data in investigations related with signal tracking performance during scintillation. The main focus of this thesis is on the suggested approach to estimate the DLL jitter variance as an alternative to the Conker model. it is also included in this research how the I/Q can be considered to estimate the PLL jitter variance, as discussed later in this section.

■ Devising a Technique to Assess the DLL Jitter Variance During Scintillation Using I/Q Post-Correlator Samples:

An alternative technique has been proposed to use I,Q post-correlation data at 50Hz rate made available by the Septentrio PolaRxS receiver to estimate the DLL jitter variance such that even during strong levels of amplitude scintillation an estimation can be possible as long as the signal is tracked.

Considering the representation of the variance of the DLL jitter variance by the Conker model, which is mathematically similar to the variance of the thermal noise contribution to the total PLL jitter variance, (Eq. 22 in

Section 3.2.2.2.), the relationship between "I" and DLL jitter *STD* can be stated as:

$$-|I| \cong DLL\,jitter\,std\,(chips) = \sqrt{\frac{B_{n,DLL}\cdot d}{c/n_0\cdot(1-S_4^2)}\cdot\left(\frac{1}{2}+\frac{1}{2\cdot\eta\cdot c/n_0\cdot(1-2S_4^2)}\right)}$$

$$= \sqrt{B_{n,DLL}\cdot d\cdot G/K} \qquad \text{(Eq. 39)}$$

In Eq. 39, $G = \frac{1}{2}+\frac{1}{2\cdot\eta c/n_0\cdot(1-2S_4^2)}$, $K = c/n_0\cdot(1-S_4^2)$, $B_{n,DLL}$ is the DLL loop filter bandwidth in Hz and d is the correlator spacing of the receiver.

The strategy is to approximate c/n_0 and S_4 in terms of I/Q such that G and K can be all in terms of I/Q. The approximation for c/n_0 and S_4 was devised by testing signal amplitude obtained with I/Q to see when a best fit is achieved for these two parameters. In this sense, it was observed that:

$$c/n_0 \cong \frac{2}{10} * (mean(I^2+Q^2))^2 \qquad \text{(Eq. 40)}$$

$$S_4 \cong \frac{2}{mean(\sqrt{I^2+Q^2})/std(\sqrt{I^2+Q^2})} \qquad \text{(Eq. 41)}$$

where "mean" is for arithmetic mean of signal envelope/magnitude calculated as $\sqrt{I^2+Q^2}$ over a second or a minute (depending on the rate at which these parameters are required to be estimated; and "STD" is the standard deviation of $\sqrt{I^2+Q^2}$, again, over a second or a minute.

Next these approximations, Eq. 40 and Eq. 41, are substituted into the Eq. 39 and only the first term is regarded to give the following for DLL jitter std (i.e. a first order approximation is performed):

$$DLL\,jitter\,std\,(chips) \approx \sqrt{\frac{B_{n,DLL}/10}{\left[mean(\sqrt{I^2+Q^2})\right]^2-\left[2*std(\sqrt{I^2+Q^2})\right]^2}} \qquad \text{(Eq. 42)}$$

It is important to note that in this approximation, Eq. 42, the correlator spacing (which in general is a constant within a receiver for tracking different modulation codes, 0.04 chips in a Septentrio PolaRxS for GPS L1) and predetection integration time (in this case 100ms for DLL in a

Septentrio PolaRxS receiver) are absorbed into the constant 10 in the Eq. 42. For other receivers' specifications, this equation would be derived with different coefficients leading to a constant term different from 10.

Since in principle the derivation of Eq. 42 is based on the approach of Conker for the DLL jitter variance, it is expected that the result should be in chips^2 units despite the approximations involved. Comparison of the results obtained with this approach to those obtained with the Conker model is shown in Fig. 4.8.

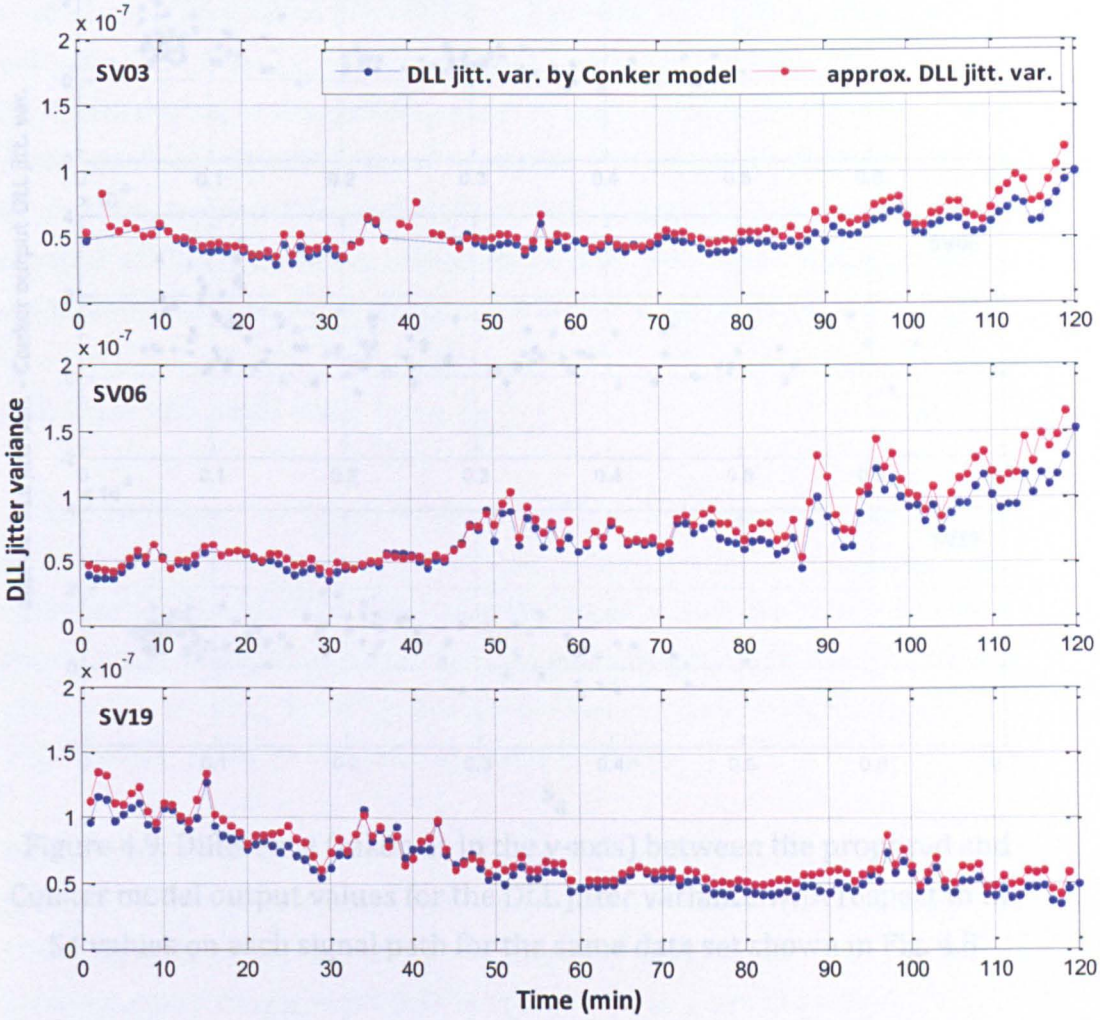

Figure 4.8. DLL jitter variance calculated respectively from the Conker model and approximated with the proposed model using I/Q; considering data collected at PRU2 for GPS L1CA with SV03 (*top*), SV06 (*middle*) and SV19 (*bottom*) on 11 March 2011.

Some differences between the results of the two methods can be noticed: for instance, after about 74th minute for SV06 (middle plot in Fig. 4.8.) and during the first ten minutes for SV19 (bottom plot in Fig. 4.8.). Considering

the S4 values for these three satellites (shown on x-axis in Fig. 4.9.), it can be observed that the differences between the two series in Fig. 4.8. are greater especially for S4 values less than about 0.2. Another aspect is that such deviation between the two time series in Fig. 4.8. does not necessarily occur for larger jitter variances, for SV19 the difference between the two time series occurs during both high and low values of the jitter variance.

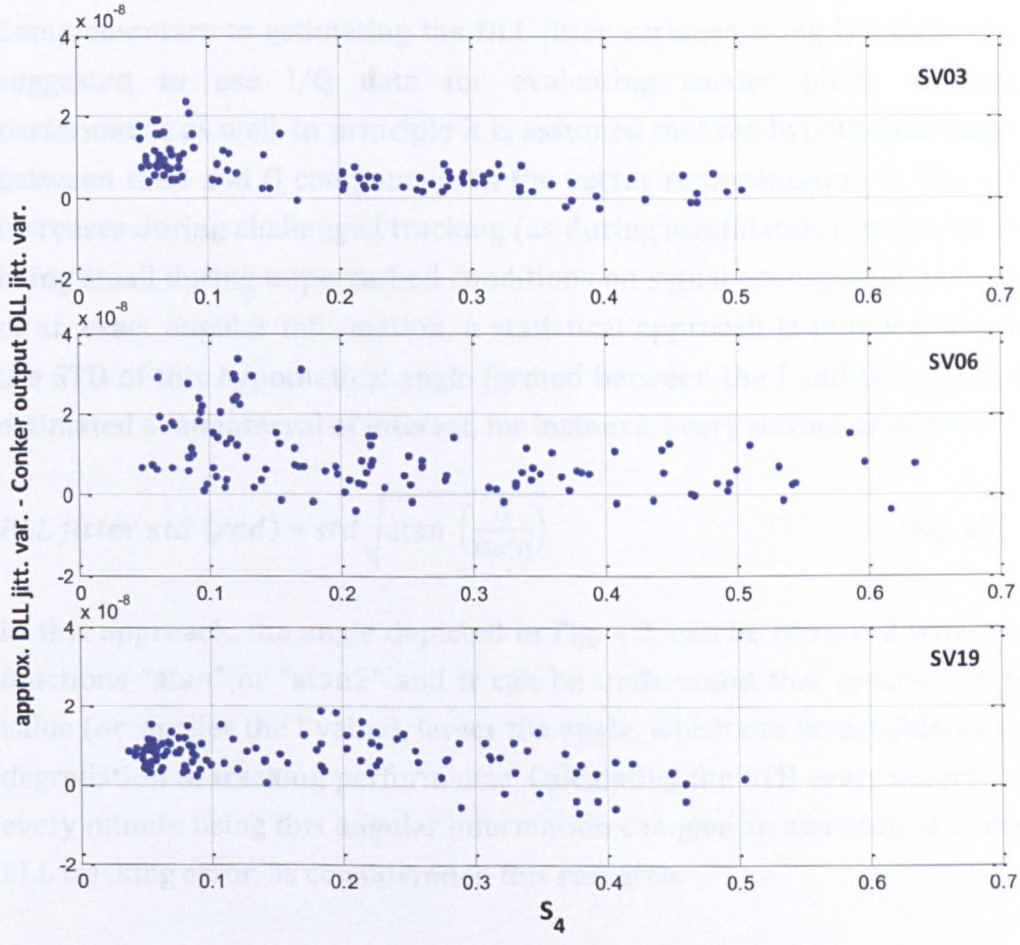

Figure 4.9. Difference (taken as in the y-axis) between the proposed and Conker model output values for the DLL jitter variance with respect to the S4 values on each signal path for the same data set shown in Fig. 4.8.

It can be seen in Fig. 4.9. that for non-negligible values of S4 (such as S4 > 0.2) the difference in the estimated values of the jitter between using the proposed method (Eq. 42) and the Conker model is relatively small (scatters about 0); this can support that the proposed estimation method is an acceptable alternative to the Conker model. Further analyses could be performed for stronger levels of scintillation for comparison purposes however the Conker model cannot be used in the case of strong levels of amplitude scintillation (Section 3.2.2.2.). Agreement between the two sets

of outputs presented in Fig. 4.9. can show that the proposed approach is advantageous because it reproduces the Conker model results up to S4=0.707 and also covers strong scintillation.

■ **Devising a Technique to Assess PLL Jitter Variance During Scintillation Using I/Q Post-Correlator Samples:**

Complementary to estimating the DLL jitter variance using I/Q data, it is suggested to use I/Q data for evaluating carrier phase tracking performance as well. In principle it is assumed that the hypothetical angle between the I and Q components in the vector representation in Fig. 4.3. increases during challenged tracking (as during scintillation) compared to being small during unperturbed conditions on signal propagation. Instead of an exact angular information, a statistical approach is pursued where the STD of this hypothetical angle formed between the I and Q vectors is estimated at an interval of interest, for instance, every second or minute.

$$PLL\ jitter\ std\ (rad) \approx std\sqrt{\text{atan}\left(\frac{Q}{\text{abs(I)}}\right)} \qquad \text{(Eq. 43)}$$

In this approach, the angle depicted in Fig. 4.3. can be retrieved with the functions "atan" or "atan2" and it can be understood that greater the Q value (or smaller the I value), larger the angle, which can be considered as degradation in tracking performance. Calculating the STD every second or every minute using this angular information can give an assessment of the PLL tracking error, as considered in this research.

Mao et al. (2008) also put forward that any misalignment of the input or prompt I/Q components can be detected by the carrier loop (discriminator). Results for assessing the performance of the phase tracking loop for a generic GNSS receiver is included in Chapter 6.

In Aquino et al. (2009), the Conker model was used for calculating per link per frequency the jitter variance which were employed to estimate "weights" (1/variance ~ weight) used to improve the stochastic model. However, in order to apply the technique for data with strong levels of (amplitude) scintillation, continuous assessment of the jitter variance is required. As shown in the mitigation results in chapter 6, this proposed approach is applied to provide input to the covariance matrix.

CHAPTER 5

5. DATA AND METHODOLOGY

In this chapter the data analyzed in this research and the method of investigation are discussed in sections 5.1. and 5.2., respectively. The data that was used is introduced in two parts: data recorded in the field, and data simulated using a GNSS signal simulator. The methodology adopted in this research is also considered in two parts, respectively, for investigating the ionospheric refractive effects and for investigating the diffractive effects.

5.1. DATA IN THIS RESEARCH

Important factors regarding the analyzed data are where and when data is collected, specifications of the receiver that is used while collecting the data and information about the data such as its content, rate and duration.

5.1.1. FIELD RECORDED DATA

Field recorded data was available on account of:

i) Participation in the CIGALA and POLARIS projects during this PhD,

ii) From the International GNSS Service (IGS) which provides GNSS products and data in support of research, GNSS applications and education (IGS 2012c).

- Where the data was collected:

i) Receivers deployed in the CIGALA (Fig. 5.1.) and POLARIS projects at a wide latitudinal coverage are considered as a data source. The importance of the data from the CIGALA project owes to the location of the receivers and the period of deployment. Location in the equatorial region with good proximity regarding the geomagnetic equator subjects the receivers to degrading effects of equatorial scintillation. The period of deployment coincides well with the Sunspot Cycle #24 as well as the initial phase of GNSS modernization, enabling data capture on GPS L2C and L5 signals and signals of Galileo IOV.

Figure 5.1. Receiver locations deployed in the CIGALA project are marked with a triangle.

Extensive analysis of data collected at the station in Presidente Prudente, PRU2, (22.1^{0}S, 51.4^{0}W) in the CIGALA network has been performed after this station started to be deployed in February, 2010. Its early deployment, multipath-free environment and proximity to another station by about 300m (for differential positioning purposes) were the main reasons why data from the PRU2 station was considered largely during this PhD.

Receivers in the POLARIS project cover a wider range of latitudes and deployment of the receivers started in 2011. Data from the receivers in Bronnoysund (65^{0}N, 12^{0}E) and Cyprus (35^{0}N, 33^{0}E) were of interest due to their high and mid latitude locations, respectively. However in terms of significant scintillation events no data could be analyzed during the research period of this thesis.

ii) Data from three stations TRO1 (Norway), HERS (UK) and MATE (Italy) involved in the International GNSS Service (IGS) network were also selected to consider the mid and high latitudes in Europe (Fig. 5.2.). Stations coordinates are given in Table 5.1.

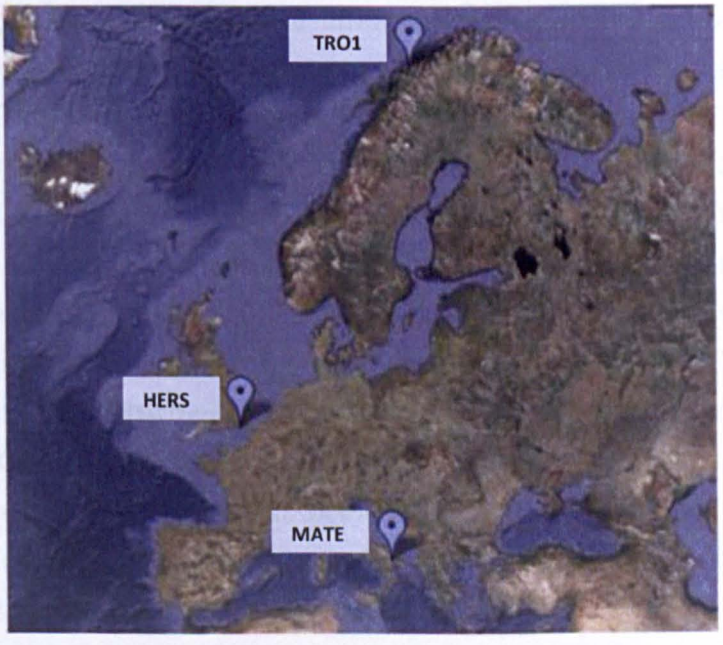

Figure 5.2. IGS stations considered in this work.

	TRO1	HERS	MATE
Latitude (deg), N	69.6627	50.8673	40.6491
Longitude (deg), E	18.9396	0.3362	16.7045
Height (m), U	138.0000	76.4990	534.5000

Table 5.1. Coordinates of the IGS stations considered in this work.

- When the data was collected: Regarding the period of data collection, timeliness of the analyzed data can be appreciated regarding the background solar, geomagnetic and ionospheric conditions.
  i) Data from the CIGALA project was available from February 2010 onwards and from the POLARIS project since 2011. These years fall well into Solar Cycle #24 whose peak is expected at around 2013. Indeed, enhancements in the ionization levels and a few scintillation events were observed in this data.

ii) Regarding the data from IGS, a selection of days for analysis was aimed at not only the peak period of the Solar Cycle #23 (when solar radiation can be regarded as the main influence on ionospheric conditions) but also during the presence of geomagnetic storms that may occur even during low solar activity and still may cause enhanced levels of ionization and disturbances in the geomagnetic field. In this sense, four sets of days (Table 5.2.) are selected: in order to investigate the impact of solar activity devoid of disturbances in the geomagnetic field, periods with day-of-year (DOY) 312-316 in 2001 and DOY 321-326 in 2006 were selected. For these two periods, the planetary geomagnetic index, K_p, is less than 4, which is a good threshold to exclude the influence of geomagnetic storms (NOAA 2005). For a more disturbed geomagnetic field, DOY 294-296 in 2001 and DOY 301-307 in 2003 were selected, when K_p is equal to or greater than 4. Table 5.2. provides the three-hourly K_p (first value corresponding to 00:00 GPS Time) indices for each day analyzed.

N.B. Other geomagnetic indices like the Auroral Electrojet index (AE) or Disturbance Storm Time index (Dst) could also be considered (WDC 1996) while selecting the days for analysis; however, the K_p index is deemed well representative for the considered latitudinal coverage and adequate for analyses given the fact that the focus is confined to the mid-to-high latitudes.

		DOY	K_p indices (3 hourly)	
2001	08-Nov	312	21221221	Active period of the Solar Cycle
	09-Nov	313	10001222	
	10-Nov	314	11002233	
	11-Nov	315	21021221	
	12-Nov	316	10001211	
2001	21-Oct	294	23323667	Geomagnetic storms during active period of the Solar Cycle
	22-Oct	295	65465765	
	23-Oct	296	45322221	
2003	28-Oct	301	34443434	Geomagnetic storms during post-peak of the Solar Cycle
	29-Oct	302	43987798	
	30-Oct	303	87655899	
	31-Oct	304	87766544	
	01-Nov	305	45433333	
	02-Nov	306	34333443	
	03-Nov	307	33232323	
2006	17-Nov	321	22112101	Quiet period of the Solar Cycle
	18-Nov	322	00001001	
	19-Nov	323	11111000	
	20-Nov	324	00001101	
	21-Nov	325	00000001	
	22-Nov	326	00001133	

Table 5.2. The four sets of days with different solar and geomagnetic background conditions with the K_p index for each day.

- Receivers used during data collection:
  i) Receivers deployed in the CIGALA and POLARIS projects are scintillation monitor receivers[a], the GPS Ionospheric Scintillation and TEC Monitor (GISTM) system Model GSV4004B from GPS Silicon Valley and the PolaRxS from Septentrio, respectively. These receivers are equipped with oven-controlled crystal oscillators (OCXO) which have low phase noise[b] that is necessary for precise monitoring of phase scintillation and measurements.

[a] A scintillation monitor receiver is a single or dual frequency GNSS receiver specifically designed to monitor scintillation in real time with a wide tracking bandwidth that helps maintain signal lock during strong scintillation. With a high sampling rate, it can calculate amplitude and phase scintillation indices.

[b] The phase noise of the reference oscillator in a receiver is important since this noise can dominate the phase

measurement which could then prevent precise monitoring of phase scintillation and measuring SigmaPhi index. Therefore, the choice of a stable, low noise reference oscillator is important for an ionosphere monitoring receiver (Shanmugam et al. 2012).

- GSV4004B is a GPS L1/L2 dual frequency receiver (NovAtel's Euro-3M card) containing a low phase noise OCXO housed in NovAtel's EuroPak-3M enclosure (CHAIN 2013).
- PolaRxS receiver, manufactured by Septentrio N.V. Belgium, is a multi-frequency, multi-constellation GNSS receiver dedicated to space weather and ionosphere monitoring applications. It is equipped with a triple frequency receiver engine and an ultra low noise oscillator frequency reference (Septentrio 2010).

Both receivers estimate ionospheric scintillation statistics for all visible satellites and store data for (mostly) post processing. They can be programmed to store data in files of, for instance, 15 or 60min at user choice - during this research GSV4004B outputs were 15-min long "scintillation (indices) data files" and 60-min long high rate raw (signal intensity and phase) data files whereas PolaRxS receiver outputs were hourly files for scintillation indices (along with other parameters) and high rate raw signal data. Both receivers provide S4, SPhi, TEC, C/N_0, lock time (the time elapsed while a lock is maintained on the signal) etc. every minute (per frequency per SV per constellation) in the scintillation indices data files. Regarding the high rate data, GSV4004B provides signal intensity and carrier phase (latter in the form of accumulated Doppler range, ADR, in cycles) at 50Hz and PolaRxS provides signal intensity in terms of post-correlator outputs I/Q (such that the square root of the sum of their squares is proportional to intensity of the received signal) and carrier phase as ADR at up to 100Hz rate. Both receivers can be configured by user to change the detrending and filter cut-off

parameters involved in the calculation of the scintillation indices.

ii) Receivers used in the IGS data belong to the IGS network and each station in this case was equipped by a receiver from a different manufacturer. Details on environment where receiver is mounted, default elevation cutoff setting, receiver model and clock type can be found in the "Older Mail" section for a particular IGS station in the IGS network list (IGS 2012b).

- Data content:

i) Receivers in the CIGALA and POLARIS projects provide observation files in RINEX format. These scintillation monitor receivers also provide additional data in separate files: one about scintillation related parameters, referred to as a "scintillation data file" in this thesis, that contains scintillation indices and parameters per SV per frequency such as lock time on carrier, C/N_0, TEC and TEC rate, and another high rate signal intensity and carrier phase measurements[c] at a high rate referred to as a "high rate data file". Receiver data is obtained through ftp connection to the server held at UNESP, where a secure log in is needed for data access. Table 5.3. briefly summarizes the details of the data content.

Data File:	Observation File	Scintillation Data file	High Rate Signal Data file
Data Content:	Range measurements	Scintillation indices, Lock Time on carrier, TEC, C/N_0, Elevation, Azimuth, etc.	Accumulated Carrier Phase (ADR), Intensity
File format:	RINEX	Text file	Text file
Data Rate:	1s, 30s, 60s	Every 60s	20ms (in this work)

Table 5.3. Details of the data content for the receivers deployed in the CIGALA and POLARIS projects.

[c] *Signal intensity and phase data is also used as a source of scintillation effects which can be extracted to be re-implemented on simulated GNSS signals as discussed later in Section 5.1.2.*

ii) IGS data has GPS observations in RINEX format for each station and DOY analyzed. These files are obtained from the JPL website for the DOY of interest.

- Data rate and duration:
  i) Data obtained from the receivers deployed in the projects constitute observation files in RINEX format at interval of interest, scintillation data files at 60s interval and high rate data files at 20ms interval. Data duration depends on the amount of data that is of interest for analysis.
  ii) RINEX observation files obtained from IGS network are at 30s interval.

In the data analysis, much of the data comes from a Septentrio PolaRxS receiver. The main reason for this is the fact that this type of receiver was deployed at the stations where data collection is of interest (at low latitude stations in the CIGALA project). Another reason is the novel output of I/Q data from this receiver type, which has been used in this thesis for studying scintillation effects.

5.1.2. SIMULATED DATA

The NGI has pioneered *GPS* ionospheric scintillation monitoring in Europe covering most of the last solar maximum between June 2001 - December 2003 at 53^0-71^0N, by operating a network of scintillation specific receivers. However, there are two main limitations of exploiting this open sky data source for the purposes of this research: (i) the data is GPS only, lacking not only observations for GLONASS or newly emerging Galileo but also the new signals of GPS itself, (ii) the data output of high rate signal intensity and phase cannot be incorporated into the analyses conducted in this thesis based on I/Q type data. Therefore, simulated data has been primarily helpful to study scintillation effects within the scope of GNSS modernization and at any level - simulations provide a controlled environment where scintillation effects can be studied in the absence of other error sources such as multipath and clock and orbit errors.

The Spirent GSS8000 GNSS signal simulator, available for researchers at the NGI and which can provide RF outputs for GPS and Galileo signals, was

used in scintillation-oriented simulations. By connecting a GNSS receiver to the antenna output of the simulator, it is possible to test receiver signal tracking robustness against scintillation.

Figure 5.3. shows how simulations with scintillation effects were performed during this PhD.

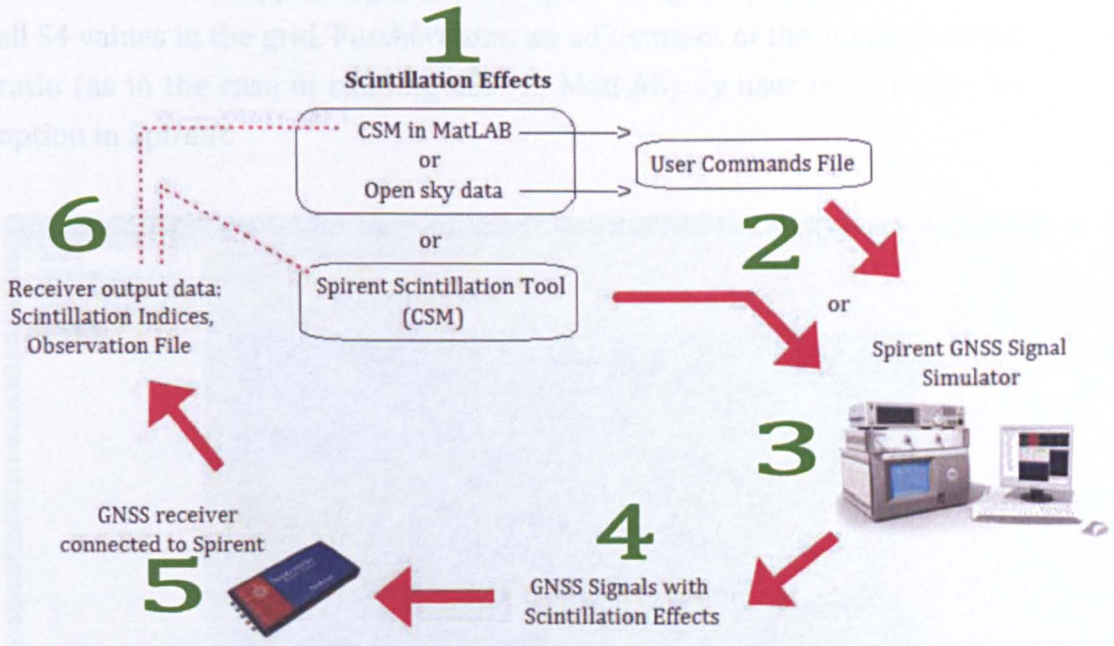

Figure 5.3. Closed loop diagram followed in simulations for studying scintillation effects. It can be understood that Step 1 and 2 reduce to one step (elucidating the preparation of a *.ucd* file) if the Spirent simulator's scintillation tool is enabled.

Step 1 is about obtaining scintillation effects, i.e. time series of high rate fluctuations in signal intensity and phase, for which a model like Cornell Scintillation Model (CSM) or Global Ionospheric Scintillation Model (GISM) or open sky data with scintillation event can be used. A model in this case provides time series of realistic signal intensity and phase variations depending on input parameters (S4 and time decorrelation parameter Tau0 (τ_0) for CSM) that determine level of scintillation. Similarly, scintillation induced perturbations (i.e. high frequency fluctuations) from received signal intensity and phase can also be extracted from open sky data to provide scintillation time series – the role of "User Commands File" related with this is explained in Step 2.

Another source for scintillation effects is the Spirent simulator's scintillation tool: In 2010, the simulation firmware was updated for its atmospheric modelling to provide user means of inserting scintillation effects in simulation scenarios. CSM was selected as its scintillation tool, which has a user interface of a scintillation grid (Fig. 5.4.). While using CSM through Spirent, the value for Tau0 parameter ("Channel de-correlation time" appearing below the grid in Fig. 5.4.) stays the same for all S4 values in the grid. Furthermore, an adjustment of the signal-to-noise ratio (as in the case of running CSM in MatLAB) by user is no longer an option in Spirent.

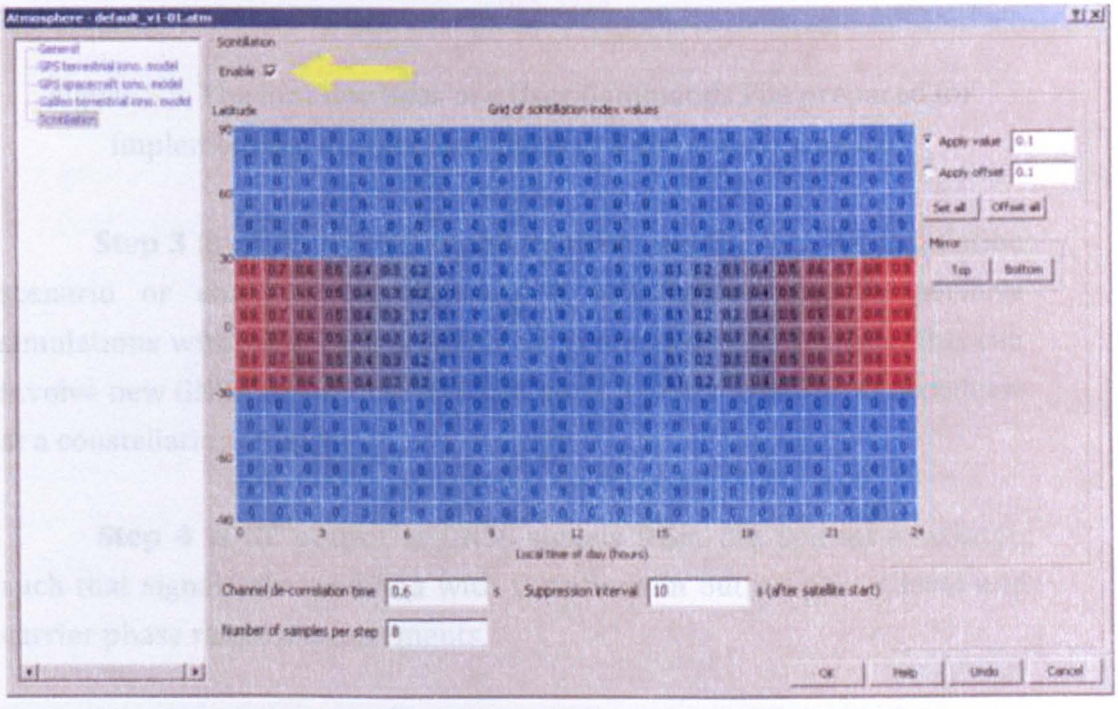

Figure 5.4. Spirent Scintillation tool user interface. Yellow arrow indicates that the scintillation tool is enabled.

Step 2 is taken *only if* scintillation time series are obtained externally, either from a model or from open sky data. Whereas the use of a model necessitates scintillation time series to be formatted into a commands file, the simulator scintillation tool elucidates such formatting. Scintillation time series obtained in Step 1 need to be written into a specific file with time stamps and in correct units to *mod*ify the generated GNSS signals by the Spirent simulator. For this purpose, a User Commands File (*.ucd* file) with "MOD" command is generated, which contains time-stamped information of how much signal power level and carrier phase

range on a particular signal path of a constellation should be *mod*ified. Figure 5.5. shows the first few lines of a User Commands File.

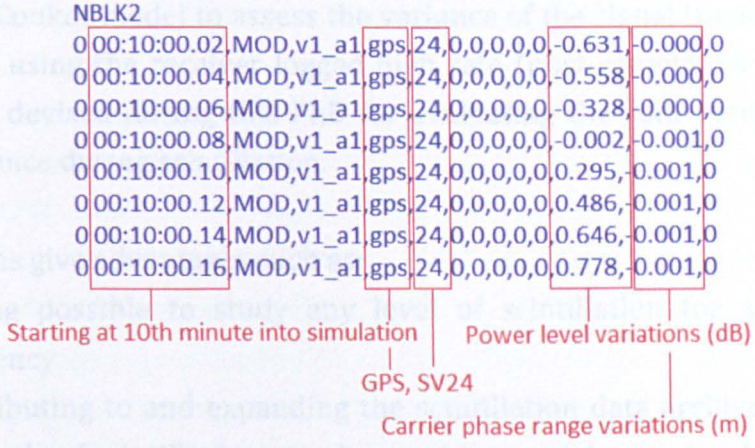

Figure 5.5. The first few lines of a User Commands File prepared for implementing scintillation effects in a simulation scenario.

Step 3 involves uploading the relevant *.ucd* file into the simulation scenario or enabling the simulator's scintillation tool to perform simulations with scintillation effects on generated GNSS signals. This can involve new GNSS signals like GPS L2C and L5 which are not yet broadcast at a constellation level.

Step 4 is RF output of GNSS signals from the Spirent simulator, such that signals are modified with variations in output power level and carrier phase range measurements.

Step 5 is what characterises a simulation "hardware-in-the-loop": connecting a GNSS receiver to the antenna output of the Spirent simulator subjects the receiver to scintillation effects. In order to study scintillation effects in isolation, other error sources such as orbit and clock errors, troposphere and multipath were not included in the simulations during this PhD research.

Step 6 involves receiver output data (scintillation indices data, (high rate signal data), observation file etc.). Scintillation indices recorded by receiver can be compared to those in the open sky data from which effects were extracted; this ensures (and helps to establish the routine for) the correct extraction of scintillation induced fluctuations from raw signal data. Furthermore, the receiver output S4 can be compared to that input in

the grid or CSM MatLAB GUI; this indeed was done while testing the Spirent simulator's implementation of CSM into its firmware. Moreover, the receiver signal tracking performance can be evaluated, for instance, by using the Conker model to assess the variance of the signal tracking error, as well as using the receiver logged high rate (post-correlator) data in a technique devised during this PhD for evaluating the code tracking loop jitter variance during scintillation.

Simulations give advantages such as:

1. Making possible to study any level of scintillation for any signal frequency.
2. Contributing to and expanding the scintillation data archive (at NGI) for levels of scintillation not observed in open sky data and involving new GNSS constellations and signals.
3. Repeating tests for different receivers (or same receiver with different configurations) connected to the simulator or connecting more than one receiver per simulation

The main contribution of this PhD regarding simulations with scintillation effects has been the methodology of implementing scintillation effects in simulation scenarios. In this sense, Step 1 and 2 shown in Fig. 5.3. were investigated and implemented for the first time at NGI during the course of this PhD.

The first attempt was the use of CSM (through MatLAB) when the model was published by the School of Electrical and Computer Engineering at Cornell University, USA, in 2009. CSM was developed for hardware-in-the-loop testing of GNSS receivers against scintillation and it targets the equatorial scintillation effects in particular which are challenging for the receiver tracking loops. The authors observe in their analysis of open sky data deep signal fades accompanied by half cycle phase jumps, which they term as "canonical fades", and claim that these are the principal cause of carrier unlock during severe equatorial scintillation (Humphreys et al. 2009a; Kintner et al. 2009). CSM simulates ionosphere-induced "equatorial" scintillation effects (in terms of time histories of signal phase and intensity variations) to test GPS receiver tracking loops for scintillation robustness (Humphreys et al. 2009a). In principle, this model aims to properly shape the spectrum of the complex scintillation signal

(Humphreys et al. 2009b) such that the amplitude and phase spectra are interrelated; this way CSM is aimed to realistically capture the effects of the equatorial scintillation on the signal tracking loops (Kintner et al. 2009; Humphreys et al. 2008b).

CSM can be run externally in MatLAB (scripts available at gps.ece.cornell.edu under the "Space Weather" link.) for the two input parameters of S_4 and Tau0. Figure 5.6. shows the user interface for CSM on the left where the S4 and Tau0 parameters are given the values 0.7 and 0.5, respectively, in this case. The scintillation time histories contain how much the signal power level and carrier phase range offset should be changed, in dB and meters, respectively. CSM output time series of signal intensity and phase fluctuations (Fig. 5.6.) are then written to a user commands file (*.ucd* file) that is included in the simulation scenario. Further details on CSM are available in Appendix M.

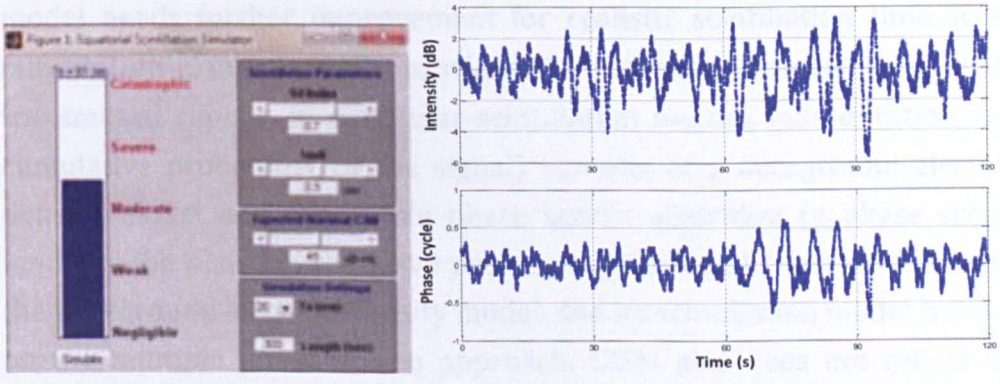

Figure 5.6. (*left*) CSM Graphical User Interface; (*right*) output time series.

To alleviate the lack of open sky data to study scintillation during this research, CSM was a "tool at hand" used in simulations to "colour" the generated GPS signals with scintillation-like effects to investigate receiver signal tracking performance subject to scintillation-induced perturbations.

In October 2010, Spirent Communications adopted CSM as an embedded part of their SimGEN software, providing it to users as a "scintillation tool", which can be found among the ionosphere modelling tools to the users for simulating realistic scintillation environments in simulations. This helps users to avoid inserting an external *.ucd* file when they want to simulate not only the background ionosphere but also its "patchy" character

associated with electron density gradients/irregularities leading to scintillation effects on GNSS signals. Subjecting GNSS receivers to realistic scintillation effects in simulation helps in testing signal tracking to the stress caused by scintillation on code and carrier tracking loops, and consequently how the receiver navigation solution can be affected. Work related with validating the CSM using the Spirent simulator were presented by Elmas et al. (2010b-d). From these works it was understood that CSM can induce signal power fades that are not always realistic when compared with the level of scintillation determined in CSM by the amplitude scintillation index, S4. For this reason CSM can cause false losses of lock in the carrier phase tracking loops.

Another model that outputs scintillation time series is GISM (Béniguel & Buonomo 1999) which, however, falls rather far from the purpose of implementing its output scintillation time series into simulations (From personal communication with Roberto Cerdeira it was understood that the model needs further improvement for realistic scintillation time series outputs). In principle, GISM provides the statistical characteristics of the transmitted signals, in particular scintillation indices, fade duration, and cumulative probability of the signal) consists of a background electron density model and a multiple phase screen algorithm (a phase screen modifies the phase of the wave penetrating through it); uses NeQuick for the background electron density model, and its scintillation model is based on the multiple phase screen approach. GISM also does not reflect the patchiness of the ionosphere and variation in the morphology of scintillation may not be captured except its intensity. For further details on the GISM, see the Appendix N.

In parallel to using such models, insertion of scintillation effects on simulated GNSS signals is also possible by exploiting open sky data of signal intensity and phase collected at a high sampling rate by an ionospheric scintillation monitoring receiver during a scintillation event. This requires extraction of high frequency signal intensity and phase fluctuations from raw signal data – estimation of SigmaPhi parameter from raw signal phase data as shown by Aquino et al. (2007) was taken as principle for extracting carrier phase fluctuations due to scintillation from raw data. It was completed by extraction of amplitude fluctuations from raw signal intensity data in this research. Figure 5.7. provides a flow

diagram for the steps involved in using open sky data for scintillation oriented simulations.

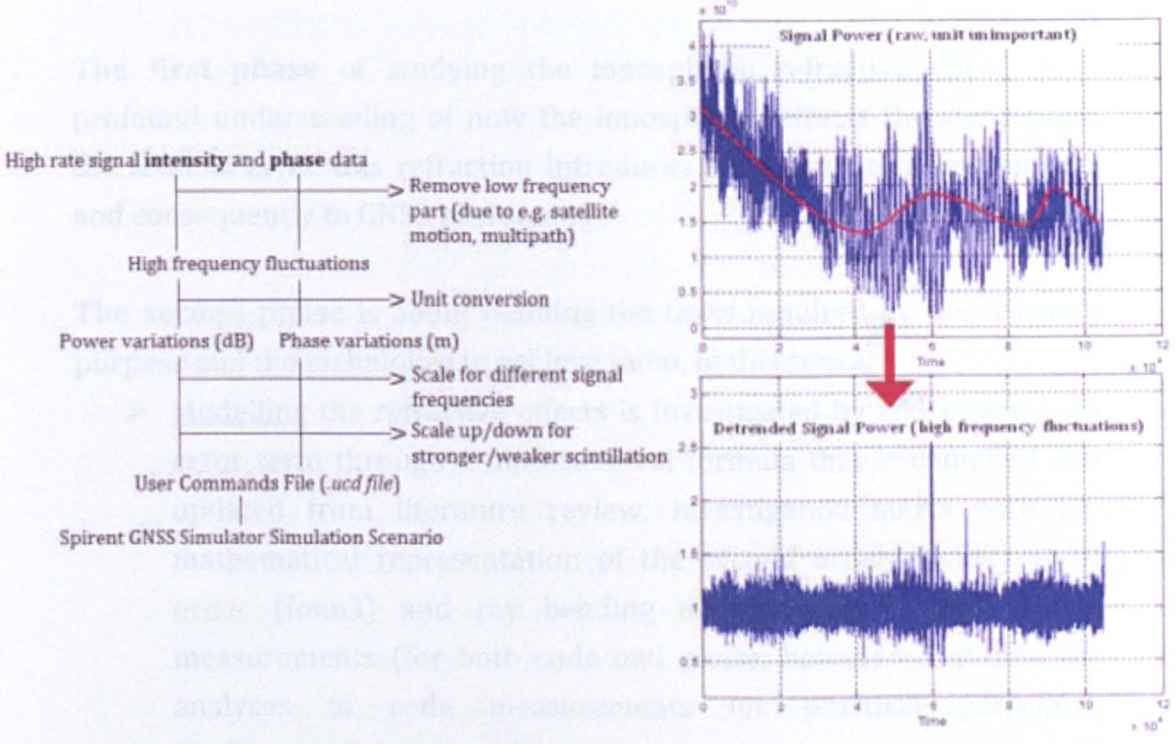

Figure 5.7. (*left*) Flow diagram for extracting fluctuations in signal intensity and phase; (*right top*) Raw signal intensity from which the low frequency part (red curve in the top plot) is removed; (*right bottom*) Resultant high frequency fluctuations.

After detrending the signal intensity and phase to take out their low frequency component that is associated with satellite motion and multipath, high frequency fluctuations are converted into proper units (dB for intensity and meters for phase) to be written into a specific file format (User Commands File using *MOD* command of the Spirent simulator firmware) that is recognized by the simulation firmware. This file is then included in the simulation scenario. Appendix 0 involves algorithm details for extracting the scintillation effects from raw phase and intensity data.

5.2. METHODOLOGY

Modelling, *monitoring* and *mitigating* ionospheric effects within the scope of GNSS modernization is the research purpose of this PhD work. In this sense, the methodology of the research is described respectively for the refractive and diffractive ionospheric effects.

5.2.1. INVESTIGATION OF THE IONOSPHERIC REFRACTIVE EFFECTS

The first phase of studying the ionospheric refractive effects is a profound understanding of how the ionosphere refracts the signals and the level of error this refraction introduces to the range measurements and consequently to GNSS positioning.

The second phase is about defining the tasks required by the research purpose and the techniques to achieve them. In this sense,

- Modelling the refractive effects is investigated by addressing each error term through a mathematical formula that is compiled and updated from literature review. Investigation starts with the mathematical representation of the second order (Iono2), third order (Iono3) and ray bending error terms in GNSS range measurements (for both code and phase, however confining the analyses to code measurements for practical purposes). Mathematical formulas for the error terms are written in MatLAB to analyze error bounds under different ionospheric conditions, which are determined by the values of the involved parameters, such as the geomagnetic field for Iono2 and the maximum electron density for Iono3. It is based on these mathematical models, implemented in MatLAB, that plots (in Section 3.1.2.) of the higher order error terms for different GNSS signals and background physical conditions are constructed.
- Monitoring is shown to be feasible through use of the mathematical formulae which, if updated in real time with necessary input information, can provide monitoring of the refractive effects.
- Mitigating the refractive effects is possible through estimation or elimination of the error terms. For *estimation* purposes, mathematical models for each error term can suggest how they can be used realistically to estimate the error in range measurements *including* the new GNSS signals: an interested user needs to provide values or ranges of values for the parameters involved in these error terms to obtain estimates for the error in code/carrier range measurements.

  For *elimination* purpose, creating linear combinations of observations can be useful. Considering the order of the error term

that needs to be eliminated (excluding ray bending error term), different orders of approximations are shown. A first order approximation helps eliminate the first order error term through combination of observations on two different signal frequencies that leads to an ionosphere-free observable (however containing residual errors due to higher order error terms). A second order approximation, possible thanks to triple-frequency GNSS, helps eliminate both first and second order ionospheric error terms leading to a further improved ionosphere-free observable with *less* residual error.

The third phase of the methodology consists of the data and routines that are exploited for the tasks mentioned above. These consist of:

- *Data*: IGS field recorded data from stations in Europe and open sky data collected by receivers in the projects involving NGI are considered for practical assessment of the refractive effects.
- *MatLAB routines*: For estimating the error bounds and eliminating the first and second order error terms by linearly combining observations in dual and triple frequency approach, respectively.
  Rinex_HO program: It applies the mathematical foundations described in Chapter 3 with necessary input ionospheric information to estimate per range measurement per frequency (L1 and L2) Iono2 and Iono3 for a particular receiver location (using observations from the receivers chosen in the IGS network in Europe in this work) and DOY. The program also "corrects" the range measurements in the observation file in accordance with the estimated Iono2 and Iono3 terms which yields a "corrected observation file" in RINEX format. Figure 5.8. describes the steps involved in processing with the Rinex_HO program, which was compiled and run in Windows platform in this work. In principle, the two input files "Rinex_ha.inp" and "Rinex_ha_param.dat" need to be updated according to the particular data that is processed, for instance, the former to contain the names of the necessary files such as the observation and navigation, and the latter to contain the parameter values such as the precision of the observables. All necessary files should be made available in the folder where the program is run from. The program returns the output files into the same folder where it is run from (Marques et al. 2011).

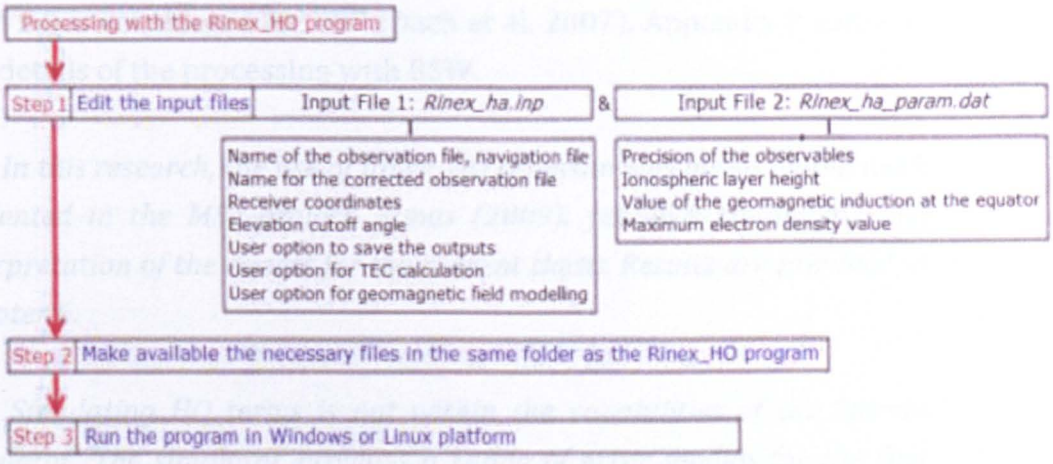

Figure 5.8. Steps involved in the Rinex_HO program.

In addition to investigating the ionospheric refractive effects *as individual error terms* under different ionospheric conditions and methods of estimating or eliminating them, it may be of interest to the GNSS community an assessment of the impact of HO terms on GNSS positioning. In this sense, the corrected observation files by Rinex_HO are considered for position computation to assess the influence of such corrections in new estimates of station coordinates. Analysis of differences in the estimated station coordinates helps to determine how much positioning error the higher order error terms can cause under different physical backgrounds. This has been the method for studying how much the higher order error terms (neglecting ray bending) can impact the estimated station coordinates under different solar / geomagnetic / ionospheric background conditions.

- *Positioning software*: For assessing the impact of using "corrected" (against Iono2 and Iono3) observation files output by Rinex_HO as opposed to using the original observation files. PPP is a high accuracy (cm level) positioning method which can be performed by a dual-frequency receiver (to create the IF observable) in stand-alone mode, such that the satellite orbit and clock corrections are assumed to be known from precise satellite orbit and clock data products with cm level accuracy (Gao 2006) instead of differencing (as in differential positioning) or estimating (Beutler et al. 2007). Therefore, PPP is the choice of positioning technique in this project so that the effect of correcting the observation files for HO ionospheric effects can be analyzed. The positioning software BSW

V5.0 is considered for PPP (Dach et al. 2007). Appendix P contains details of the processing with BSW.

N.B. In this research, the use of Rinex_HO program was based on the work presented in the MSc project, Elmas (2009), yet with re-analysis and interpretation of the results for the current thesis. Results are provided in Chapter 6.

N.B. Simulating HO terms is not within the capabilities of the Spirent simulator. The simulator provides a range of error models for the first order ionospheric error term that is based on TEC only (Spirent 2009).

5.2.2. INVESTIGATION OF THE IONOSPHERIC DIFFRACTIVE EFFECTS

The first phase of studying the ionospheric diffractive (scintillation) effects involves understanding the diffractive nature of the ionosphere, gaining further knowledge about impact of scintillation on GNSS signals, and acquiring a perspective of receiver architecture for signal tracking loops to carry out the investigation in a cause and effect approach regarding how the affected signals pose a challenge for the tracking loops and thereby for the positioning solution.

Second phase involves tasks that are required by the research purpose of this thesis which, in this case, can be stated in terms of the diffractive effects as:

- Modelling the impact of scintillation effects on signal tracking performance during especially strong levels of (amplitude) scintillation. This task was born out of necessity while using Conker model, which contains inherent limitation for application during adverse scintillation conditions.
- Monitoring the scintillation effects especially on the new signal frequencies such as GPS L2C, L5 and Galileo E1 – as long as scintillation events occur during the period when receivers deployed in the field were capable of tracking these new signals.
- Mitigating the scintillation effects in GNSS positioning is considered in this research in two approaches:

(i) *Considering all observations* in LoS where the observations are made to contribute to the GNSS positioning solution depending on the degrading effect of scintillation on them,
(ii) *Excluding "some" observations* from contributing to the GNSS positioning solution when the scintillation effect on particular signals is above a predefined threshold about severity of scintillation.

Regarding approach (i) where all observations are considered, the impact of scintillation in the positioning solution is mitigated through improving the GNSS stochastic model by tuning the statistical quality of the individual observations, as shown in prior work by Aquino et al. (2009). Such statistical quality of the observations is determined in terms of the jitter variance, which in the work of Aquino et al. (2009) is estimated using the Conker model. As highlighted earlier in Section 3.2.2.2, the use of Conker model can be limited at times to assist the approach (i) and this PhD proposes an estimation technique for the jitter variance that can facilitate the mitigation approach in (i) for times of strong sctintillation as well as for the new GNSS signals.

In a typical GNSS data processing strategy for the navigation/ positioning solution, the Least Squares (LSQ) approach can be considered (Amiri-Simkooei 2007; Ebner 2008; Elmas et al.2010c), where the user position is estimated on an epoch-by-epoch basis after the linearization of the measurement equations (Kaplan & Hegarty 2006). The LSQ approach aims to minimize the sum of the squares of the residual errors in the estimated position solution per epoch. (Kaplan & Hegarty 2006; Misra & Enge 2006). Whereas the functional model of the LSQ adjustment describes the relation between the measurements and the unknown parameters (position coordinates and the unknown clock bias), the stochastic model gives the variance-covariance matrix of the estimated unknown parameters (Elmas et al. 2010c).

The LSQ model for a receiver "A" observing satellites i, j, k and l, considers the inverse of the covariance matrix of the observations as the weight matrix, W, of the form:

$$W = \begin{bmatrix} 1/\sigma_A^{i\,2} & 0 & 0 & 0 \\ 0 & 1/\sigma_A^{j\,2} & 0 & 0 \\ 0 & 0 & 1/\sigma_A^{k\,2} & 0 \\ 0 & 0 & 0 & 1/\sigma_A^{l\,2} \end{bmatrix} \qquad \text{(Eq. 44)}$$

where no correlation between the observations is assumed (therefore the off-diagonal elements in the W matrix have the value of 0), and the observable variance for the receiver "A" and the satellite i/j/k/l, $\sigma_A^{i\,2}$, is assumed to be the same (i.e. same observation precision) for all receiver/satellite pairs, i.e.

$$\sigma_A^i = \sigma_A^j = \sigma_A^k = \sigma_A^l = \sigma$$

This simplifies the weight matrix into an identity matrix. I, which can be written as:

$$W = 1/\sigma^2(I) \qquad \text{(Eq. 45)}$$

The idea of "improving" the stochastic model is based on "redefining" each variance in the weight matrix, $\sigma_A^{i\,2}$, in terms of the tracking error – this makes the weights matrix more realistic regarding the physical scintillation effects on different receiver/satellite paths. For each receiver-satellite link the particular jitter variance estimated for that link is assigned, and the inverse of this variance becomes the weight for that observation in the W matrix such that greater the jitter variance, less is the weight.

The mitigation approach "improves" the stochastic model by re-defining the precision that is associated with each observation; this re-definition is done in terms of the tracking error associated with each observation. In this approach, formerly studied by Aquino et al. (2009), the degrading effect of scintillation on the signal tracking is evaluated in terms of (an increase in) the variance of the signal tracking error in code and carrier tracking loops. As such, larger variances (as expected during stronger scintillation) are associated

with poorer tracking performance which can be linked with less accurate range measurements during scintillation. Estimates for the variances (for code and carrier tracking loops) are considered for "weighing" the observations such that larger tracking error variance estimated for a particular observation on a particular link implies assigning it a smaller weight, i.e. reciprocal of the estimated variance defines the weight for that observation. The common practice of assigning predefined precision values to the different observables such as L1, L2, C1, P2 (independent of link) in the stochastic model may not realistically take into account the impact of scintillation. Assigning different precisions per observations on different signal paths can be *more* representative of the scintillation effect which can be "link-specific". This helps to reflect the "per link effect" of the ionospheric scintillation enabling the contribution of each observation be proportional to its estimated weight[d].

Aquino et al. (2009) show the results for baseline positioning where the authors modify the stochastic model as described earlier. They consider data from the high latitudes with moderate level of scintillation and use the scintillation sensitive model of Conker et al. (2003) to estimate the jitter variances of the tracking error for the coded (GPS L1C/A) and semicodeless (for GPS P(Y)) delay and phase locked loops. Using the Conker model requires to input the scintillation indices (S_4 and SigmaPhi), signal-to-noise ratio and spectral parameters (p and T) every minute. In addition to the issue raised earlier (Section 3.2.2.2.) about the Conker model regarding its use for data with strong amplitude scintillation, the need for reliable and on-time (when the processing is in real time although the mitigation approach can also be implemented in post processing) prediction of the spectral parameters can make the use of this model further complicated.

[d] *Significant levels of ionospheric disturbance may lead to correlation between different observation types which, as observed by Lui (2001), can be insignificant. However, temporal correlation may occur as pointed out in studies of El-Rabbany (1994) and Wang et al. (2002).*

For results of the mitigation technique for approach (i), the jitter variances for the code observables are calculated based on the technique proposed in Section 4.2., where calculation is performed for the L1 signal and scaled[e] for the L2. For the carrier phase observables on GPS L1, the jitter STD estimation method is applied for the L1 signal as described in Section 4.2. and scaled[f] for the L2. Appendix Q provides details about the steps involved in the application of the mitigation technique in the GNSS positioning software RT_PPP and GPSeq considered in this thesis.

The height component is focused on in the results shown for the approach (i) given above as the height error in general varies more than that of the horizontal components.

[e] *Scaling the DLL jitter STD for the L2 frequency is achieved by multiplying the estimated STD values for L1 by a factor decided by exhaustive testing (based on the similar ratio between precision values for C1 and P2 in standard positioning): scale factors of 5, 10 and 20 were tested to multiply the jitter STD estimated for the C1 observable to be usable for the P2 observable in the weight matrix. Testing such different scale factors and observing the positioning results with mitigation indicated that a scale factor of 20 gives better results (and a larger value beyond 20 does not bring any significant improvement); thus this value was adopted in the mitigation analyses. The reason that the jitter STD cannot be estimated directly for the P2 observable (and needs to be obtained from C1) is due to non-availability of I/Q output from the receiver for semicodeless tracking, which is the case for this observable.*

[f] *Scaling of the PLL jitter STD for the L2 frequency is achieved by multiplying the jitter STD values obtained for the L1 signal with the ratio of the frequencies, "f_1/f_2" where f_1 and f_2 are frequencies for the L1 and L2 signals. This leads to "scaling up" the jitter STD values obtained for L1 by about 1.28 to be used for the L2 observable; and this ratio is also observed to exist between the precision values assigned to these observables in the non-mitigated case.*

Regarding approach (ii) where selected observations are excluded, results are shown in this section where observations corresponding to instances of *significant* scintillation levels associated with high elevation angle signal paths are excluded from the observation file, which can be performed in real-time or post-processing. This is similar to Receiver Autonomous Integrity Monitoring, RAIM, whereby a faulty measurement can be detected and excluded from the positioning solution based on a self-consistency check performed with the available observations – the least squares position solution residual can be used for such consistency check (Kirkko-Jaakkola et al. 2009; DLR 2012). Here, the attempt is to detect possible "faulty" observations based on the scintillation level while the elevation angle is "high enough" to assume that multipath can be neglected. Scintillation level and the respective elevation angle define a threshold, which is determined by the user, such as when $S_4>0.8$ with corresponding elevation angle being greater than 45^0. Mitigation in this approach is performed in post-processing (as in approach (i)) where first a particular data set is analyzed for the amplitude scintillation index S_4 along with the respective elevation angle to determine instances when both parameters are greater than user-specified thresholds. Corresponding observations are then excluded from the observation file and positioning is performed with the original observation file as well as the one from which the flagged observations are excluded. GNSS positioning in this approach is performed with NRCan software.

The third phase of the methodology for investigating the diffractive effects consists of the data and routines that are necessary to achieve the above defined tasks. These tools consist of:

- *Data*: Field recorded and simulated data both of which are made available by receivers in terms of high rate signal intensity and phase (in particular I/Q data in the case of PolaRxS receiver) data and 60s data including the scintillation indices and other parameters..

  - *Field recorded data* has been analyzed for frequency dependent impact of scintillation on GNSS signals; this helps in particular for implementing scintillation effects (extracted or generated by a model) on different signal frequencies in simulations. Field

recorded data is also exploited for extracting scintillation induced intensity and phase fluctuations (through MatLAB routines).

- *Simulated data* has been useful to correlate the simulated scintillation effects and receiver signal tracking performance where the tracking loops can be set to different configurations to arrive at an optimum tracking configuration depending on the scintillation level.

High rate signal intensity and phase data from the GSV4004B receiver was considered mainly during the start of this PhD – its use was mainly for extraction of scintillation effects from signal intensity and phase in order to perform simulations with these effects implemented on the generated signals. With the availability of data logged by the Septentrio PolaRxS receiver through the CIGALA project, high rate data was predominantly obtained from this receiver deployed at low latitude stations. Therefore the majority of the data analyzed between 2010-2012 was from the PolaRxS receiver. One main reason for this was that this receiver makes raw signal measurements available[g] to the user in the form of post-correlator signal samples (I/Q) that provide a genuine source to study the actually effects on signal propagation.

- *MatLAB routines*: For data handling, extraction of scintillation effects from open sky data and formatting into a user commands file for insertion into simulation scenarios, evaluation of receiver signal tracking performance based on the Conker model and a proposed technique using I/Q data. Investigation of scintillation effects starts with loading receiver logged high rate (50Hz) and 60s data into MatLAB, where data parts of interest are made available for use in calculations and plots. Processing 60s data in MatLAB enables characterization of the level of scintillation regarding different signal frequencies and this helps to decide whether the

[g] *The receiver records I/Q as part of its high rate data file that is input into MatLAB to separate out IQ with timestamps per constellation, frequency and SVID. More details about I/Q data are provided in Chapter 4.*

corresponding high rate data shall be considered for extracting[h] scintillation effects or applying the mitigating technique. For the specific file formats of GSV4004B and PolaRxS receivers, MatLAB routines were created to read a file with specific data columns and sort data for a signal of interest to the user.

The evaluation of receiver signal tracking performance starts with the use of the Conker model and focuses in particular on its limited use for receivers at the low latitudes where amplitude scintillation can render the model inapplicable (Section 3.2.2.2.). For continuous evaluation of code tracking performance independent of S4 and for any GNSS signal, an innovative approach is proposed in this PhD work that uses high rate receiver logged data (from the *prompt, "P",* correlators, Fig. 3.18.) for evaluating scintillation induced increase in thermal noise in the tracking loops, which is fundamental to estimate the DLL jitter variance, as suggested by Conker et al. (2003). This new technique was initiated with the analysis of the limitation in the Conker model for the thermal noise term (Section 3.2.2.2.) that is modelled as a function of S_4 and C/N_0. In principle, if S4 and C/N_0 can be approximated in terms of the I/Q data (after all, I/Q is related with signal amplitude which is related with C/N_0 and thereby S4 i.e. such approximation is reasonable and possible), then the model of Conker related with the thermal noise and the DLL jitter variance can be approximated in terms of the I/Q data. Section 4.2. includes details of this approximation for evaluating the DLL error variance. MatLAB routines were devised during this PhD to take I/Q data as input from receiver logged high rate signal data file and approximate the DLL jitter variance.

[h] *For extracting the scintillation effects from high rate carrier phase data, a routine from Aquino et al. (2007) about estimating the SigmaPhi index from high rate carrier phase data was considered (see Appendix O). This routine was completed to include extraction of perturbations from signal intensity data. Extracting perturbations from signal intensity and phase is automated in MatLAB to format the perturbations into specific files recognized by the Spirent simulator so that they can be included in simulation scenarios.*

- *Spirent GNSS Signal Simulator*: For performing scintillation oriented simulations, the Spirent simulator was an important tool for the methodology of investigating scintillation effects on GNSS signals, in particular for studying extreme ionospheric conditions and considering the new signals that are not yet being broadcast.
- *GNSS receivers*: For capturing open sky data in the field and in simulations. The NovAtel GSV4004B receiver was used at the beginning of this research in simulations where it was subjected to GNSS signals with scintillation effects applied through the use of open sky data (as described in Section 5.1.2.). Later in 2010, the Septentrio PolaRxS receiver was started to be deployed in the field at the low latitudes as well as used in simulations. The PolaRxS receiver was used significantly more than the GSV4004B receiver due to its multi-frequency tracking capability, user options for the receiver configuration and the novel I/Q data output feature.
- *Positioning software:* For assessing the *impact* of scintillation i.e. the level of degradation in accuracy/availability of a positioning solution during scintillation and applying mitigation against scintillation in positioning based on previous work by Aquino et al. (2009), different types of GNSS positioning software such as the real time PPP software *RT_PPP*, baseline positioning software *GPSeq* and online GNSS positioning tool provided by the Natural Resources Canada, *NRCan*[i], were considered in this thesis. The first two, made available by colleagues at UNESP, Presidente Prudente, Brazil, for research purposes, are especially helpful for applying the mitigation technique against range errors induced by scintillation. They were also used in the work by Aquino et al. (2009) about baseline positioning. However, in this present work

[i] *NRCan is an online post-processing tool that allows users to submit GPS observation files over the internet and receive PPP results either in the Canadian Spatial Reference System or the International Terrestrial Reference Frame (ITRF) (the latter is considered in this work). NRCan considers the antenna phase center for height estimation and applies a 10° elevation cut-off angle. Single station position estimates are obtained from NRCan in static mode using precise GPS orbits and clocks.*

they were used for scintillation data of stronger levels. The choice of the RT_PPP and GPSeq programs for the mitigation work has two main reasons:

1. Possibility of user interface to implement the mitigation technique (developed earlier by Aquino et al. (2009)) which assumes different weights per SV per observations type unlike the common concept of assigning the same weights per observable in stochastic modelling. User interface for implementing the mitigation algorithm requires the use of a file containing weights as inverse jitter variances. The user provides weights (per link per frequency) in the form of a text file that RT_PPP and GPSeq can read. (More details can be found in Appendix Q)

2. Option to decide the type of positioning to perform such as point or differential (baseline) positioning (GPSeq) or precise point positioning (RT_PPP). Furthermore, the user can opt for kinematic, static or epoch-by-epoch solutions.

- Use of the online positioning tool NRCan was considered for showing the impact of scintillation on different data sets recorded at the PRU2 station (22.1^{0}S, 51.4^{0}W) in Presidente Prudente, Brazil. Further use of the NRCan program is related with the exclusion of selected observations from the observation file according to the corresponding satellite elevation angle and scintillation index S4 (as explained in Section 6.2.4.2.).

A brief summary for the Sections 5.2.1. and 5.2.2. is provided herein:

- Regarding the investigation of the *ionospheric refractive effects* (Section 5.2.1.), the first step involves understanding the ionospheric refractivity on GNSS signals and the ranging errors induced by refractivity. The second step involves investigating the refractive effects from the aspects of modelling, monitoring and mitigating. Modelling was studied on the basis of the mathematical formulae for the refractive error terms analyzed in MatLAB; monitoring was aimed to be shown with the help of the mathematical formulae introduced, and mitigating these error terms was discussed through the methods of elimination and estimation. The final step is related with the data considered and the routines performed for these tasks. The data for studying the refractive effects is obtained from the IGS network stations selected from the

European region and the open sky data collected by NGI through the projects participated in. The investigations of refractive effects involved MatLAB code to assist the estimation and elimination of the first and HO refractive errors; the Rinex_HO program, which not only estimates the HO error terms but also corrects the observation files against them; and the BSW V5.0 positioning software for performing coordinate estimation.

- Regarding the investigation of the *ionospheric diffractive effects* (Section 5.2.2.), scintillation in particular, the first step involves understanding the diffractive effects of the ionosphere on GNS signals and acquiring a perspective of GNSS receiver architecture. The second step focuses on the modelling, monitoring and mitigating tasks for the scintillation effects. Modelling considers the impact of scintillation on GNSS signals (with keen interest in the new signals) and receiver signal tracking performance. Monitoring is concerned with the data collected in the field during scintillation events, especially including the new GNSS signals. Mitigating the scintillation effects is based on the earlier work by Aquino et al. (2009), for which the investigation here makes use of the post-correlator data for estimating the tracking error variances that are used to "weigh" the observations. The final step consists of the data considered for the tasks and the routines for executing these tasks. The data analyzed for the diffractive effects is the field recorded and simulated data. The investigation of diffractive effects involved MatLAB codes (for data handling, formatting, detrending and evaluating the signal tracking error variance); the Spirent simulator; GNSS receivers (NovAtel GSV4004B and Septentrio PolaRxS) and GNSS positioning software (RT_PPP, GPSeq and NRCan).

CHAPTER 6

6. RESULTS AND DISCUSSION

This chapter presents the results for the investigation about the ionospheric effects on GNSS considering the new GNSS signals. The ionospheric effects introduced theoretically in Chapter 3 are supported in practice through the field data recorded data in this chapter. Results are presented in two main sections for the refractive and diffractive effects, and each section ends with a discussion of the results.

6.1. RESULTS FOR THE IONOSPHERIC REFRACTIVE EFFECTS

Results presented in this section are about the ionospheric refractive (delay) effects and their impact on the GNSS measurements and positioning solutions subject to different ionospheric conditions. It is also included how the new GNSS signal frequencies can be exploited to eliminate the first and second order ionospheric error terms, respectively.

The results related to the impact of the higher order ionospheric effects in PPP are based on the data which was analyzed in the author's MSc project submitted to IESSG, University of Nottingham, in 2009. The data was reanalyzed and interpreted to incorporate the results into this thesis. These results were presented at the General Assembly of European Geosciences Union in Austria in 2010 (Elmas et al. 2010a) and earned the Outstanding Student Poster Award, which led to publishing the work in Annales Geophysicae (Elmas et al. 2011a).

6.1.1. IMPACT ON GNSS MEASUREMENTS

Results describing how much the ionosphere can induce errors in the GNSS measurements obtained using the Rinex_HO program are shown in this section. Regarding the field recorded data obtained from the IGS stations (Fig. 5.2.) in the form of observation files in RINEX format, the error contribution of Iono1, Iono2 and Iono3 to the total range error calculated by the Rinex_HO program for the days analyzed (given in Table 5.2.) and the results are shown in this section. In these calculations, the ray bending error term is neglected. Results are presented for the GPS L1

signal frequency per station during the four periods of days corresponding to different solar/geomagnetic/ionospheric background conditions. For the other GNSS signal frequencies, the frequency dependence of the error terms described in Section 3.1. can be applied to inspect the error terms for different observables.

Considering the dual-frequency open sky data from the IGS stations, the results for the Iono1 (Section 6.1.1.1.) and HO error terms (6.1.1.2.) do not take into account the new GNSS signals, such as GPS L2C, L5 and Galileo E1, E5a/b. This is mainly due to:

(i) The dates for the data obtained from IGS stations in these analyses which do not overlap with GNSS modernization to include the newly broadcast signals;

(ii) The fact that even when observation files containing the new signals were available, the Rinex_HO program in its version used in this research was not upgraded to process the new observables of the modernized GNSS (such as C2, C5, L5[a]).

Estimating the ionospheric error terms is explained in Section 3.1.; elimination techniques that are outlined *mathematically* in Section 4.1. for the Iono1 and Iono2 terms are investigated in this section based on *open sky data*.

6.1.1.1. FIRST ORDER IONOSPHERIC EFFECT

Results are shown in Fig. 6.1. - 6.4. for Iono1 error term for the GPS L1 signal calculated by Rinex_HO using the IGS open sky data for the four sets of analysis days. The top plot in each figure shows the calculated Iono1 term in meters for each station (colour coded) and the subsequent plots show STEC (computed by using GIMs in Rinex_HO) for each station (Station coordinates can be found in Fig. 5.2.). Plots for STEC are provided to highlight the importance of STEC for the Iono1 error term computation, which contributes about 99% of the total range error induced by the ionosphere (Klobuchar 1996; Hofmann- Wellenhof et al. 2001).

[a] *C2 and C5 are the code observables for the GPS L2C and L5 signals; L5 is the carrier phase observable for GPS L5 signal.*

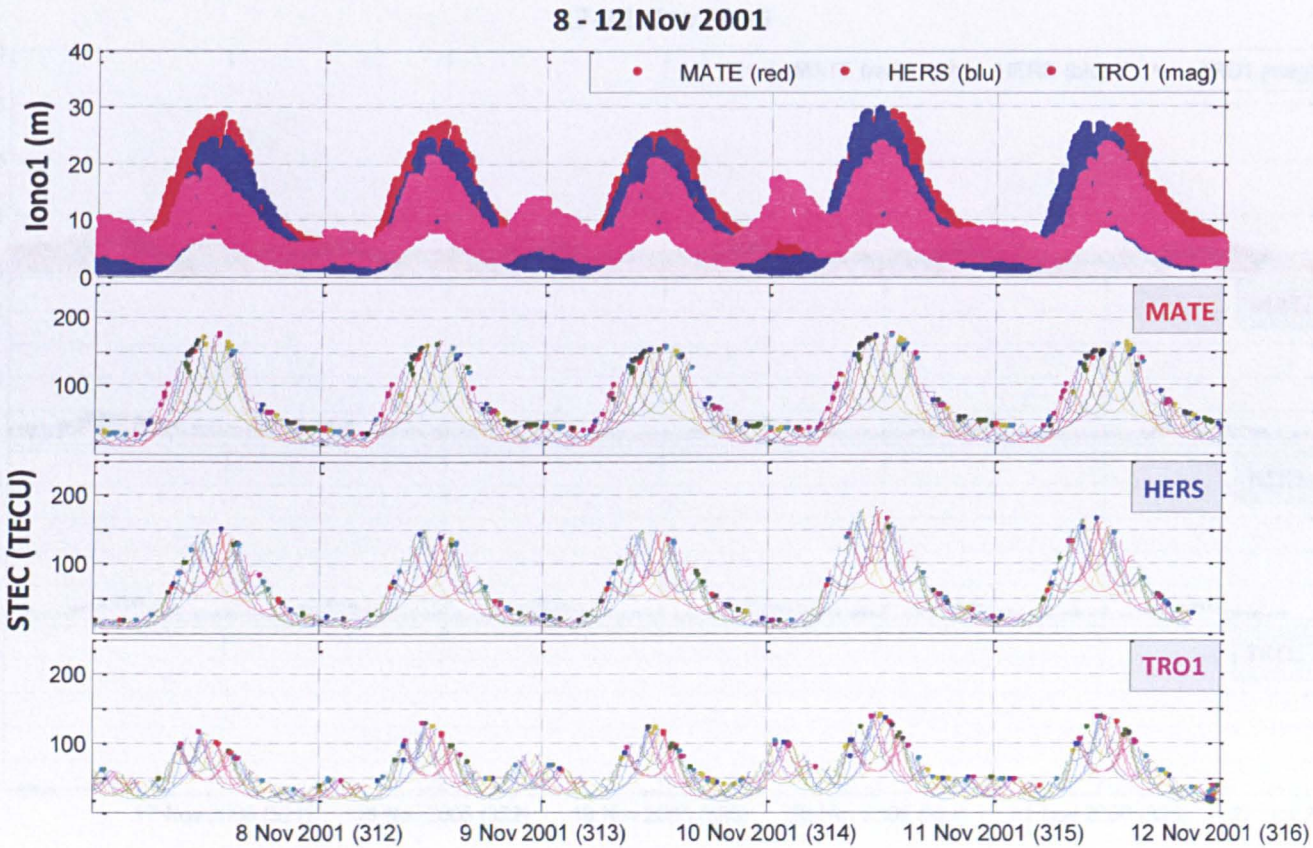

Figure 6.1. The magnitude of the Iono1 term (*top*) and the STEC values for each station are provided in the second (MATE), third (HERS) and fourth (TRO1) plots from the top. The results refer to the period 8-12 Nov 2001 (DOY 312-316).

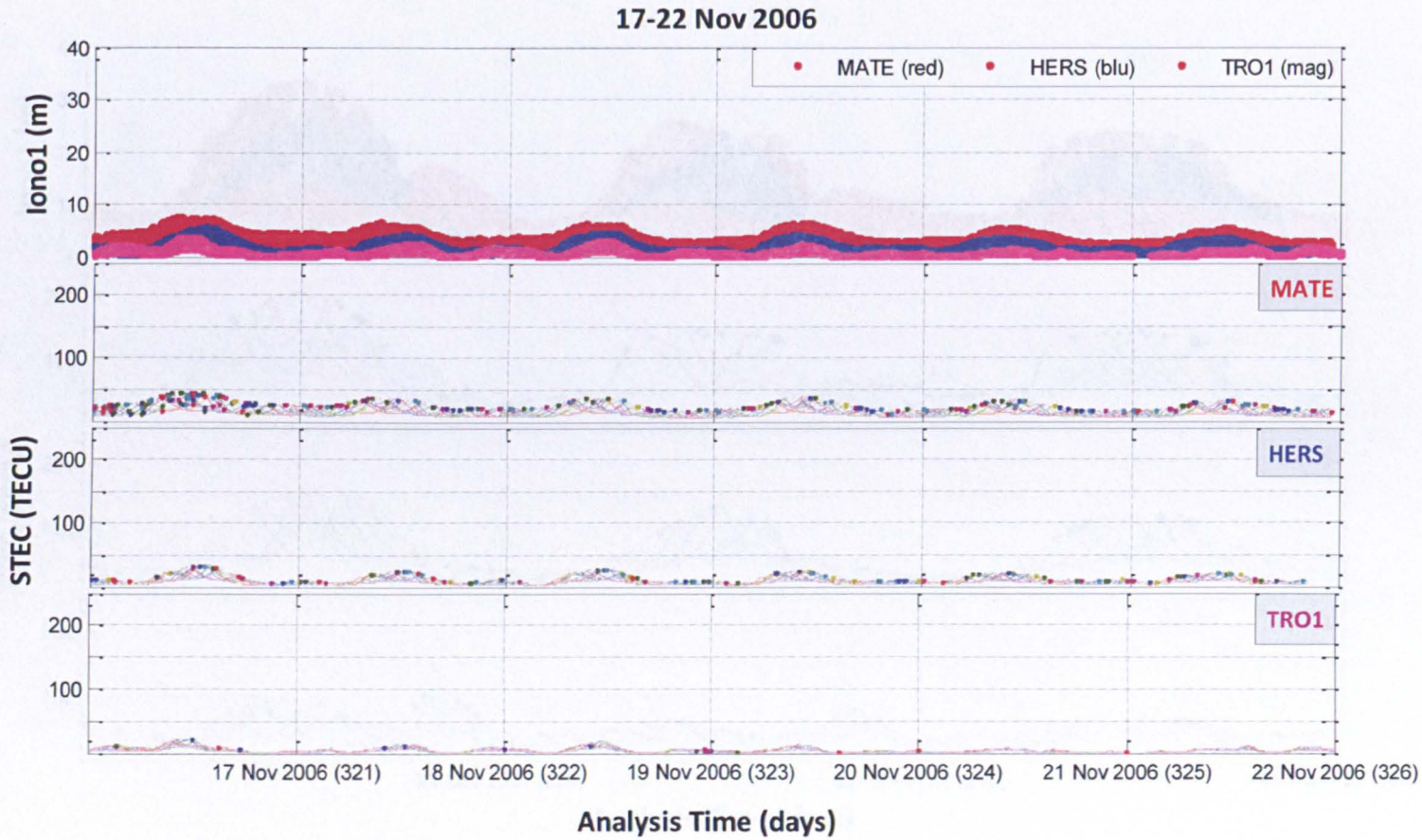

Figure 6.2. The magnitude of the Iono1 term (*top*) and the STEC values for each station are provided in the second (MATE), third (HERS) and fourth (TRO1) plots from the top. The results refer to the period 17-22 Nov 2006 (DOY 321-326).

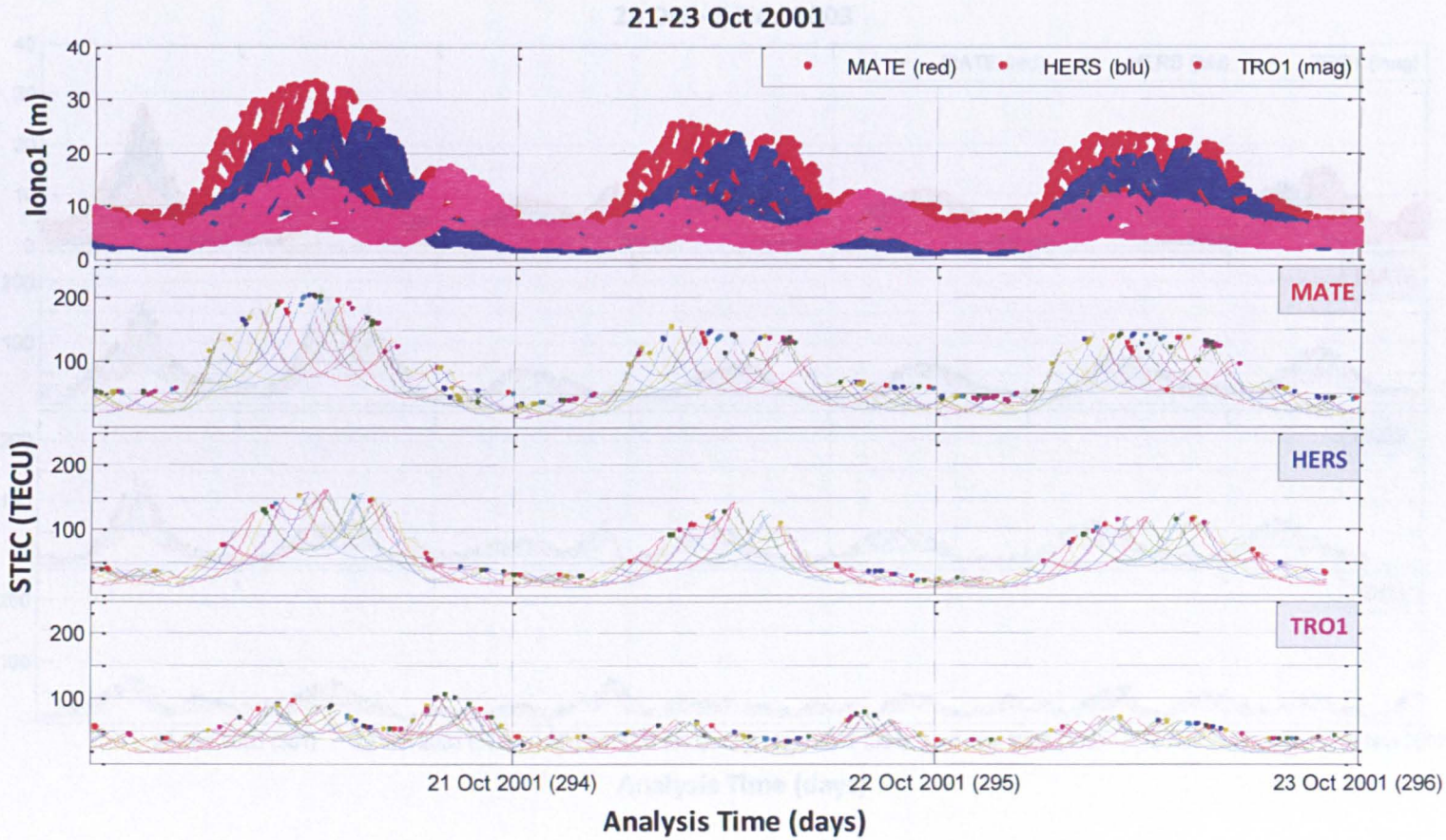

Figure 6.3. The magnitude of the Iono1 term (*top*) and the STEC values for each station are provided in the second (MATE), third (HERS) and fourth (TRO1) plots from the top. The results refer to the period 21-23 Oct 2001 (DOY 294-296).

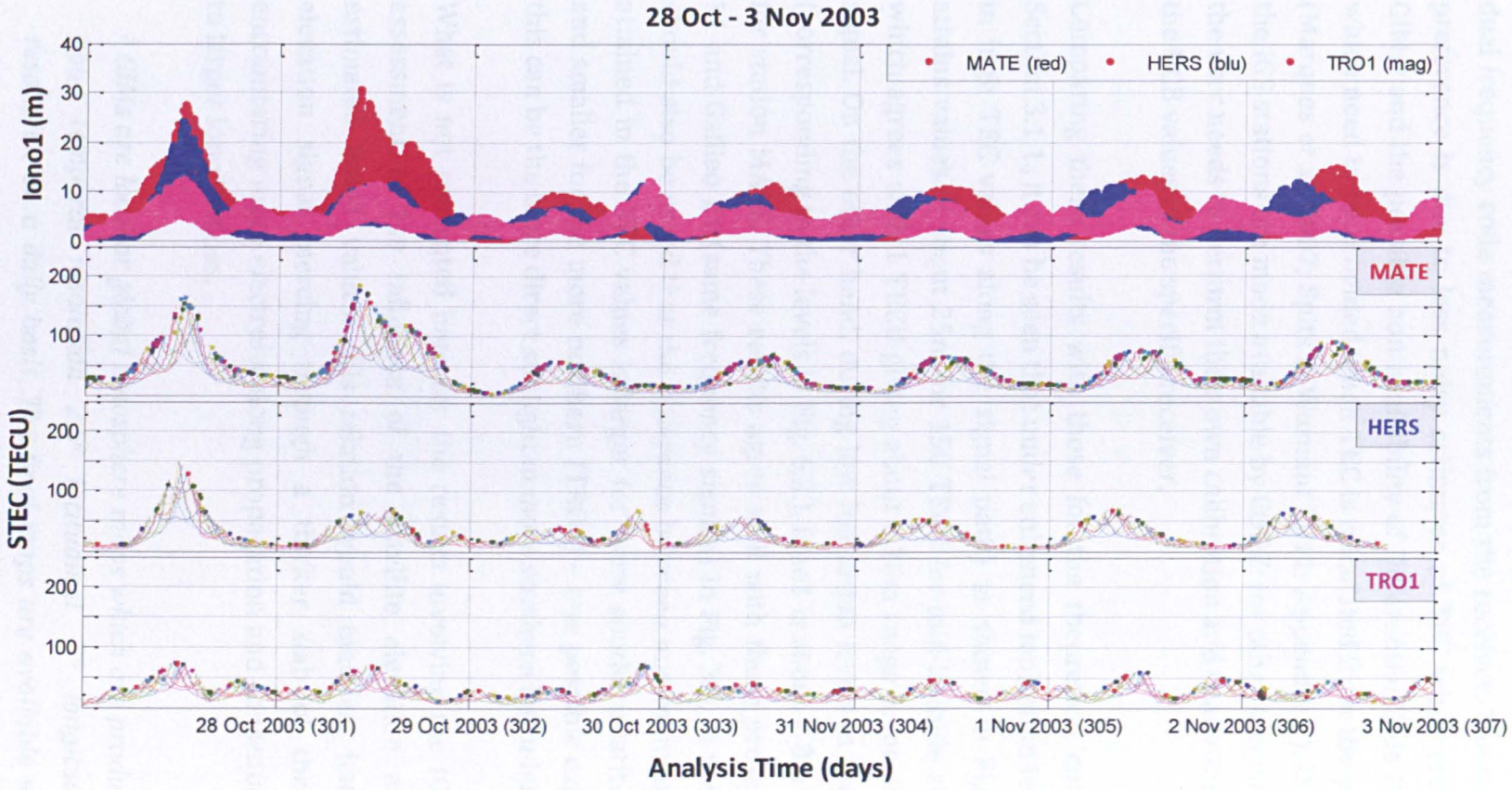

Figure 6.4. The magnitude of the Iono1 term (*top*) and the STEC values for each station are provided in the second (MATE), third (HERS) and fourth (TRO1) plots from the top. The results refer to the period 28 October – 3 Nov 2003 (DOY 301-307).

For evaluating the Iono1 term using Rinex_HO, the option of using GIMs was selected to estimate the TEC data per signal path instead of the use of dual frequency code measurements from the receiver. The reason for this preference is due to less noisy estimates of TEC when computed from GIMs[b] and the possible non-availability of Differential Code Biases (DCBs) which need to be provided when TEC is calculated from the pseudoranges (Marques et al. 2007; Spits & Warnant 2011; Appendix B). DCB values for the IGS stations are made available by CODE; for other receivers, however, the user needs to perform their own calibration and computation to obtain the DCB values of the specific receiver.

Comparing these results with those for the theoretical computation in Section 3.1.1., it can be seen that under enhanced ionization levels (evident in high TEC values along the signal path) as shown in Fig. 6.3., Iono1 attains values of about 25m for 150 TECU for mid-latitude station MATE, which agrees with 1 TECU giving about 0.16m range error on the GPS L1 signal. On the other hand, during low ionization levels in the ionosphere (corresponding to the levels in Fig. 6.2.), Iono1 is about 7-8m for 40 TECU, for station MATE. These results agree well with those presented for GPS L1 and Galileo E1 (same frequency signals) in Fig. 3.5. in Section 3.1.1. It should also be noted that the difference between minimum and maximum attained in the TEC values is larger for more southern latitudes (MATE) and smaller for the more northern (TRO1) – one possible explanation for this can be the more direct sunlight in more southern latitudes.

What is not presented here for the results involving the IGS data is an assessment of the influence of the satellite elevation angle on the estimated Iono1 values: this relation would manifest itself in a low elevation signal piercing through a thicker slab of the ionosphere encountering more electrons along propagation and consequently leading to larger Iono1 values.

[b] *GIMs are local or global ionosphere maps which are produced with two hour temporal resolution 2.5^0 latitudinal -5^0 longitudinal spatial resolution on a daily basis. The final maps are available within 3 days (Schaer et al. 1998).*

In addition to the IGS data analyzed within the context of the Iono1 error term, the investigation is expanded to focus on the elimination of the Iono1 term making use of data collected at PRU2 station containing measurements for the new GNSS signals GPS L2C and L5 that are considered in constructing the IF observable. The data was collected on 14 November 2011, during two periods of the day: an hour in the local morning, 08:00-09:00 (observing SV01) and another hour in the local post-sunset, 21:00-22:00 (observing SV25). The reason of this choice is to consider two relatively different background ionospheric conditions: quieter during the local morning and adverse during the local post-sunset. The scintillation level given by the S4 index observed for the triple frequency signal link with SV01 during the morning hour is plotted in Fig. 6.5. at the top, and that with SV25 during the post-sunset hour is plotted in the same figure at the bottom. It should be mentioned that the elevation angle for SV01 changes from 64^0 to 74^0, and that for SV25 from 32^0 to 52^0 during the hours of analysis.

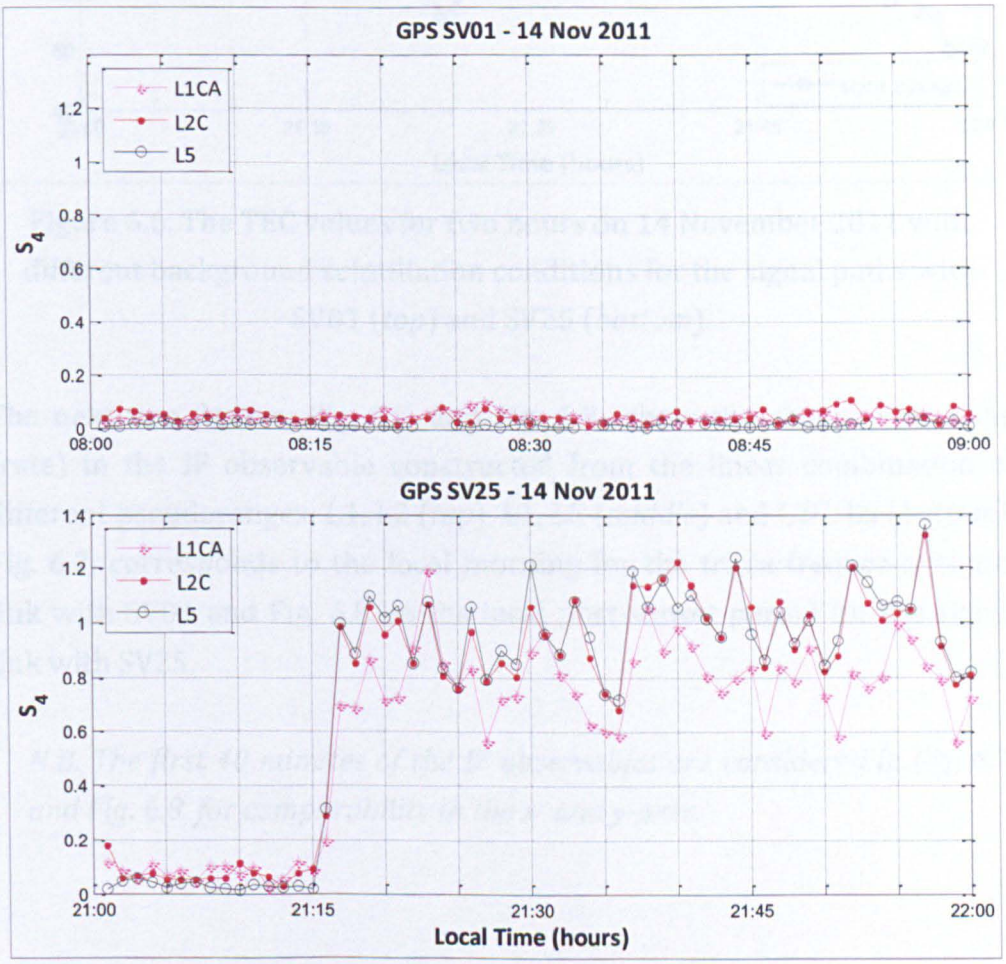

Figure 6.5. The S4 index for local morning (*top*) and post-sunset (*bottom*) hours for L1C/A, L2C and L5 signals.

The values for TEC during the two hours (shown in Fig. 6.5 for PRU2 station) are shown in Fig. 6.6. to describe the ionospheric conditions during these two hours considered here.

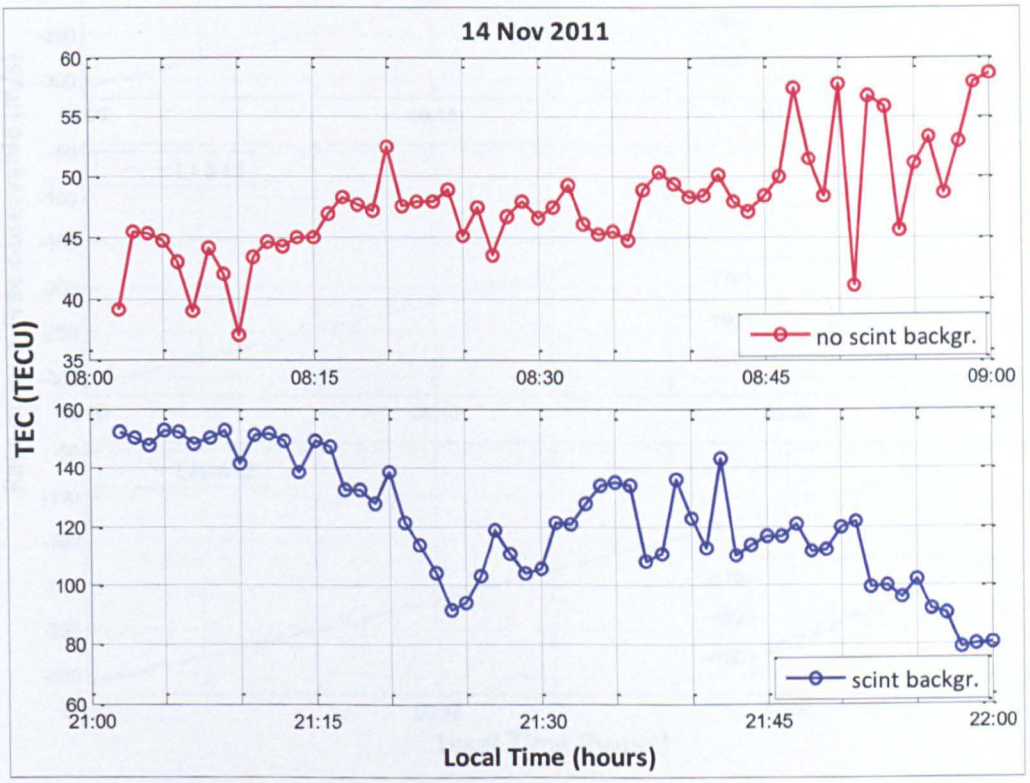

Figure 6.6. The TEC values for two hours on 14 November 2011 with different background scintillation conditions for the signal paths with SV01 (*top*) and SV25 (*bottom*).

The next two figures, Fig. 6.7. and Fig. 6.8., show the change over time (rate) in the IF observable constructed from the linear combination of different pseudoranges: L1, L2 (*top*), L1, L5 (*middle*) and L2C, L5 (*bottom*). Fig. 6.7. corresponds to the local morning for the triple frequency signal link with SV01 and Fig. 6.8. to the local post-sunset period for the signal link with SV25.

N.B. The first 40 minutes of the IF observables are considered in Fig. 6.7. and Fig. 6.8. for comparability in the x- and y-axes.

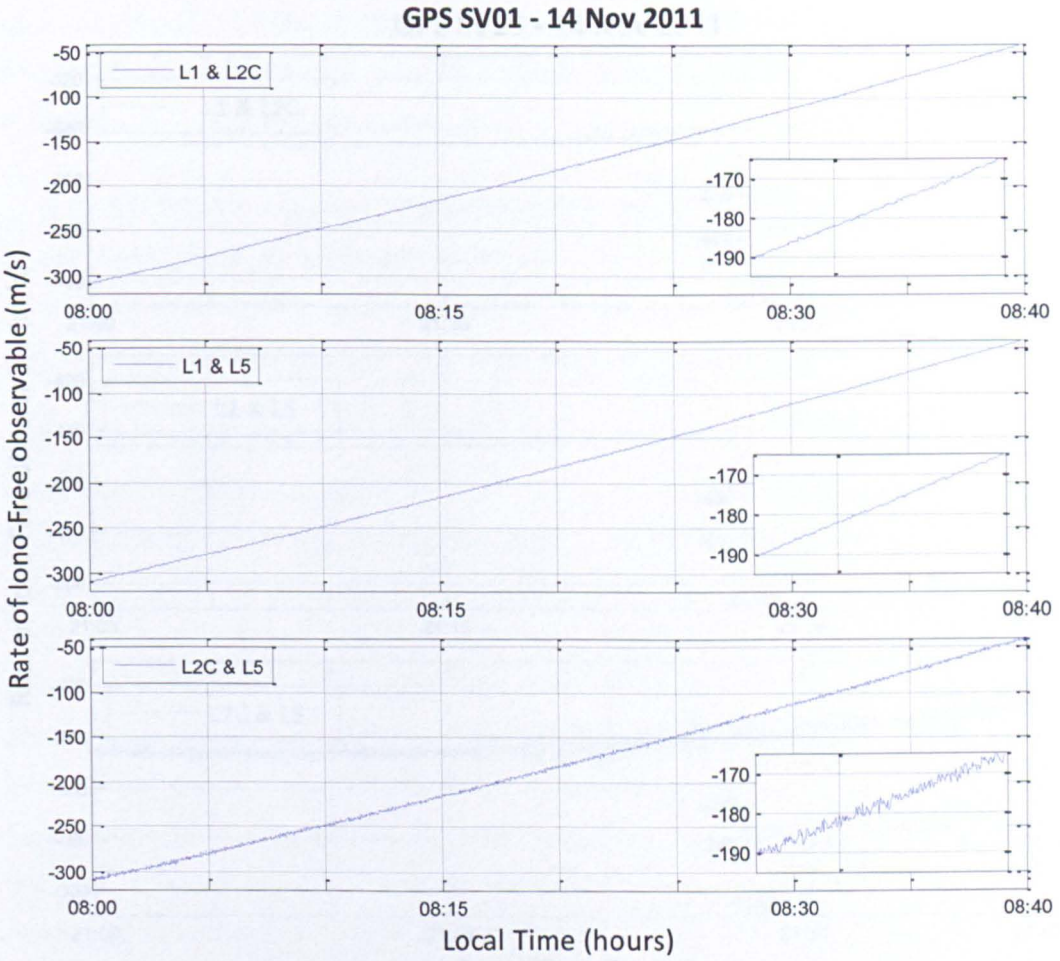

Figure 6.7. The rate of the IF observable constructed from the pseudoranges for L1, L2C (*top*), L1, L5 (*middle*) and L2C, L5 (*bottom*) signals; data for the local morning on 14 November 2011.

It can be seen that during negligible levels of scintillation on this signal path for which the satellite elevation changes from 64^0 to 74^0, the rate of change of the IF observable is comparable when L1 and L2C or L1 and L5 signals are considered for the linear combination. More variations in time can be noted in the case of when L2C and L5 signals are considered for the IF observable: inset in the bottom plot in Fig. 6.7. shows more variations compared with those in the top and middle plots.

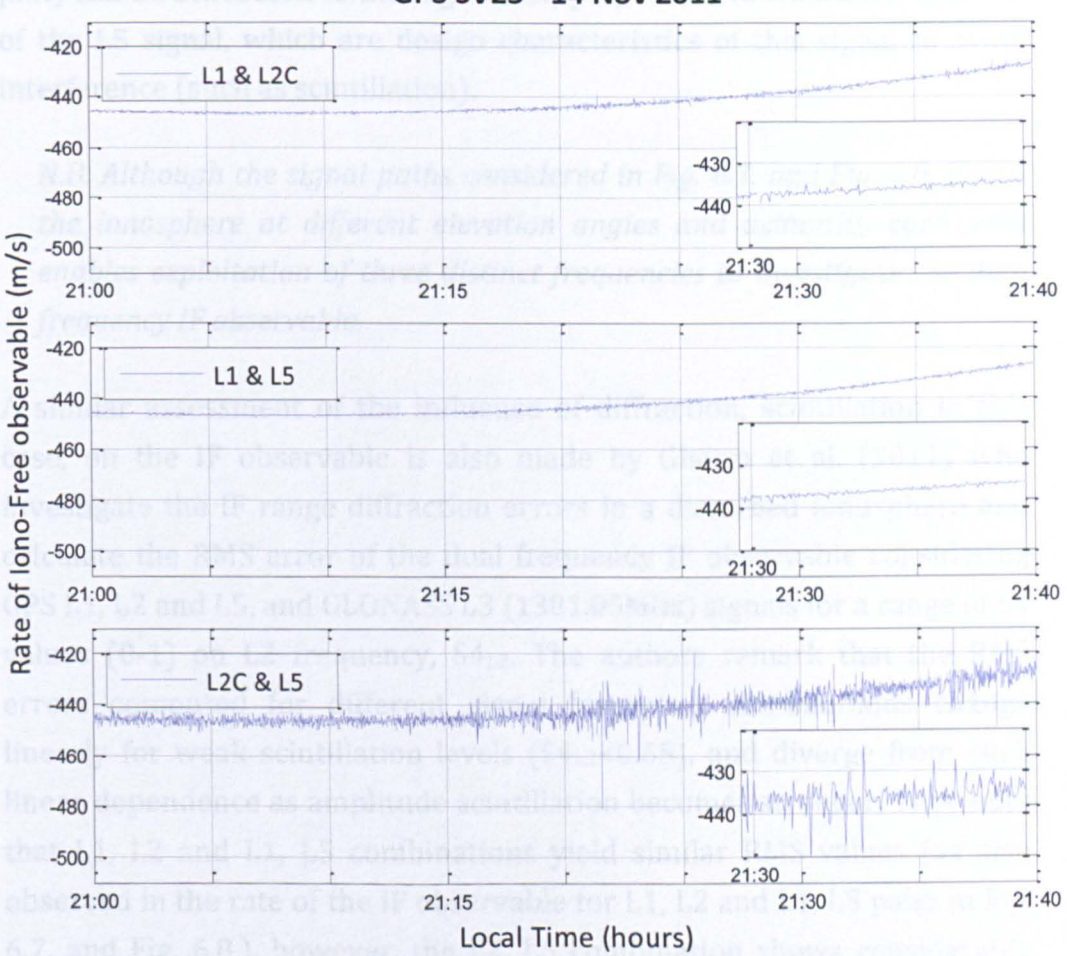

Figure 6.8. The rate of the IF observable constructed from the pseudoranges for L1, L2C (*top*), L1, L5 (*middle*) and L2C, L5 (*bottom*) signals; data for local post-sunset on 14 November 2011.

However, under strong scintillation levels, considering the signal path with SV25 which has elevation changing from 32^0 to 52^0, the rate of change of the IF observable constructed from different observables is remarkable: it can be noted that combining L2C and L5 signals in particular may not be an optimum choice for eliminating the first order ionospheric effect given that the resultant IF observable shows more variations in time especially with the onset of scintillation from about 21:15 local time onwards affecting the L2C and L5 band signals at saturating levels, which can be noted in the bottom plot of Fig. 6.5. Comparing the first two plots in Fig. 6.8., where the L2C and L5 signals are considered for the linear combination with the L1 signal, the slightly better performance of the linear combination L1, L5 (inset in the middle plot shows slightly less variations in time compared with that in the first

plot) can be attributed to the higher chipping rate and transmitted power of the L5 signal, which are design characteristics of this signal to avoid interference (such as scintillation).

N.B. Although the signal paths considered in Fig. 6.7. and Fig. 6.8. pierce the ionosphere at different elevation angles and azimuths, each path enables exploitation of three distinct frequencies to investigate the dual frequency IF observable.

A similar assessment of the influence of diffraction, scintillation in this case, on the IF observable is also made by Gherm et al. (2011) who investigate the IF range diffraction errors in a disturbed ionosphere and calculate the RMS error of the dual frequency IF observable considering GPS L1, L2 and L5, and GLONASS L3 (1381.05MHz) signals for a range of S4 values (0-1) on L2 frequency, $S4_{L2}$. The authors remark that the RMS errors computed for different signal frequency combinations change linearly for weak scintillation levels ($S4_{L2}<0.65$), and diverge from such linear dependence as amplitude scintillation becomes stronger. They note that L1, L2 and L1, L5 combinations yield similar RMS values (as also observed in the rate of the IF observable for L1, L2 and L1, L5 pairs in Fig. 6.7. and Fig. 6.8.), however, the L2, L5 combination shows considerably larger RMS values (as also observed in the higher rate of the IF observable for L2, L5 pair, Fig. 6.8.)

6.1.1.2. HIGHER ORDER IONOSPHERIC EFFECTS

Results for the Iono2 and Iono3 terms, respectively, are shown in Fig. 6.9. and 6.10. for the GPS L1 signal. STEC data for each station during the specific period of analysis can be retrieved from the bottom three plots in Fig. 6.1. - 6.4. introduced earlier. It should be remarked that the STEC parameter is not the only variable for Iono2 and Iono3 - Iono2 depends further on the magnitude of the geomagnetic field as well as the angle between the signal link and the geomagnetic field vector at the IPP and Iono3 on the maximum electron density along the propagation path.

The results for Iono2 and Iono3 are shown in Fig. 6.9. and 6.10., respectively, for the pseudoranges on GPS L1 (for the other GNSS signals the frequency dependency given in Section 3.1.2. can be applied). In the case of the pseudoranges, Iono2 results for the L1 signal frequency need to

be multiplied by about 2.11 for L2 and 2.40 for L5 signal frequencies. Similarly, Iono3 results for the L1 signal frequency need to be multiplied by about 2.71 for L2 and 3.22 for L5 signal frequencies. For the contribution of the error terms to carrier phase measurements, the Iono2 term needs to be divided by 2, and Iono3 by 3 (Eq. 9 in Section 3.1.) for all signal frequencies.

Regarding the results in Fig 6.9., it should be remembered that the Iono2 term has LoS dependence through the $B_0 cos\theta$ term, which can attain positive or negative values depending on the relative satellite-receiver geometry. In this sense, a mid-latitude station (MATE) can track satellites with a wider range of elevation angles, whereas a high latitude station (TRO1) tracks with a more confined range of elevation angles. Therefore, "how" positive or negative the values are attained by Iono2 depends on the receiver location; and, as expected, the mid-latitude station MATE shows larger magnitudes for the Iono2 error term than the other relatively higher latitude stations. Furthermore, background solar physical conditions affecting the ionization levels are also expected to influence the contribution of Iono2 to the total delay error. Due to these two major factors, different magnitudes of positive and negative values are attained by the Iono2 term during the analysis periods for the stations considered.

The top two plots in Fig. 6.9. refer to the peak of the Solar Cycle (2001) where the first plot pertains to a period of geomagnetic activity as evidenced by the K_p values during these three days (Table 5.2.). It can be claimed that geomagnetic activity influences the contribution of Iono2 to the total range error since DOY 294 when K_p is as large as 7 corresponds to higher Iono2 error values during these three days. The $B_0 cos\theta$ term in Iono2 is calculated by IGRM, which does not in general take into account the actual geomagnetic disturbances, therefore the enhanced values of Iono2 can be more correctly related with the enhancement in TEC during geomagnetic storms. The similarity between the Iono2 profile and the corresponding TEC values along the signal paths suggests strong dependence of Iono2 on TEC along the signal path (see Fig. 6.1. – 6.4. in earlier figures of Iono1 for TEC plots)

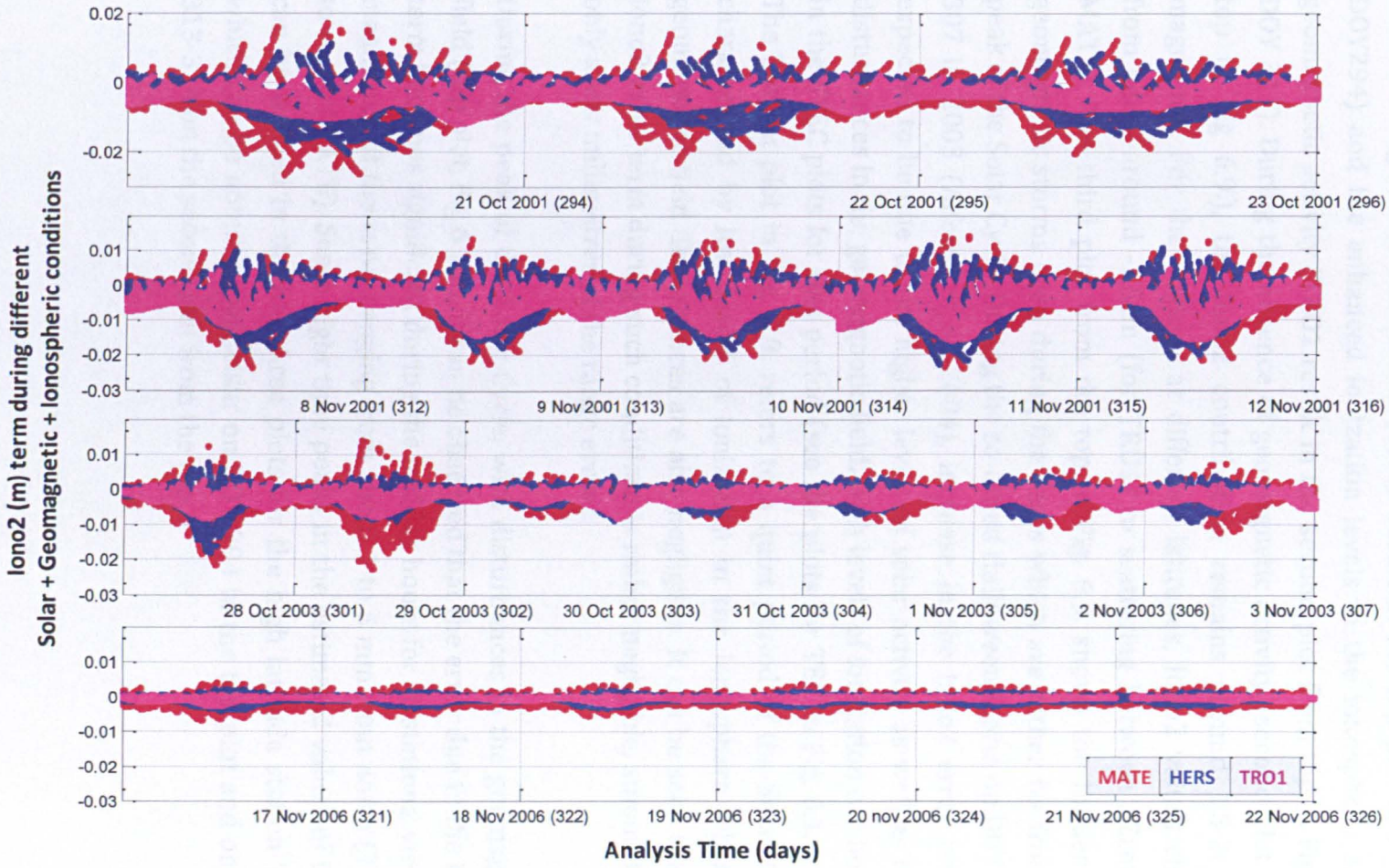

Figure 6.9. The Iono2 term calculated during four periods (*from the top to bottom*) with different background conditions.

During DOY 294-296 with high background geomagnetic activity, the error due to Iono2 is overall within 1-2cm in magnitude. Night time enhancement in Iono2 for the high latitude station TRO1 can be explained in terms of geomagnetic storms (TRO1 result in the top plot in Fig 6.9., DOY294) and the enhanced ionization levels in the ionosphere during geomagnetic activity (TRO1 result in the second plot from top in Fig 6.9., DOY 315). During the absence of geomagnetic activity (second plot from top in Fig 6.9.), the Iono2 contribution remains around 1.5-2cm in magnitude. For the stations at different latitudes, Iono2 values change from being around -1.5cm (for TRO1) to scattering between ±2cm (for MATE). The third plot from the top in Fig. 6.9. shows the influence of geomagnetic storms even during the years which are rather far from the peak of the Solar Cycle. During the so-called Halloween Storm on DOY 301-307 in 2003 (Alfonsi et al. 2004), increase in the Iono2 error term is expected to be due to the higher levels of solar activity as well as to the disturbances in the geomagnetic field. High levels of ionization can be seen in the STEC plots for this period (see the plots for TEC in Fig. 6.1. – 6.4.). The bottom plot in Fig. 6.9. refers to a quiet period of the Solar Cycle, characterised by low levels of ionization in the ionosphere when the geomagnetic field disturbances are also negligible. It can be seen that the Iono2 error term during such conditions is rather negligible, amounting to only a few millimetres of the range errors.

During the peak of the Solar Cycle, with disturbances in the geomagnetic field (top plot, Fig 6.10.), it can be observed that the error due to the Iono3 term becomes significant during the midday hours for all stations, with the magnitude of the error ranging from about 1 to 5 mm from north (TRO1) to south (MATE). Some night time peaks in the estimated values of Iono3 can be noticed in the top three plots for the high latitude station TRO1 which can be noted in particular on DOY 294 in the top plot and on DOY 313-314 on the second plot from the top.

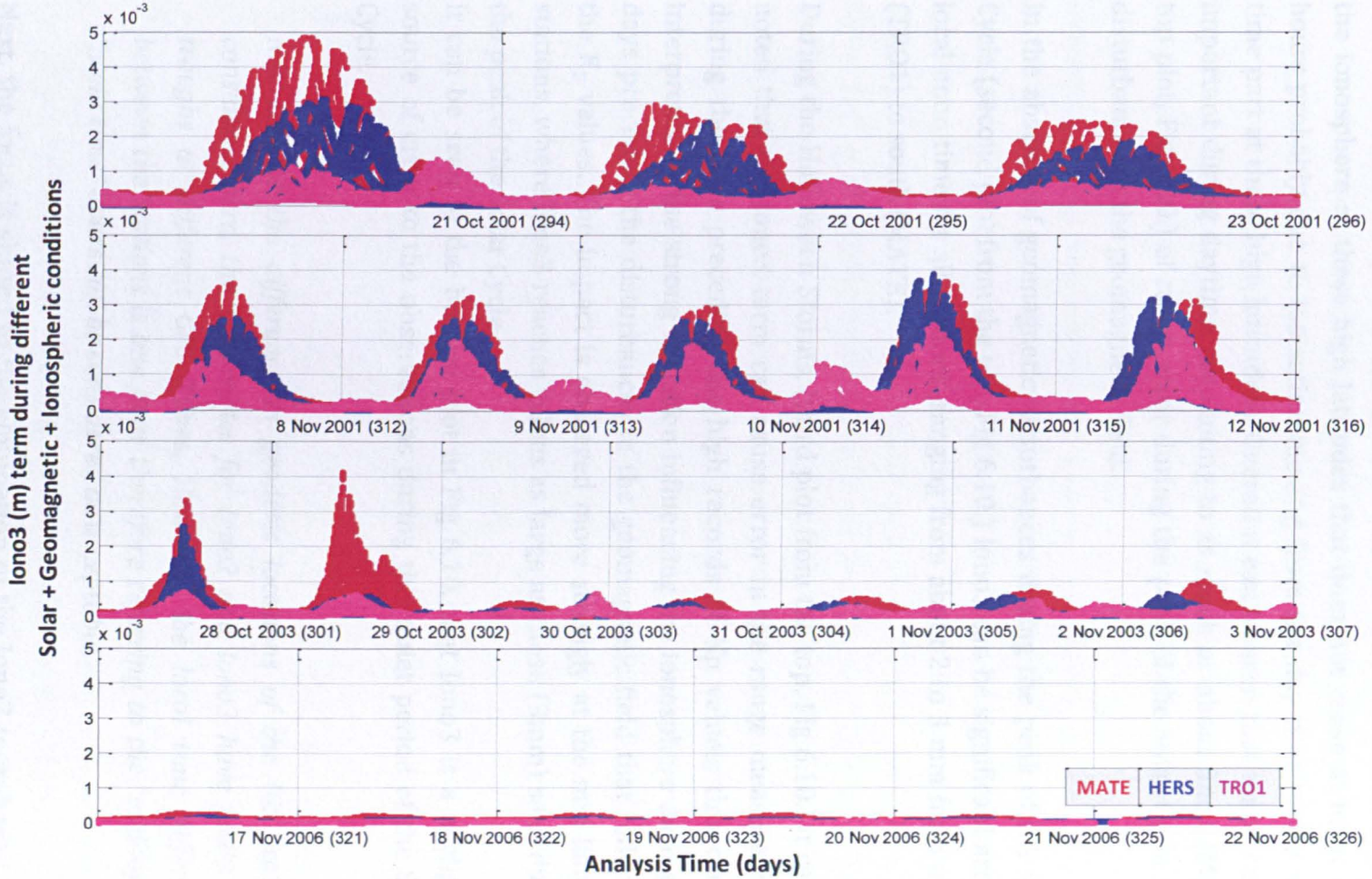

Figure 6.10. The Iono3 term calculated during four periods (*from the top to bottom*) with different background conditions.

Both of these plots refer to the peak of the Solar Cycle when the ionization levels are high due to strong solar radiation, therefore it can be concluded that at the high latitudes in particular, errors may arise due to the Iono3 term in the absence of daylight (due to continuous levels of ionization in the ionosphere at these high latitudes that does not cease at night time hours probably due to ionization moving from the day time to the night time part at these high latitudes). Overall it can be seen that Iono3 can be important during daytime, amounting to as much as about 5mm (MATE, top plot, Fig 6.10.) of range error during the peak of the Solar Cycle with disturbances in the geomagnetic field.

In the absence of geomagnetic disturbances during the peak of the Solar Cycle (second plot from the top, Fig 6.10.) Iono3 can be significant around local noon time for all stations, ranging from about 2 to 3 mm from north (TRO1) to south (MATE).

During the Halloween Storms, (third plot from the top, Fig 6.10.) it can be noted that the Iono3 term can cause error in the range measurements during the days preceding the high records of Kp values; this can be interpreted as the strong radiation influencing the ionosphere during the days preceding the disturbances in the geomagnetic field that reflect on the K_p values. The impact is observed more strongly at the mid latitude stations, where Iono3 reaches values as large as those (3mm) seen during the peak of the Solar Cycle.
It can be seen in the bottom plot in Fig 6.10. that Iono3 is a negligible source of error to the observations during this quiet period of the Solar Cycle.

N.B. Due to the difference in geodetic locations of the IGS stations considered here, the time series for Iono2 and Iono3 have peaks and troughs at different GPS Times. However, the local time difference between the stations is one hour therefore referring to the "midday" or "night time" hours can be considered as acceptable.

Next, the focus is shifted to the elimination of the Iono2 term based on a triple frequency approach involving the new GPS signals L2C and L5. This analysis is based on the triple frequency GPS data collected at PRU2 station on 14 November 2011. The signal paths for SV01 and SV25 are

considered for the local morning and post-sunset hours, respectively, for each receiver-satellite path. As also analyzed earlier in Section 6.1.1.1., this two-hour data set enables a comparison of how a strong scintillation level can influence the triple frequency linear combination that can eliminate the Iono2 error term. Contribution from other error sources (such as multipath) to the residual error when considering the triple frequency "reduced" (the Iono2 term eliminated) IF observable should be noted. The increase in the noise level of such triple frequency IF observable should also be acknowledged.

Regarding these points and similar to the earlier results shown in Fig, 6.7. and 6.8., the rate of the *triple*-frequency IF observable is considered and compared to those of the *dual*-frequency IF observables in Fig. 6.11.: on the left is the comparison of the rate for the triple and dual frequency IF observables during 08:00-09:00 local time for the triple signal link with SV01 during negligible scintillation level, and on the right is a similar analysis during 21:00-22:00 local time for the triple signal link with SV25 during strong scintillation level. It can be seen in both plots of Fig. 6.11. that the variations in the IF observable are greater in the triple frequency case; the inset in the left plot aims to show that this is the case even during negligible scintillation level.

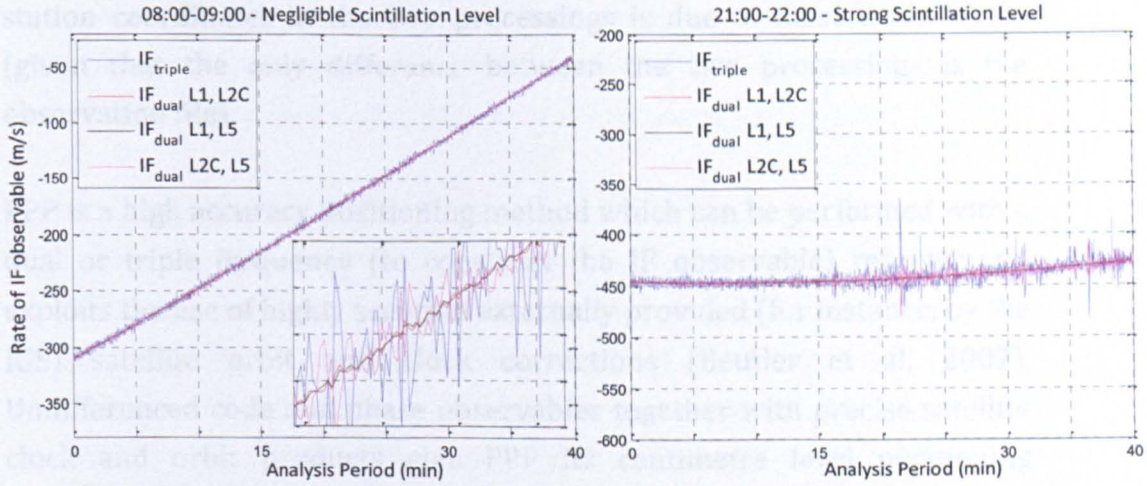

Figure 6.11. Rate of the IF observable compared between the triple and dual frequency cases, where negligible scintillation level with SV01 (*left*) is compared to strong scintillation level with SV25 (*right*).

N.B. (1) Bending error is excluded in these analyses.

(2) The first 40 minutes of observations are considered during both 08:00-09:00 and 21:00-22:00 local time periods.

(3) Triple frequency was only available on a limited number of signal paths while the analyses were conducted during this PhD.

The influence of diffraction, scintillation as analyzed here, on the IF observable can be understood from these results where this influence is observed to depend on not only the number of frequencies considered for the IF observable (dual or triple) but also on the individual signal frequencies considered in the linear combinations (in the case of dual frequency). It can be observed that the triple frequency linear combination has more variations compared with the dual frequency combinations (Fig. 6.11., left plot).

6.1.2. IMPACT OF THE HIGHER ORDER IONOSPHERIC EFFECTS IN PRECISE POINT POSITIONING

In this section, results for the impact of the HO ionospheric effects in precise point positioning (PPP) are shown, aiming to assess the influence on coordinate estimation. By considering the corrected observation files (for Iono2 and Iono3) output by Rinex_HO program and the original files in PPP; it is expected that the difference between the estimates of the station coordinates in the two processings is due to these error terms (given that the only difference between the two processings is the observation file).

PPP is a high accuracy positioning method which can be performed with a dual or triple frequency (to construct the IF observable) receiver and exploits the use of highly accurate externally provided (for instance, by the IGS) satellite orbit and clock corrections (Beutler et al. 2007). Undifferenced code and phase observables together with precise satellite clock and orbit products give PPP its centimetre level positioning accuracy. PPP is applied in this work using BSW V5.0 (Dach et al. 2007) to investigate the impact of correcting the (GPS) code and phase measurements for the Iono2 and Iono3 terms. While using the BSW PPP, the satellite orbits define the coordinate system to which the estimated station coordinates refer to (Beutler et al. 2007; Dach et al. 2007).

It should be noted that only the GPS observations are considered in this work, i.e. both the original observation files from IGS and the corrected ones include GPS observations only. Furthermore, the orbit and clock products used in positioning do not include corrections for the Iono2 or Iono3 terms; this is due to non-availability of such corrected products from IGS during the time that this work was undertaken, as in the IGS data reprocessing campaign, a common model was not agreed regarding the corrections for the higher order ionospheric effects (IGS 2012a).

Figure 6.12. shows how much the station coordinates were observed to differ in latitude, longitude and ellipsoidal height: in this case, the differences in the coordinate components are computed by subtracting the PPP results obtained with the original observation (uncorrected) files from those obtained with the corrected files. Table 6.1. provides the magnitudes of these differences.

During DOY 294-296, 2001, which corresponds to the peak of the Solar Cycle with disturbed geomagnetic conditions (K_p values as large as 7 notable in the corresponding plot in Fig. 6.12.), it is difficult to observe a general trend for the shifts in the latitude and longitude components that are of the order of a few millimetres in general. The vertical component (height) gets upward corrections overall except for the mid-latitudes where the trend is downward at sub-cm level on average. It should be noted here that the short observation period (of 3 days) may hinder a more conclusive analysis of the shifts in the station coordinates.

During DOY 312-316, 2001, which is a period of high solar activity with negligible disturbances in the geomagnetic field, corrections for Iono2 and Iono3 can be considered to account mainly for the impact of the solar activity. Differences in the PPP results show northward shifts in the coordinates of about 2-3mm for high latitude station and southward corrections of about 1cm for mid-latitude stations. Hernandez-Pajares et al. (2007), who focus only on the Iono2 term and its impact on positioning show that applying Iono2 correction to sub-daily *differential* positioning

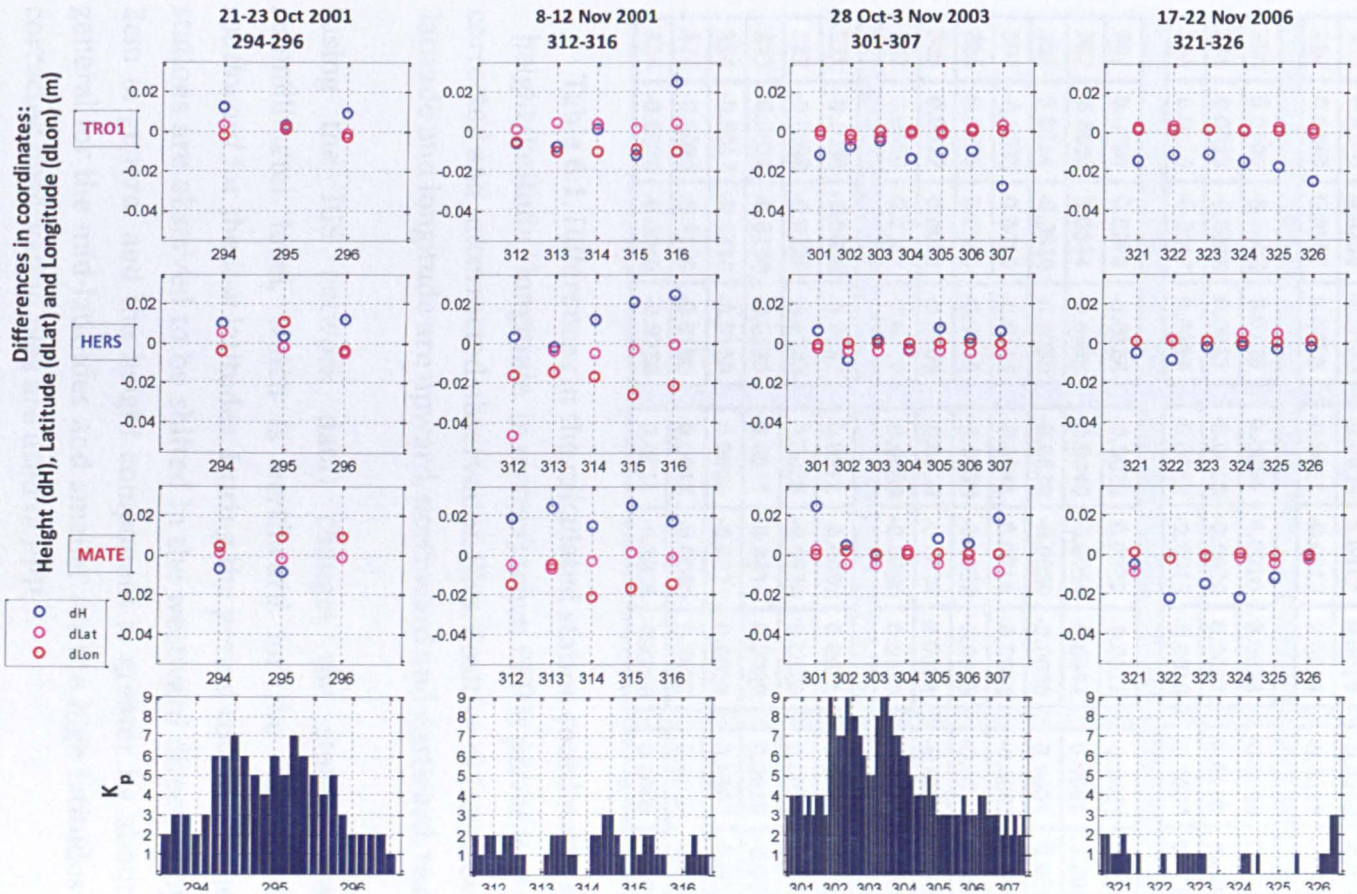

Figure 6.12. Difference between the corrected and uncorrected PPP results (in meters) for latitude (dlat), longitude (dlon) and ellipsoidal height (dH).

CORRECTED - UNCORRECTED

DOY	delta height (m)			delta latitude (m)			delta longitude (m)		
	HERS	MATE	TRO1	HERS	MATE	TRO1	HERS	MATE	TRO1
312	0.0035	0.0180	-0.0060	-0.0470	-0.0054	0.0013	-0.0160	-0.0150	-0.0054
313	-0.0018	0.0245	-0.0080	-0.0040	-0.0072	0.0040	-0.0145	-0.0048	-0.0100
314	0.0120	0.0147	0.0012	-0.0052	-0.0033	0.0037	-0.0170	-0.0210	-0.0100
315	0.0206	0.0251	-0.0123	-0.0033	0.0012	0.0019	-0.0260	-0.0165	-0.0090
316	0.0240	0.0167	0.0250	-0.0011	-0.0012	0.0039	-0.0215	-0.0146	-0.0104
294	0.0100	-0.0072	0.0120	0.0054	0.0010	0.0028	-0.0040	0.0040	-0.0019
295	0.0033	-0.0088	0.0032	-0.0018	-0.0020	0.0027	0.0110	0.0088	0.0014
296	0.0120	-0.0017	0.0089	-0.0052	-0.0015	-0.0010	-0.0037	0.0089	-0.0030
301	0.0064	0.0240	-0.0124	-0.0025	0.0022	-0.0017	-0.0006	-0.0001	0.0001
302	-0.0089	0.0044	-0.0080	-0.0040	-0.0050	-0.0042	0.0001	0.0015	-0.0015
303	0.0014	-0.0010	-0.0050	-0.0039	-0.0050	-0.0030	0.0001	0.0001	-0.0001
304	-0.0035	0.0018	-0.0140	-0.0041	0.0014	-0.0014	-0.0001	-0.0001	0.0001
305	0.0075	0.0080	-0.0110	-0.0038	-0.0052	-0.0013	-0.0001	-0.0001	0.0001
306	0.0022	0.0056	-0.0105	-0.0050	-0.0034	0.0012	-0.0001	-0.0001	0.0001
307	0.0059	0.0182	-0.0280	-0.0060	-0.0090	0.0030	-0.0001	-0.0001	0.0001
321	-0.0050	-0.0050	-0.0152	0.0012	-0.0088	0.0021	0.0008	0.0013	0.00121
322	-0.0090	-0.0220	-0.0120	0.0018	-0.0020	0.0029	0.0010	-0.0020	0.00105
323	-0.0018	-0.0150	-0.0120	0.0011	-0.0014	0.0009	0.0010	-0.0009	0.00108
324	-0.0017	-0.0216	-0.0158	0.0046	-0.0021	0.0010	0.0007	0.0007	0.00066
325	-0.0030	-0.0120	-0.0180	0.0044	-0.0045	0.0022	0.0007	-0.0006	0.00071
326	-0.0020	-0.0010	-0.0256	0.0011	-0.0026	-0.0008	0.0009	-0.0004	0.00089

Table 6.1. Differences in the calculated station coordinates (delta height/latitude/ longitude, in meters) when PPP is performed with the corrected and uncorrected observation files. Positive differences in height, latitude and longitude are upward, northward and eastward, respectively.

(using the IGS network data) changes the station positions at submillimeter level, which is *northward* for the *high* latitudes and *southward* for the *low* latitudes. During the period considered here, all the stations are observed to be shifted in the westward direction by about 1-2cm in general and the height component is greater by about 2-3cm in general for the mid-latitudes and smaller for the high latitudes when the corrected observation files are used in PPP.

During DOY 321-326, 2006, in the presence of low background solar activity and quiet geomagnetic conditions, it can be seen that for the horizontal coordinate components the PPP results do not show significant differences when the observation files are corrected for Iono2 and Iono3,

however for the height component, stations get shifted by up to 2cm vertically (especially at TRO1 and MATE).

Table 6.2 shows the average and STD values for the differences in the estimated station coordinates during each period per station. Overall, smaller STD values are encountered more often during the quiet period DOY 321-326, 2006, and larger STD values during the active period DOY 312-316, 2001. Furthermore, the calculated averages are larger during the active period DOY 312-316, 2001, especially for the longitude component for all stations, than during the other periods.

	delta height (m)			delta latitude (m)			delta longitude (m)			
DOY	HERS	MATE	TRO1	HERS	MATE	TRO1	HERS	MATE	TRO1	
312-316	0.0110	0.0047	0.0148	0.0196	0.0033	0.0013	0.0047	0.0059	0.0021	STD
	0.0117	0.0198	0.0000	-0.0121	-0.0032	0.0030	-0.0190	-0.0144	-0.0090	mean
294-296	0.0046	0.0037	0.0045	0.0054	0.0016	0.0022	0.0086	0.0028	0.0023	STD
	0.0084	-0.0059	0.0080	-0.0005	-0.0008	0.0015	0.0011	0.0072	-0.0012	mean
301-307	0.0060	0.0091	0.0074	0.0011	0.0040	0.0024	0.0002	0.0006	0.0006	STD
	0.0016	0.0087	-0.0127	-0.0042	-0.0034	-0.0011	-0.0001	0.0002	-0.0002	mean
321-326	0.0029	0.0086	0.0051	0.0017	0.0028	0.0013	0.0001	0.0012	0.0002	STD
	-0.0037	-0.0128	-0.0164	0.0024	-0.0036	0.0014	0.0009	-0.0003	0.0009	mean

Table 6.2. The average and STD values of the differences in the estimated station coordinates for each period and station.

Considering that PPP can potentially provide centimetre level accuracy for the estimated station coordinates and that the corrections for Iono2 and Iono3 per signal path per frequency are at about centimetre and millimetre levels, respectively, it can be expected that the shifts in the estimated station coordinates observed in this work are mostly influenced by the corrections against the Iono2 term.

6.1.3. DISCUSSION

Different ionospheric conditions in terms of the background ionization and scintillation levels can affect the temporal variations of the dual frequency IF observable, as noted in this work. Considering the triple frequency signal paths during two hours with different levels of scintillation (Fig. 6.5.) and different ionization levels (Fig. 6.6.), the rate of the IF observable was observed to be different for these two hours. During negligible scintillation levels (S4 on GPS L1<0.2, top plot in Fig. 6.5.) and normal ionization conditions (TEC~40-50 TECU, top plot in Fig. 6.6.), the

rate of the IF observable is similar between the different dual frequency combinations for the IF observable (Fig. 6.7.). However, during strong scintillation levels (S4 on GPS L1~0.8, bottom plot in Fig. 6.5.) and enhanced ionization levels (TEC~120-140 TECU, bottom plot in Fig. 6.6.), it can be observed that with the onset of scintillation at about 21:30 local time, the temporal variations in the L2C, L5 case (Fig. 6.8. bottom plot) become more distinguished, which can make the choice of L2C and L5 for the IF observable less favourable for such adverse ionospheric conditions.

Enhancement in TEC can occur due to greater solar activity, as during the peak of the Solar Cycle. Similarly the geomagnetic field disturbances can also instigate mechanisms that enhance ionization in the ionosphere, leading to large TEC values. As TEC is a prominent parameter for the ionosphere induced error in the GNSS observations, the ionosphere is expected to contribute more to the GNSS error budget during the periods of high solar and geomagnetic activities. Tracking low elevation satellites when signal paths through the ionosphere encounter greater electron content along the signal path is also anticipated to contribute to the ionosphere induced range errors.

Due to the influence of TEC on the error induced along the propagation of GNSS signals through the ionosphere, it is vital to estimate TEC with high accuracy in order to account for the ionospheric error along the satellite/receiver signal path. It has been mentioned in this work that TEC can be estimated per link using GIMs due to their high accuracy and availability (Marques et al. 2007) and from the pseudoranges (as carrier phases are ambiguous) as shown in Appendix B. It is important to remark the benefit of GNSS modernization for estimating TEC more accurately when, for instance, the GPS L5 signal is considered in the calculations. The accuracy of TEC when estimated from pseudoranges involving the L5 signal increases, which is shown with the error propagation law in Appendix B.

During the post-peak period of the Solar Cycle, enhanced levels of ionization can be observed linked with the presence of the geomagnetic field disturbances (DOY 301-307 in 2003). In this case, HO ionospheric error terms are observed to attain magnitudes comparable to those

occurring during the peak of the Solar Cycle in the absence of such disturbances (DOY 312-316 in 2001).

During the post-peak period of the Solar Cycle, high TEC values can be observed under the conditions of a disturbed geomagnetic field. Particularly at the high latitudes where the geomagnetic field lines are almost oriented vertically towards the surface of the Earth, the incoming solar particles can be routed to the lower altitudes in the ionosphere, enhancing TEC in these regions. Therefore, increased geomagnetic activity can be a factor for enhanced TEC levels at the high latitudes even during the non-peak periods of the Solar Cycle.

During the quiet period of the Solar Cycle with low ionization levels in the ionosphere and negligible geomagnetic field disturbances (DOY 321-326 in2006), HO ionospheric error terms are observed to be insignificant.

It is expected that the strong diurnal variation in TEC (minimum values before sunrise and after sunset, maximum values around local noon as well as enhancement during night hours at the high latitudes) causes the diurnal variation observed in the Iono2 and Iono3 terms. Comparing the values calculated for Iono2 and Iono3, the diurnal variation is observed to be stronger (i.e. the relative difference between the minimum and maximum being larger over a day) for Iono3 than for Iono2. This can be explained by the fact that in addition to the dependence on STEC of both terms, Iono2 depends on the projection of the geomagnetic field onto the signal path at the IPP, whereas Iono3 is associated with the maximum electron density in the ionosphere.

In the former case, IGRM's modelling of the geomagnetic field is considered in this work for Iono2 and this does not take into account the geomagnetic disturbances which may be linked with the observed TEC values. In the latter case, however, a diurnal variation can be anticipated since the maximum electron density (associated with Iono3) normally reaches a maximum around the local afternoon (Ratcliffe 1956). Therefore, a more defined diurnal variation in the Iono3 error term rather than in Iono2 can be observed.

The impact of the HO error terms on GNSS coordinate estimation can be assessed from the results based on PPP using respectively the original (not corrected for the HO error terms) and corrected observation files. The results are summarized in Table 6.3, where for the four sets of days analyzed during different solar and geomagnetic conditions, the average calculated shifts in the estimated station coordinates are given distinguishing between the high and mid-latitude stations.

	Active Period of Solar Cycle	Quiet Period of Solar Cycle	Active Period of Solar Cycle with Geomagnetic Storms		
	DOY 312-316, 2001	DOY 321-326, 2006	DOY 294-296, 2001	DOY 301-307, 2003	
Lat.	3-4mm N	1-2mm N	NOP	3-4mm S	High Lat.
Lon.	1cm W	NOP	NOP	NOP	
Height	1cm up	1-2cm down.	8-10mm up	1-2cm down.	
Lat.	3-4mm S	4-6mm S	1-2mm S	1-2mm S	Mid-Lat.
Lon.	1-2cm W	NOP	5-7mm E	NOP	
Height	1-2cm up	1-2cm down.	6-8mm down.	1-2cm up	

Table 6.3. The average observed shifts in latitude (Lat.), longitude (Lon.) and height components. "N" denotes a northward shift, "S" southward, "E" eastward, "W" westward, "down." downward and "up" upward. "NOP" stands for no obvious pattern.

In general, during the active period of the solar cycle, a southward shift occurs in the estimated station coordinates for the mid-latitude and a northward shift for the high latitude. During the same period, a general westward correction in the longitude and upward in the height component can be observed. During the active period of the solar cycle with geomagnetic storms, both high and mid latitudes get southward corrections, with the magnitudes being greater for the high latitudes. During this period, it is difficult to observe a general pattern for changes in the longitude and height components. During the quiet period of the solar cycle, it is difficult to observe a pattern in the horizontal components, and a downward direction in the corrections for the height component is observed in general. Overall, the horizontal and vertical components of the estimated station coordinates in the PPP results are observed to differ at cm-mm level when the corrected observation files are used. As also

suggested by the findings of (Elsobeiey & El-Rabbany 2009), neglecting the Iono2 error term introduces error in the order of 2cm in the GPS satellite orbit and clock corrections.

Although the data set considered here is limited in terms of the days analyzed and the background solar/magnetic conditions, it can be commented that the corrections for the HO error terms calculated for the non-peak period of the Solar Cycle (DOY 301-307 in 2003) can be comparable to those during the peak period (DOY 312-316 in 2001) *if* the non-peak period is influenced by strong geomagnetic activity. It can be seen in Fig. 6.9. and Fig. 6.10. that the results for DOY 301-307 in 2003 (the third plot from the top in both figures) are similar to those in magnitude for DOY 312-316 in 2001 (the second plot from the top in both figures) especially around the days when high K_p values are recorded (Table 5.2.). This highlights the influence of the geomagnetic conditions on the ionospheric error terms through enhancing the ionization levels, which can affect both the mid and high latitudes, as observed in this work.

Another remark that should be mentioned is that in the approach followed in this work only the observation files are corrected for the Iono2 and Iono3 error terms. It is possible that the net effect of correcting the observations against these error terms is obscured in this approach. It would be more enlightening and systematic if the corrected satellite orbit and clock products were available for use in PPP. Indeed, as discussed by Elsobeiey & El-Rabbany (2009), use of such products corrected against the Iono2 term could show improvement in the convergence and accuracy of the PPP solution; the same authors show in their work focusing on the Iono2 error term that correcting the Iono2 term can benefit the accuracy of the PPP solution.

6.2. RESULTS FOR THE IONOSPHERIC DIFFRACTIVE EFFECTS

In this section, the field data recorded is considered in the results for the ionospheric diffractive, *scintillation* in particular, effects in terms of their impact during signal propagation and on the receiver signal tracking performance, the degradation they can induce in the GNSS positioning solution and the mitigation technique to account for the scintillation induced errors in the observations that can affect the GNSS positioning

solution. First, the impact of scintillation is shown regarding signal intensity, phase and lock time for the L1, L2 and L5 band signals. Next, the results for receiver signal tracking performance are presented during moderate-to-strong levels of scintillation, where calculations are based on both the Conker model and the proposed technique using receiver post-correlator data (see Section 4.2.). Then the impact of scintillation in the GNSS positioning solution is shown from the positioning results obtained with the online PPP tool NRCan considering the open sky data with significant levels of scintillation. The concluding part of the results presented in this section are for the mitigation of scintillation in GNSS positioning where the previously introduced (Section 5.2.2.) positioning software GPSeq (for relative), RT_PPP (for PPP), and NRCan (for PPP) are utilized.

6.2.1. IMPACT OF SCINTILLATION ON GNSS SIGNALS

A GNSS receiver in general can be capable of tracking signals up to certain levels of scintillation, when fluctuations in the received signal's amplitude and phase start challenging the tracking loops of the receiver. Signal lock can still be maintained and therefore range measurements can still be made available by the receiver; however, the precision of these measurements may be affected. Scintillation can increase the possibility of cycle slips and, if strong enough, can cause loss of carrier lock on the signal. It can be seen in the observation files considered in the following analyses that gaps in the observations are present during strong levels of scintillation.

Regarding the values attained by the S4 and SigmaPhi indices on LoS paths with 10^0 elevation cutoff angle for the data collected at PRU2 station, it can be seen in Fig. 6.13. and Fig. 6.14 that saturated levels of amplitude and phase scintillation are possible to affect GNSS receivers at the low latitudes. In the top plot in Fig. 6.13. strong amplitude scintillation persists throughout the hour (00:00-01:00 GPS Time) with saturated levels being observed abound the 20^{th} minute onwards. The bottom plot in Fig. 6.13., which seems to be less populated compared with the top plot in the same figure due to rapid losses of phase lock that hinder SigmaPhi calculation, indicates moderate-to-strong level phase scintillation.

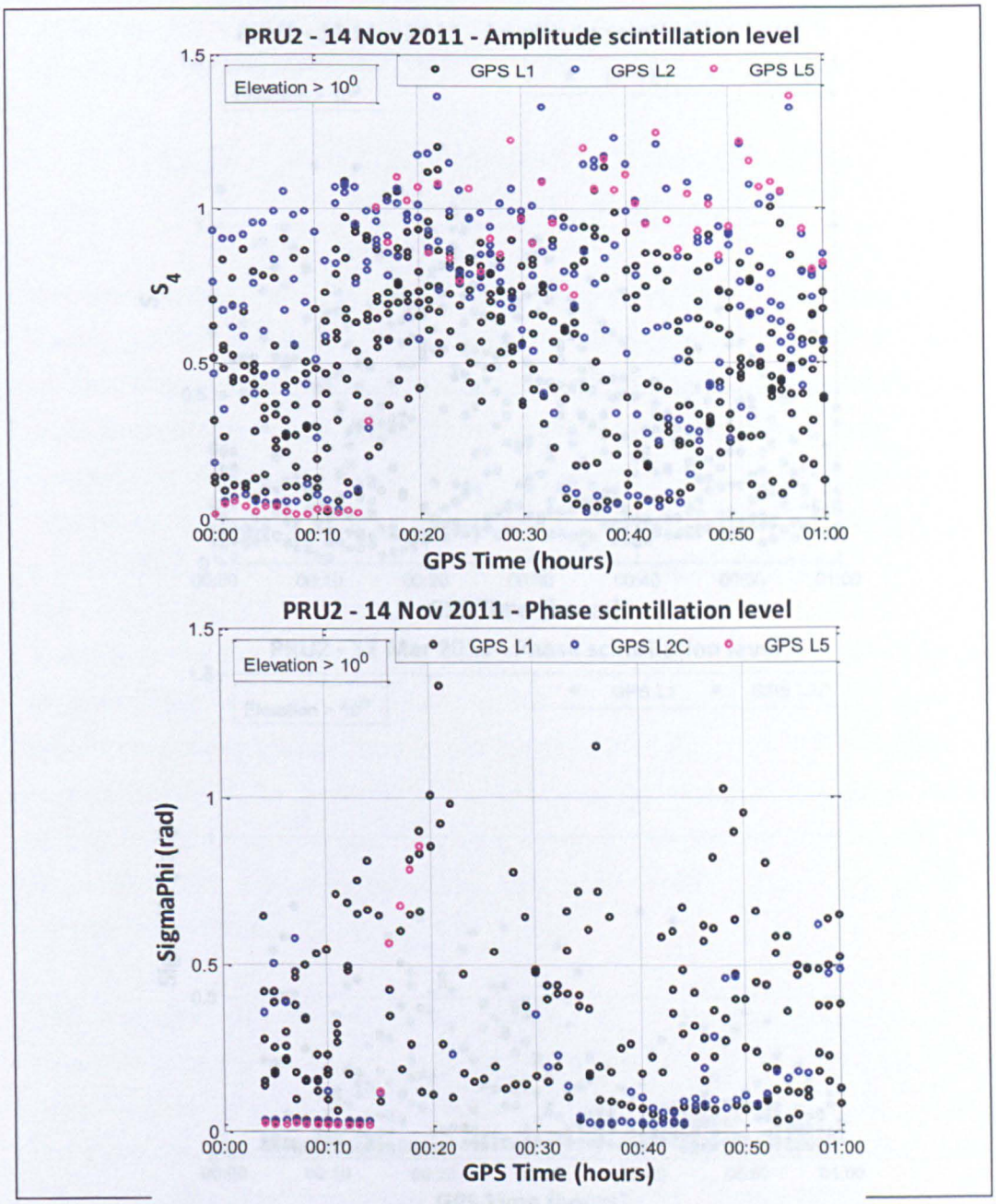

Figure 6.13. Amplitude and phase scintillation indices for all LoS above 10^0 elevation cutoff angle on 14 November 2011.

In the top plot in Fig. 6.14. strong amplitude scintillation can be observed during the first half hour with the S4 values scattered around 1 and moderate level in the second half with the S4 values scattered around 0.5. The bottom plot in Fig. 6.14. indicates moderate level phase scintillation throughout the hour. It should furthermore be mentioned that SigmaPhi values around 1 may be unavailable for plotting due to losses of lock encountered during strong phase scintillation.

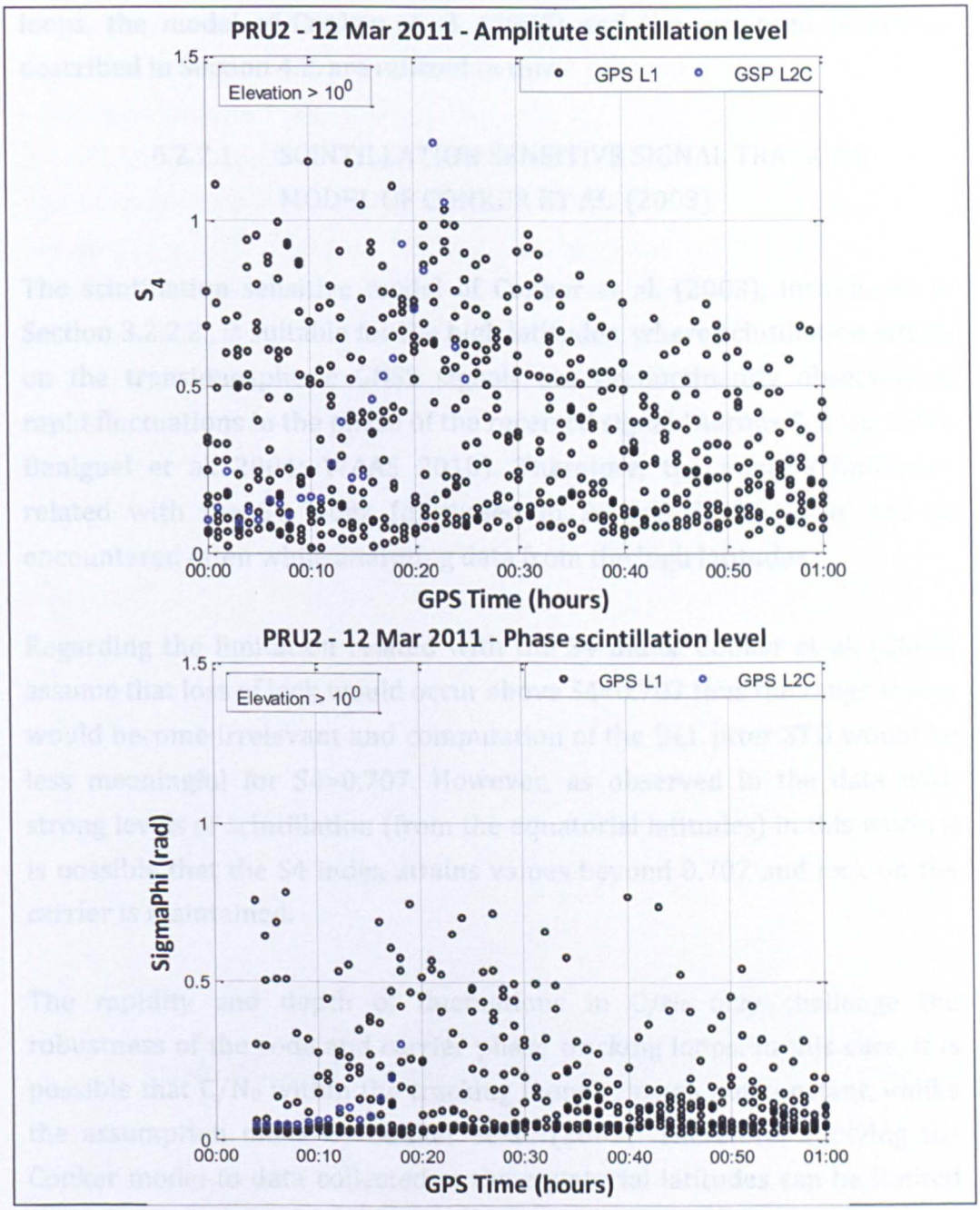

Figure 6.14. Amplitude and phase scintillation indices for all LoS above 10^0 elevation cutoff angle on 12 March 2011.

6.2.2. IMPACT OF SCINTILLATION ON RECEIVER SIGNAL TRACKING PERFORMANCE

This section presents the results on the evaluation of the receiver signal tracking performance during scintillation in terms of the jitter variance at the output of the code and carrier tracking loops, DLL and PLL, respectively. For estimating the jitter variance in the case of both tracking

loops, the model of Conker et al. (2003) and the proposed technique described in Section 4.2. are utilized in turn.

6.2.2.1. SCINTILLATION SENSITIVE SIGNAL TRACKING MODEL OF CONKER ET AL. (2003)

The scintillation sensitive model of Conker et al. (2003), introduced in Section 3.2.2.2., is suitable for the high latitudes, where scintillation effects on the transionospheric GNSS signals are predominantly observed as rapid fluctuations in the phase of the received signal (Aarons & Basu 1994; Beniguel et al. 2004; WAAS 2010). Therefore, the model's limitation related with the S4 index (discussed in Section 3.2.2.2) may not be encountered often while analyzing data from the high latitudes.

Regarding the limitation related with the S4 index, Conker et al. (2003) assume that loss of lock would occur above S4=0.707 thus the range errors would become irrelevant and computation of the DLL jitter STD would be less meaningful for S4>0.707. However, as observed in the data with strong levels of scintillation (from the equatorial latitudes) in this work, it is possible that the S4 index attains values beyond 0.707 and lock on the carrier is maintained.

The rapidity and depth of fluctuations in C/N_0 may challenge the robustness of the code and carrier phase tracking loops. In this case, it is possible that C/N_0 within the tracking loops remains not constant, unlike the assumption made by Conker et al. (2003). Therefore, applying the Conker model to data collected at the equatorial latitudes can be limited due to an S_4 related mathematical limitation inherent in the model for the DLL jitter variance estimation.

N.B. Comparing the high and equatorial latitudes, plasma bubbles at the equatorial latitudes are observed at local sunset towards midnight and this is diurnal and quite predictable. However, such predictability may not hold as much at the high latitudes where scintillation is observed often as coupled with geomagnetic storms. Moreover, amplitude fades observed at the high latitudes in general may not be as severe as those observed at the low latitudes.

The estimated results for the DLL and PLL jitter variances are shown in Fig. 6.15. and Fig. 6.16., respectively. The data considered is from the equatorial latitude PRU2 station, focusing on the signal path of GPS SV02 for GPS L1 C/A signal. For the DLL jitter variance estimation, it can be seen that stronger amplitude scintillation causes greater code tracking error at the output of DLL (Fig. 6.15.). It can also be remarked that a continuous estimation is not possible while utilizing the Conker model in this case: instances of S_4>0.707 (emphasized by the horizontal red line in the bottom plot of Fig. 6.15.) lead to gaps in monitoring the performance for the code tracking loop.

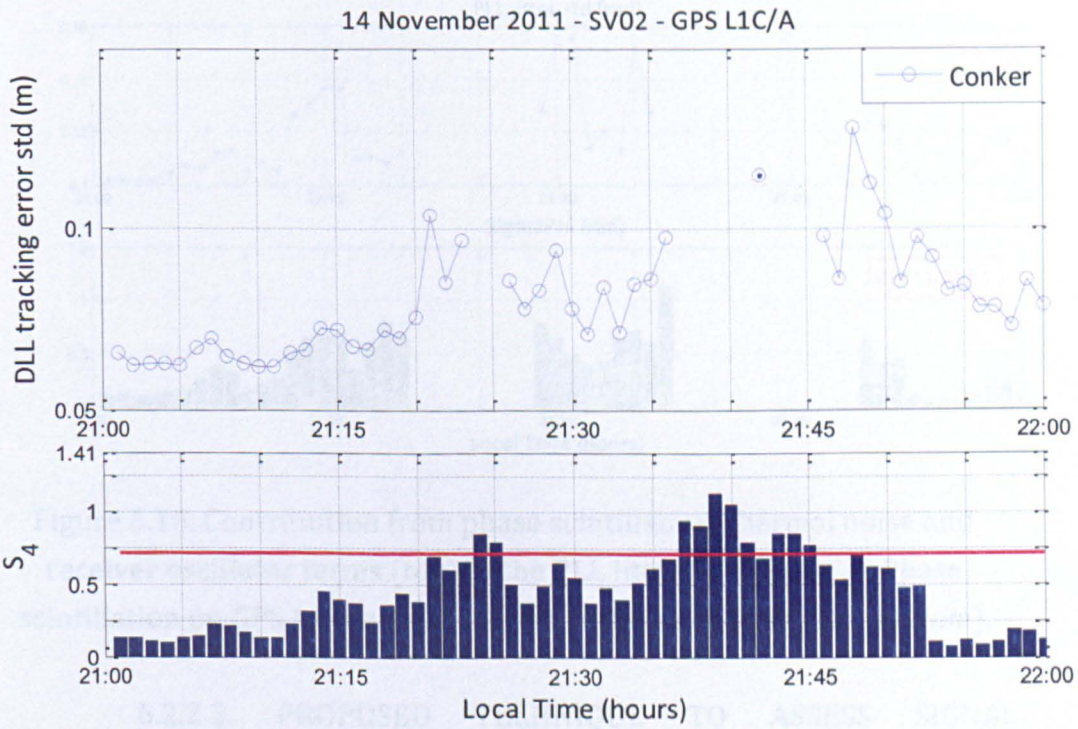

Figure 6.15. (*top*) DLL tracking error STD estimated using the Conker model for data collected at PRU2 station. (*bottom*) The S4 index during the hour of analysis is for GPS L1 signal with SV02.

For the PLL jitter variance estimation, the first row in Fig. 6.16. shows (for the same data set considered in Fig. 6.15.) the contribution from the three terms (represented by the three plots in the first row) described in Section 3.2.2.2 to the PLL jitter variance (STD plotted): the term related with the phase scintillation effect ("Phase scint.term"), that related with the increase in the thermal noise due to scintillation ("Thermal term") and the contribution of the receiver oscillator ("Rec. oscill. term") to the PLL jitter variance. The middle plot shows the PLL jitter STD as the accumulation of

these three error sources and in the bottom plot the values for the SigmaPhi index on GPS L1 are given for the signal path (GPS SV02) considered here. It can be seen that during this one hour observation period with strong phase and amplitude scintillation, monitoring and assessing the signal tracking performance is not possible at all times.

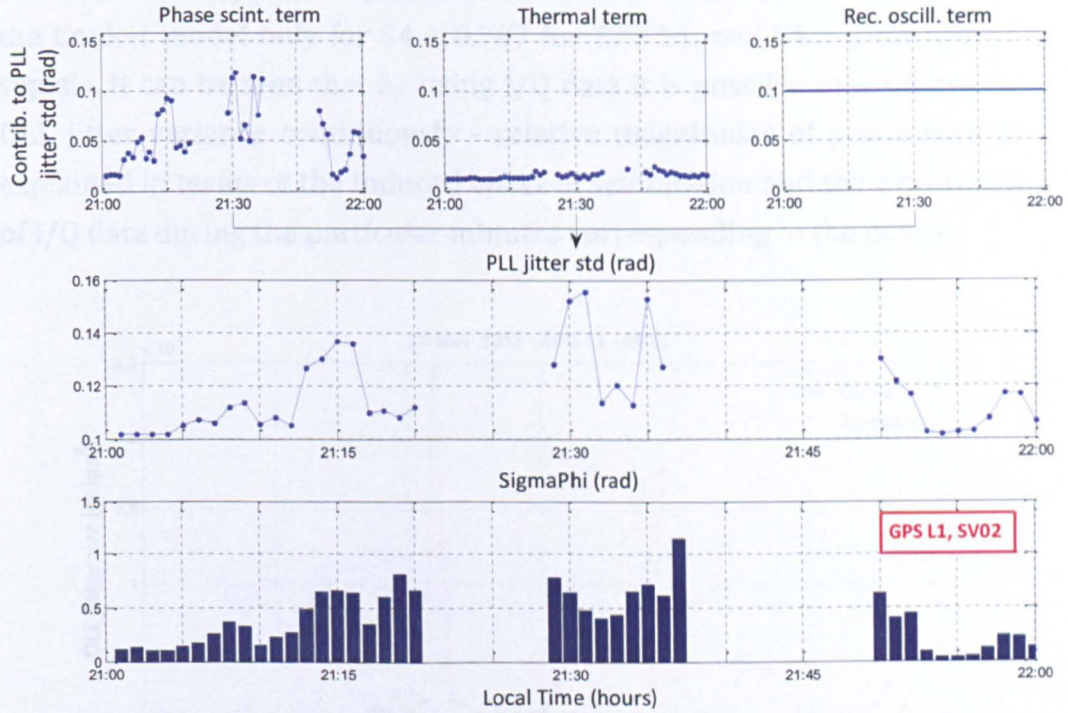

Figure 6.16. Contribution from phase scintillation, thermal noise and receiver oscillator terms (*top*) to the PLL jitter STD (*middle*). Phase scintillation on GPS L1 for SV02 is given in terms of SigmaPhi (*bottom*).

6.2.2.2. PROPOSED TECHNIQUE TO ASSESS SIGNAL TRACKING PERFORMANCE DURING SCINTILLATION

A method is proposed in Section 4.2. that makes use of the post-correlator I/Q signal data for estimating the DLL jitter variance when scintillation may affect the signal. In this section, the results of this estimation are shown in Fig. 6.17. - 6.20. including comparison with the results obtained using the Conker model. In addition to the results regarding the DLL, the I/Q post-correlator data is also used for estimating the PLL jitter STD as described in Section 4.2; these results are shown in Fig. 6.22.

Figures 6.17. and 6.18. refer to the data collected at PRU2 station on 14 November 2011 for the signal path from GPS SV25, for which the civil GPS

L1 and L5 signals are presented, respectively. Moderate to strong levels of scintillation can be noted from the values of the S_4 index provided in the middle plot in each figure. A horizontal pink line in the plots of S_4 indicates the threshold beyond which the Conker model is not applicable. Singularity conditions imposed by the mathematical formulae (introduced in Section 3.2.2.2) make it possible to estimate the DLL jitter variance with the Conker model only for S4 < 0.707 for GPS L1, and S4 < 1 for GPS L5 signals. It can be seen that by using I/Q data it is possible to estimate the DLL jitter variance continuously - relative magnitudes of peaks may be explained in terms of the induced effect of scintillation and the availability of I/Q data during the particular minutes corresponding to the peaks.

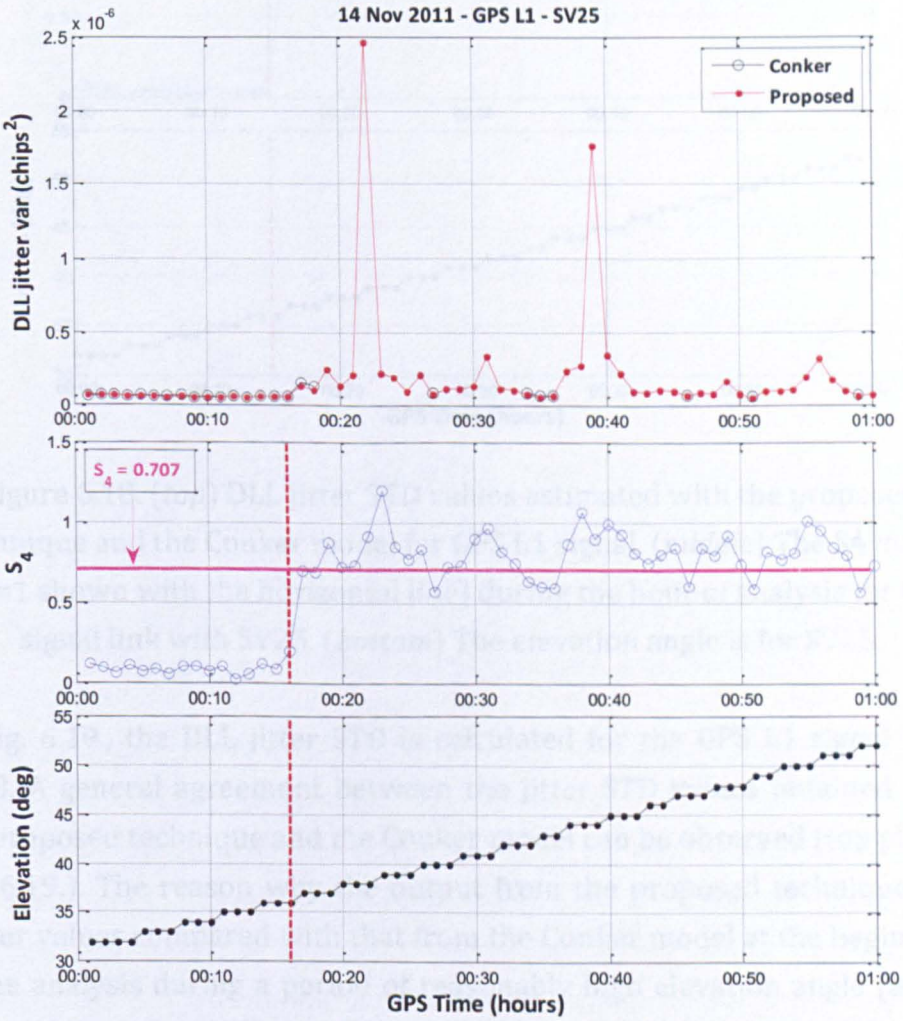

Figure 6.17. (*top*) The DLL jitter variance estimated with the proposed technique and the Conker model for GPS L1 signal. (*middle*) The S4 index (S4=0.707 shown with the horizontal line) during the hour of analysis for this signal link with SV25. (*bottom*) The elevation angle is for SV25.

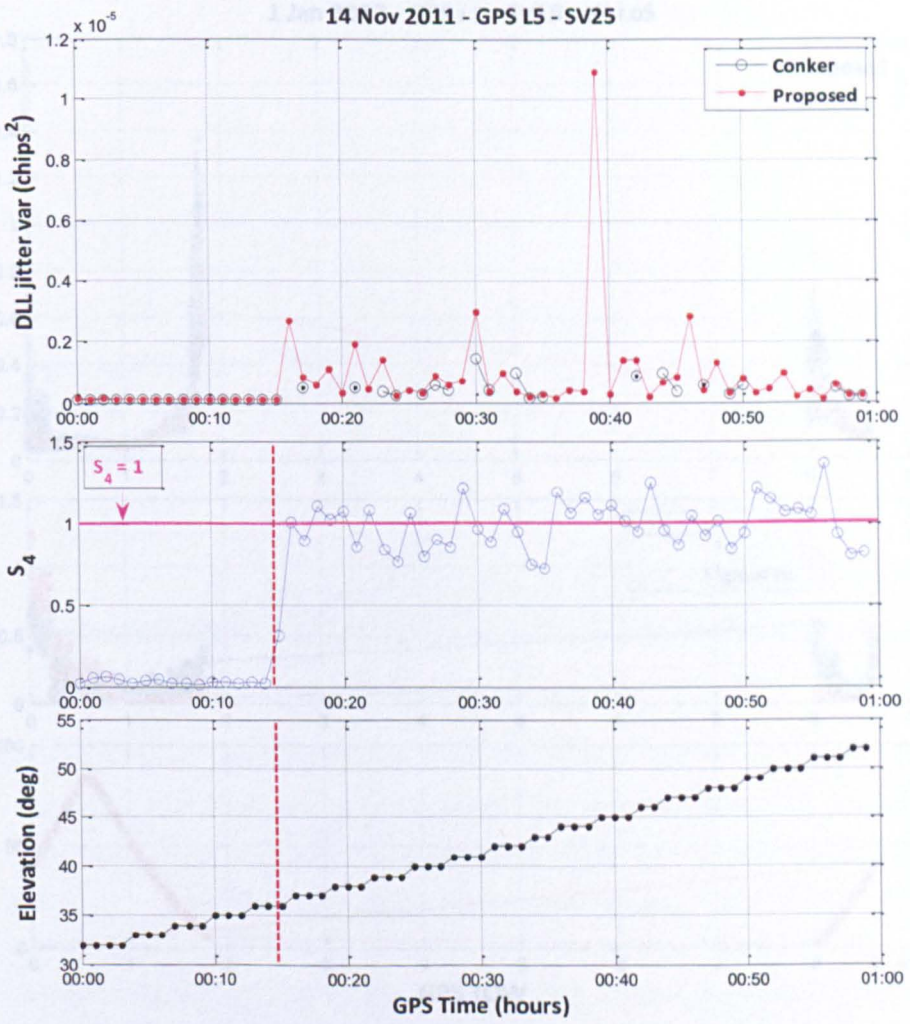

Figure 6.18. (*top*) DLL jitter STD values estimated with the proposed technique and the Conker model for GPS L1 signal. (*middle*) The S4 index (S4=1 shown with the horizontal line) during the hour of analysis for this signal link with SV25. (*bottom*) The elevation angle is for SV25.

In Fig. 6.19., the DLL jitter STD is calculated for the GPS L1 signal with SV18. A general agreement between the jitter STD values obtained with the proposed technique and the Conker model can be observed (top plot in Fig. 6.19.). The reason why the output from the proposed technique has higher values compared with that from the Conker model at the beginning of the analysis during a period of reasonably high elevation angle (about 40^0) and strong scintillation (both S4 and SigmaPhi about 0.8-1) is due to the difference in estimating the DLL jitter std through both approaches - per second estimation with the proposed technique versus per minute with the Conker model.

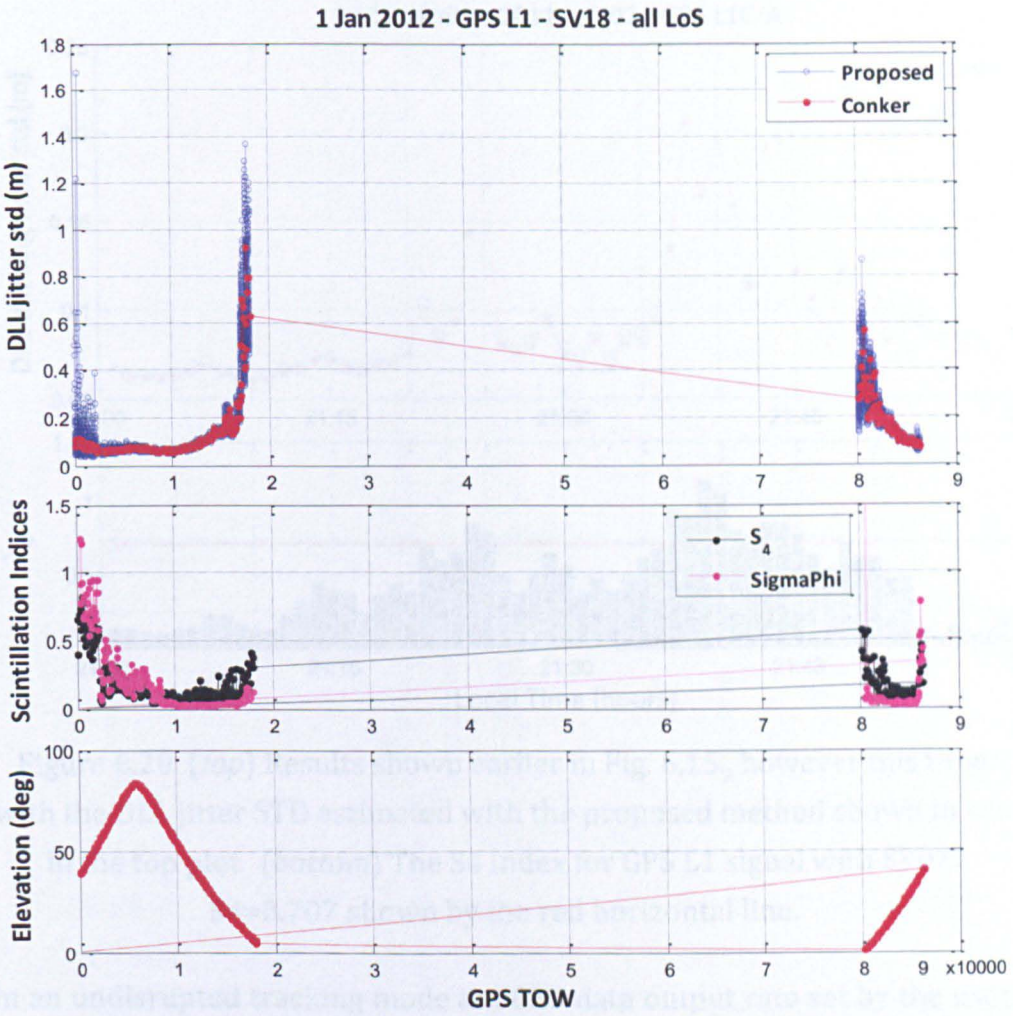

Figure 6.19. (*top*) Comparison of DLL jitter STD estimated with the proposed technique and Conker model for the data set collected at PRU2 on 1 January 2012; data analyzed for GPS L1 signal with SV18. (*middle*) Scintillation indices for GPS L1 with SV18 during the hour of analysis. (*bottom*) Elevation angle is for SV18.

Figure 6.20. refers to the same data set analyzed earlier in Fig. 6.15. – here, it can be noted that the code tracking error (DLL jitter) STD is estimated with the proposed technique based on using the I/Q post-correlator data (red series in the top plot). The instances of S4 when S4>0.707 can be seen with the help of the red horizontal line in the bottom plot in Fig. 6.20. – at such instances, when an estimate with the Conker model is not possible, the approach using I/Q data can provide estimates of the DLL jitter STD. As such, continuous monitoring for the code tracking error can be achieved for weak-to-strong levels of (amplitude) scintillation.

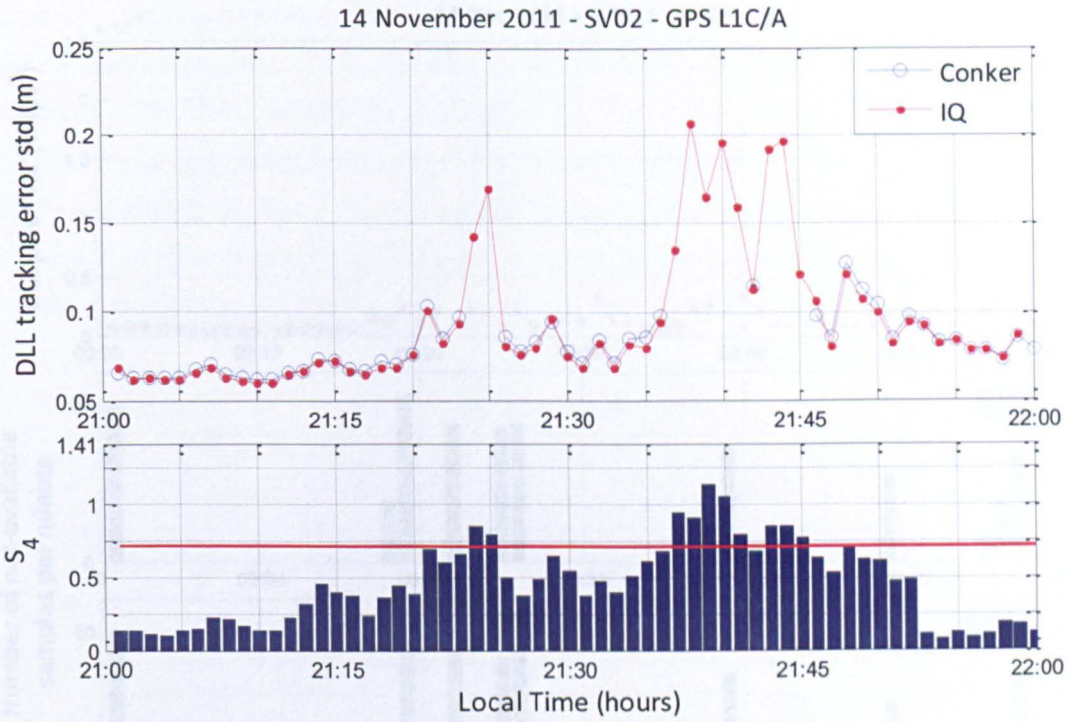

Figure 6.20. (*top*) Results shown earlier in Fig. 6.15., however this time with the DLL jitter STD estimated with the proposed method shown in red in the top plot. (*bottom*) The S4 index for GPS L1 signal with SV02; S4=0.707 shown by the red horizontal line.

In an undisrupted tracking mode at 50Hz data output rate set by the user, there should be 50 samples of I/Q data bits per second. In "stressed" conditions due to scintillation this number can fall below 50 per second, which may lead to statistically less reliable results for estimating the DLL jitter variance using I/Q data. Figure 6.21. illustrates this point: the results for the DLL jitter variance obtained with the Conker model and the proposed technique utilizing the I/Q data are shown and it is aimed to call attention to non-availability of I/Q samples per *minute* (ideally 3000 bits per minute). It can be noted that during, for instance, 1st and 19th minutes, there are about a second's worth I/Q data not available for the jitter variance estimation performed during these minutes, as shown in the top plot of Fig. 6.21.

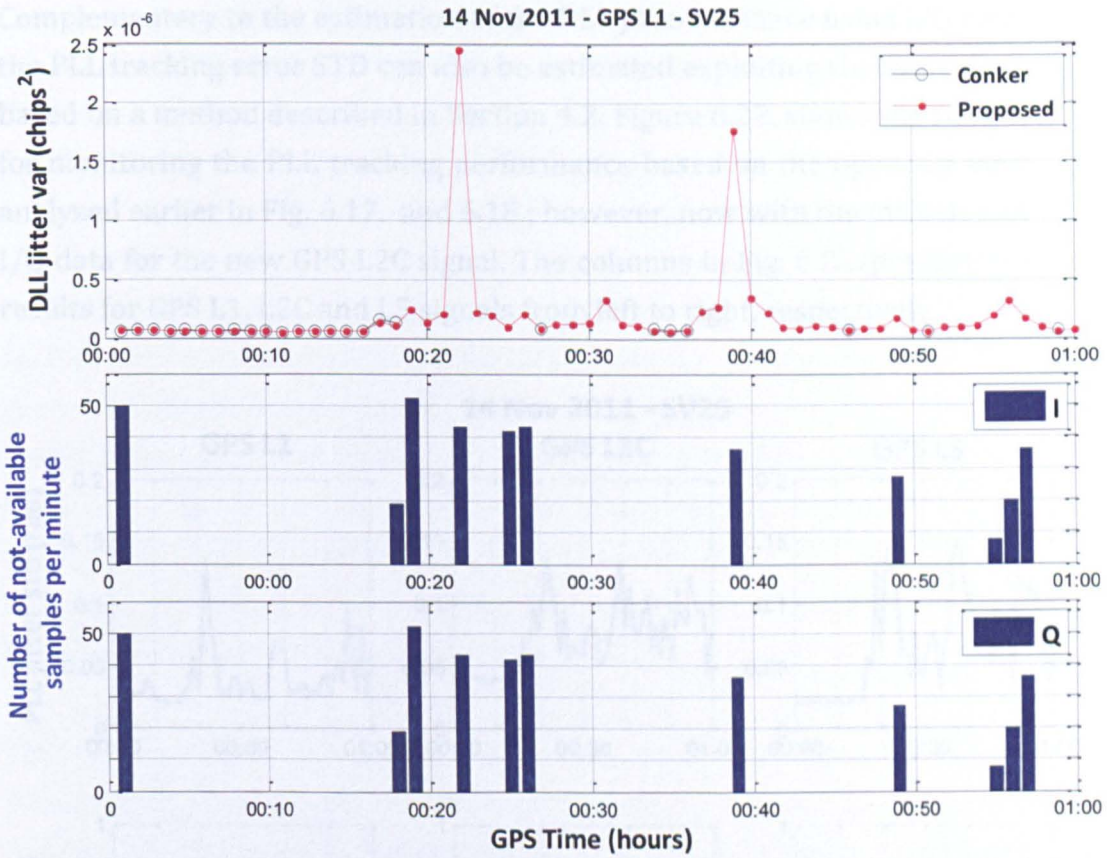

Figure 6.21. (*Top*) The DLL jitter variance ("var") estimated using the Conker model (black) and post-correlator I/Q data (red) by the proposed method for the data collected at PRU2 for GPS L1 signal link with SV25 on 14 November 2011. (*Middle)* Number of missing I and (*Bottom*) Q samples in the high rate data during each minute (i.e. out of 3000 samples for a rate of 50Hz) considering for the analyzed data set with SV25.

The aim is to highlight that such peaks can be related with non-availability of the post-correlator data utilized for such estimation in this case, and not necessarily represent a genuine tracking error. If the DLL jitter variance was estimated every second instead of every minute, then such non-availability of I/Q data could render impossible the estimation for the corresponding epochs.

It should be noted that all results in Fig. 6.17. - 6.21. are at 60s intervals which is the estimation rate possible with the Conker model. These results can be obtained at smaller intervals of interest if I/Q data is applied alternatively,

Complementary to the estimation of the DLL jitter variance using I/Q data, the PLL tracking error STD can also be estimated exploiting the same data, based on a method described in Section 4.2. Figure 6.22. shows the results for monitoring the PLL tracking performance based on the open sky data analyzed earlier in Fig. 6.17. and 6.18.; however, now with the inclusion of I/Q data for the new GPS L2C signal. The columns in Fig. 6.22. present the results for GPS L1, L2C and L5 signals from left to right, respectively.

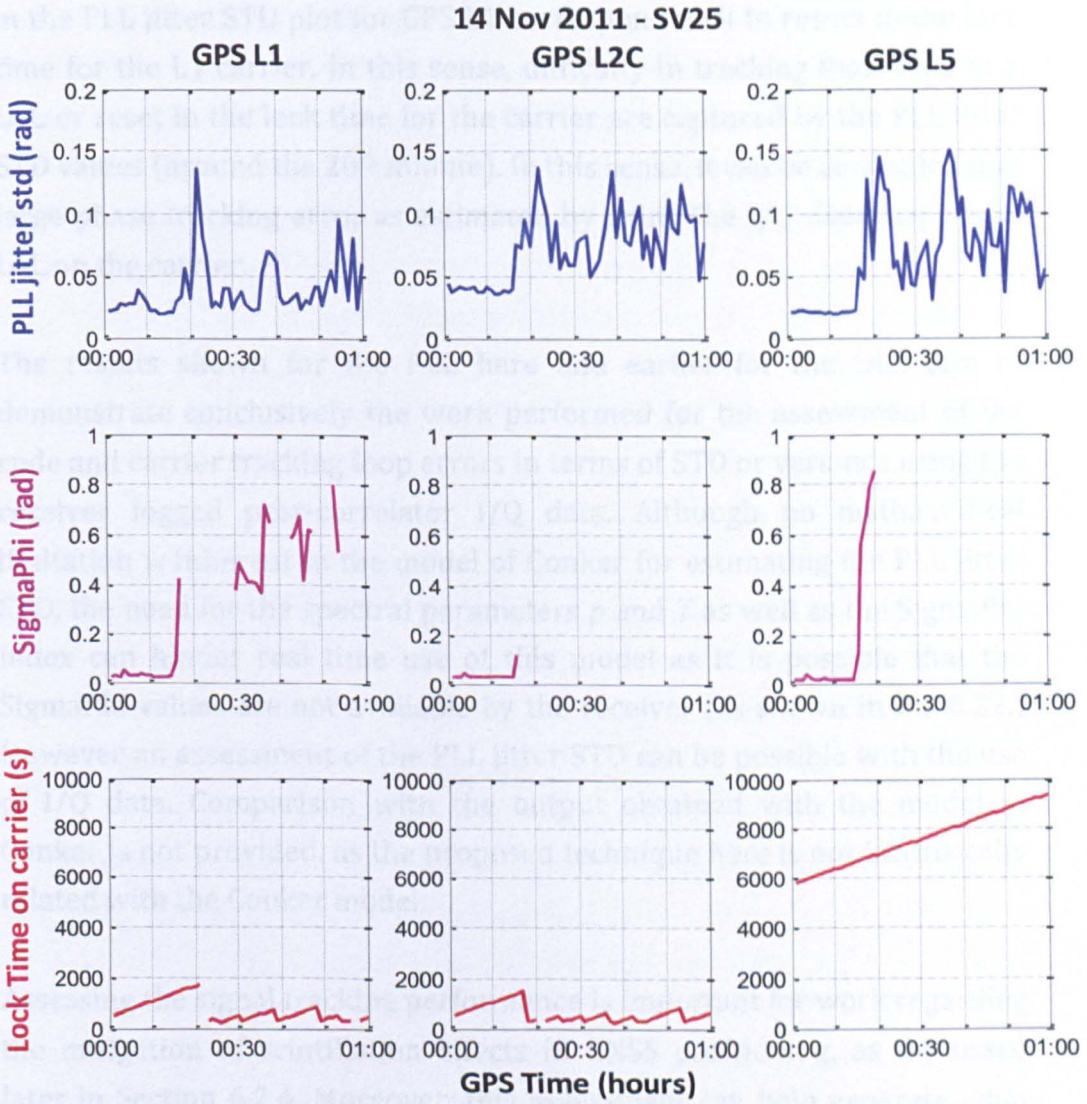

Figure 6.22. (*top*) The PLL jitter STD calculated every second and given in units of radians; (*middle*) SigmaPhi index which in this case could not be output by the receiver continuously; (*bottom*) carrier lock time.

Results for the STD of the carrier phase tracking error at the output of the PLL are shown in the first row in Fig 6.22., respectively, for the GPS signals L1, L2C and L5. It can be seen by inspecting the corresponding L1

SigmaPhi values (second row, leftmost plot) that moderate-to-strong levels of scintillation challenge the carrier tracking from especially about the 20th minute onwards: resets on the lock time are observed (except for the GPS L5 signal which can be related with the specific firmware related with tracking of the GPS L5 signal) and non-availability of SigmaPhi index can be noted. It can be seen that a continuous assessment of the PLL jitter STD is possible when the post-correlator I/Q data is used as described in Section 4.2. The results obtained for GPS L1 are promising: the peaks seen in the PLL jitter STD plot for GPS L1 correspond well to resets in the lock time for the L1 carrier. In this sense, difficulty in tracking that leads to a LoL or reset in the lock time for the carrier are captured by the PLL jitter STD values (around the 20th minute). In this sense, it can be concluded that large phase tracking error as estimated by using the I/Q data may cause LoL on the carrier.

The results shown for the PLL here and earlier for the DLL aim to demonstrate conclusively the work performed for the assessment of the code and carrier tracking loop errors in terms of STD or variance using the receiver logged post-correlator I/Q data. Although no mathematical limitation is inherent in the model of Conker for estimating the PLL jitter STD, the need for the spectral parameters p and T as well as the SigmaPhi index can hinder real time use of this model as it is possible that the SigmaPhi values are not available by the receiver (as shown in Fig 6.22.) However an assessment of the PLL jitter STD can be possible with the use of I/Q data. Comparison with the output obtained with the model of Conker is not provided, as the proposed technique here is not intrinsically related with the Conker model.

Assessing the signal tracking performance is important for work regarding the mitigation of scintillation effects in GNSS positioning, as discussed later in Section 6.2.4. Moreover, this assessment can help generate what are introduced as "Jitter maps" by the authors Sreeja et al. (2011b), which represent receiver signal tracking performance under scintillation based on the proposed technique in this section. Such maps can refer to both the code and carrier tracking loops of a reference station to provide users information about current (now-casting) or predicted tracking conditions under scintillation.

6.2.3. IMPACT OF SCINTILLATION ON GNSS POSITIONING

Stress induced on the tracking loops of a GNSS receiver by scintillation can manifest itself as degradation in the precision and availability of observations which can reflect on the accuracy, reliability and availability of a positioning solution. As an example, to highlight the impact of scintillation on GNSS positioning, in Fig. 6.23. the height error (calculated as the difference between the reference and estimated height) is shown for the PRU2 station using RT_PPP for PPP performed at a 60s interval. The background amplitude scintillation for this 4-hour-long period is shown in terms of the maximum S_4 observed on LoS paths from 22:00 UTC Time onwards on 31 December 2011. It can be noted that the time series for the height error is similar to that of the S4 index – it can be seen that at 00:00 UTC, the height error makes a peak crossing the zero error line. This is related with the change of date which causes a gap in the positioning solution.

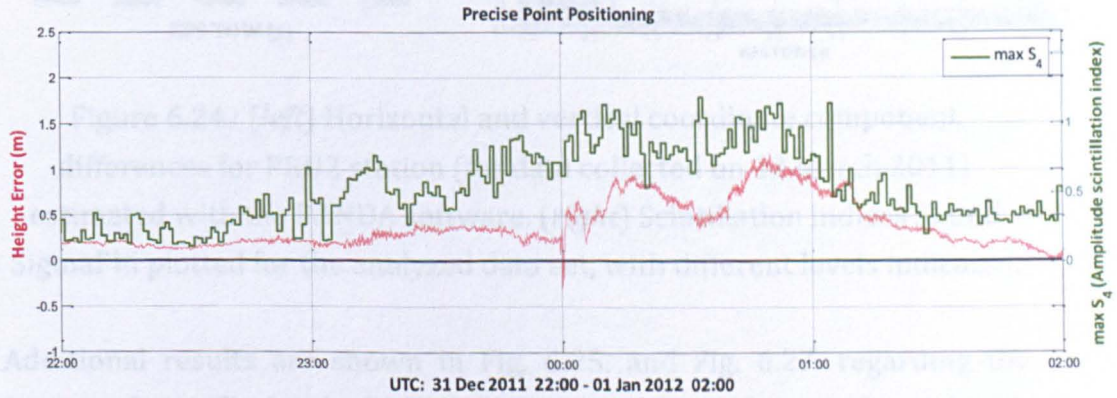

Figure 6.23. The height error (calculated as the difference between the reference and estimated height) for PRU2 station estimated with RT_PPP. The background amplitude scintillation is shown in terms of the maximum S_4 observed on all LoS paths.

Another result (courtesy of Dr Jianghui Geng for performing PPP with *P*ositioning *A*nd *N*avigation *D*ata *A*nalyst, PANDA[c], software) drawing

[c] *PANDA (Positioning and navigation data analyst) is a PPP tool developed by the Wuhan University in China. It combines dual-frequency GPS measurements to eliminate the first-order ionospheric errors, estimates zenith tropospheric delays, epoch-wise receiver position, receiver clock and the carrier phase ambiguity for a single receiver.*

attention to the impact of scintillation in PPP is shown in Fig. 6.24., which contains on the left the PPP result for the horizontal and vertical components, and on the right the scintillation indices (S_4 at the top and SigmaPhi at the bottom) that are marked for different (moderate and strong) levels. The large variation observed in the estimated coordinate differences during 0-14400s (4 hours) is due to strong scintillation in the background that is presented by the scintillation indices on the RHS in Fig. 6.24.

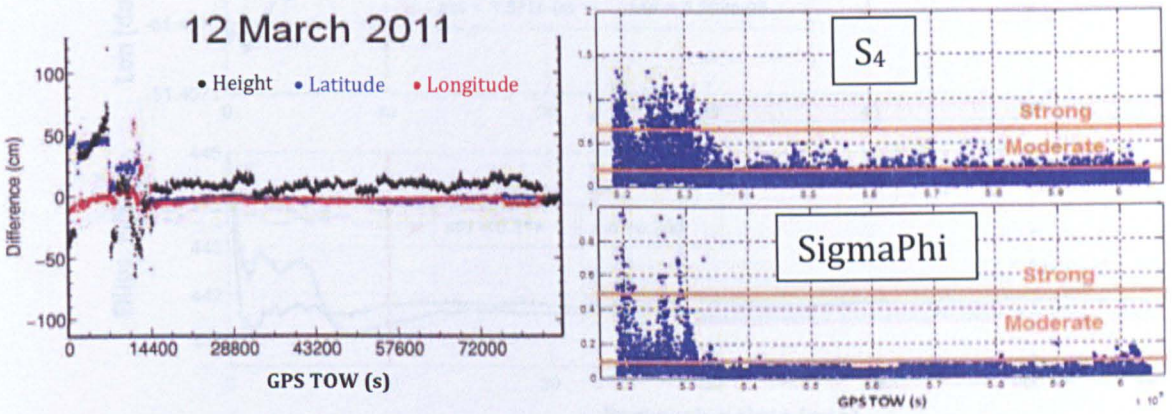

Figure 6.24.: (*left*) Horizontal and vertical coordinate component differences for PRU2 station (for data collected on 12 March 2011) estimated with the PANDA software. (*right*) Scintillation indices S_4 and SigmaPhi plotted for the analyzed data set, with different levels indicated.

Additional results are shown in Fig, 6.25. and Fig. 6.27. regarding the impact of scintillation in GNSS positioning where PPP is performed with the online positioning tool NRCan, introduced in Section 5.2.2., for the data collected on 13-14 November 2011 (Fig. 6.25.) and 12 March 2011 (Fig. 6.27.) at the PRU2 station. PPP results for each day involve comparison between two hours, where each hour has a different (strong versus weak) scintillation level. The local post-sunset hours (about 00:00-01:00 GPS Time) with significant scintillation levels are compared with local morning hours (11:00-12:00 GPS Time) when there is no significant scintillation. It is aimed to show how the differences in the background scintillation levels, shown in Fig. 6.26., can influence the positioning solution obtained with NRCan for a static receiver, allowing for the fact that variations in position over the first ten minutes are due to convergence of the PPP solution.

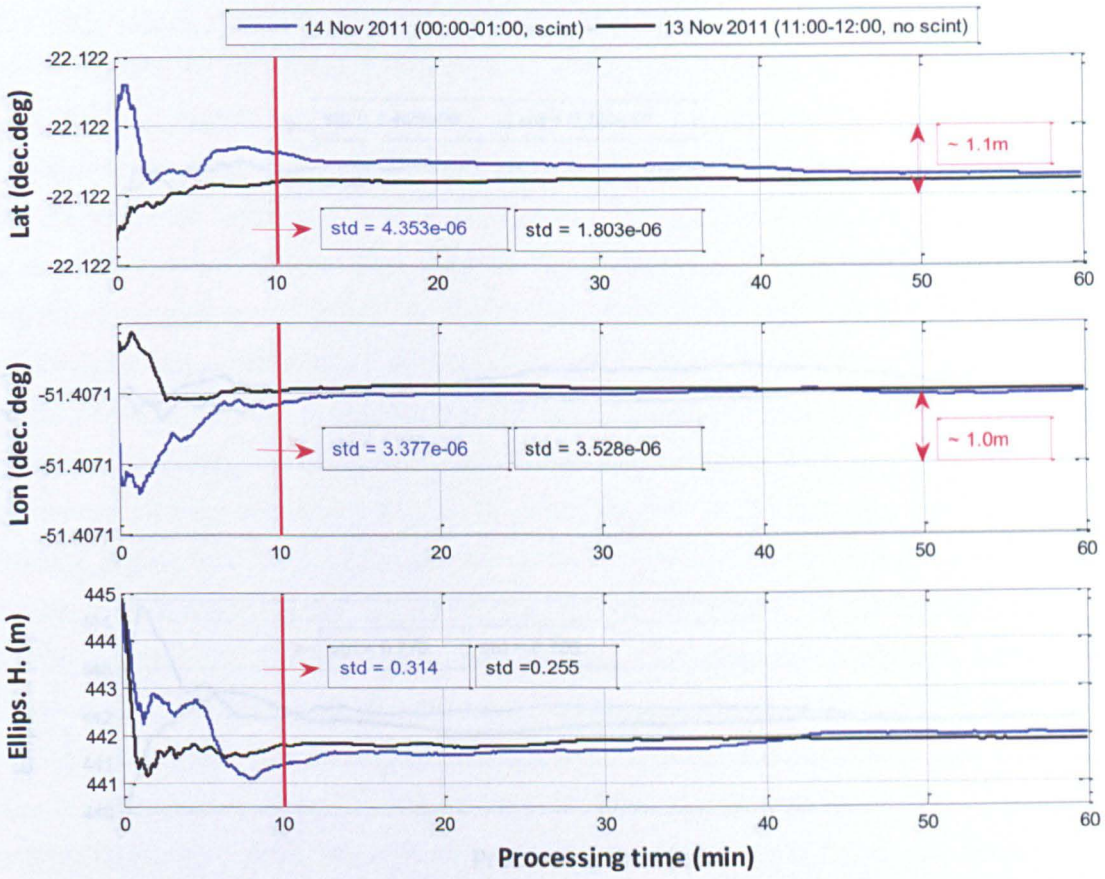

Figure 6.25. NRCan PPP results as differences in latitude ("Lat"), longitude (Lon) and ellipsoidal height ("Ellips.H.") for two one-hour observation periods. The top and middle plots are in decimal degrees, "dec.deg.".

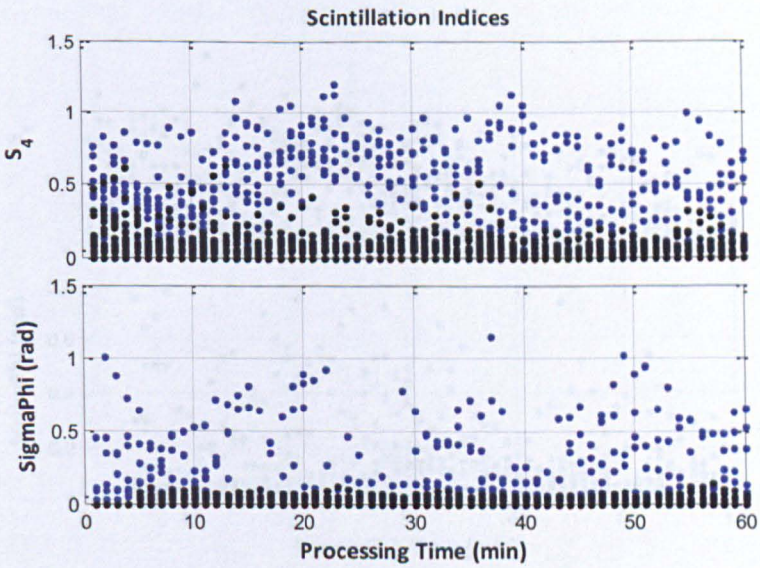

Figure 6.26. Background scintillation levels for the data considered in Fig. 6.15 (blue: 14 November 2011, 00:00-01:00 GPS Time, black: 13 November 2011, 11:00-12:00 GPS Time). An elevation cutoff angle 10^0 is applied, which agrees with the NRCan cutoff angle.

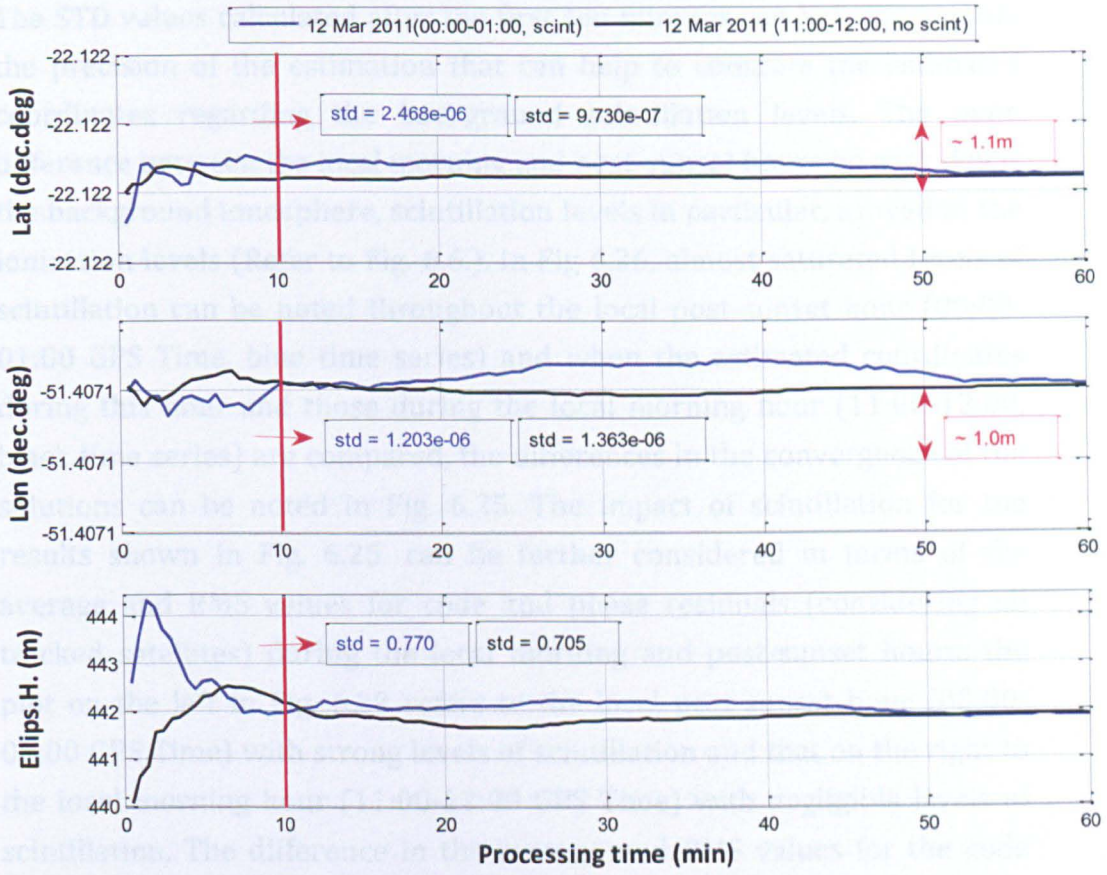

Figure 6.27. NRCan PPP results as differences in latitude ("Lat"), longitude (Lon) and ellipsoidal height ("Ellips.H.") for two one-hour observation periods. The top and middle plots are in decimal degrees, "dec.deg.".

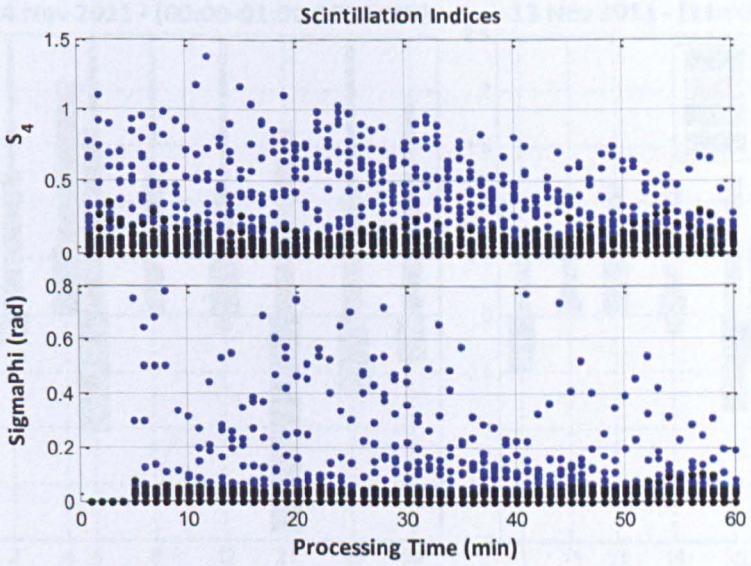

Figure 6.28. Background scintillation levels for the data considered in Fig. 6.15 (blue: 12 March 2011, 00:00-01:00 GPS Time, black: 12 March 2011, 11:00-12:00 GPS Time). An elevation cutoff angle 10^0 is applied, which agrees with the NRCan cutoff angle.

The STD values calculated after the first ten minutes can help to quantify the precision of the estimation that can help to compare the estimated coordinates regarding the background scintillation levels. The main difference between the local morning and post-sunset hours on each day is the background ionosphere, scintillation levels in particular, as well as the ionization levels (Refer to Fig. 6.6.). In Fig 6.26. almost saturated levels of scintillation can be noted throughout the local post-sunset hour (00:00-01:00 GPS Time, blue time series) and when the estimated coordinates during this hour and those during the local morning hour (11:00-12:00, black time series) are compared, the differences in the convergence of the solutions can be noted in Fig. 6.25. The impact of scintillation for the results shown in Fig. 6.25. can be further considered in terms of the average and RMS values for code and phase residuals (considering all tracked satellites) during the local morning and post-sunset hours: the plot on the left in Fig. 6.29 refers to the local post-sunset hour (00:00-01:00 GPS Time) with strong levels of scintillation and that on the right to the local morning hour (11:00-12:00 GPS Time) with negligible levels of scintillation. The difference in the average and RMS values for the code and phase measurements between the two hours compared for this particular station can be attributed to the differences in background ionospheric conditions (Fig. 6.6., Fig. 6.26) during these two hours.

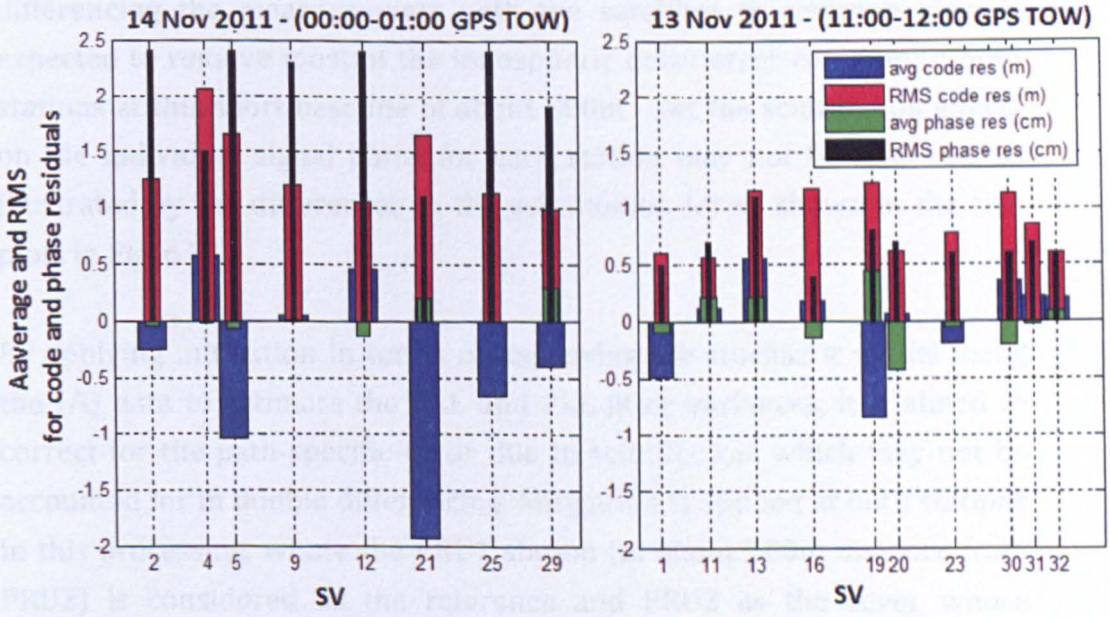

Figure 6.29. Average ("avg") and RMS values for code and phase residuals ("res") for the data collected on 13-14 November 2011, which is previously analyzed in Fig. 6.25.

6.2.4. MITIGATION OF SCINTILLATION IN GNSS POSITIONING

Mitigation of the possible scintillation-induced range errors in GNSS positioning can help attain more precise positioning solutions especially at times of strong scintillation. Coco et al. (1999) show that strong amplitude scintillations can increase the pseudorange RMS values and introduce less reliable pseudorange measurements. As described in Section 5.2.2., mitigation of the scintillation effects in GNSS positioning is considered in two approaches and the results are presented here.

6.2.4.1. MITIGATION IN RELATIVE POSITIONING

Figure 6.30. shows the results of a baseline positioning solution obtained with the GPSeq positioning software for the two stations PRU1 and PRU2 at a baseline of about 300m, in Presidente Prudente, Brazil. The data was collected on 15 November 2011 at 00:00-01:00 GPS Time. The scintillation levels for each station are provided in Fig. 6.31. Positioning is performed to estimate the station coordinates of PRU2 station as an epoch-by-epoch solution at 30s interval considering 4 types of observables: C1, L1, P2, L2. The precision considered for these four observables are given in Table 6.4. A cycle slip threshold of 3 and an elevation cutoff angle of 5^0 are chosen. No ionospheric correction is applied to the measurements as double differencing the measurements with the satellites in common view is expected to remove most of the ionospheric delay error common to both stations at this short baseline of about 300m - yet the scintillation effects on the individual signal paths for each station may not be removed, as illustrated by the differences in the scintillation levels shown in the two plots in Fig. 6.31.

By applying mitigation in terms of improving the stochastic model using the I/Q data to estimate the DLL and PLL jitter variances, it is aimed to correct for the path-specific error due to scintillation, which may not be accounted for in double differencing. Mitigation is applied at both stations in this processing, where the PRU1 station (at about 300m distance from PRU2) is considered as the reference and PRU2 as the rover whose coordinates are estimated.

The mitigated solution in Fig. 6.30. for the height estimate ("mitigated", blue series) refers to the case when the stochastic model is improved in terms of the weights calculated as the inverse of the jitter variances. The non-mitigated solution refers to the case when the stochastic model is based on the precision values for the observables as the predefined values given in Table 6.4.

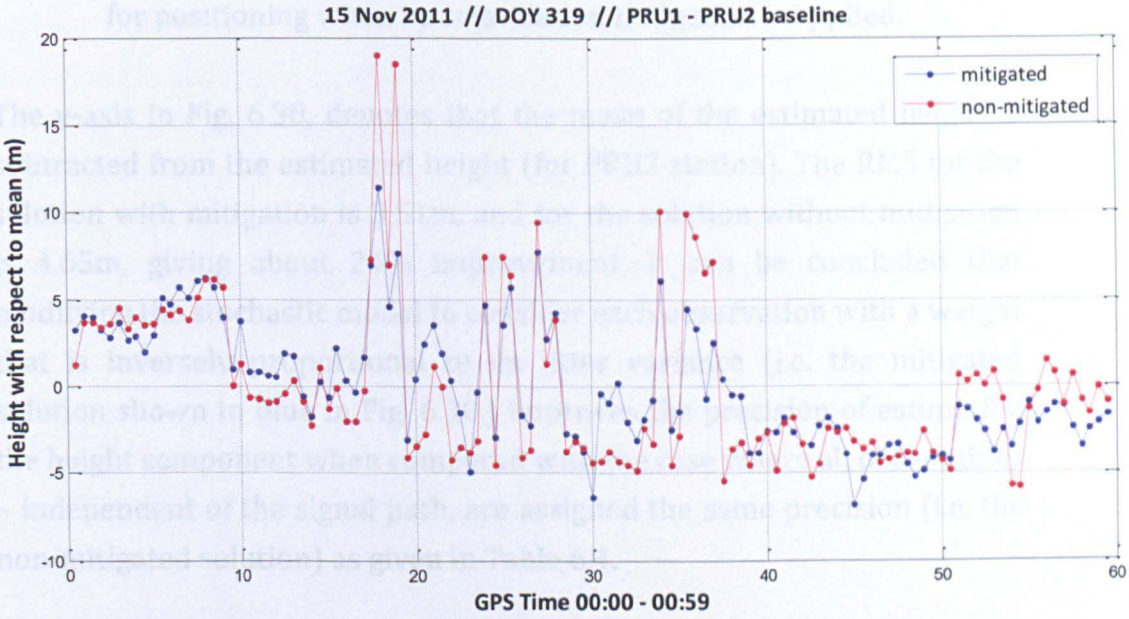

Figure 6.30. Estimated height with respect to mean in (short) baseline positioning with (blue series) and without (red series) scintillation mitigation.

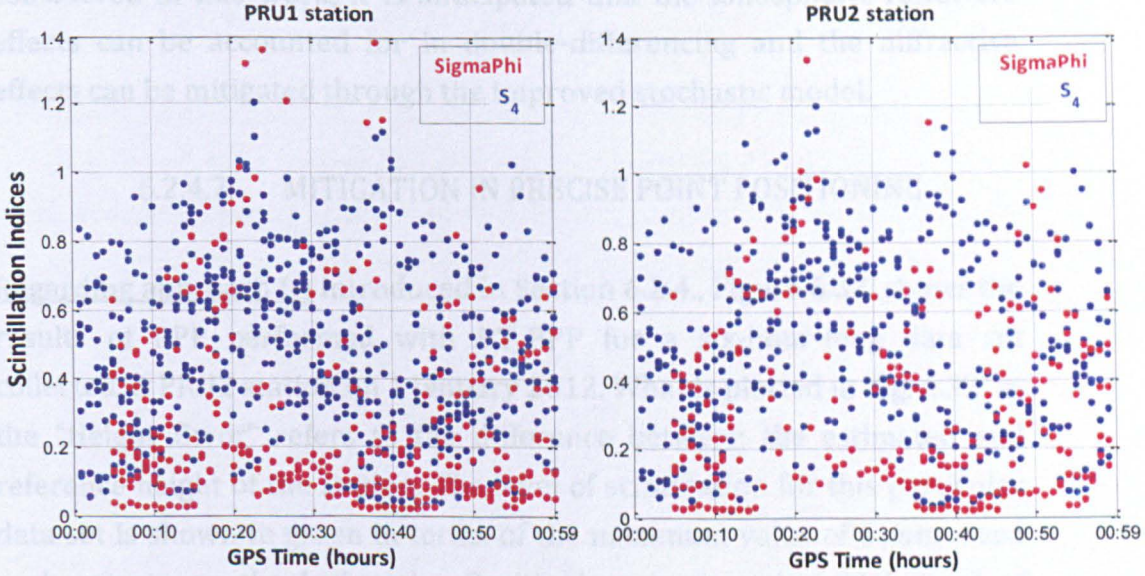

Figure 6.31. Scintillation levels (given by the scintillation indices SigmaPhi and S4) for the baseline stations PRU1 and PRU2 for the data analyzed in Fig. 6.30.

Observable	Precision
C1	0.3m
P2	5.85m
L1	0.004m
L2	0.006m

Table 6.4. Precision of the observables considered in the stochastic model for positioning when no scintillation mitigation is applied.

The y-axis in Fig. 6.30. denotes that the mean of the estimated height is subtracted from the estimated height (for PRU2 station). The RMS for the solution with mitigation is 3.51m, and for the solution without mitigation is 4.65m, giving about 24% improvement. It can be concluded that modifying the stochastic model to consider each observation with a weight that is inversely proportional to its jitter variance (i.e. the mitigated solution shown in blue in Fig. 6.30.) improves the precision of estimating the height component when compared with the case where all observables – independent of the signal path, are assigned the same precision (i.e. the non-mitigated solution) as given in Table 6.4.

The method introduced and the preliminary results presented here can help to set out a method for investigating how the scintillation effects can be mitigated in baseline positioning. For the short baseline of about 300m considered in this work, it is anticipated that the ionospheric refractive effects can be accounted for in double-differencing and the diffractive effects can be mitigated through the improved stochastic model.

6.2.4.2. MITIGATION IN PRECISE POINT POSITIONING

Regarding approach (i) introduced in Section 6.2.4., Figure 6.32. shows the results of PPP performed with RT_PPP for a six-hour-long data set collected at PRU2 station on 1 January 2012. What is plotted in Fig. 6.32. as the "Height Error" refers to the difference between the estimated and reference height of the station. The level of scintillation for this particular data set is shown in green in terms of the maximum value of S_4 observed each minute on the LoS paths. Positioning starts with a high level of scintillation from 00:00 GPS Time onwards and persists until about 01:00 which may also delay the convergence of the estimated height solution to

be achieved; therefore, the first hour of positioning (marked with a black solid line) is considered as the convergence period. "Conventional technique" refers to the positioning solution where no mitigation against scintillation is applied, and "New technique" indicates when the scintillation mitigation technique is considered in RT_PPP. In this processing with RT_PPP, the IF observable is used to eliminate the first order ionospheric error, a static solution is adopted while estimating the station coordinates, the receiver clock is estimated per epoch and the ambiguities are taken as floating values. While the mitigation technique modifies the weight matrix according to the precision values estimated per observable per receiver-satellite, standard precision values are taken for the observables (independent of path) when scintillation mitigation is not applied (C1=0.4m, P2= 0.8m, L1=0.005m , L2=0.008m).

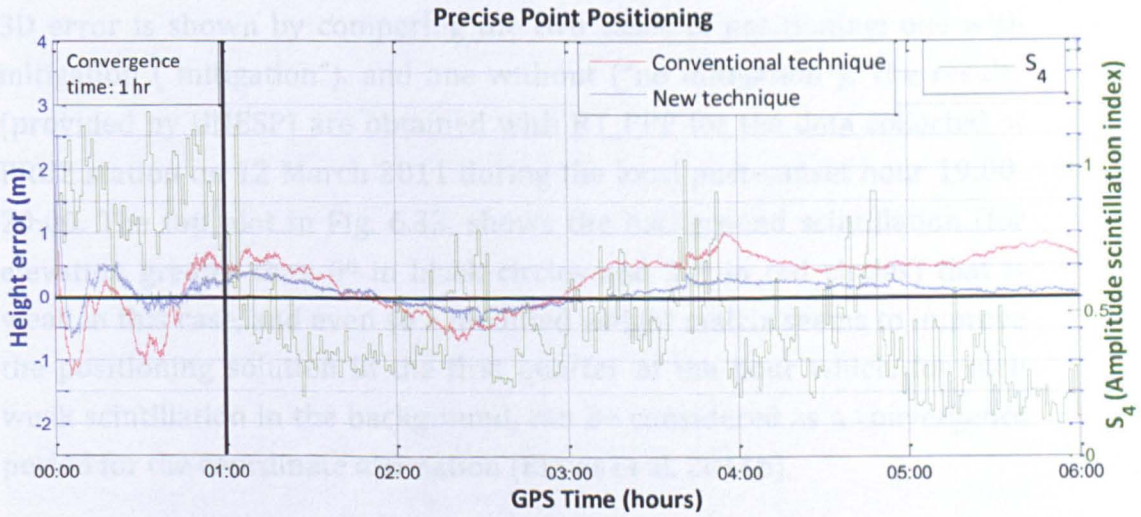

Figure 6.32. Comparison of the error in the estimated height with ("New technique", blue series) and without ("Conventional technique", red series) scintillation mitigation in PPP. Background amplitude scintillation is given in terms of the maximum S4 in all LoS paths (green series).

Comparing the two series of results for the error in height, it can be seen that for the strong level of amplitude scintillation during the convergence time between 00:00-01:00 GPS Time, the mitigation technique benefits the coordinate estimation by making the height estimates to fluctuate less within a more confined error bound – the height error in the red series of the "Conventional technique" fluctuates up to about a meter, whereas for the blue series representing the "New technique" this fluctuation is within about ±0.5m. Beyond 01:00, it can be seen that the height error in both

series starts decreasing towards 02:00 while the level of scintillation also gets milder. For the period of 01:00-06:00 GPS Time, the comparison of RMS values obtained from the two positioning solutions shows that the scintillation mitigation technique brings advantage to the estimated height overall: the STD value of the height error for the conventional technique is about 0.52m and about 0.18m for the new technique, which gives an improvement of about 65% in the estimated height solution.

N.B. During the convergence period, RMS for the conventional and new techniques are 0.59m and 0.41m, respectively. This gives an improvement of about 29%.

Another result for mitigating the effect of scintillation in PPP following approach (i) is shown in (the bottom plot of) Fig. 6.33. where this time the 3D error is shown by comparing the two cases of positioning: one with mitigation ("mitigation"), and one without ("no mitigation"). The results (provided by UNESP) are obtained with RT_PPP for the data collected at PRU2 station on 12 March 2011 during the local post-sunset hour 19:00-20:00. The top plot in Fig. 6.33. shows the background scintillation (for elevation greater than 0^0 in black circles and 30^0 in red circles) that is weak in this case, and even so a modified weight matrix seems to improve the positioning solution in the first quarter of the hour which, for such weak scintillation in the background, can be considered as a convergence period for the coordinate estimation (Elmas et al. 2011b).

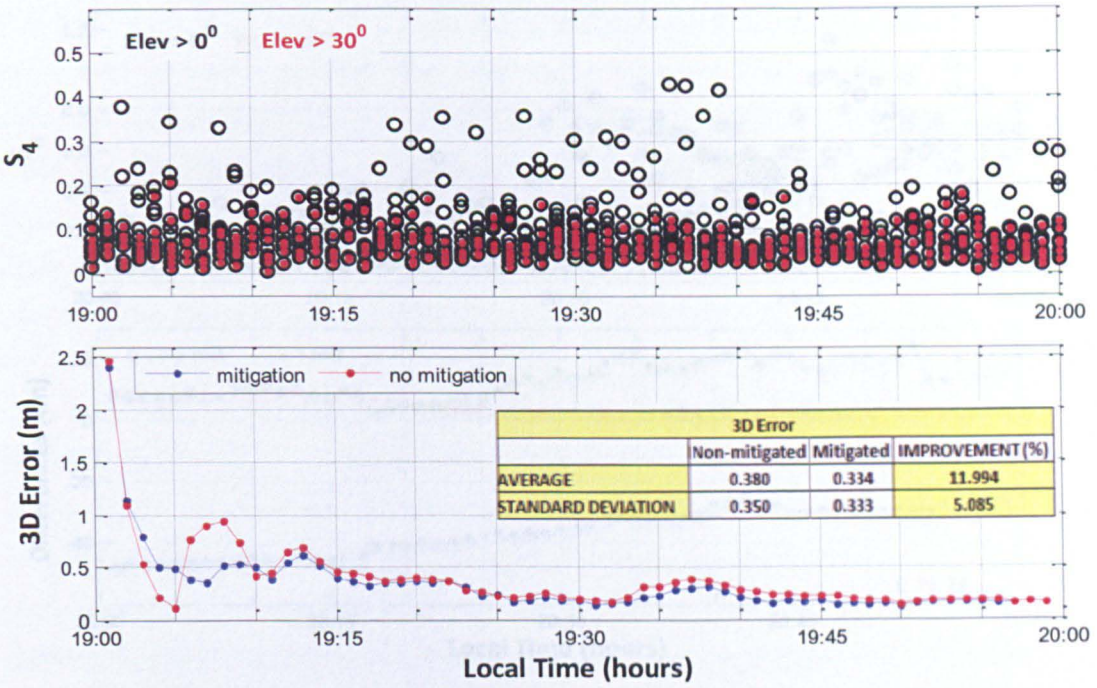

Figure 6.33. (*top*) The S4 values for all signal paths and those above 30^0 elevation angle for the data collected at PRU2 station on 11 March 2011 between 22:00-23:00 GPS Time. (*bottom*) PPP results shown for the 3D error for the same data set (vales in the inset are in meters).

This result shows that for such weak level of scintillation, there is no significant improvement in the estimated station coordinates when the mitigation technique is applied except during the convergence period when more accurate estimates can be possible. On average, about 12% improvement is observed in the average 3D error during the hour and the STD is improved by about 5%.

Another example for scintillation mitigation in PPP regarding approach (i) is shown in Fig. 6.34. (in the bottom plot), which is provided by Dr. J. Geng (colleague at NGI during the course of this PhD) who processed the open sky data collected at PRU2 station during the local post-sunset hour 20:00-21:00 on 11 March 2011 using the PANDA software. Modification of the stochastic model in the PANDA software in order to allow for testing the mitigation technique in this software was carried out through this PhD. The top plot in Fig. 6.34. shows the amplitude scintillation level in terms of S_4 index indicating that scintillation affects some paths, especially in the second half of the hour (Elmas et al. 2011b).

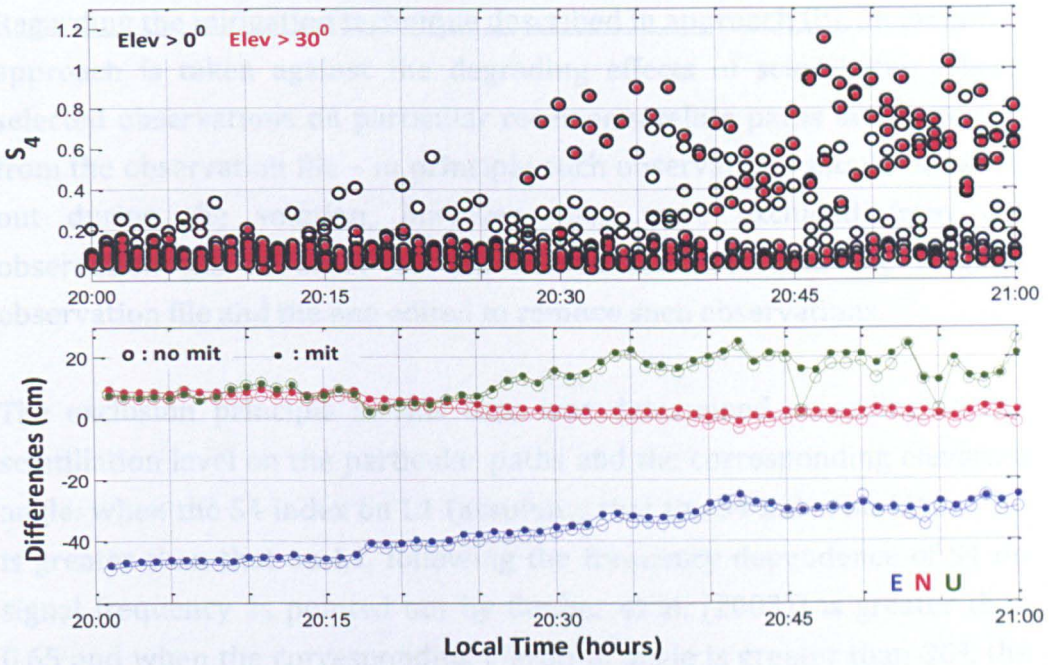

Figure 6.34. (*top*) The S4 index for elevation greater than 0^0 (black) and greater than 30^0 (red). (*bottom*) The estimated station coordinates (East, "E", in blue; North, "N", in red; Up, "U", in green) plotted (against a ground truth) in empty circles when the scintillation mitigation technique is *not* applied, and in filled circles when it *is* applied.

It can be noticed that during the second half of the hour, the mitigation technique seems to improve the coordinate estimation, which can be observed in the less scattering of results for the Upward component, in particular. Focusing on the second half of the processed hour, the STD values for the three position components and the improvement calculated from the STD values in terms of a percentage are shown in Table 6.5.

	STD values (cm)		
	No mitigation case	With mitigation	Improvement
East	3.0192	2.7172	10%
North	5.2325	3.5581	32%
Up	1.1817	0.9764	17%

Table 6.5. The STD values and improvements for the East, North and Up components with and without the mitigation technique, referring to 20:30-21:00 local time.

Regarding the mitigation technique described in approach (ii), an *exclusion* approach is taken against the degrading effects of scintillation where selected observations on particular receiver-satellite paths are neglected from the observation file – in principle such observations should be taken out during the solution, however, they were excluded from the observation file in order to use NRCan for PPP with the original observation file and the one edited to remove such observations.

The exclusion principle in this case was determined according to the scintillation level on the particular paths and the corresponding elevation angle: when the S4 index on L1 (assuming that the S4 index on L2 and L5 is greater than that on L1, following the frequency dependence of S4 on signal frequency as pointed out by Conker et al. (2003)) is greater than 0.65 and when the corresponding elevation angle is greater than 30^0, the observations were flagged for the selected signal paths.

For the one hour long (21:00-22:00 local time) open sky data collected at PRU2 station on 1 January 2012, the threshold for excluding the observations from the observation file is set as 0.65 for S_4 on GPS L1 frequency and 30^0 for the elevation angle; this means that whenever the S4 index is greater than 0.65 with the corresponding elevation angle being larger than 30^0 for a receiver-satellite link, the range measurements on that signal link are removed from the observation file. First the data set is examined to detect instances when this threshold is encountered considering all LoS paths. Once the observations are flagged, they are excluded from the observation file. In this particular data set analyzed here, observations with the GLONASS satellites are also considered.

PPP is performed with both the original observation file (no observations taken out) and the one edited to remove the flagged observations. Figure 6.35. shows for this particular data set the three signal paths (two with GPS SVs and one with a GLONASS SV) which, at certain times, are excluded from the observation file. The red horizontal line shows when S_4 values are greater than 0.65 and all plots refer to elevation angles greater than 30^0.

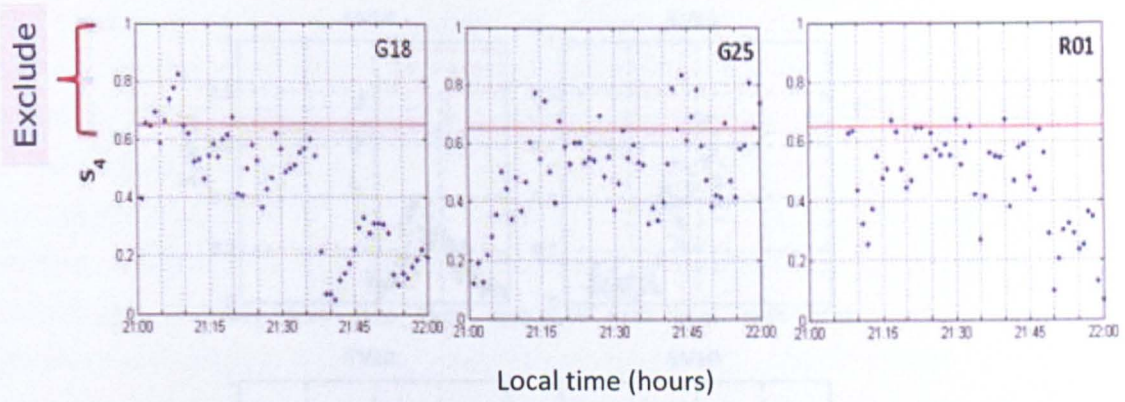

Figure 6.35. Red line shows S4=0.65. Instances of S_4 above the red line when elevation angle is greater than 30^0 are excluded from the observation file.

Results for PPP with the original and edited observation files are given in Table 6.6. It can be seen that neglecting the flagged observations in this case has exacerbated (sigma values, "Sigmas", are almost twice as large) the precision with which latitude (Lat), longitude (Lon) and ellipsoidal height (Ell. H) coordinates are estimated.

			Lat (m)	Lon (m)	Ell. H (m)
Impact	GPS + GLO	Sigmas (95%)	0.110	0.153	0.369
	GPS + GLO excl'd SV	Sigmas (95%)	0.253	0.415	0.797

Table 6.6. The impact of mitigation through elimination of satellite paths in PPP with NRCan considering the GPS and GLONASS ("GLO") constellations.

In another data set, the same threshold in terms of the S4 index and elevation angle is considered for a GPS-only observation file. The data analyzed was collected at the PRU2 station on 22 January 2012, during 00:00-03:59 GPS Time. As shown in Fig. 6.36., with four signal paths (with GPS SV14, SV16, SV22 and SV30) instances of S4>0.65 (marked with a horizontal red line in each plot) on GPS L1 frequency are observed with an elevation angle greater than 30^0 (Fig. 6.36.). The corresponding measurements are taken out from the observation file. PPP is performed with a 10^0 elevation cutoff angle and at a 60s interval.

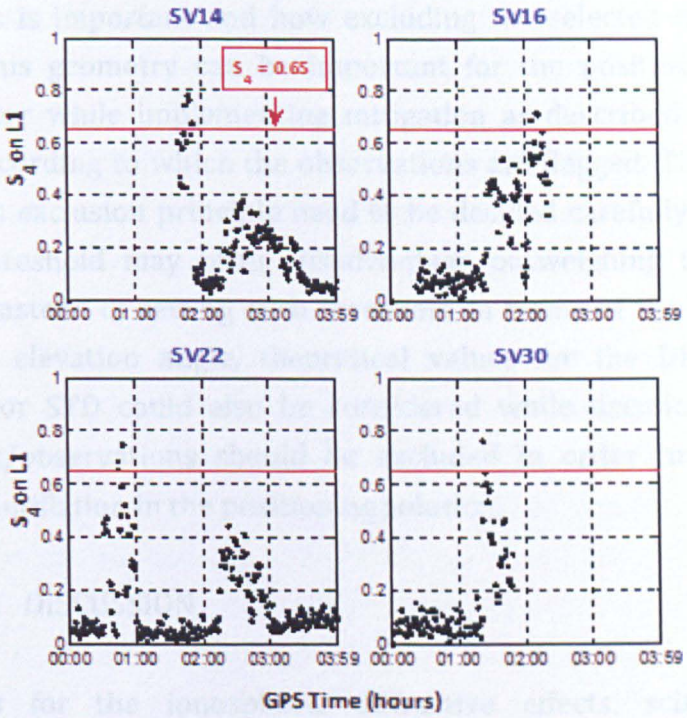

Figure 6.36. Four signal paths (with an elevation cutoff angle of 30^0) for instances of S4>0.65, with a red line in each plot marking S4=0.65.

Table 6.7. shows the precision of the coordinate estimation when the original and the edited observation files are considered in PPP. Unlike the earlier case (in Table 6.6.), this time excluding the observations has slightly improved the precision of the estimation: about 8.3%, 4.9% and 12.5% improvement is achieved for latitude, longitude and ellipsoidal height components when scintillation mitigation is applied in an approach similar to RAIM.

		Lat (m)	Lon (m)	Ell. H. (m)
GPS	Sigmas (95%)	0.036	0.081	0.128
GPS excl'd SVs	Sigmas (95%)	0.033	0.077	0.112

Table 6.7. Changes in the precision of the estimates for latitude (Lat), longitude (Lon) and ellipsoidal height (Ell. H.) components when the selected observations are excluded ("excl'd") from PPP.

One important factor to consider while excluding the observations is the elevation angle of the particular signal path and the number of tracked satellites per epoch. Thus, the relative geometry between the receiver and

the satellites is important and how excluding the selected observations influences this geometry can be important for the positioning results. Another factor while implementing mitigation as described here is the threshold according to which the observations are flagged. The threshold values for an exclusion principle need to be decided carefully as too high or low a threshold may bring disadvantage outweighing the possible advantage. Instead of setting such threshold in terms of the scintillation indices and elevation angle, theoretical values for the DLL and PLL tracking error STD could also be considered while deciding on which signal paths/observations should be excluded in order to reduce the impact of scintillation in the positioning solution.

6.2.5. DISCUSSION

The results for the ionospheric diffractive effects, scintillation in particular, are presented in Section 6.2., where open sky data collected at low latitude stations (PRU1 and PRU2) (during the years 2011-2012) are considered for the analyses. From this aspect, the analyses were limited by the scintillation events that were observed during this period of the ascending phase of Solar Cycle #24.

The impact of scintillation on GNSS signals was studied for weak to strong levels of scintillation, and also considering the new GNSS signals such as GPS L2C and L5. As for the Galileo signals, tracked by the receivers at the high and mid latitude stations in Bronnoysund and Cyprus (Section 5.1.1.), respectively, the data collected during the research period of this thesis did not contain significant levels of scintillation; therefore, investigation of the new signals for scintillation effects could not be expanded to include the Galileo signals.

Regarding the impact of scintillation on receiver signal tracking performance, results are presented for assessing the jitter variance with the scintillation sensitive model of Conker et al. (2003) and with the proposed technique making use of the post-correlator data (Section 4.2.). The Conker model is limited for use when S4>0.707 for GPS L1 signal – the authors state that assessment of the jitter variance becomes not meaningful under such condition as LoL occurs with the carrier; however, it was observed in the data analyzed during this research that the carrier

lock can be maintained when S4>0.707. For such instances, i.e. when the scintillation level is strong and signal lock is maintained, the proposed technique is shown to provide continuous estimation of the jitter variance based on data available by the receiver and independent of any external input information, such as the scintillation indices and the spectral parameters as in the case of the Conker model.

Impact of scintillation on GNSS positioning is shown based on the low latitude data with strong levels of scintillation. It was observed in the field recorded data that scintillation is a threat to GNSS receivers; it can cause rapid phase and intensity fluctuations in the received signal (evident in the values of the scintillation indices), challenge signal tracking and cause gaps in the range measurements recorded by the receiver, lead to a delay in obtaining a position solution and affect the *quality* of the IF observable.

The results for scintillation mitigation in GNSS positioning, in relative positioning and PPP, as considered here, constitute an important part of this thesis. Based on the mitigation technique suggested by Aquino et al. (2009), who proposed improving the stochastic model in order to account for the degradation in measurements due to scintillation, the approach here makes it possible to apply this mitigation technique to data sets with *strong* levels of scintillation. This is achieved by improving the stochastic model in terms of the jitter variances computed per observation (as also done by Aquino et al. (2009)) making use of the post-correlator data (instead of using the Conker model as in the case of Aquino et al. (2009)). This enables mitigation to data sets with weak-to-strong levels of scintillation as long as the signal is tracked so that the post-correlator data is available for subsequent jitter variance calculations.

Another approach for mitigating the scintillation effects is attempted in PPP through excluding the observations, which correspond to a level of scintillation and an elevation angle that are greater than predefined values for these two parameters.

In the baseline positioning for two receivers at about 300m distance from each other, scintillation mitigation (applied in the GPSeq program through improving the stochastic model) helps to improve the estimated station height component for the rover by about 24% (Fig. 6.30.). In PPP,

scintillation mitigation applied in the RT_PPP program (through improvement of the stochastic model) helps to improve the precision for the height component as presented in Section 6.2.4.2. As for the case where an exclusion principle is applied to mitigate the scintillation effects (using NRCan) it was observed that such exclusion of the measurements from a position solution improved the precision of coordinate estimation in one of the cases considered, and degraded the precision further in another case. This brings into attention the importance of the relative receiver-satellite geometry that is affected when the observations are excluded for a particular signal link as well as the values in the predefined threshold for the parameters of interest (such as S4 and elevation angle, in this case).

CHAPTER 7

CONCLUSIONS AND RECOMMENDATIONS FOR FUTURE WORK

In this chapter, a comprehensive summary is made of the conclusions drawn from this research and recommendations are given for future work in the field of modelling, monitoring and mitigating the ionospheric effects in GNSS within the scope of GNSS modernization.

- Conclusions:

[1] An important contribution of GNSS modernization is the availability of at least two signal frequencies for the civil users to correct for the frequency dependent ionospheric error. In addition, three distinct frequencies provide redundancy in a dual-frequency approach to the ionospheric error and make available a further reduced IF observable by e.g. accounting for the second order ionospheric error term in a triple frequency approach; however, the increased noise level of this approach outweighs the benefit of reducing the ionospheric error further. Other benefits of GNSS modernization include the new modulation techniques, which can provide more robust tracking in poor conditions, such as during scintillation, and an increase in the number of satellites, which can contribute to a better sampling of the ionosphere as well as providing a good relative geometry between the receiver and satellites.

[2] Scintillation effects should be taken into account as they may cause loss of lock on the carrier, reduce the accuracy of the pseudoranges and carrier phase measurements and affect the availability of a position solution. Performance of the code and carrier tracking loops can be affected during scintillation such that precise carrier phase estimation in the phase-locked loop and good alignment of the code in the delay locked loop can be affected. (new) Poorer performance in the tracking loops reflects on the precision of the range measurements obtained from the receiver, and this can sequentially impair the accuracy and availability of a positioning solution.

[3] Scintillation may cause additional ranging error in the dual and triple frequency IF observables. It was observed that for the change in

time (rate) of the dual and triple frequency IF observables there is greater scattering in the rate once scintillation starts affecting the signal paths. Comparing the rate of triple and dual frequency IF observables during different (negligible and strong) levels of scintillation, it was observed that in general the dual frequency approach yields an IF observable that has less scattering during scintillation. Greater scattering in the triple frequency IF can be associated with the enhanced noise level of this observable.

[4] Considering multiple frequencies for constructing the IF observable in a dual frequency approach, the rate of IF when constructed from the L2C, L5 signals showed greater scattering compared to when constructed from L1,L5 and L1,L2 during scintillation (at negligible and strong levels). This can be explained by the small frequency difference between L2C and L5 compared with that between L1 and L2C, and L1 and L5. Good performance of the IF observable based on L1, L5 signals was noticed in particular during strong scintillation from less scattering observed in the rate.

[5] TEC can be calculated more precisely by using observations on L1 and L5 signal frequencies in the dual frequency approach instead of L1 and L2. As more satellites start broadcasting the GPS L5 signal, users can gradually shift to L1, L5 signals to estimate TEC more precisely.

[6] Through participation in the CIGALA and POLARIS projects during this thesis, it was possible to have access to field data recorded at low to high latitudes while approaching the next peak of the Solar Cycle (Solar Cycle #24) predicted for 2013. Although the receivers deployed at these latitudes were limited by the number of new GNSS signals they could track, the data was important for including measurements for some new signals, such as GPS L2C and L5, which play an important role in modernization of GPS. Furthermore, the open sky data was also limited in terms of adverse conditions of the ionosphere, for instance, regarding the level of enhancement in the ionization levels and significant scintillation events. Nevertheless, the open sky data was essential for understanding the actual physical effects of the ionosphere on GNSS signals and investigating this impact on receiver signal tracking and positioning performance.

[7] The tools available during this research in hardware (GNSS receivers and the Spirent signal simulator) and software (the positioning programs RT_PPP and GPSeq; the Rinex_HO program for study of the HO error terms; scintillation models CSM and GISM) played an important role in investigations. In this sense, the Septentrio PolaRxS receiver was notable for its novel output feature of signal intensity in terms of post-correlator data. The Spirent simulator was helpful to apply scintillation effects on the generated signals to test the routines developed for extracting the scintillation effects from open sky data and to assess receiver signal tracking performance, giving the capability to consider the new GNSS signals that were not yet broadcast at a constellation level. The positioning programs RT_PPP and GPSeq were outstandingly helpful in providing a user interface to test and validate scintillation mitigation in terms of modifying the stochastic model in the LSQ positioning solution. The Rinex_HO program was particularly useful to obtain the observation files corrected for the higher order, Iono2 and Iono3, error terms so that these files could be used in positioning. The scintillation model CSM was a helpful source to generate scintillation time series for simulation scenarios to investigate receiver signal tracking robustness during scintillation.

[8] Regarding the study of scintillation effects on GNSS signals through simulation, use of an external user commands file to modify the signal intensity and carrier phase ranges has been well exhausted during this PhD. In order to obtain scintillation effects (as time series) that can be formatted into command files for simulations in order to simulate realistic scintillation conditions, the scintillation models CSM and GISM as well as of open sky data have been considered during this PhD. The scintillation models in this case provide outputs of signal intensity and carrier phase variations in time that can be formatted into specific files recognized by the Spirent simulator. An important part of this research was about the use of open sky data with scintillation in the background in order to extract scintillation effects in terms of high frequency fluctuations in signal intensity and phase. For this purpose, a routine is suggested to extract amplitude fluctuations from the signal intensity data; and extraction of phase fluctuations the signal phase data is adapted from the work of Aquino et al. (2007) (based on estimating the SigmaPhi index from high rate carrier phase data). Routines in MatLAB were made applicable for

multi-frequency signals as well as to include constellations such as GLONASS and Galileo (multi-constellation). Use of open sky data to perform scintillation-oriented simulations through command files allows users to implement genuine scintillation characteristics in the rapidity of fluctuations and depth of signal fades.

[9] Another task well practiced within the investigation of scintillation was the use of the Spirent simulator's scintillation tool, (CSM implemented into the simulation firmware), which was tested and evaluated as part of the methodology for studying scintillation effects. The model is part of the ionospheric modelling of the simulation firmware, and a few differences were noticed between running the model externally in MatLAB and through the simulation firmware. For instance, the time decorrelation parameter Tau0 can only be assigned a (user input) constant value to correspond to the (user input) S4 values provided in the scintillation grid. While using CSM externally in MatLAB, it is possible to set a different Tau0 value with each S4 value. Another difference is the signal-to-noise ratio, which is not a parameter to be adjusted by the user while using CSM as Spirent's scintillation tool. However, running CSM externally allows the user to define the value of signal-to-noise ratio per link for a pair of S4-Tau0.

[10] Regarding the study of the ionospheric refractive effects, the mathematical formulae representing the first and HO effects can help the understanding of the parameters constituting these effects and provide a means to focus on the methods to eliminate and estimate these effects. It was shown that a first order approximation can help to eliminate the Iono1 term by linearly combining observations on two distinct frequencies (dual frequency approach), such as L1, L2P(Y) in common practice, and L1, L2C or L1, L5 as expected to be more widely applied in future practice. Since the higher order error terms do not cancel out in the first order approximation, they can degrade the accuracy of GNSS positioning, depending on the solar, magnetic and ionospheric conditions. The Iono2 term contributes errors of several centimetres, and Iono3 by several millimetres. These higher order ionospheric errors should be accounted for as they may influence the position solution. For this purpose, a second order approximation was discussed to show that the Iono2 term can be further reduced in the IF observable by linearly combining observations

on three distinct frequencies (triple frequency approach). This, however, may result in a significantly noisier observable. As the Iono2 error term is in general an order of magnitude larger than the Iono3 error term, it can in particular benefit the convergence and accuracy of the PPP solution if it is accounted for.

[11] Based on the mathematical formulae presented for the contribution of the HO error terms to pseudoranges, error bounds are provided in a theoretical approach taking into account the TEC in both Iono2 and Iono3, and furthermore the angle between the signal path and geomagnetic field at IPP in the case of Iono2, and the maximum electron density in the case of Iono3. These formulae can help to estimate the HO error terms highlighting the parameters that an accurate estimation of these terms will depend on. It can be noted that cm to mm level range errors are possible under certain solar/magnetic conditions for the Iono2 and Iono3 terms, respectively.

[12] With the use of the Rinex_HO program and considering observations from three IGS stations selected in the European region as input to this program, the magnitudes of Iono2 and Iono3 were investigated for different background solar/geomagnetic/ionospheric conditions. It was observed that the magnitudes of the HO error terms are greater during the peak of the Solar Cycle when enhanced ionization levels occur due to larger solar activity (leading to larger TEC values) and disturbances in the geomagnetic field can cause enhanced ionization levels which can increase the magnitudes of Iono2 and Iono3 during post-peak period of the Solar Cycle with geomagnetic storms.

[13] The impact of Iono2 and Iono3 on GNSS positioning (PPP) was investigated making use of the observation files (from three IGS stations selected for this work) which were corrected (for Iono2 and Iono3) by the Rinex_HO program. PPP was performed with the BSW V5.0 software with both the original and corrected observation files in order to assess the impact on the estimated station coordinates when the HO error terms are corrected for. Although a more systematic analysis could be performed with the use of satellite orbit and clock products that are corrected for the HO error terms, it was observed in this work that the estimated station

coordinates were shifted when only the observation files were corrected for the HO error terms.

[14] The jitter variance at the output of tracking loops can be considered for assessing the impact of scintillation on receiver signal tracking performance. The model of Conker et al. (2003) can be used for assessing the tracking error (jitter) variance for the GPS L1, L2P and L5 signals; however, application of the model is better suited for the high latitudes where strong amplitude scintillation may occur less often; otherwise applicability of the model is only possible for weak-to-moderate amplitude scintillation. The model of Conker has limitations for (especially real time) mitigation purpose. One difficulty is that the model cannot estimate the DLL tracking error variance or the thermal noise contribution to the PLL tracking error variance, as discussed in Section 3.2.2.2.. Another difficulty is with the real time availability of the spectral parameters, p and T, which require FFT on the signal phase. It can also be mentioned that any non-availability (over a minute) of the scintillation indices also poses a problem for using this model.

[15] Regarding the assessment of signal tracking performance, an important and novel contribution of this PhD is in the use of high rate post-correlator I/Q data for estimating the jitter variance for the DLL and PLL during scintillation. The use of I/Q data for estimating the DLL jitter variance involves in principle approximating S4 and C/N0 in terms of I/Q and then considering (the first term of) each approximation to use in a relationship with other parameters (such as the loop bandwidth and correlator spacing) in a similar approach as in the model of Conker. Similarly, I/Q data was also considered to estimate the PLL jitter variance. MatLAB routines were devised to take as input I/Q data from receiver output data at 50Hz rate, and approximate the DLL and PLL jitter variances during scintillation. Compared with the Conker model, the use of I/Q data for the DLL and PLL jitter variance can obviate the need for the scintillation spectral parameters p and T as well as for the scintillation indices S4 and SigmaPhi – these two sets of data are needed to apply the Conker model. The use of I/Q data for such monitoring purposes can be advantageous for a receiver especially in a real-time application as less number of input parameters are required to facilitate the computational steps. The advantage of using the post-correlator data for assessing

receiver signal tracking performance is that robust, continuous, estimation at any scintillation level is possible for any GNSS signal that is tracked.

[16] An application of the use of I/Q data for estimating the jitter variance is shown in the work of Sreeja et al. (2011b) for the concept of jitter variance maps, which could inform users (who may not have receivers capable of performing similar calculations if I/Q data access is not available) about current tracking conditions.

[17] The impact of scintillation in GNSS positioning can be mitigated by an approach that involves modifying the stochastic model in the LSQ positioning solution, as shown by Aquino et al. (2009), by assigning weights to the observations in the variance-covariance matrix in terms of the jitter variance associated with each observation. In this approach, where the weight matrix becomes more representative of the actual ionosphere, the "per link effect" of scintillation on the precision of observations is taken into account. In the aforementioned work, the authors use the scintillation-sensitive model of Conker et al. (2003) to estimate the DLL and PLL jitter variances for the GPS L1C/A and P(Y) codes, respectively, for their data set; however, as discussed in this thesis this model can be limited in applicability to different data sets depending on the values attained by the S4 index, .i.e. the level of scintillation.

[18] In this thesis, the mitigation technique suggested by Aquino et al. (2009) was applied in relative (short baseline) positioning and PPP, where the post-correlation I/Q data is used for estimating the DLL and PLL jitter variances for the open sky data with strong scintillation levels collected at the low latitude stations (PRU1 and PRU2). The fact that any receiver can make such correlator data available and these products show sensitivity to the perturbations of ionospheric scintillation inspired the technique introduced here. The technique is applied in the GPSeq and RT_PPP programs, which provide a user interface to modify the stochastic model by assigning precision to each observation. The height component is focused on in the positioning results with the mitigation technique, as it is the more sensitive component compared with the horizontal coordinates. It was observed that the precision of estimating the station height can be improved when scintillation mitigation is applied.

[19] A patent application has been filed (by the Nottingham Geospatial Institute, file number JL59468P.GBA) regarding the abovementioned technique of mitigating the scintillation effects in GNSS positioning by improving the stochastic model based on the use of I/Q data (University of Nottingham, 2013). This patent claims to improve GNSS positioning accuracy, in particular during adverse ionospheric conditions such as scintillation, without the need for external models (to predict scintillation) or input data (for instance, about the physical conditions of the ionosphere). The technique is advantageous as it can be applied in real time within the receiver without the need for external data paths and in particular for positioning applications requiring high degree of accuracy, which may be hindered by fluctuations in signal phase and amplitude caused by irregularities in the ionosphere.

[20] Another approach investigated in this work to mitigate the impact of scintillation in positioning was by excluding selected observations from contributing to the position solution, according to a threshold defined in order to detect measurements at certain paths with strong scintillation. In this work, this threshold was set in terms of the S4 index and corresponding to a reasonably high elevation angle to avoid error sources such as multipath. Taking out such measurements from the observations in PPP and comparing the two cases of PPP with all observations and without the detected ones, it was observed that the precision of the estimated coordinates improved in one case and degraded in the other. The choice of a threshold to flag the signal paths and the impact of excluding the signal paths on relative receiver-satellite geometry are important.

- Recommendations for future work:

[1] One of the recommendations for future work is related to an improved version of the Rinex_HO program, which can correct the observations for the new signals (such as GPS L2C and L5 and Galileo E1 and E5a/b) against the Iono2 and Iono3 terms. This would enable assessment of the impact of correcting the HO error terms in positioning when considering a larger set of observables available with GNSS modernization.

[2] When the IGS repro2 orbit and clock products corrected for Iono2 and Iono3 are available for use in PPP, a more systematic investigation can then be performed to assess the impact of accounting for the HO term in GNSS positioning.

[3] Mitigation work in this thesis was limited to consider only the C1, P2, L1 and L2 observables since during the progress of this thesis the positioning programs, RT_PPP and GPSeq, were not able to process the new observables with GPS L2C, L5 and Galileo E1, E5a/b signals. Mitigation work based on improving the stochastic model can be carried forward if the new observables can be considered in these programs. When the new observables are included in the mitigation work, the files (containing the jitter variances per observation) which are used to update the weight matrix need to be formatted to contain data for these new observables.

[4] The post-correlator I/Q data can also be further considered for the multipath effect, another type of "interference" perturbing the propagation of GNSS signals.

CHAPTER 8

REFERENCES

Aarons, J. (1982), "Global morphology of ionospheric scintillations", Proceedings of the IEEE, Vol. 70(4), pp. 360-378.

Aarons, J. (1985), "Construction of a model of equatorial scintillation intensity", Radio Science, Vol.20, pp. 397-402.

Aarons, J., & Basu, S. (1994), "Ionospheric amplitude and phase fluctuations at the GPS frequencies". In Proceedings of the 7th International Technical Meeting of the Satellite Division of The Institute of Navigation (ION GPS 1994) pp. 1569-1578.

Abramovitch, D. (2002), "Phase-locked loops: A control centric tutorial", In American Control Conference, 2002. Proceedings of the 2002, Vol. 1, pp. 1-15, IEEE.

Alfonsi, L., De Franceschi, G., Romano, V. Aquino, & M. Dodson, A. (2004), "Positioning errors during space weather - Event of October 2003" [online] Available at http://www.earth-prints.org/bitstream/2122/4035/1/40.pdf [Accessed 18 December 2012]

Amiri-Simkooei, A. (2007),"Least-squares variance component estimation: Theory and GPS applications" [PhD dissertation], Delft University of Technology, Netherlands.

Anandan, S. (2010), "Launch of first satellite for Indian Regional Navigation Satellite system next year" [online] Available at http://www.thehindu.com/sci-tech/article393892.ece [Accessed 18 November 2012]

Anderson, D. N., Mendillo, M., & Herniter, B. (1987). "A semi-empirical low-latitude ionospheric model (No. AFGL-TR-88-0282)". AIR FORCE GEOPHYSICS LAB HANSCOM AFB MA.

Andreotti, M. (2011) "GNSS Signals: The old, the new and so what?", [presentation notes], Nottingham Geospatial Institute (NGI).

Anon. (2012), "The Almanac, Orbit Data and Resources on Active GNSS Satellites", GPSWorld, Vol 23. No 12

AppInSys (2010), "Earth's Magnetic Field and Climate Variability" [online] Available at http://www.appinsys.com/globalwarming/earthmagneticfield.htm [Accessed 15 November 2012]

Aquino, M., Andreotti, M., Dodson, A. & Strangeways, H. (2007) "On the Use of Ionospheric Scintillation Indices as Input to Receiver Tracking Models" Journal Advances in Space Research, 40(3), pp. 426-435.

Aquino, M., Monico, J. F., Dodson, A. H., Marques, H., De Franceschi, G., Alfonsi, L., ... & Andreotti, M. (2009), "Improving the GNSS positioning stochastic model in the presence of ionospheric scintillation", Journal of Geodesy, 83(10), pp. 953-966.

Ascheid, G. & Meyr, H. (1982), "Cycle slips in phase-locked loops: A tutorial survey", IEEE Transactions on Communications, vol. COM-30, no. 10, pp. 2228–2241.

Banks, P. M. (1976), "High-Latitude Ionosphere-Atmosphere Interactions", In Atmospheric Physics from Spacelab: Proceedings of the 11th ESLAB Symposium, Organized by the Space Science Department of the European Space Agency, Held at Frascati, Vol. 61, p. 19. Springer.

Barclay, L. W. (2003), "Propagation of radiowaves", Institution of Electrical Engineers.

Bassiri, S. & Hajj, G.A. (1993),"Higher-order ionospheric effects on the global positioning system observables and means of modelling them", In Manuscripta Geodaetica, 18, pp. 280-289.

Basu, S., (1981), "Equatorial Scintillations – A Review" Journal of Atmospheric and Terrestrial Physics, Vol. 43, Nº. 5/6, pp. 473-489

Basu, S., Basu, Sa. & Khan, B.K. (1976), "Model of equatorial scintillation from in-situ measurements", Radio Science, Vol.11, pp. 821-832.

Basu, S., Basu, Sa., Weber, E.J., & Coley, W.R. (1988), "Case study of polar cap scintillation modeling using DE 2 irregularity measurements at 800 km", Radio Science,Vol. 23, pp. 545-553.

Beach, T. L. (1998), "Global Positioning System studies of equatorial scintillations" [PhD dissertation], Cornell University, U.S.A.

Béniguel, Y., & S. Buonomo (1999), "A multiple phase screen propagation model to estimate fluctuations of transmitted signals", Phys. Chem. Earth (C), Vol.24, 333-338.

Beniguel, Y., Forte, B., Radicella, S. M., Strangeways, H. J., Gherm, V. E., & Zernov, N. N., (2004), "Scintillations Effects on Satellite to Earth Links for Telecommunication and Navigation Purposes", Annals of Geophysics, Vol. 47, pp. 1179-99.

Betz, J. W. (1999), "The offset carrier modulation for GPS modernization", In Proceedings of the 1999 National Technical Meeting of The Institute of Navigation, pp. 639-648.

Beutler, G., & Brockmann, E. [Editors](1993), "Proceedings of the 1993 IGS Workshop", Astronomical Institute, University of Berne, pp. 351-360.

Beutler, G., Brockmann, E., Fankhauser, S., Gurtner, W., Johnson, J., Mervart, L., ... & Weber, R. (2007). Bernese GPS software version 5.0. Astron. Inst., Univ. of Bern, Bern, Switzerland.

Bhaskaranarayana, A. (2008), "Indian IRNSS and GAGAN – Presentation to COSPAR Meeting" [online] Available at http://www.oosa.unvienna.org/pdf/icg/2008/expert/2-3.pdf [Accessed 12 December 2012]

Bilitza, D., & Reinisch, B. W. (2008), "International reference ionosphere 2007: Improvements and new parameters", Advances in Space Research, Vol. 42(4), pp. 599-609.

Borio, D. & Lo Presti, L., (2007) "How will the Open Service Galileo signal in space change acquisition process in GNSS receivers?", GNSS Solutions, InsideGNSS, Nov/December 2007, pp. 22-25.

Bouin, M. N., & Wöppelmann, G. (2010), "Land motion estimates from GPS at tide gauges: a geophysical evaluation", Geophysical Journal International, Vol. 180, pp. 193-209.

Brunner, F. K., & Gu, M. (1991), "An improved model for the dual frequency ionospheric correction of GPS observations", Manuscripta Geodaetica, Vol. 16(3), pp. 205-214.

Bureau of Meteorology –Australian Government (2009), "Educational - Everything you always wanted to know about the Sun, space weather and much more" [online] Available at http://www.ips.gov.au/Educational [Accessed 14 November 2012].

Bureau of Meteorology –Australian Government (2010), "About Ionospheric Scintillation"[online] Available at http://www.ips.gov.au/Satellite/6/3#whatis [Accessed 2 July 2012]

Bureau of Meteorology –Australian Government (2013), "Ionospheric Scintillation – Latest Conditions" [online] Available at http://www.ips.gov.au/Satellite/1/1 [Accessed 20 January 2013]

Burian, A., Lohan, E. S., & Renfors, M. K. (2007), "Efficient delay tracking methods with sidelobes cancellation for BOC-modulated signals", EURASIP Journal on Wireless Communications and Networking, 2007(2), pp. 18-18.

Cairo, L., & Cerisier, J. C. (1976), "Experimental study of ionospheric electron density gradients and their effect on VLF propagation", Journal of Atmospheric and Terrestrial Physics, Vol. 38(1), pp. 27-36.

Calais, E., Mattioli, G., DeMets, C., Nocquet, J. M., Stein, S., Newman, A., & Rydelek, P. (2005), "Tectonic strain in plate interiors?", NATURE, Vol. 438, p. 15.

Celestino, U. (2012) "Galileo & EGNOS Programmes Status" [online] Available at http://www.euromedtransport.org/En/image.php?id=2073 [Accessed 03 January 2013]

Cerruti, A. P., Kintner Jr, P. M., Gary, D. E., Mannucci, A. J., Meyer, R. F., Doherty, P., & Coster, A. J. (2008), "Effect of intense December 2006 solar radio bursts on GPS receivers", Space Weather, Vol. 6(10), S10D07.

CHAIN (2013), "Global Positioning System (GPS Receiver) - GSV 4004B" [online] Available at http://chain.physics.unb.ca/chain/pages/gps/ [Accessed 15 January 2013]

China Satellite Navigation Office (2011), "Development of the BeiDou Navigation Satellite System (BNSS)" [online] Available at http://www.oosa.unvienna.org/pdf/sap/2011/un-gnss/04.pdf [Accessed 22 September 2012].

Ciraolo, L., Azpilicueta, F., Brunini, C., Meza, A., & Radicella, S. M. (2007), "Calibration errors on experimental slant total electron content (TEC) determined with GPS", Journal of Geodesy, 81(2), pp. 111-120.

Clore, R. E. (2011), "U.S. GPS Policy and Constellation Status"[online] Available at http://www.gps.gov/multimedia/presentations/2011/06 /moscow/clore.pdf [Accessed 10 November 2012]

Coco, D. S., Coker, C., Valladares, C. E., Bishop, G. J., Mazzella, A. J., Fremouw, E. J., & Howell, D. (1999). "High Speed GPS Scintillation Measurements", Proceedings of the Ionospheric Effects Symposium - IES 99, pp. 2A6-1 to 2A6-6.

Collins, J.P. & R.B. Langley (1996). "Mitigating Tropospheric Propagation Delay Errors in Precise Airborne GPS Navigation." Proceedings of PLANS '96, the 1996 IEEE Position, Location and Navigation Symposium, Atlanta, GA, U.S.A., 22-26 April, 1996; pp. 582-589.

Conker, R. S., El-Arini, M. B., Hegarty, C. J., & Hsiao, T. (2003), "Modeling the effects of ionospheric scintillation on GPS/Satellite-Based Augmentation System availability", Radio Science, Vol. 38(1), p. 1001.

Coordinates (2011), "Indian plan for Satellite-Based Navigation Systems for Civil Aviation" [online] Available at http://mycoordinates.org/indian-

plan-for-satellite-based-navigation-systems-for-civil-aviation/ [Accessed 26 April 2013.]

Dach, R., Hugentobler, U., Fridez, P. & Meindl, M. (2007), "Bernese GPS Software Version 5.0.", p 259.

Datta-Barua, S., Walter, T., Blanch, J., & Enge, P. (2008), "Bounding Higher Order Ionospheric Errors for the Dual Frequency GPS Users", Radio Science, Vol.43, p. 15.

Davies, K. (1966), "Ionospheric Radio Propagation", Dover Publications, Inc.

Davies, K. (1990), "Ionospheric radio", Vol. 31, Peter Peregrinus Ltd.

Davydov, V., & Revnivykh, S. (2012), "GLONASS Today and Tomorrow - Fully Operational System Modernizes for the Multi-GNSS World". GPS World, Vol. 23(12), p. 16.

Dawoud, S. (2010) "GNSS principles and comparison" [online] Available at http://www.snettu-berlin.de/fileadmin/fg220/courses/WS1112/snet-project/gnss-principles-and-comparison_dawoud.pdf [Acessed 1 November 2012]

Dingding, X. (2011), "Satellite navigation system launched" [online] Available at http://europe.chinadaily.com.cn/business/2011-12/28/content_14343656.htm [Accessed 22 December 2012]

DLR, "Receiver Autonomous Integrity Monitoring (RAIM)"[online] Available at http://www.dlr.de/kn/en/desktopdefault.aspx/tabid-7569/12812_read-32120/ [Accessed 23 November 2012]

Doherty, P. H., Dehel, T., Klobuchar, J. A., Delay, S. H., Datta-Barua, S., de Paula, E. R., & Rodrigues, F. S. (2001), "Ionospheric effects on low-latitude space based augmentation systems", In Proceedings of the 15th International Technical Meeting of the Satellite Division of The Institute of Navigation (ION GPS 2002) pp. 1321-1329.

Doherty, P. H., Delay, S. H., Valladares C. E., & Klobuchar, J. A.(2000), "Ionospheric Scintillation Effects in the Equatorial and Auroral Regions." in Proceeding of ION GPS-2000.

Du, J., Caruana, J., Wilkinson, P., Thomas, R., & Cervera, M. (2001). "Determination of Equatorial Ionospheric Scintillation S4 by dual frequency GPS", In Beacon Satellite Symposium (Vol. 2001).

Dubey, S., Wahi, R., & Gwal, A. K. (2006), "Ionospheric effects on GPS positioning", Advances in Space Research, 38(11), pp. 2478-2484.

Ebner, A. (2008), "On the attainable accuracy of multi-system GNSS positioning in high-multipath urban environments" [Master Thesis], Technical University Graz, Austria.

El-Arini, M. B., Conker, R. S., Ericson, S. D., Bean, K. W., Niles, F., Matsunaga, K., & Hoshinoo, K. (2003), "Analysis of the effects of ionospheric scintillation on GPS L2 in Japan", In Proceedings of the 16th International Technical Meeting of the Satellite Division of The Institute of Navigation (ION GPS/GNSS 2003) pp. 314-327.

Elmas, Z.G. (2009), "The Higher Order Ionospheric Effects in GNSS Positioning in the European Region", [Master Thesis], University of Nottingham, Nottingham, UK.

Elmas, Z. G., Aquino, M., & Dodson, A. (2010a), "Using ionospheric scintillation indices to estimate GPS receiver tracking performance", *In*: EGU General Assembly Conference Abstracts, Vol. 12, p. 14936.

Elmas, Z.G., & Aquino, M. (2010b),"Using ionospheric scintillation indices to estimate GPS receiver tracking performance" [poster presentation], *In*: AGU Meeting of the Americas, Foz do Iguacu, Brazil, 2010.

Elmas, Z.G., Aquino, M., Moore, T., Marques, H., & Monico, & J.F.G. (2010c). "Higher order ionospheric effects on GNSS positioning in the European Region" [poster presentation], European Geophysical Union, May 2010, Vienna, Austria.

Elmas, Z., Aquino, M., Forte, B., Moore, T, & Hill, C. (2010d), "Analysis of GNSS receiver tracking performance under ionospheric scintillation" *In*: The Navigation Conference and Exhibition, London, UK.

Elmas, Z. G., Aquino, M., Marques, H. A., & Monico, J. F. (2011a), "Higher order ionospheric effects in GNSS positioning in the European region", Annales Geophysicae-Atmospheres Hydrospheresand Space Sciences, 29(8), 1383.

Elmas, Z., Aquino, M., Geng, J., Monico, J.F.G., da Silva, H.A., & Marques, H. (2011b),"The Impact and Mitigation of Ionospheric Scintillation on Precise Point Positioning" the Institute of Navigation, ION GNSS 2011, Portland, OR, USA.

El-Rabbany, A. (2002), "Introduction to GPS: the global positioning system", Artech House Publishers.

El-Rabbany, A.E. (1994) "The effect of physical correlations on the ambiguity resolution and accuracy estimation in GPS differential positioning", [PhD Dissertation], Department of Geodesy and Geomatics Engineering, University of New Brunswick, Canada.

Elsobeiey, M. & El-Rabbany, A. (2009) "Rigorous Modeling of GPS Residual Errors for Precise Point Positioning" Proceedings of the International Technical Meeting of the Institute of Navigation, ION GNSS 2009, CD-ROM.

Elsobeiey, M. & El-Rabbany, A. (2011), "Convergence Time Improvement of Precise Point Positioning" In Proceedings of the International Federation of Surveyors (FIG) Working Week 2011 (FIG Working Week 2011)

Elsobeiey, M. & El-Rabbany, A. (2012), "An Improved GPS-Based Precise Point Positioning Model" In Proceedings of the International Federation of Surveyors (FIG) Working Week 2012 (FIG Working Week 2012)

EU METSAT (2008), "Study on Ionospheric Effects in GNSS Radio Occultation, TEchnical Report" [online] Available at http://www.eumetsat.int/groups/pps/documents/document/pdf_peps_rep10.pdf [Accessed 28 November 2012]

Europa Press Releases (2010), "Commission awards major contracts to make Galileo operational early 2014" [online] Available at http://europa.eu/rapid/press-release_IP-10-7_en.htm [Accessed 26 October 2012]

European Commission (2011a), "EGNOS Safety of Life Service Definition Document" [online] Available at http://ec.europa.eu/enterprise/policies/satnav/egnos/files/egnos-sol-sdd-v1.0_en.pdf [Accessed 23 November 2012]

European Commission (2011b), "One Soyuz Launcher, Two GALILEO Satellites, Three Success for Europe" [online] Available at http://www.esa.int/esaNA/SEM167GURTG_index_0.html [Accessed 15 December 2012]

European Commission (2011c), "REPORT FROM THE COMMISSION TO THE EUROPEAN PARLIAMENT AND THE COUNCIL - Mid-term review of the European satellite radio navigation programmes" [online] Available at http://ec.europa.eu/enterprise/newsroom/cf/_getdocument.cfm?doc_id=6321 [Accessed 10 August 2012]

European Commission (2012), "Satellite navigation: Galileo - What do we want to achieve?" [online] Available at http://ec.europa.eu/enterprise/policies/satnav/galileo/programme/index_en.htm [Accessed 10 October 2012]

European Commission (2013),"What Is GALILEO?" [online] Available at http://www.esa.int/esaNA/galileo.html [Accessed 10 February 2013]

FAA (2008), "What's Next for WAAS?" [online] Available at http://www.

faa.gov/about/office_org/headquarters_offices/ato/service_units/techops/navservices/gnss/library/satnav/media/SatNav_March08.pdf [Accessed 22 November 2012]

FAA (2009), "Navigation Programs - History - Satellite Navigation" [online] Available at http://www.faa.gov/about/office_org/headquarters_offices/ato/service_units/techops/navservices/history/satnav/index.cfm [Accessed 25 September 2012]

FAA (2010a), "Navigation Programs - WAAS – News" [online] Available at http://www.faa.gov/about/office_org/headquarters_offices/ato/service_units/techops/navservices/gnss/waas/news/ [Accessed 20 July 2012]

FAA (2010b), "Navigation Programs - Wide Area Augmentation System (WAAS)" [online], Available at http://www.faa.gov/about/office_org/headquarters_offices/ato/service_units/techops/navservices/gnss/waas/ [Accessed 20 July 2012]

FAA (2013), "GNSS – GPS/WAAS Approaches" [online] Available at http://www.faa.gov/about/office_org/headquarters_offices/ato/service_units/techops/navservices/gnss/approaches/index.cfm [Accessed 13 December 2012]

Fontana, R. D., Cheung, W., & Stansell, T. (2001), "The modernized L2 civil signal", GPS world, 12(9), 28-35.

Forte, B. (2011), "Analysis of the PLL phase error in presence of ionospheric scintillation", *In*: XXXth URSI General Assembly and Scientific Symposium, Istanbul, 13-20 August 2011.

Fremouw, E.J. & Rino, C.L. (1973), "An empirical model for average F-layer scintillation at VHF-UHF", Radio Sci, Vol. 8, pp.213-222.

Fritsche, M., Dietrich, R., Knöfel, C., Rülke, A., Vey, S., Rothacher, M., & Steigenberger, P. (2005), "Impact of higher-order ionospheric terms on GPS estimates", Geophysical Research Letters, 32(23), L23311.

Fu, W., Han, S., Rizos, C., Knight, M., & Finn, A. (1999), "Real-time ionospheric scintillation monitoring", In 12th Int. Tech. Meeting of the Satellite Division of the US Inst. Of Navigation GPS ION99, Nashville, Tennessee.

Ganguly, S., Jovancevic, A., Brown, A., Kirchner, M., Zigic, S., Beach, T., & Groves, K. M. (2003), "Ionospheric scintillation monitoring and mitigation using a software GPS receiver", Radio Science, 39(1), RS1S21.

Gao, Y. (2006),"Precise Point Positioning and its challenges", Inside GNSS, Vol. 1(8), pp. 16-18.

Gardner, F. M. (2005), "Phaselock techniques", Wiley-Interscience.

Georgia State University (2008), "Magnetic Field of the Earth" [online] Available at http://hyperphysics.phy-astr.gsu.edu/hbase/magnetic/magearth.html [Accessed 28 October 2012]

Gherm, V. E., N. N. Zernov, & H. J. Strangeways. (2011) "Effects of diffraction by ionospheric electron density irregularities on the range error in GNSS dual-frequency positioning and phase decorrelation", Radio Sciences, 46, RS3002.

Gibbons, G. (2008), "Russia Approves CDMA Signals for GLONASS, Discussing Common Signal Design" [online] Available at http://www.insidegnss.com/node/648 [Accessed 20 August 2012]

Gleason, S., & Gebre-Egziabher, D. (2009), "GNSS applications and methods", Artech House Publishers.

GNSS Solutions (2006), "New GNSS frequencies, advantages of M-Code, and the benefits of a solitary Galileo satellite" [online] Available at http://www.insidegnss.com/auto/MayJune06GNSSSolutions.pdf [Accessed 28 July 2012]

GPS Governance (2012a), "GPS Governance" [online], Available at http://www.gps.gov/governance/ [Accessed 28 December 2012]

GPS Governance (2012b), "GPS Modernization" [online] Available at http://www.gps.gov/systems/gps/modernization/ [Accessed 28 December 2012]

GPS Governance (2013a), "New Civil Signals" [online] Available at http://www.gps.gov/systems/gps/modernization/civilsignals/ [Accessed 18 January 2013]

GPS Governance (2013b), "Space Segment" [online] Available at http://www.gps.gov/systems/gps/space/ [Accessed 18 January 2013]

GPSLAB (2004), "Wide Area Differential GPS (WADGPS)" [online] Available at http://waas.stanford.edu/research/waas.htm [Accessed 3 December 2012].

Groves, K. M., Basu, S., Weber, E. J., Smitham, M., Kuenzler, H., Valladares, C. E., ... & Kendra, M. J. (1997), "Equatorial scintillation and systems support", Radio Science, 32(5), 2047-2064.

Gruber, B. J. (2012), "Plans Set in Motion for GPS", GPS World, Vol. 23, No 12.

Gupta, S. (1975), "Phase-locked loops", In Proceedings of the IEEE, vol. 63, no. 2, pp. 291–306.

Hartmann, R., & Leitinger, R. (1984), "Range errors due to ionospheric and tropospheric effects for signal frequencies above 100MHz", Bull. Geod. Vol. 58 pp. 109-136.

Hegarty, C. J., & Chatre, E. (2008), "Evolution of the Global Navigation Satellite System (GNSS)", Proceedings of the IEEE, 96(12), 1902-1917.

Hegarty, C., El-Arini, M.B., Kim, T., & Ericson, S. (2001), "Scintillation modelling for GPS-Wide Area Augmentation System receivers", Radio Science, Vol.36(5) pp.1221-1231.

Hein, G. W., Godet, J., Issler, J. L., Martin, J. C., Lucas-RodrigueZ, R., & Pratt, T. (2002), "Status of Galileo frequency and signal design", In in CDROM Proc. ION GPS.

Hernandez-Pajares, M., Juan, J. M., Sanz, J., & Orus, R. (2007), "Second-order ionospheric term in GPS: implementation and impact on geodetic estimates", Journal of Geophysical Research, Vol. 112(B8), B08417.

Hernández-Pajares, M., Fritsche, M., Hoque, M. M., Jakowski, N., Juan Zornoza, J. M., Kedar, S., ... & Sanz Subirana, J. (2008), "Methods and other considerations to correct higher order ionospheric delay terms in GNSS", In IGS Analysis Center Workshop 2008.

Hofmann-Wellenhof, B., Lichtenegger, H., & Collins, J. (2001), "Global positioning system: theory and practice", Springer-Verlag.

Hoque, M. M., & Jakowski, N. (2007), "Higher order ionospheric effects in precise GNSS positioning", Journal of Geodesy, 81(4), 259-268.

Hoque, M. M., & Jakowski, N. (2008), "Estimate of higher order ionospheric errors in GNSS positioning", Radio Science, Vol. 43(5), RS5008.

Hoque, M. Mainul & Jakowski, Norbert (2012), "New correction approaches for mitigating ionospheric higher order effects in GNSS applications", Institute of Navigation. ION GNSS 2012, Nashville, USA.

Humphreys, T.E., Psiaki, M.L., Kintner, P.M. Jr., & Ledvina, B.M. (2005), "GPS Carrier Tracking Loop Performance in the presence of Ionospheric Scintillations", Proceedings of ION GNSS, The Institute of Navigation.

Humphreys, T. E., Psiaki, M. L., & Kintner, P. M. (2009a), "Modeling the effects of ionospheric scintillation on GPS carrier phase tracking", Aerospace and Electronic Systems, IEEE Transactions on, Vol. 46(4), pp. 1624-1637.

Humphreys, T. E., Psiaki, M. L., Hinks, J. C., O'Hanlon, B., & Kintner, P. M. (2009b), "Simulating ionosphere-induced scintillation for testing GPS receiver phase tracking loops", Selected Topics in Signal Processing, IEEE Journal of, Vol. 3(4), pp. 707-715.

Humphreys, T. E., Psiaki, M. L., Ledvina, B. M., Cerruti, A. P., & Kintner, P. M. (2008b), "Data-driven testbed for evaluating GPS carrier tracking loops in ionospheric scintillation", Aerospace and Electronic Systems, IEEE Transactions on, Vol. 46(4), pp.1609-1623.

Humphreys, T., Young, L., & Pany, T. (2008a), "Considerations for future IGS receivers" In IGS Analysis Center Workshop.

Hunsucker, R. D. (1991), "Radio techniques for probing the terrestrial ionosphere", Physics and Chemistry in Space, p. 22.

ICTP (2012), "NeQuick model" [online] Available at t-ict4d.ictp.it/ nequick2 [Accessed 05 January 2013]

ICTP (2013)," Workshop on GNSS Data Application to Low Latitude Ionospheric Research"[online] Available at http://cdsagenda5.ictp. trieste.it/full_display.php?ida=a12180 [Accessed 13 February 2013]

IEEA (2010), "GISM (ionospheric model)" [online] Available at http://www.ieea.fr/en/softwares/gism-ionospheric-model.html [Accessed 10 July 2012]

IEEA (2011), "Global Ionospheric propagation Model (GISM) USER MANUAL - release n° 6.53" [online] Available at http://www.ieea.fr/ help/gism-user-manual.pdf [Accessed 12 July 2012]

IGS (2012a), "Data Reprocessing Campaign: a first full reanalysis of all IGS GPS data collected since 1994" [online] Available at http://acc.igs.org/ reprocess.html [Accessed 23 July 2012]

IGS (2012b), "IGS Stations" [online] Available at http://igscb.jpl.nasa.gov/ network/list.html [Accessed 20 December 2012]

IGS (2012c), "International GNSS Service" [online] Available at http://igscb.jpl.nasa.gov/ [Accessed 23 January 2013]

IGS (2013), "SBAS Status Information" [online] Available at http://igs.org/mgex/Status_SBAS.htm [Accessed 6 May 2013]

Inside GNSS (2009a), "China Reveals Updated Compass/ Beidou-2 GNSS Signal Plan" [online] Available at http://www.insidegnss.com/node/1624 [Accessed 20 October 2012].

Inside GNSS (2009b), "ISRO Extends Raytheon Contract for GAGAN GPS Augmentation System" [online] Available at http://www.insidegnss.com/node/1604 [Accessed 10 August 2012]

Inside GNSS (2011), "ussia's First GLONASS-K In Orbit, CDMA Signals Coming" [online] Available at http://www.insidegnss.com/node/2487 [Accessed 10 August 2012]

Inside GNSS (2012), "India's Second GAGAN Payload Heads into Space" [online] Available at http://www.insidegnss.com/node/3227 [Accessed 23 August 2012]

IS-GPS-200F (2011), "GLOBAL POSITIONING SYSTEM DIRECTORATE SYSTEM ENGINEERING & INTEGRATION INTERFACE SPECIFICATION", NAVSTAR 2011.

IS-GPS-705A (2010), "GLOBAL POSITIONING SYSTEM WING (GPSW) SYSTEMS ENGINEERING & INTEGRATION INTERFACE SPECIFICATION", NAVSTAR 2010.

IS-QZSS (2011), "Quasi Zenith Satellite System Navigation Service - Interface Specifications for QZSS" [online] Available at http://qz-vision.jaxa.jp/USE/is-qzss/index_e.html [Accessed 16 July 2012]

ISRO (2012), "Indian Space Research Organization - Future Programme" [online] Available at http://www.isro.org/scripts/futureprogramme.aspx [Accessed 13 December 2012]

Jakowski, N., Mayer, C., Hoque, M. M., & Wilken, V. (2011) "Total electron content models and their use in ionosphere monitoring" Radio Science, Vol. 46(5), RS0D18.

Jakowski, N., Mayer, C., Wilken, V., & Hoque, M.M. (2008), "Ionospheric Impact on GNSS Signals", Fisica de la Tierra, Vol. 20 pp. 11-25.

JPL (2012), "Global Ionospheric Maps" [online] Available at http://iono.jpl.nasa.gov/gim.html [Accessed 26 August 2012]

Kaplan, E. D., & Hegarty, C. J. (2006), "Understanding GPS: principles and applications", Artech House Publishers.

Kedar, S., Hajj, G. A., Wilson, B. D., & Heflin, M. B. (2003), "The effect of the second order GPS ionospheric correction on receiver positions", Geophysical Research Letters, Vol. 30(16), p. 1829.

Kibe, S. V. (2008), "GAGAN and IRNSS" [online], Available at http://www.oosa.unvienna.org/pdf/icg/2008/icg3/07.pdf [Accessed 15 September 2012]

Kim, B. C., & Tinin, M. V. (2007), "Contribution of ionospheric irregularities to the error of dual-frequency GNSS positioning", Journal of Geodesy, Vol. 81(3), pp. 189-199.

Kim, B. C., & Tinin, M. V. (2011), "Potentialities of multifrequency ionospheric correction in Global Navigation Satellite Systems", Journal of Geodesy, Vol. 85(3), pp. 159-169.

Kim, T., Conker, R. S., Ericson, S. D., Hegarty, C. J., Tran, M., & El-Arini, M. B. (2001),"Preliminary Evaluation of the Effects of Scintillation on L5 GPS and SBAS Receivers Using a Frequency Domain Scintillation Model and Simulated and Analytical Receiver Models", In Proceedings of the 2003 National Technical Meeting of The Institute of Navigation , pp. 833-847.

Kintner, P. M., Kil, H., Beach, T. L., & de Paula, E. R. (2001), "Fading timescales associated with GPS signals and potential consequences", Radio Science, Vol. 36(4), pp. 731-743.

Kintner, P. M., Ledvina, B. M., & De Paula, E. R. (2007), "GPS and ionospheric scintillations", Space Weather, Vol. 5(9), S09003.

Kintner, P., Humphreys, T., & Hinks, J. (2009), "GNSS and ionospheric scintillation: How to survive the next solar maximum", Inside GNSS, Vol. 4(4), pp. 22-31.

Kirkko-Jaakkola, M., Traugott, J., Odijk, D., Collin, J., Sachs, G., & Holzapfel, F. (2009), "A RAIM approach to GNSS outlier and cycle slip detection using L1 carrier phase time-differences", In Signal Processing Systems, 2009. SiPS 2009. IEEE Workshop pp. 273-278. IEEE.

Klobuchar, J.A. (1987), "Ionospheric time-delay algorithm for single-frequency GPS useres" IEEE Transactions on Aerospace and Electronic Systems, pp. 325-331.

Klobuchar, J. A. (1991), "Ionospheric Effects on GPS" [online] Available at http://gauss.gge.unb.ca/gpsworld/EarlyInnovationColumns/Innov.1991.04.pdf [Accessed 2 October 2012].

Klobuchar, J. (1996), "Ionospheric effects on GPS", In Global Positioning System: Theory and applications., Vol. 1, pp. 485-515

Klobuchar, J. A., & Kunches, J. M. (2003), "Comparative range delay and variability of the earth's troposphere and the ionosphere", GPS solutions, Vol. 7(1), pp. 55-58.

Knight M. (2000), "Ionospheric scintillation effects on Global Positioning System receivers" [PhD Dissertation], Department of Electrical and Electronic Engineering, The University of Adelaide.

Knight, M., & Finn, A. (1998). "The effects of ionospheric scintillations on GPS", In Proceedings of the 11th International Technical Meeting of the Satellite Division of The Institute of Navigation (ION GPS 1998) pp. 673-685.

Knight, M., Cervera, M., & Finn, A. (1999), "A comparison of predicted and measured GPS performance in an ionospheric scintillation environment", In Proceedings of the 12th International Technical Meeting of the Satellite Division of The Institute of Navigation (ION GPS 1999), pp. 1437-1450.

Langley, R. B. (2000), "GPS, the Ionosphere, and the Solar Maximum", GPS world, 11(7), pp. 44-49.

Langley, R.B. (2010) "GLONASS Update Delves into Constellation Details", GPS World Tech Talk.

Lashley, M., & Bevly, D. (2009). "What about vector tracking loops?" Inside GNSS, 16-21.

Leandro, R. F., Thirumurthi, T., Sukeova, L., Langley, R. B., & Santos, M. C. (2001), "Analysis of GPS L2C signal quality and its impact on PPP performance", In Proceedings of the 2008 National Technical Meeting of The Institute of Navigation pp. 1020-1031.

Leick, A. (1995), "GPS Satellite Surveying", pp. 560.

Lejeune, R., El-Arini, M. B., & Klobuchar, J. (2002), "Adequacy of the SBAS Ionospheric Grid Concept for Precision Approach in the Equatorial Region", In ION GPS 2002: 15th International Technical Meeting of the Satellite Division of The Institute of Navigation.

Lightsey, G. & Humphreys, T. (2011), "FOTON: A Software-Defined, Compact, Low-Cost GPS Radio Occultation Sensor", GEOScan Planning Workshop 2011.

Liu, J.Y., Lin, C.H., Tsai, H.F., & Liou, Y.A. (2004), "Ionospheric solar flare effects monitored by the ground-based GPS receivers: Theory and observation", Journal of Geophysical Research, Vol. 109, A01307.

Loh, R., Wullschleger, V., Elrod, B., Lage, M., & Haas, F. (1995), "The U.S. wide-area augmentation system (WAAS)", Navigation, Vol. 42(3), pp. 435-465.

Lohan, E. S. (2011), "Global Navigation Satellite Systems (GNSS): present and future" [Lecture Notes] [online] Available at http://geta.aalto.fi/en/courses/simona_lohan.pdf [Accessed 23 December 2012]

Macmillan, S. (2005), "IAGA V-MOD Geomagnetic Field Modeling: International Geomagnetic Field IGREF-10" [online] Available at

http://www.ngdc.noaa.gov/IAGA/vmod/igrf.html [Accessed 5 November 2012].

Mao, W. L., Tsao, H. W., & Chang, F. R. (2004), "Intelligent GPS receiver for robust carrier phase tracking in kinematic environments", In Radar, Sonar and Navigation, IEE Proceedings- Vol. 151(3), pp. 171-180.

Mao, W.L., Lee, P.H., & Chen, H.Y. (2008), "Bandwidth Optimization of Carrier/Code Tracking Loops in GPS Receiver", IEEE APWCS 2008.

Marques, H. A., Monico, J. F., & Aquino, M. (2011), "RINEX_HO: second-and third-order ionospheric corrections for RINEX observation files", GPS solutions, Vol. 15(3), pp. 305-314.

Marques, H. A., Monico, J. F., & Rosa, G. P. (2007), "Analysis of the second and third order ionospheric effects for GNSS positioning in Brazil", In AGU Fall Meeting Abstracts Vol. 1, p. 0914.

Memarzadeh, Y. (2009), "Ionospheric Modeling for Precise GNSS Applications" [Master Thesis], Delft University of Technology, Netherlands.

MikroElektronica (1998), "Finite Impulse Response (FIR) Filter" [online] Available at http://www.mikroe.com/chapters/view/72/chapter-2-fir-filters/ [Accessed 18 October 2012]

Misra, P. & Enge, P. (2006). "Global Positioning System. Signals, Measurements and Performance", (2nd ed.). Ganga-Jamuna Press. p. 115. ISBN 0-9709544-1-7.

Moore, R. C., & Morton, Y. T. (2011), "Magneto-ionic polarization and GPS signal propagation through the ionosphere", Radio Science, Vol. 46(1), RS1008.

Morrissey, T. N., Shallberg, K. W., Van Dierendonck, A. J. & M. J. Nicholson (2004), "GPS receiver performance characterization under realistic ionospheric phase scintillation environments", Radio Science, Vol. 39, Rs1S20, pp. 1-18.

Morton, J. (2008), "Second Order Ionosphere Error: Should We Worry About Them?" GPS World Tech Talk.

Morton, Y. T., Zhou, Q., & van Graas, F. (2009), "Assessment of second-order ionosphere error in GPS range observables using Arecibo incoherent scatter radar measurements", Radio Science, Vol. 44, p. 1002.

Nakagami, M. (1960), "The m-distribution: A general formula of intensity distribution of rapid fading". Statistical Methods in Radio Wave Propagation, pp. 3-36, Pergamon.

NASA (2012), "Spot_Num.txt" [online] Available at http://solarscience.msfc.nasa.gov/greenwch/spot_num.txt [Accessed 15 October 2012]

NOAA (2005), "NOAA Space Weather Scales" [online] Available at http://www.swpc.noaa.gov/NOAAscales/index.html#GeomagneticStorms [Accessed on 28 December 2012]

NovAtel (2012), "Weathering the Storm- GNSS and the Solar Maximum Next Generation GNSS Ionospheric Scintillation and TEC Monitoring", NovAtel White Paper, 2012.

Oleynik, E., & Revnivykh, S. (2011) "GLONASS status and modernization", Civil GPS Service Interface Committee, Portland, Oregon, p. 19.

Orus, R., Hernandez-Pajares, M., Juan, J.M., Sanz, J., & Garca-Fernandez, M. (2002), "Performance of different TEC models to provide GPS ionospheric corrections", J. Atmos. and Solar-Terrestrial. Phys. 64 (2002) 2055-2062.

Pany, T., Irsigler, M., Eissfeller, B., & Winkel, J. (2002), "Code and Carrier Phase Tracking Performance of a Future Galileo RTK Receiver", In Proc. of ENC-GNSS 2002.

Parkins, A.J. (2009), "Performance of precise marine positioning using future modernised global satellite positioning systems and a novel partial ambiguity resolution technique" [PhD Dissertation].

Petrie, E. J., Hernández-Pajares, M., Spalla, P., Moore, P., & King, M. A. (2011), "A review of higher order ionospheric refraction effects on dual frequency GPS", Surveys in Geophysics, 32(3), 197-253.

Petrie, E. J., King, M. A., Moore, P., & Lavallée, D. A. (2010), "A first look at the effects of ionospheric signal bending on a globally processed GPS network", Journal of Geodesy, Vol. 84(8), pp. 491-499.

Pi, X., Boulat, B.M., Mannucci, A.J. & Stowers, D.A. (2002), "Latitudinal characteristics of L-band ionospheric scintillation", Proceedings of the ION GPS 2002, Portland, OR.

Pireaux, S., Defraigne, P., Wauters, L., Bergeot, N., Baire, Q., & Bruyninx, C. (2010), "Higher-order ionospheric effects in GPS time and frequency transfer", GPS solutions, Vol. 14(3), pp. 267-277.

Pullen, S., Opshaug, G., Hansen, A., Walter, T., Enge, P., & Parkinson, B. (1998), "A preliminary study of the effect of ionospheric scintillation on WAAS user availability in equatorial regions", in Proceedings of ION GPS-98, Institute of Navigation, Alexandria, VA.

Ratcliffe, J. A. (1956), "Some Aspects of Diffraction Theory and their Application to the Ionosphere", Reports on Progress in Physics, Vol. 19, pp. 188-267.

Richert, T., & El-Sheimy, N. (2007), "Optimal linear combinations of triple frequency carrier phase data from future global navigation satellite systems", GPS Solutions, 11(1), 11-19.

Ries, L., Lestarquit, L., Armengou-Miret, E., Legrand, F., Vigneau, W., Bourga, C., ... & Issler, J. L. (2002), "A software simulation tool for GNSS2 BOC signals analysis", In Proceedings of the 15th International Technical Meeting of the Satellite Division of The Institute of Navigation (ION GPS 2002) pp. 2225-2239.

Rino, C.L., Livingston, R.C., Tsunoda, R.T. et al. (1983), "Recent studies of the structure and morphology of auroral zone F region irregularities", Radio Science, Vol. 18, pp. 1167-1175.

Rodriguez, R. Lucas, Toran, F., Dellago, R., Arbesser-Rastburg, B., & Flament, D. (2009), "EGNOS Evolution Plans and the GNSS Evolutions Programme," Proceedings of the 2009 International Technical Meeting of The Institute of Navigation, pp. 284-288.

Schaer, S., W. Gurtner, & J. Feltens, (1998), "IONEX: The IONosphere Map Exchange Format Version 1", Proceedings of the IGS AC Workshop, Darmstadt, Germany.

Secan, J.A. (1996), "WBMOD: Ionospheric Radiowave Scintillation Model, Version 13.04", NorthWest Res. Assoc. Inc.

Seeber, G. (1993), "Satellite geodesy: foundations, methods, and applications", Berlin; New York: W. de Gruyter, 1993., 1.

Seo, J., Walter, T., Marks, E., Chiou, T. Y., & Enge, P. (2007), "Ionospheric scintillation effects on GPS receivers during solar minimum and maximum", In Proceedings of the International Beacon Satellite Symposium, pp. 11-15.

Septentrio (2010), "PolaRxS Application Manual" Version 2.1.0, Septentrio Satellite Navigation.

Shanmugam, S., Jones, J., MacAulay A., & Van Dierendonck, A.J. (2012) "Evolution to Modernized GNSS Ionospheric Scintillation and TEC Monitoring", IEEE/ION PLANS 2012.

Sharawi, M.S., & Korniyenko, O.V. (2007), "Software Defined Radios: A Software GPS Receiver Example", AICCSA, 2007 IEEE/ACS International Conference on Computer Systems and Applications, pp.562-565

Shen, J. (2009), "COMPASS/Beidou-China's GNSS" [online] Available at http://www.filasinternational.eu/sidereus-project/pdf/02.pdf [Accessed 25 October 2012].

Simsky, A., & Sleewaegen, J. M. (2005), "Galileo/GPS Receivers for Geodetic Applications - Report on the Symposium of the IAG Subcommission for Europe (EUREF)" [online] Available at http://www.euref.eu/symposia/2005Vienna/7-03.pdf [Accessed 27 August 2012]

Simsky, A., Mertens, D., Sleewaegen, J. M., De Wilde, W., Hollreiser, M., & Crisci, M. (2008), "Multipath and tracking performance of Galileo ranging signals transmitted by GIOVE-B", Proceedings of ION GNSS 2008.

Skone, S. & Knudsen, K. (2001), "GPS receiver tracking performance under equatorial and high latitude ionospheric scintillations", In Proceeding of 3rd International Symposium on Mobile Mapping Technology, p. 14.

Skone, S., Lachapelle, G., Yao, D., Yu, W., & Watson, R. (2005), "Investigating the Impact of Ionospheric Scintillation using a Software Receiver" , In Proceedings of ION GPS/GNSS 2005, pp. 1126-1137.

Spirent (2009), "SimGEN software user manual", Spirent Communications.

Spits, J., & Warnant, R. (2011), "Enhancement of Total Electron Content monitoring using triple frequency GNSS data", Presented at Scientific and Fundamental Aspects of the Galileo Programme, 2011.

Sreeja, V. V., Aquino, M., Forte, B., Elmas, Z., Hancock, C., De Franceschi, G., ... & Ferreira Da Silva, E. (2011a), "Tackling ionospheric scintillation threat to GNSS in Latin America", Journal of Space Weather and Space Climate, 1(1).

Sreeja, V., Aquino, M., & Elmas, Z. G. (2011b), "Impact of ionospheric scintillation on GNSS receiver tracking performance over Latin America: Introducing the concept of tracking jitter variance maps", Space Weather, Vol. 9(10), S10002.

Stevanovic, D. (2012), "Study of small scale plasma irregularities in the ionosphere" [online] Available at http://www.ung.si/~sstanic/teaching/Seminar/2012/20120312_Stevanovic.pdf [Accessed 16 December 2012]

Strangeways, H. J. (2009). "Determining scintillation effects on GPS receivers", Radio Science, 44(1), RS0A36.

Strangeways, H. J., & Ioannides, R. T. (2002), "Rigorous calculation of ionospheric effects on GPS Earth-Satellite paths using a precise path determination method", Acta Geod Geoph Hung, Vol. 37(2-3), pp. 281-292.

Strangeways, H. J., Ho, Y. H., Aquino, M. H., Elmas, Z. G., Marques, H. A., Monico, J. G., & Silva, H. A. (2011), "On determining spectral parameters, tracking jitter, and GPS positioning improvement by scintillation mitigation", Radio Science, 46(null), RS0D15.

Tran, M., & Hegarty, C. (2004), "Performance Evaluation of the New GPS L5 and L2 Civil (L2C) Signals", Navigation: Journal of the Institute of Navigation, Vol.51, No.3.

Tsyganenko, N. A. (2005), "Geopack-2005" [online] Available at http://modelweb.gsfc.nasa.gov/magnetos/databased/Geopack_2005.html [Accessed 14 September 2012].

University of Nottingham (2013), [online] Available at http://uon.technologypublisher.com/technology/8848 [Accessed 14 September 2012].

Urquhart, L. (2009), "An Analysis of Multi-Frequency Carrier Phase Linear Combinations for GNSS.", Senior technical report, Department of Geodesy and Geomatics Engineering Technical Report No. 263, University of New Brunswick, Fredericton, New Brunswick, Canada, p. 71.

Valladares, C. E., Alcaydé, D., Rodriguez, J. V., Ruohoniemi, J. M., & Van Eyken, A. P. (1999). "Observations of plasma density structures in association with the passage of traveling convection vortices and the occurrence of large plasma jets". In Annales Geophysicae, Vol. 17(8), pp. 1020-1039.

Van Dierendonck, A.J., (1999) "Measuring ionospheric scintillation effects from GPS signals", Proceedings of Ionospheric Effects Symposium, JMG Associates, Alexandria, VA, pp. 271-278.

Volpe, J.A. (2001), "Vulnerability assessment of the Transportation Infrastructure relying on the Global Positioning System", Final Report prepared for the Office of the Assistant Secretary for Transportation Policy, U.S. Department of Transportation.

WAAS (2010), "Effect of Ionospheric Scintillations on GNSS - A White Paper" [online] available at http://waas.stanford.edu/~wwu/papers/gps/PDF/IWG/sbas_iono_scintillations_white_paper.pdf [Accessed on 18 November 2012]

Walt, M. (1994), "Introduction to geomagnetically trapped radiation", Cambridge University Press.

Wang J., Satirapod, C., & Rizos, C. (2002), "Stochastic assessment of GPS carrier phase measurements for precise static relative positioning" Journal of Geodesy, Vol. 76, No. 2, pp. 95-104.

Wang, Z., Wu, Y., Zhang, K., & Meng, Y. (2005), "Triple-frequency method for high-order ionospheric refractive error modelling in GPS modernization", Journal of Global Positioning Systems, 4(1-2), 291-295.

Wanner, B. (2002), "SBAS Testbed Planning and Issues" [online] Available at http://apecgit.org/bbs/download.php?bo_table=presentation&wr_id=35 &no=0&page=26 [Accessed on 11 May 2013]

Wanninger, L. (1993). "Effects of the Equatorial Ionosphere on GPS." GPS World, Vol.4, No. 7, pp. 48-53.

WDC (1996), "Geomagnetic Data Service" [online] Available at http://wdc.kugi.kyoto-u.ac.jp/wdc/Sec3.html#INDICES [Accessed on 25 November 2012]

Wernik, A. W., Liu, C. H., Franke, S. J., & Gola, M. (1990), "High-latitude irregularity spectra deduced from scintillation measurements", Radio Science, Vol. 25(5), pp. 883-895.

Wernik, A.W., Alfonsi, L, & Materassi, M. (2007), "Scintillation modelling using in situ data", Radio Science, Vol.42, RS1002.

Woo, K. T. (1999), "Optimum semi-codeless carrier phase tracking of L2", In ION GPS'99 pp. 289-305.

Wu, S., Peck, S., Schempp, T., Shloss, P., Wan, H., Buckner, P., ... & Angus, J. (2001, June), "A single frequency approach to mitigation of ionospheric depletion events for SBAS in equatorial regions", In Proceedings of the 19th International Technical Meeting of the Satellite Division of The Institute of Navigation (ION GNSS 2006), pp. 939-952.

CHAPTER 9

APPENDICES

9.1. **APPENDIX A** – IONOSPHERIC SCINTILLATION MODELS

Realistic scintillation models for predicting the scintillation activity for a receiver location and time can be grouped into analytical, climatological and those based on in-situ data. More engineering-inspired statistical scintillation models can also be added to this categorization.

Analytical models are built in for specific regions; they require specific satellite-receiver geometry for signal path dependent calculations: such as those suggested by Fremouw and Rino (1973) and Aarons et al. (1982; 1985). The advantage of these models is that they do not need propagation model, for instance, maps of foF2. For instance, the model by Fremouw and Rino (1973) needs as input sunspot number, DOY, local time and geomagnetic latitude; and gives S4 for weak scattering conditions estimated based on an analytical formula and as such not applicable for equatorial latitudes where weak scattering assumption may not hold.

Climatological models: based on transionospheric scintillation data, modeling scintillation as a stochastic process (such that signal amplitude and phase obey certain distributions under scintillation activity) which takes location, date, time, geophysical conditions (i.e. solar and geomagnetic activity levels) as input and returns the scintillation spectral parameters and scintillation indices for a given time, location and satellite-receiver geometry (Knight 2000)

WBMOD is a global model for ionospheric scintillation activity that provides predictions for scintillation occurrence statistics and level of activity (through scintillation indices and spectral parameters) for a user defined time (local sunset), date and (satellite and receiver) location (also defined are signal carrier frequency and geophysical conditions). WBMOD has two parts: the first part named "Environment models", which is a set of models based on empirical data to provide worldwide climatology of ionospheric density irregularities; and the second part is a signal propagation (phase screen) model which calculates the effects of irregularities on transionospheric GNSS signals with respect to a user defined time and location. The fact that the environment models are worldwide, extreme day-to-day variations in scintillation may not be well

described; however, for long term modelling purposes they work fine. Furthermore, patchiness of irregularities may not be well represented by this model, and it is difficult to predict scintillation on a given signal path. WBMOD can help to estimate performance of individual signal paths and to calculate accuracy of positioning solution in advance. (Latest version allows estimation of the time that scintillation exceeds a given threshold or scintillation level at a user specified percentile). Further details can be found at Secan (1996).

GISM: See the Appendix N.

In-situ data based: this model provides temporal and spatial coverage. Examples are the WAM model (Wernik et al. 2007) and those suggested by Basu et al. (1976) and Basu et al. (1988), for high and equatorial latitudes, respectively. Other models collect open sky scintillation data from a network of scintillation specific monitors and process the data (using models of plume formation / evolution / dissipation) to predict/forecast scintillation activity (Knight 2000). In principle, scintillation statistics (i.e. obtained values of scintillation parameters) are benefitted from to make predictions for receiver performance at a given time and location.

Statistical models: like the CSM (Humphreys et al. 2009b) which creates scintillation perturbations on signal amplitude and phase based on the Nakagami-m distribution; Cornell Scintillation Model (CSM) which has been extensively used during this thesis to "synthesize" scintillation effects when simulating scintillation effects in a hardware GNSS signal simulator.

9.2. **APPENDIX B** – TEC ESTIMATION AND NEW SIGNALS

TEC along the signal path, STEC, can be calculated, for instance, by using the pseudoranges, based on the fact that within the first order approximation the pseudoranges contain ionospheric error that is inverse squared frequency dependent (Hofmann-Wellenhof et al. 2001). Calculation for STEC using pseudoranges (PRs) is shown in Eq. 46 for L1 and L2 signals, this representation can involve L5 signal in future applications ($\varepsilon_{1,2}$ represent errors independent of PRs (Marques et al. 2007)).

$$STEC = \frac{f_1^2 f_2^2}{40.3 \cdot (f_2^2 - f_1^2)} \cdot \{PR_1 - PR_2 - c \cdot (DCB_{rec} + DCB^{sat}) + \varepsilon_{1,2}\} \quad \text{(Eq. 46)}$$

It can be seen that input for the receiver and satellite differential code biases (DCBs) which are non-negligible error sources with magnitudes in the range of 5-10ns (Beutler et al. 2007) are needed for reconstructing STEC using code observations. For instance, in Rinex_HO program, (monthly) P1-C1 and P1- P2 DCB files need to be used (if STEC is estimated from pseudoranges) which can be retrieved from CODE (ftp.unibe.ch/aiub/CODE/yyyy) for the particular IGS stations. Another method would be for users to carry out their own computation to assess their receiver's code biases, for instance, by following the approach described by Ciraolo et al. (2007).

It can be noted in Eq. 46 that the estimation of STEC not only depends on the availability of the DCB terms on RHS of Eq. 46 but also the precision with which it is estimated is influenced by the precision of the RHS terms. The latter can be illustrated with the error propagation law:

$$\sigma_{STEC}^2 = \left(\frac{f_1^2 f_2^2}{40.3\cdot(f_2^2 - f_1^2)}\right)^2 \cdot \left\{\sigma_{PR_1}^2 + \sigma_{PR_2}^2 + c^2\sigma_{DCB_{rec}}^2 + c^2\sigma_{DCB^{sat}}^2\right\} \qquad \text{(Eq. 47)}$$

Equation 47 shows that precision of the estimated STEC depends on the precision of the pseudoranges themselves and the DCBs. It should be noted that multipath which is another important error source for the code measurements can cause additional uncertainty. DCBs can be regarded as constant in time which can allow neglecting their variances. This brings into attention that the precision of the pseudoranges is an important factor for precise estimation of STEC such that "less noisy" pseudoranges would favour more precise estimation of STEC. If the DCB variances are neglected, then the frequency dependent term in the parenthesis and the sum in the curly brackets on RHS determine the variance of STEC. Regarding these two factors, calculations reveal that even when all the code observables have the same precision[a], the frequency dependent term yields a smaller value for the final variance of STEC when the frequencies of L1 and L5 signals are considered. In this case, L1, L5 combination can yield about 18% smaller variance than L1, L2 combination in Eq. 47. Further consideration of the less noisy and better multipath performance of GPS L5 signal, the improvement in the variance of STEC can be even higher making the use of L1 and L5 more preferable to L1 and L2.

[a] *Although pseudoranges on L5 are expected to be more precise due to the higher chipping rate of the PRN code on this signal.*

In addition to considering a dual frequency approach based on the pseudoranges to estimate STEC more precisely making use of the new signals, it is also possible to improve the precision by using the third frequency on the L5 band (available in both GPS and Galileo) through a triple frequency method. As shown by Spits & Warnant (2011), using undifferentiated measurements on L1, L2, L5 frequencies, different combinations of triple frequency code and phase measurements can be formed to solve the ambiguities by successive approximations (Spits & Warnant 2011): the first step resolves the EWL ambiguities (successfully at their correct integer values) by combining the dual-frequency code and phase measurements on L2 and L5 frequencies (Code measurements are considered only in this step thus the dominant error sources in the code measurements such as multipath and DCBs do not influence the precision of TEC obtained in the final stage). In the next step, the WL ambiguities are resolved by combining dual frequency phase measurements on L1 and L2 as L1-L2. In the final step, the EWL and WL ambiguities are obtained from the two sets of dual frequency phase combinations and TEC is retrieved.

9.3. **APPENDIX C** – ADVANTAGES OF NEW CIVIL GNSS SIGNALS

At present the civil users cannot take *full* advantage of the code based dual frequency operation (since they cannot demodulate the P code) to create the ionosphere free observable; but access to L2C and L5 (civil codes) enable a complete "civilian" method to eliminate the first order ionospheric effect. Acquisition and tracking in challenging conditions (such as due to ionospheric scintillation, interference) requires higher signal-to-noise power ratio (C/N_0) which is better achieved in coded tracking compared with semicodeless tracking.

Hegarty et al. (2001) show that the semi-codeless tracking of the L2 carrier is vulnerable to scintillation; even weak scintillation can cause LoL to satellites at low elevation angles. This can be explained by the fact that in semi-codeless technique, there is the need for L1 carrier aiding to overcome the signal-to-noise degradation inherent in tracking the L2 carrier without knowing the Y code; under scintillation, L1 and L2 carrier

phases can lose coherence which can invalidate the assumption of common dynamics on L1 and L2 which enables the use of narrow loop bandwidths for the semicodeless tracking of the L2 carrier. The same authors also show that narrow bandwidth *code* tracking loops are less affected by scintillation compared to *carrier* tracking loops which suffer from an increase in the thermal noise. Thus, access to civil codes on multi-frequencies can benefit the acquisition and tracking processes.

It is generally accepted that scintillation has a greater impact on codeless and semicodeless tracking than on coded tracking (Knight 2000). This is mainly due to the fact that in codeless and semicodeless tracking, the difference between the L1 and L2 phase measurements is taken. This difference cancels systematic effects due to satellite motion, satellite and receiver clock and tropospheric effects; however the measurements in such codeless cross-correlation receivers are very noisy which makes them less favourable for scintillation monitoring. The tracking loops of codeless and semicodeless receivers generally have a reduced C/N_0 and narrow bandwidth; such receivers may track only the L1 signal under strong scintillation - this may not degrade the positioning accuracy, however it may prevent eliminating the ionospheric error with the IF observable or hinder calculating the TEC. Introduction of the new civil codes is expected to reduce the use of semicodeless and codeless tracking cases.

9.4. **APPENDIX D** – ELECTRON DENSITY IRREGULARITIES RESPONSIBLE FOR THE SCINTILLATION EFFECTS

The scintillation inducing irregularities (mostly at an altitude of 250-400km of the ionosphere) are in general either "random ionospheric irregularities" or "travelling ionospheric disturbances (TIDs)". Dimensions of these irregularities and their growth rate may vary according to the processes that cause them. Irregularities smaller than the Fresnel scale (scale size of scintillation pattern, Du et al. 2001), i.e. less than about 300m, are responsible for scintillation since much smaller irregularities cause very low intensity diffraction effects on the signals and larger scale irregularities cause little amplitude variations and gradual phase variations (intermediate size irregularities i.e. larger than Fresnel radius in dimensions do not cause scintillation effects but cause a frequency-

dependent deviation of the ray trajectory different than a straight line between the satellite and receiver; it is this deviation from straight-line propagation that the ionospheric delay effect is observed). In general, the ionospheric irregularities have the following shapes (Rino et al. 1983):

1) Rod-shaped irregularities (latitudes above 70^0 are common regions for observing such rod shaped irregularities which are circular in cross section extending along the geomagnetic field lines);

2) Sheet-like irregularities (extending along geomagnetic field lines but sheet-like in cross section located at invariant latitudes less than 65^0);

3) Wing-shaped irregularities.

9.5. **APPENDIX E** - DETAILS FOR DERIVATION OF EQ. 1

Following from Bassiri and Hajj (1993)

$$X = \frac{Ne^2}{\varepsilon_0 m 4\pi^2 f^2} = \left(\frac{f_p}{f}\right)^2$$

where the plasma frequency $f_p = \sqrt{\frac{Ne^2}{4\pi^2 \varepsilon_0 m}} \approx 8.9$ MHz i.e. $f_p <<$ 10MHz. Under this approximation for f_p, X becomes less than 4.4×10^{-5}.

N.B. Plasma frequency "f_p" is the minimum frequency for GNSS signals to penetrate an ionospheric layer and it depends on the geomagnetic field.

$$Y = \frac{eB_0}{2\pi f m} = \frac{e\mu_0 H_0}{2\pi f m} = \frac{f_H}{f}$$

where $f_H = \frac{e\mu_0 H_0}{2\pi m} \approx 0.59$ MHz i.e. $f_H < 10^{-3}$ MHz.

Expanding the refractive index formula for X<<1 and Y as above, phase refractive index to the first order approximation becomes (Brunner and Gu, 1991):

$$n_{-,p} = 1 - \frac{X(1-X)}{(1-X) - \frac{Y_{\prime}^2}{2} - \sqrt{\frac{Y_{\prime}^4}{4} + (1-X)^2 Y_{||}^2}}$$

$$= 1 - X(1-X) \cdot \frac{1}{1 - \left(X + \frac{Y_{\prime}^2}{2} + \sqrt{\frac{Y_{\prime}^4}{4} + (1-X)^2 Y_{||}^2}\right)}$$

$$= 1 - X(1-X)\cdot\left(1 + X + \frac{Y_{\perp}^2}{2} + \sqrt{\frac{Y_{\perp}^4}{4} + (1-X)^2 Y_{||}^2} + \cdots\right)$$

$$= 1 - \frac{X}{2} - \frac{X^2}{8} - \frac{XY_{||}}{2}$$

where $Y_{||} = Y\cos\theta$, and $Y_{\perp} = Y\sin\theta$. Replacing X and $Y_{||}$ gives:

$$n_{-,p} = 1 - \frac{1}{2}\cdot\frac{Ne^2}{4\pi^2\varepsilon_0 m f^2} - \frac{1}{8}\left(\frac{Ne^2}{4\pi^2\varepsilon_0 m f^2}\right)^2 - \frac{1}{2}\cdot\frac{Ne^2}{4\pi^2\varepsilon_0 m f^2}\cdot\frac{\mu_0 e H_0 \cos\theta}{2\pi f m}$$

$$n_{-,p} = 1 + \frac{a_1}{f^2} + \frac{a_2}{f^3} + \frac{a_3}{f^4}$$

where

$$a_1 = -\frac{1}{2}\cdot\frac{Ne^2}{4\pi^2\varepsilon_0 m}$$

$$a_2 = -\frac{1}{2}\cdot\frac{Ne^2}{4\pi^2\varepsilon_0 m}\cdot\frac{\mu_0 e H_0\cos\theta}{2\pi m}$$

$$a_3 = -\frac{1}{8}\cdot\frac{N^2e^4}{16\pi^4\varepsilon_0{}^2 m^2}$$

Using

$$n_g = n_p + f\cdot\frac{dn_p}{df}$$

the group refractive index can be obtained as:

$$n_{-,g} = 1 - \frac{a_1}{f^2} - \frac{2a_2}{f^3} - \frac{3a_3}{f^4}$$

Hereafter, it can be concluded that:

$$\delta\rho_g = \int (n_g - 1)ds = \int\left(-\frac{a_1}{f^2} - \frac{2a_2}{f^3} - \frac{3a_3}{f^4}\right)ds$$

$$= \frac{1}{2f^2}\int\frac{Ne^2}{4\pi^2\varepsilon_0 m}ds + \frac{1}{f^3}\int\frac{Ne^2}{4\pi^2\varepsilon_0 m}\cdot\frac{e\mu_0 H_0}{2\pi m}\cos\theta\, ds + \frac{3}{8f^4}\int\frac{N^2e^4}{16\pi^4\varepsilon_0{}^2 m^2}ds$$

$$= \frac{e^2}{8\pi^2\varepsilon_0 m f^2}\int N ds + \frac{e^3\int N B_0 \cos\theta\, ds}{8\pi^3\varepsilon_0 m^2 f^3} + \frac{3e^4}{128\pi^4\varepsilon_0{}^2 m^2 f^4}\int N^2\, ds$$

$$= \frac{K}{f^2}\int N ds + \frac{Ke\int N B_0\cos\theta\, ds}{\pi m f^3} + \frac{3K^2}{2f^4}\int N^2\, ds$$

$$\delta\rho_g = \frac{K}{f^2}\,STEC + \frac{KeB_0\cos\theta}{\pi m f^3}\,STEC + \frac{3K^2}{2f^4}\,\eta\, N_{max}\,STEC$$

And similarly,

$$\delta\rho_p = \int (n_p - 1) ds = \int \left(\frac{a_1}{f^2} + \frac{a_2}{f^3} + \frac{a_3}{f^4}\right) ds$$

$$= -\frac{1}{2f^2}\int \frac{Ne^2}{4\pi^2\varepsilon_0 m} ds - \frac{1}{2f^3}\int \frac{Ne^2}{4\pi^2\varepsilon_0 m}\cdot\frac{e\mu_0 H_0}{2\pi m}\cos\theta\, ds - \frac{1}{8f^4}\int \frac{N^2e^4}{16\pi^4\varepsilon_0{}^2 m^2} ds$$

$$= -\frac{e^2}{8\pi^2\varepsilon_0 m f^2}\int N ds - \frac{e^3\int N B_0\cos\theta\, ds}{16\pi^3\varepsilon_0 m^2 f^3} - \frac{e^4}{128\pi^4\varepsilon_0{}^2 m^2 f^4}\int N^2\, ds$$

$$= -\frac{K}{f^2}\,STEC - \frac{Ke\int N B_0\cos\theta\, ds}{2\pi m f^3} - \frac{K^2}{2f^4}\int N^2\, ds$$

$$\delta\rho_p = -\frac{K}{f^2}\,STEC - \frac{KeB_0\cos\theta}{2\pi m f^3}\,STEC - \frac{K^2}{2f^4}\,\eta\, N_{max}\,STEC$$

9.6. **APPENDIX F** – COMMONLY USED INCIDES FOR GEOMAGNETIC ACTIVITY

Geomagnetic activity can be parameterized and monitored by the following commonly used indices:

Kp: planetary index computed from *K* indices reported by observatories worldwide; it is a measure of geomagnetic activity averaged from 13 observatories. *K* is a local measure (determined by 13 observatories that lie between 46-63^0 N and S geomagnetic latitudes) of fluctuations in the horizontal component of the geomagnetic field at mid-latitude (thus Kp is considered mostly for the level of geomagnetic activity at mid-latitudes). It is measured every 3hrs (of every UT day) from data

collected during those 3 hrs. Its value ranges from 0 (quiet) to 9 (strong disturbance) (NOAA 2005).

Dst: Disturbance Storm Time index, Dst, is a measure of fluctuations in the horizontal component of the geomagnetic field in the equatorial region such that a negative value for Dst indicates a storm (inducing ring currents around the Earth) in progress. Dst is in general taken as a good measure of geomagnetic activity at low latitudes. The geomagnetic field is "reduced" by currents during an ionospheric storm which gives negative Dst values during especially adverse conditions.

Ap: Another parameter for geomagnetic activity is Ap index which is a daily, planetary average of A index which is K index converted to a linear scale with a range of 0-400. Ap values of 30-50 indicate minor, 50-100 major and >100 severe geomagnetic storm. During the last Solar Cycle peak (year 2001), ionospheric storm activity in terms of Ap can be given as in the below plot where Ap>100 corresponds to severe storm conditions.

9.7. **APPENDIX G** – DETAILS ON THE KLOBUCHAR AND NEQUICK IONOSPHERIC MODELS

Klobuchar model is a predicted ionospheric correction model for single frequency GPS users, which was designed to reduce the group delay error by about 50% in a root-mean-square sense (Klobuchar 1991). Eight parameters (coefficients to two 3rd order polynomials) are broadcast in the GPS navigation message to represent the vertical ionospheric delay that is converted to slant delay for each signal path using a mapping function (Klobuchar 1987). Klobuchar model is updated every 6 days which may not be able to account for changes in TEC. At such update rate, it is difficult in practice for the model to account for rapid changes in ionospheric electron content (equatorial anomalies which consists of maxima for electron density, around abot 150 N-S of magnetic equator (Skone and Knudsen, 2001).

A new ionospheric model is the NeQuick model (ICTP 2012) introduced for single frequency users of Galileo system, which approximates the ionosphere as a thin shell – unlike the Klobuchar model. NeQuick is a three dimensional electron density model. Effective ionization parameters are calculated for NeQuick model by sensor stations that monitor TEC. These parameters are then transmitted in the navigation message to Galileo

users. Using these coefficients, users can calculate effective ionization level and STEC. The NeQuick model can perform better than the Klobuchar model; related research can be found in Memarzadeh (2009).

9.8. **APPENDIX H** – DETAILS FOR EQ. 15

HF_2 in the denominator of this formula can be obtained from another formula suggested by the same authors:

$$STEC \approx \frac{HF_2 * (h_m + R_E) * N_m * \sqrt{2\pi \exp(1)}}{\sqrt{(h_m + R_E)^2 - (R_h + R_E)^2 * cos^2\beta}}$$

N_m is the peak electron density (e/m^3); h_m is the height of the peak density; R_h is the receiver altitude, and R_E is the radius of the Earth. It can be noted that for the vertical case, $\beta=\pi/2$, the above formula yields HF_2 as:

$$HF_2 \approx \frac{VTEC}{N_m * \sqrt{2\pi \exp(1)}}$$

9.9. **APPENDIX I** – GLOBAL REGIONS FOR SCINTILLATION

Mechanisms that cause scintillation can be different at high and low latitudes and this leads to different characteristics for scintillation observed at these regions (Knight 2000). For instance, at high latitudes around the polar cap (a region of *open* magnetic field lines) and auroral regions where the ionosphere is very dynamic due to the influence of IMF and has little diurnal variation and can start at any time lasting from a few hours to a few days.

At high latitudes (80^0-90^0), more fluctuations are observed in phase than in amplitude (a generally low S4 and high SigmaPhi). Such phase fluctuations may seem related to the influence of the geomagnetic activity at these latitudes. Geomagnetic activity can trigger scintillation even when the solar flux is low. In the polar regions, scintillation is closely related to the solar flux and geomagnetic storms – even when there is low geomagnetic activity, a high solar flux can introduce intense scintillation. At the auroral region / oval (60^0-80^0) where strong ionospheric activity and geomagnetic storms take place, severe scintillation is observed in and

to the north of the auroral oval such that the effects can be observed when the signal propagation path intersects the auroral oval. Extension of scintillation at the polar region towards the equator can affect mid-latitudes.

At mid latitudes (30^0-60^0), except during ionospheric storms, scintillation is weak (Beutler and Brockmann, 1993).

Scintillation at equatorial (low) latitudes ($\pm 30^0$ of the magnetic equator), more pronounced in this case, is linked with high sunspot number and observed typically after sunset and especially at local night time hours. Equatorial scintillation can be characterized with S4 which is in this case proportional to TEC fluctuations such that S4 can be estimated from these fluctuations (Du et al. 2001). At low latitudes, severe (amplitude) scintillation effects (at saturating intensity levels) can be observed near the geomagnetic equator ($\pm 10^0$-15^0). These boundaries in latitude may change according to the time of day and year, sunspot number and magnetic activity etc.

9.10. **APPENDIX J** – LINEAR COMBINATION OF OBSERVATIONS IN A TRIPLE FREQUENCY APPROACH

Details on linear combination of observations on three frequencies such that there is no Iono1 or Iono2 related terms in the final IF observable.

$$\alpha \cdot PR_1 + \beta \cdot PR_2 + \gamma \cdot PR_5 = PR_{triple\ IF}$$

Considering that each of the code measurements contains the geometric range (with all non-frequency dependent errors absorbed into the geometric range) and ionospheric error as:

$$\begin{aligned} PR_1 &= \rho + c(dt_r - dT^S) + Iono1_{f1} + Iono2_{f1} + Iono3_{f1} \\ PR_2 &= \rho + c(dt_r - dT^S) + Iono1_{f2} + Iono2_{f2} + Iono3_{f2} \\ PR_5 &= \rho + c(dt_r - dT^S) + Iono1_{f5} + Iono2_{f5} + Iono3_{f5} \end{aligned}$$

The following conditions need to be met for a triple frequency linear combination "$PR_{triple\ IF}$" to yield an ionosphere free observable in which both Iono1 and Iono2 terms are eliminated:

$$\alpha + \beta + \gamma = 1 \text{ (Geometric constraint)}$$
$$\alpha \cdot Iono1_{f1} + \beta \cdot Iono1_{f2} + \gamma \cdot Iono1_{f5} = 0$$
$$\alpha \cdot Iono2_{f1} + \beta \cdot Iono2_{f2} + \gamma \cdot Iono2_{f5} = 0$$

These three conditions lead to:

$$\alpha + \beta + \gamma = 1 \text{ (Geometric constraint)}$$

$$\frac{\alpha}{f_1^2} + \frac{\beta}{f_2^2} + \frac{\gamma}{f_5^2} = 0$$

$$\frac{\alpha}{f_1^3} + \frac{\beta}{f_2^3} + \frac{\gamma}{f_5^3} = 0$$

Solution of this system of equations gives for the coefficients α, β *and* γ:

$$\alpha = \frac{f_1^3}{(f_1 - f_2)(f_1 - f_5)(f_1 + f_2 + f_5)}$$
$$\beta = \frac{-f_2^3}{(f_1 - f_2)(f_2 - f_5)(f_1 + f_2 + f_5)}$$
$$\gamma = \frac{f_5^3}{(f_1 - f_5)(f_2 - f_5)(f_1 + f_2 + f_5)}$$

When substituted into the above equation for $PR_{triple\ IF}$, the resultant IF observable is:

$$PR_{triple\ IF} = \rho + \frac{3\,K^2 \eta\, N_{max}\, STEC}{2} \cdot \frac{1}{f_1^2 (f_2 - f_5)(f_1 + f_2 + f_5)} \cdot \left(\frac{f_2 + f_1}{f_2} - \frac{f_5 + f_1}{f_5} \right)$$

Precision of the new IF observable (with reduced ionospheric error) depends on those of each pseudorange and the coefficients involved in the linear combination. If precision of the pseudoranges for L1, L2 and L5 signals are taken as 0.3m, 0.5m and 0.5m, respectively, then the resultant IF observable in this triple frequency combination has precision of about 17m.

9.11. **APPENDIX K** - RELATION BETWEEN THE SIGNAL ENVELOPE AND ANGLE CONSTRUCTED FROM THE I/Q CORRELATOR DATA

Additional results showing the relation between the signal envelope (x-axis) and angle (y-axis), where both quantities are calculated from I/Q post-correlator data using the data collected at PRU2 station during weak to strong scintillation levels. Left plot in the middle row corresponds to negligible level of scintillation, for which it can be noted that the Q values are very small, and I values are confined around a constant value.

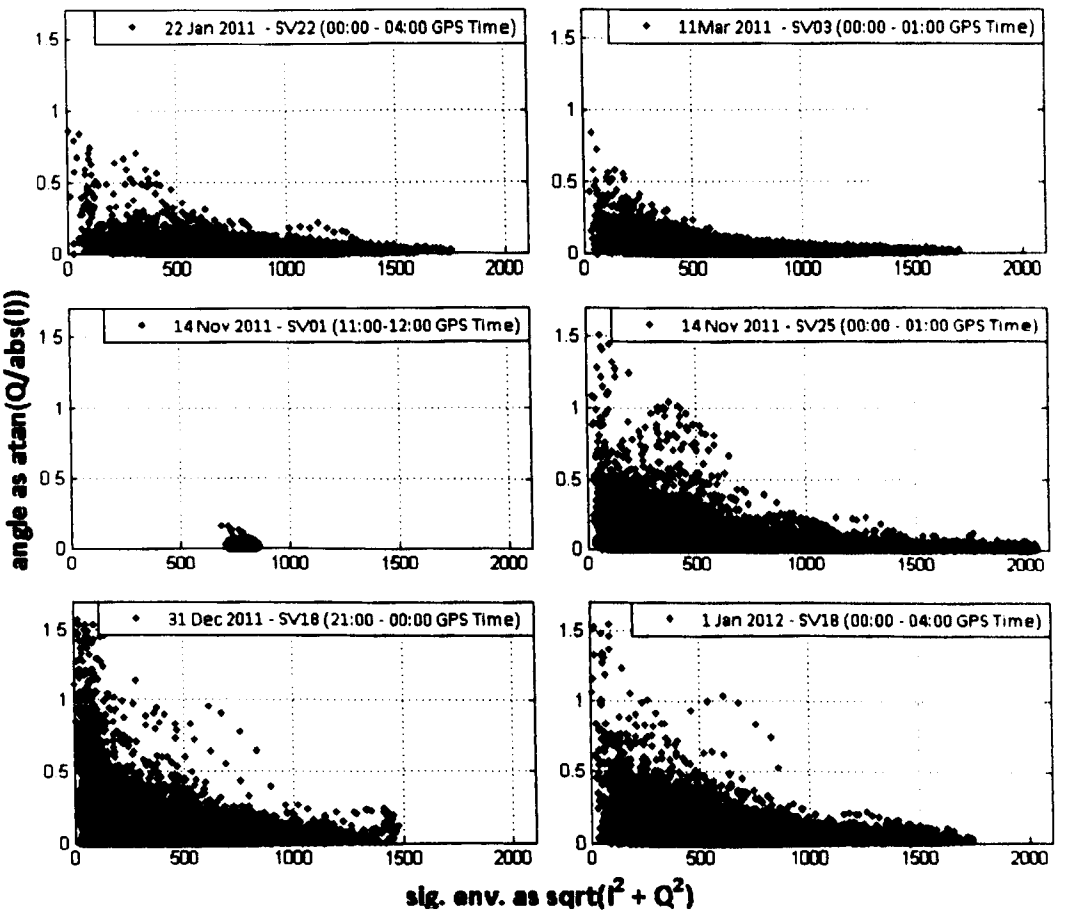

Figure 9.1. Relation between signal angle and envelope for GPS L1 with different satellites during different levels of scintillation.

9.12. **APPENDIX L** - RELATION BETWEEN THE CORRELATOR OUTPUTS AND SCINTILLATION LEVEL

Additional results showing the relation between the I/Q correlator outputs and S4 index for different satellites and scintillation levels. The second row corresponds to negligible scintillation.

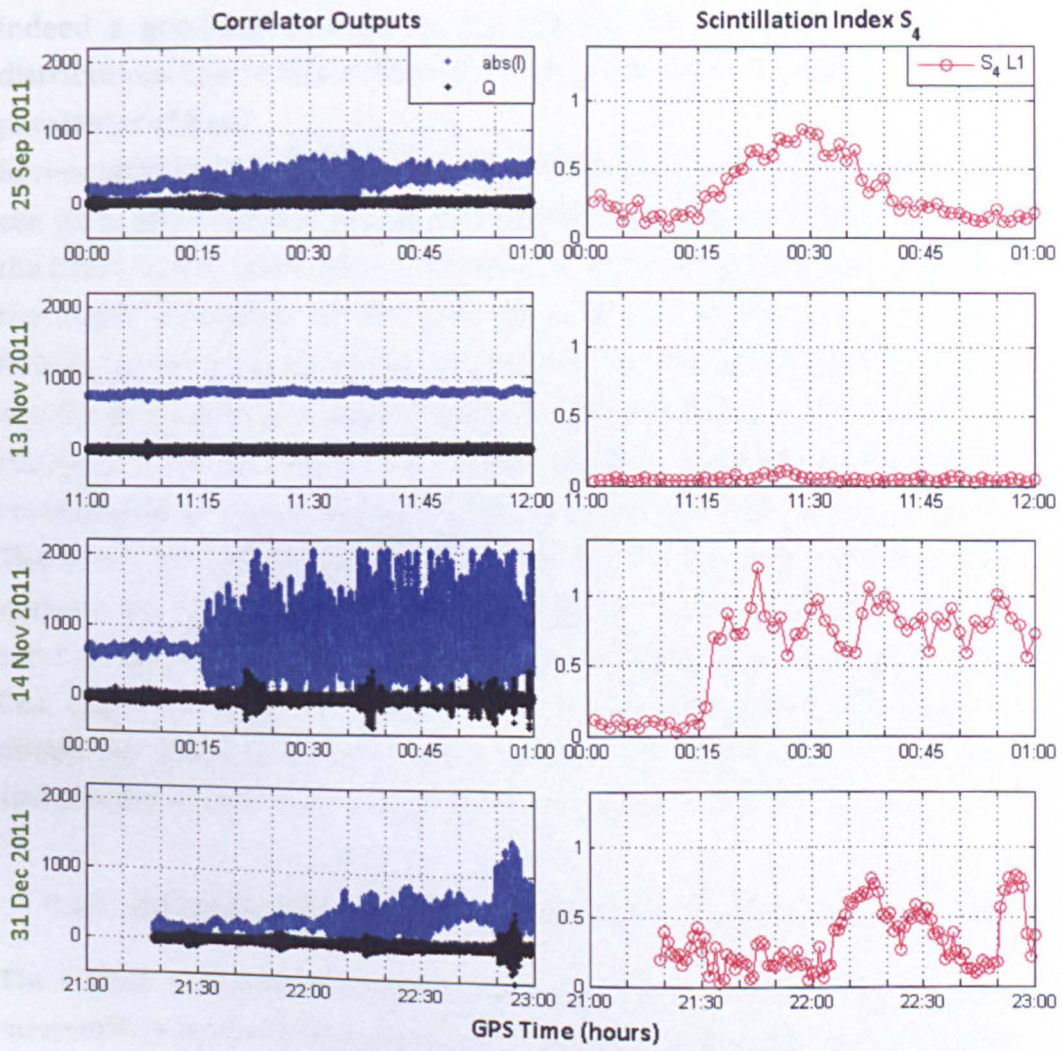

Figure 9.2. Relation between the I/Q data and S4 index for SV02, 01, 25 and 18 from the top to bottom row, respectively.

9.13. **APPENDIX M** – CORNELL SCINTILLATION MODEL

There are two main assumptions in CSM: (i) Amplitude of the GNSS signal follows the Rice distribution (owing to the implementation simplicity of Rice distribution) under the (equatorial) scintillation environment; and (ii) the rapidly varying component (the "scintillation component") of the complex scintillation signal has a spectrum similar to that of complex white noise that is low-pass-filtered with a 2nd order Butterworth filter (Humphreys 2009b). These two assumptions are justified and validated by Humphreys et al. (2008b, 2009a-b). Indeed, the Nakagami-m distribution has been shown to best fit the empirical data (Humphreys 2009a-b). The authors of CSM show that Nakagami-m and Rice distributions are similar and agree well with real data for S4<1. From this aspect and choice, Rice is

indeed a good-approximate to the Nakagami-m distribution. The two distributions can be linked through the m parameter of Nakagami-m and K parameter of Rice.

Severe scintillation may lead to LoL such that the receiver tracking loops can no longer cope due to increased phase dynamics, and degradation on the C/N0. In this sense, the input parameters pair such that as t0 increases, the cutoff frequency of this low pass filter decreases, so only lower frequency components of the white noise are passed through the filter; equally for larger t0 values the autocorrelation function of the scintillating component of the scintillation signal attains a wider main peak which corresponds to more slowly varying scintillation (Humphreys 2009b). Therefore, for any S4, a value of Tau0 that is small in its allowed range makes the scintillation related fluctuations more challenging for the receiver tracking loops. Tau0 is used to determine the coefficients of the 2nd order low pass Butterworth filter which filters the white noise to obtain the "scintillation" component of the "scintillating" signal. Larger S4 and smaller t0 yield severe scintillation in CSM (Humphreys 2009b)

9.14. **APPENDIX N** – GLOBAL IONOSPHERIC SCINTILLATION MODEL

The Global Ionospheric Scintillation Model, GISM, allows obtaining both mean errors and scintillations due to propagation through the ionosphere. This model has been accepted by the International Telecommunications Union as a reference code for scintillation evaluation (IEEA 2010; IEEA, 2011). To produce signal scintillation, the bubbles (structures of depleted TEC) sizes should be below a typical dimension (typically one km) such that the diffracting pattern is inside the first Fresnel zone. The Fresnel zone dimension also depends on the distance from IPP (usually defined at about 350 km height) to the receiver and on the frequency.

GISM can either consider a trajectory described by a list of successive points or a constellation for which an orbit generator is introduced that requires a Yuma file as input. GISM allows considering either paths from a receiver to a satellite or a constellation, or maps.

GISM aims to calculate in particular:

- LoS errors

• Faraday rotation effect on polarization: being an anisotropic medium, ionosphere layers will impact a linear polarized wave by rotating its polarization plane.
• Propagation Delay
• Scintillation effects: phase and amplitude scintillations, shorter correlation distances with respect to space, time, signal frequency, cycle slips, LoL.

GISM allows assessing both scintillation and mean effects for propagation through ionosphere for any locations of transmitter and receiver. Two sub models are involved: one to provide the mean errors and another to provide the scintillation effects (based on a resolution of the parabolic equation).

The electron density inside the ionosphere at any time and location, which is an input of both sub models, is provided by the NeQuick model (used as a subroutine in GISM to provide the value of the electron density inside the ionosphere at any time and location.) developed by the University of Graz and the Abdus Salam International Centre for Theoretical Physics, Trieste. Inputs to NeQuick are the solar flux number, year, DOY and local time.

The GISM model uses the Multiple Phase Screen technique with which the medium is divided into successive layers each acting as a phase screen. The locations and altitudes of both the transmitter and receiver are arbitrary therefore the signal path can go through the entire ionosphere or a small part of it.

Complete calculation for one particular link is composed of two consecutive steps:
• Calculation of the Line Of Sight (LoS)
• Calculation of scintillation (requires the parabolic equation be solved at each screen located along the LoS) which involves

- Intensity and phase scintillation indexes (S4 & SigmaPhi)
- Range and phase RMS errors
- Angle of arrival fluctuations
- Coherence lengths
- Probabilities

- Spectrum

Scintillation parameters are estimated from the knowledge of the time series at receiver level using the signal intensity and phase and its correlation and structure functions. In case of strong scintillations (typically S4 > 0.7), the phase may exhibit cycle slips with consequences on the receiver PLL and may also lead to losses of lock for one or several satellites. Sample output maps with GISM are provided in Fig. 9.3.

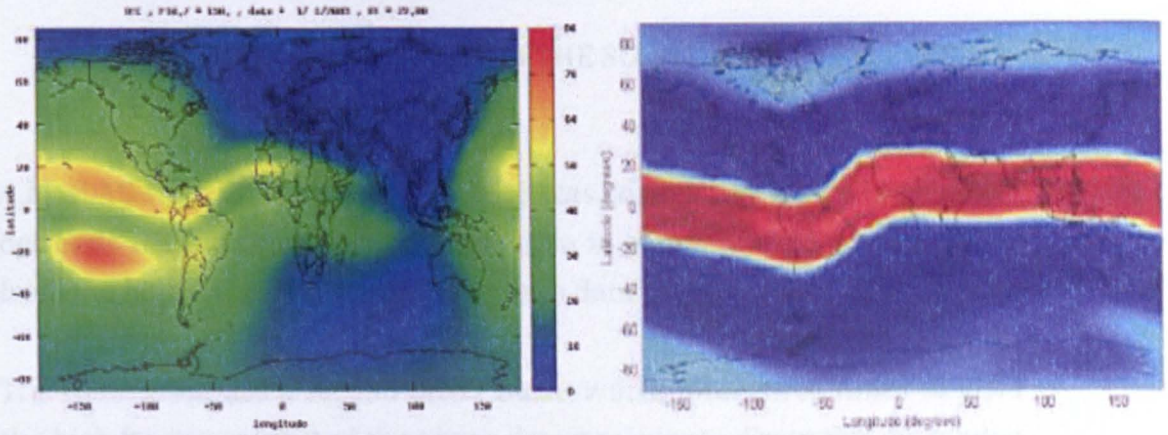

TEC map S4 map cumulated over 24 hours

Figure 9.3. Output maps with GISM for TEC (left) and S4 (right).

More details about the code organisation of GISM, input data and output files, algorithm convergence, mapping capability and typical scenario input files can be found at IEEA (2011).

Web interface for GISM is also possible at: http://www.ieea.fr/en/gism-web-interface.html. GISM functionality on this website provides "point-to-point" calculation (full version of GISM gives other options) in which ionospheric effects on a signal transmitted between two user defined points are computed (Fig 9.4.). Running GISM with the requested input data returns the GISM computation results on the same page.

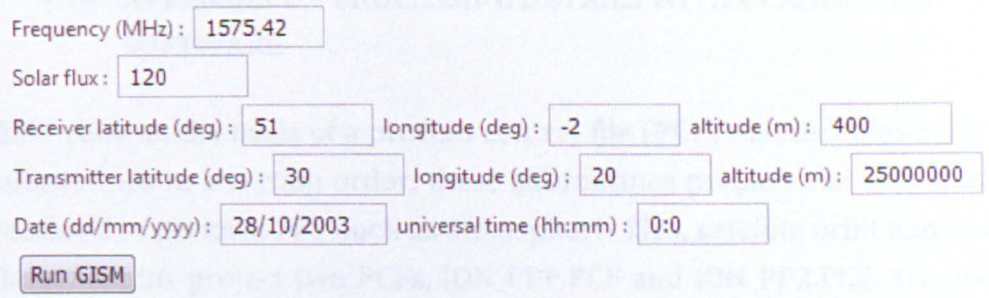

Figure 9.4. Web interface for GISM.

9.15. **APPENDIX O** – EXTRACTING THE SCINTILLATION EFFECTS FROM RAW SIGNAL DATA

A MatLAB routine from Marcio Aquino was considered, which in principle detrends the high rate carrier phase data to estimate the SigmaPhi index from the high frequency part of the phase data.

The routine applies a second order Butterworth filter three times to yield the high frequency part of the phase data per minute. From this detrended data, the SigmaPhi index is estimated as the STD per minute. The high frequency part of this detrended data is considered as the fluctuations due to phase scintillation (which lead to the estimated SigmaPhi values).

Similarly, the amplitude data is detrended with a sixth order Butterworth filter – applied directly to each minute. The detrended high frequency part of the data is considered as the fluctuations due to amplitude scintillation.

MatLAB routines are created for performing the necessary computations and formatting the data (i.e. the extracted perturbations) into a specific file format that is recognized by the Spirent simulator, i.e. a *.ucd* file.

With this technique, it is possible to extract perturbations from, for instance, GPS L1 signal and scale the perturbations (in a frequency based approach) to apply the perturbations on other signal frequencies such as GPS L2C and L5 in the simulations.

9.16. **APPENDIX P** – PROCESSING DETAILS WITH BERNESE GPS SOFTWARE

BSW runs on the basis of a process control file (PCF) that includes a list of subroutines in a certain order; these subroutines prepare the data that is required to perform PPP such as atmospheric files, satellite orbit and clock data. For this project two PCFs, ION_PPP.PCF and ION_PP2.PCF, are used: former does PPP on the uncorrected observation files and latter on the corrected ones. In the latter case, subroutines in the PCF are modified so that BSW obtains the corrected observation files from a new directory added into the existing database of observation files.

N.B. PCFs are modified for BSW to use the specific observation files (corrected observation files) instead of the observation files in its own database. The database that serves BSW contains the uncorrected GPS observation files; the corrected ones are introduced in a new folder to the database for use in this work.

A free network solution is adopted in BSW: this implies that the satellite orbits define the coordinate system in which the stations are positioned. In order to observe how the higher order ionospheric effects cause variations in the coordinates of each station, stations are considered individually in a free network solution, i.e. the coordinate system is always defined by the satellite orbits. Thus, "for each station" the estimated coordinates using the corrected and uncorrected observation files can be compared to estimate the effect of HO ionospheric effects. For high accuracy positioning, BSW considers the phase wind-up corrections, satellite antenna offsets and site-displacement effects due to the solid Earth tides and ocean tide loading effects. BSW PPP is configured not to take any elevation cut-off angle but to apply an elevation dependent weighting to the GPS observations (through "GPSEST" step) in this project.

Station coordinates estimated from BSW (in Cartesian coordinates) are transformed into geodetic coordinates (latitude, longitude and height) by applying a coordinate transformation (Elmas, 2009). Differences for latitude and longitude (in degrees) are converted into meters to assess all geodetic components at meter level.

Estimated satellite clocks and orbits can vary according to especially Iono2: work by Hernandez-Pajares et al. (2008) shows that the daily mean shift in the estimated satellite orbits can be related to the variation in global TEC values. The same authors state that corrections for RREs due to Iono2 should be applied *consistently*: first, GNSS measurements should be corrected, and then satellite orbits and clocks should be computed. They emphasize that if the GNSS observations are corrected for the effects of Iono2, then GNSS products should also be obtained through corrected GNSS measurements before such corrected observations are used in positioning.

As considered also by Fritsche et al. (2005), a consistent comparison of coordinate estimates between using the corrected (for HO error terms) and uncorrected observation files can be achieved by the following two cases (Fig. 9.5.):

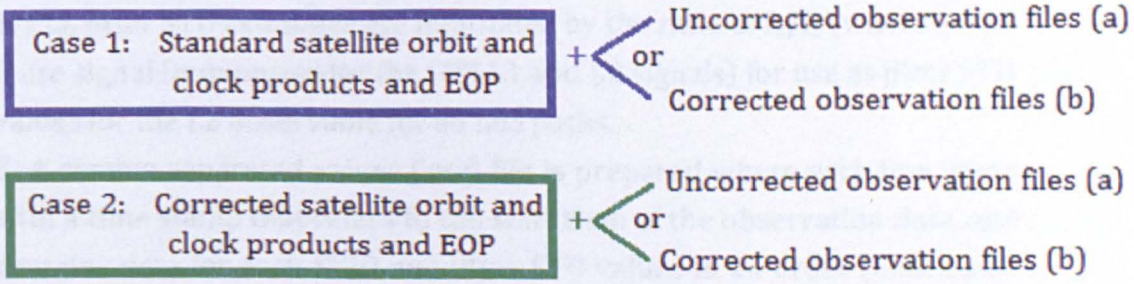

Figure 9.5. Two cases that lead to a systematic analysis of the higher order error terms in GNSS coordinate estimation.

According to Hernandez-Pajares et al. (2008), Case 1a and Case 2b are consistent for performing positioning and comparing the estimated coordinates; it can allow a more realistic analysis of the influence of HO terms on positioning results. Since the standard products (as considered in this work) do not consider HO ionospheric effects, using them with the corrected GPS observation files blurs the net effect HO errors may have on the estimated coordinates. However with the IGS products considered in this work (IGS does not apply corrections for HO error terms in its products (Hernandez-Pajares et al. 2008)) station coordinates estimated with and without correcting the observation files are compared to assess the influence of HO ionospheric errors in GNSS positioning.

In terms of the IGS products for a consistent PPP, CODE satellite orbit and clock products which do not consider HO ionospheric effects are used in this project.

9.17. **APPENDIX Q** – STEPS INVOLVED IN THE APPLICATION OF THE SCINTILLATION MITIGATION TECHNIQUE

1. DLL jitter STD is estimated for the C1 observable using GPS L1 I/Q data for all LoS paths according to the proposed technique introduced in Section 4.2.
2. DLL jitter STD estimates are multiplied by a factor of 20 for use as jitter STD values for P2 observable for all LoS paths. Refer to Section 6.2.4. for the details of this scaling.
3. PLL jitter STD values are calculated for the L1 observable using GPS L1 I/Q data for all LoS paths according to the method, as described in Section 4.2.
4. PLL jitter STD estimates are multiplied by the ratio of f_1/f_2 (where f_1 and f_2 are signal frequencies for the GPS L1 and L2 signals) for use as jitter STD values for the L2 observable for all LoS paths.
5. A comma separated values (*.csv*) file is prepared where each line starts with a time stamp that refers to the start time of the observation data, and contains data for each SVID and jitter STD values in an order (defined by columns) as determined by the positioning software. Snapshot of such a file used in RT_PPP is provided in Fig. 9.6. The contents of each column are defined in red labels for the respective columns (for illustration purposes here); 6th column onwards are the jitter STD values for the observables C1 and P2 in meters and L1 and L2 in radians. Columns occupied with "NaN" are not considered yet in the positioning software; however for future use of C2 (allocated in 7th column) and other new observables (non-specified 10th column) that can be included in PPP these columns can also be occupied. Scintillation indices are not relevant for the positioning solution and are provided in 4th and 5th columns for data purpose only, therefore these columns are filled with constant values of 0.3 (4th column) and 0.5 (5th column) for practical purposes. The line for SV16 marked in blue rectangle contains the jitter STD values that can be noted to be the same for SV14 and SV15 in the earlier lines. These (repeating) STD values are indeed "placeholders" – these SVs were present earlier in the observation period and not anymore during the period of this snapshot, therefore their

corresponding jitter STD values are assigned default values for the particular observables. These "default" values[b] are decided based on the expected precision for C1 and L1, and scaled for P2 and L2 as described earlier (by 20 for the code observable, and frequency ratio for the phase observable). In addition to such placeholder purpose of these default values, they also serve as "safety" precision values in case an estimate for the jitter STD cannot be achieved due to non-availability of I/Q data.

[b] *For C1, 0.5m, P2 (20 times that of C1) 10m, L1 pi/12 radians, and for L2 (f1/f2 times that of L1) about 0.33 radians are considered as safety precision values to be applied in such circumstances.*

GPS Time of Week

		SVID			C1	C2	L1	L2		P2
1669	54000	4	0.3	0.5	0.500000	NaN	0.261799	0.335976	NaN	10.000000
1669	54000	5	0.3	0.5	0.073828	NaN	0.019830	0.025449	NaN	1.476568
1669	54000	6	0.3	0.5	0.098452	NaN	0.029232	0.037515	NaN	1.969036
1669	54000	7	0.3	0.5	0.077973	NaN	0.026754	0.034335	NaN	1.559452
1669	54000	8	0.3	0.5	0.077973	NaN	0.026754	0.034335	NaN	1.559452
1669	54000	9	0.3	0.5	0.500000	NaN	0.261799	0.335976	NaN	10.000000
1669	54000	10	0.3	0.5	0.107279	NaN	0.026155	0.033566	NaN	2.145582
1669	54000	11	0.3	0.5	0.500000	NaN	0.261799	0.335976	NaN	10.000000
1669	54000	12	0.3	0.5	0.500000	NaN	0.261799	0.335976	NaN	10.000000
1669	54000	13	0.3	0.5	0.127321	NaN	0.031018	0.039806	NaN	2.546413
1669	54000	14	0.3	0.5	0.500000	NaN	0.261799	0.335976	NaN	10.000000
1669	54000	15	0.3	0.5	0.500000	NaN	0.261799	0.335976	NaN	10.000000
1669	54000	16	0.3	0.5	0.500000	NaN	0.261799	0.335976	NaN	10.000000
1669	54000	17	0.3	0.5	0.086259	NaN	0.021132	0.027120	NaN	1.725187
1669	54000	18	0.3	0.5	0.500000	NaN	0.261799	0.335976	NaN	10.000000
1669	54000	19	0.3	0.5	0.500000	NaN	0.261799	0.335976	NaN	10.000000

GPS Week Number

S_4 SigmaPhi Scintillation Indices

Figure 9.6. Sample lines from a *.csv* file used in the mitigation technique in RT_PPP.

N.B. for the two types of GNSS positioning software GPSeq and RT_PPP, the order of data in each line of a .csv file is different. Furthermore, in GPSeq two .csv files need to be applied, one for each of the stations on the baseline if scintillation mitigation is to be applied at both ends. If mitigation is aimed to be applied only for the reference station, then .csv file only for the reference station needs to be uploaded.

6. While running the RT_PPP software, "scintillation mitigation" can be applied during positioning which involves uploading the relevant *.csv* file

into the program before starting the positioning process. Figure 9.7. shows how positioning with mitigation is performed using the software RT_PPP: regarding the stochastic modelling (related with the statistical quality of the measurements), the scintillation file is uploaded as pointed with the red arrow.

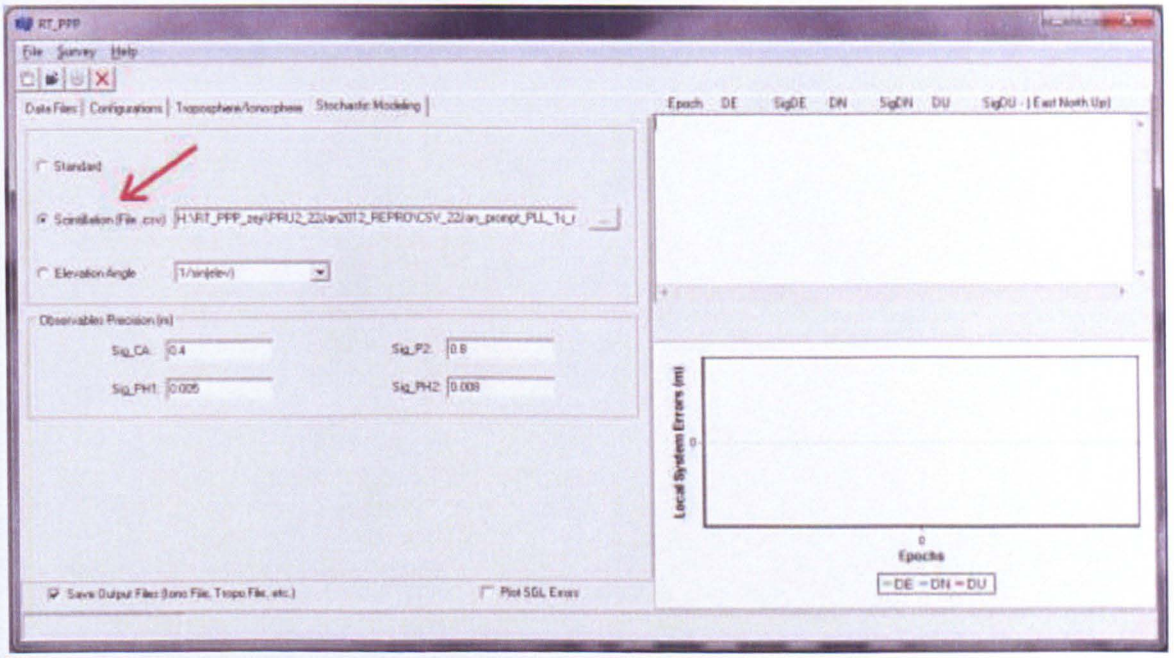

Figure 9.7. User interface for RT_PPP software showing the scintillation file option enabled with the relevant *.csv* file uploaded.